A MICROFLUIDIC PAPER-BASED ANALYTICAL DEVICE FOR EARLY DIAGNOSIS AND PROGNOSIS OF ACUTE MYOCARDIAL INFARCTION

LIM WEI YIN

FACULTY OF SCIENCE
UNIVERSITY OF MALAYA
KUALA LUMPUR

2020

University of Malaya

A MICROFLUIDIC PAPER-BASED ANALYTICAL DEVICE FOR EARLY DIAGNOSIS AND PROGNOSIS OF ACUTE MYOCARDIAL INFARCTION

LIM WEI YIN

THESIS SUBMITTED IN FULFILMENT OF THE REQUIREMENTS FOR THE DEGREE OF DOCTOR OF PHILOSOPHY

DEPARTMENT OF CHEMISTRY
FACULTY OF SCIENCE
UNIVERSITY OF MALAYA
KUALA LUMPUR

2020

University of Malaya

UNIVERSITY OF MALAYA

ORIGINAL LITERARY WORK DECLARATION

Name of Candidate: **LIM WEI YIN**
Matric No: **SHC140116**
Name of Degree: **DOCTOR OF PHILOSOPHY**
Title of Thesis ("this Work"):
A MICROFLUIDIC PAPER-BASED ANALYTICAL DEVICE FOR EARLY DIAGNOSIS AND PROGNOSIS OF ACUTE MYOCARDIAL INFARCTION
Field of Study:
ANALYTICAL CHEMISTRY

I do solemnly and sincerely declare that:

(1) I am the sole author/writer of this Work;
(2) This Work is original;
(3) Any use of any work in which copyright exists was done by way of fair dealing and for permitted purposes and any excerpt or extract from, or reference to or reproduction of any copyright work has been disclosed expressly and sufficiently and the title of the Work and its authorship have been acknowledged in this Work;
(4) I do not have any actual knowledge nor do I ought reasonably to know that the making of this work constitutes an infringement of any copyright work;
(5) I hereby assign all and every rights in the copyright to this Work to the University of Malaya ("UM"), who henceforth shall be owner of the copyright in this Work and that any reproduction or use in any form or by any means whatsoever is prohibited without the written consent of UM having been first had and obtained;
(6) I am fully aware that if in the course of making this Work I have infringed any copyright whether intentionally or otherwise, I may be subject to legal action or any other action as may be determined by UM.

Candidate's Signature Date:

Subscribed and solemnly declared before,

Witness's Signature Date:

Name:
Designation:

University of Malaya

A MICROFLUIDIC PAPER-BASED ANALYTICAL DEVICE FOR EARLY DIAGNOSIS AND PROGNOSIS OF ACUTE MYOCARDIAL INFARCTION

ABSTRACT

Acute myocardial infarction (AMI), also termed as heart attack, is often clinically screened by blood test through the measurement of cardiac biomarkers (i.e., troponin (T or I), creatine kinase (CK−MB) and myoglobin) and electrocardiography (ECG) changes which are presented to the hospital. However, the early diagnosis of AMI is challenging because the detection of biomarkers such as troponin (T or I) and CK−MB are only reliable at the intermediate and later stages (> 6 hours after chest pain onset), during myocardial injury and myocardial infarction. On the other hand, myoglobin often been used as early biomarker which is detectable within the first 3 hours of chest pain onset was found to be more specific to skeletal muscle injury rather than myocardial injury. To overcome these limitations, the detection of a new combination of cardiac biomarkers for early diagnosis and prognosis of AMI was demonstrated in this Ph.D. project. The uniqueness of this new combination of cardiac biomarkers detection was to allow an early diagnosis of the patient at risk, to provide immediate therapy and reduce mortality rate of AMI. Glycogen phosphorylase isoenzyme BB (GPBB) was detected as a potential early biomarker of ischemic myocardial injury (within the first 4 hours) while cTnT and CK−MB were detected as prognosis biomarkers of myocardial injury and myocardial infarction. The main objective of this Ph.D. project is to develop a sensitive, low-cost and disposable microfluidic paper-based device (μPAD) for simultaneous detection of multiple cardiac biomarkers utilising both colourimetric and Surface Enhanced Raman Scattering (SERS) detection techniques. The fabricated μPAD was designed with three reaction zones: G for GPBB; M for CK−MB and T for cTnT, which was connected to a central sample zone on a nitrocellulose membrane by wax-printing technique using a wax printer—Fuji Xerox ColorQube 8870. Three different colour nanoparticles (silver, gold urchin and gold) were used as detecting indicator for a particular target analyte. The colourimetric signal could be easily observed easily through the naked eye based on the appearance of the distinct colour. Whereas the SERS signals are measured by the peak characteristics of the respective Raman reporter molecules in SERS probe at the three respective reaction zones. On the other hand, smartphone-based camera and desktop scanner were used as a diagnostic tool in colourimetric quantification; whereas Renishaw InVia Raman Microscope was

University of Malaya

used in SERS. As for the obtained results, the colourimetric and SERS-based sandwich immunoassay performed on the μPAD showed good reproducibility (*RSD* approximately 10%), good intra- and inter-day precision (*CV* 10%–20%), consistent stability test results throughout the 28 days, and a strong correlation between these three developed diagnostic tools ─ smartphone–based camera (R^2 = 0.96); desktop scanner (R^2 = 0.94) and SERS (R^2 = 0.97) with the laboratory Siemens Centaur XPT Immunoassay System (a laboratory method) used at University Malaya Medical Center (UMMC). Additionally, to omit the requirement of the calibration curve for quantitative measurement, partial least squares (PLS) models were designed to quantify the levels of cardiac biomarkers with the Raman spectral data, for GPBB assay with R^2 = 0.94; CK-MB assay with R^2 = 0.80; and cTnT assay with R^2 = 0.86. This method allows for absolute quantitative measurement when the conventional calibration curve fails to provide accurate estimate of the cardiac biomarkers, especially at low and high concentration ranges. Overall, the present findings indicated the potential of μPAD platform as a point-of-care testing (POCT) device for early diagnosis and prognosis of AMI by using smartphone-based camera/desktop scanner and Raman spectroscopy as a diagnostic tool for colourimetric detection and SERS detection, respectively. Hence, this developed the μPAD with a new combination of cardiac biomarkers which potentially function as a POC device for prompt diagnosis by rapid exclusion of MI (quantified by using a calibration curve or a calibration- free predictive diagnostic model).

Keywords: Microfluidic paper-based device, Acute myocardial infarction, Multiplex detection, Colourimetric technique, Surface enhanced Raman scattering technique

University of Malaya

MIKRO-BENDALIRAN BERASASKAN KERTAS UNTUK DIAGNOSIS AWAL DAN LEWAT INFARK MIOKARD AKUT

ABSTRAK

Infark miokard akut (IMA), juga dikenali sebagai serangan jantung, boleh diuji secara klinikal melalui ujian darah dengan mengesan bio-penanda jantung (contohnya, troponin (T atau I), creatine kinase (CK−MB) dan myoglobin) dan elektrokardiografi (EKG) semasa hadir ke hospital. Walau bagaimanapun, diagnosis awal IMA) adalah mencabar kerana pengesanan bio-penanda seperti troponin (T atau I) dan CK−MB hanya boleh dikesan semasa peringkat pertengahan dan kemudian (> 6 jam selepas permulaan kesakitan dada), semasa kecederaan miokardium dan infark miokard. Selain itu, myoglobin sering digunakan sebagai bio-penanda jantung awal kerana ia dapat dikesan dalam masa 3 jam pertama dari kesakitan dada, tetapi ia didapati lebih spesifik untuk kecederaan otot rangka daripada kecederaan miokardium. Bagi mengatasi batasan ini, pengesanan gabungan baharu bio-penanda jantung untuk diagnosis awal dan lewat IMA telah dijalankandalam projek Ph.D. saya. Pengenalan unik baru pengesanan biomarker jantung adalah untuk membolehkan diagnosis awal pesakit berisiko, untuk memberikan terapi segera dan mengurangkan kadar kematian AMI. Glycogen phosphorylase isoenzyme BB (GPBB) merupakan bio-penanda jantung awal yang berpotensi pada kecederaan miokard iskemia (dalam masa 4 jam yang pertama) manakala cTnT dan CK−MB merupakan bio-penanda jantung lewat untuk mengesan kecederaan miokardium dan infark miokard. Objektif kajian Ph.D. ini adalah mereka peranti mikro-bendaliran yang berasaskan kertas,sensitif, kos rendah. Peranti tersebut boleh mengesan pelbagai bio-penanda jantung secara serentak dengan kedua-dua kaedah, iaitu kolorimetrik dan permukaan dipertingkatkan penyebaran Raman (SERS). Oleh itu, peranti mikro-bendaliran yang berasaskan kertas ini direka dengan tiga zon tindak balas: G untuk GPBB; M untuk CK−MB dan T untuk cTnT, yang bergabung dengan zon sampel pusat pada membran nitrocellulosa dengan menggunakan kaedah pencetakan lilin—Fuji Xerox ColorQube 8870 pencetak lilin. Tiga jenis warna nanopartikel yang berbeza (emas, perak, dan emas “urchin”) telah digunakan sebagai penunjuk untuk analit tertentu. Isyarat kolorimetrik boleh dilihat dengan mudah melalui mata kasar berdasarkan warna yang berbeza manakala isyarat Raman dipertingkatkan dengan menjerap molekul Raman masing-masing ke nanopartikel tertentu. Di samping itu, kamera telefon bimbit dan alat pengimbas telah dicadangkan sebagai alat diagnostik

University of Malaya

untuk kuantifikasi isyarat kolorimetrik; manakala Renishaw InVia Raman Mikroskop telah digunakan untuk kuantifikasi isyarat Raman. Maka, immunoassay sandwich berasakan kolorimetrik dan SERS yang dilaksanakan pada μPAD menunjukkan kebolehulangan (*RSD* kira-kira 10%), ketepatan intra-dan antara hari (*CV* 10%−20%), ujian kestabilan yang konsisten hasil sepanjang 28 hari, dan korelasi yang kuat antara tiga alat diagnostik yang dicadang- kamera telefon bimbit (R^2 = 0.96); pengimbas (R^2 = 0.94); SERS (R^2 = 0.97) dengan sistem makmal Siemens Centaur XPT Immunoassay (kaedah piawai) yang digunakan di Pusat Perubatan Universiti Malaya (PPUM). Di samping itu, bagi mengelakkan keperluan keluk penentukuran dalam pengukuran kuantitatif, model *Partial least squares (PLS)* direka untuk mengukur kepekatan bio-penanda jantung dari data spektrum Raman, untuk ujian GPBB dengan R^2 = 0.94; ujian CK-MB dengan R^2 = 0.80; dan ujian cTnT dengan R^2 = 0.86. Kaedah ini membenarkan pengukuran kuantitatif mutlak apabila keluk penentukuran konvensional gagal untuk memberikan anggaran yang tepat mengenai kepekatan bio-penanda jantung, terutamanya pada julat kepekatan yang rendah dan tinggi. Secara umum, penemuan penyelidikan ini menunjukkan potensi μPAD sebagai alternatif alat penjagaan untuk diagnosis awal dan lewat IMA dengan menggunakan kamera telefon bimbitsebagai alat diagnostik untuk pengesanan kolorimetrik dan spektroskopi Raman sebagai alat diagnostik untuk pengesanan SERS. Oleh itu, μPAD dengan gabungan baru bio-penandajantung berpotensi berfungsi sebagai alat penjagaan dalam diagnosis segera dengan pengecualian pesat infark miokar (dianggarkan dengan keluk penentukuran atau ramalan model diagnostik, bebas dari keluk penentukuran).

Kata kunci: Peranti mikro-bendaliran berasaskan kertas, Infark miokard akut, Pengesanan multipleks, Teknik Kolorimetrik, Teknik permukaan dipertingkatkan penyebaran Raman.

University of Malaya

ACKNOWLEDGEMENTS

I would like to express my sincere gratitude to both of my supervisor; Dr. Khor Sook Mei and Dr. Goh Boon Tong for their continuous support given throughout my entire Ph.D. study. Dr. Khor Sook Mei expertly guided and helped me in all the time of research and the writing of this thesis. She allows me to widen my research from various perspectives and keeping me improves with challenges. My sincere thanks to Dr. Goh Boon Tong, who has supported me with his patience and knowledge while permitting freedom for me to work in my own way. I would also like to thank Dr. T. Malathi who helping me in biomedical analysis as part of my study and her insightful comments for my research.

My sincere thanks go to the scientific officer, Mr. Amirul and Miss Syariah works in HIR (High Impact Research) and Miss Lela Chemistry department (Chemistry New Building) for allowing me to access the instrument and facilities for my research. My appreciation also goes all my beloved friends Steff Lim, Choo Gim Hua, Kwan Soon Seng, Goh Yuh Ha and Albert Teo, who supported and incented me to strive toward my goal. Finally, a special thank directed to my parents, Lim Kooi Thong and Lee Lay Ean; my lovely siblings, Wei Leong, Yen Sun, Wei Kheng, Wei Yih; and my boyfriend, Dr. Goh Choon Hian for supporting me spiritually and their continuous encouragements throughout my years of study. This accomplishment would not have been possible without them.

University of Malaya

TABLE OF CONTENTS

ORIGINAL LITERARY WORK DECLARATION ..... **ii**

ABSTRACT ..... **iii**

ABSTRAK ..... **v**

ACKNOWLEDGEMENTS ..... **vii**

TABLE OF CONTENTS ..... **viii**

LIST OF FIGURES ..... **xiii**

LIST OF TABLES ..... **xviii**

LIST OF SYMBOLS AND ABBREVIATIONS ..... **xix**

LIST OF APPENDICES ..... **xxiii**

CHAPTER 1: INTRODUCTION **1**

1.1 Aim and Objectives 4

1.1.1 Aim 4

1.1.2 Research Objectives 4

1.2 Organisation of Thesis 5

CHAPTER 2: LITERATURE REVIEW **7**

2.1 Acute Coronary Syndrome 7

2.2 Cardiac Biomarkers 10

2.2.1 Troponin 11

2.2.2 Creatine Kinase−MB 13

2.2.3 Glycogen Phosphorylase Isoenzyme BB 14

2.2.4 Myoglobin 14

2.3 Fabrication Techniques of Microfluidic Paper-Based Analytical Device 18

2.3.1 Photolithography 18

University of Malaya

2.3.2 Polydimethylsiloxane Plotting 20
2.3.3 Inkjet Printing 20
2.3.4 Plasma Etching 22
2.3.5 Wax Printing and Wax Dipping 22
2.3.6 Flexographic Printing 24
2.3.7 Cutting 25
2.3.8 Stamping 26
2.3.9 Origami 27
2.4 Detection Methods of Microfluidic Paper-Based Analytical Device 34
2.4.1 Colourimetric Detection 34
2.4.2 Electrochemical Detection 36
2.4.3 Chemiluminescence Detection 37
2.4.4 Electrochemiluminescence Detection 38
2.4.5 Surface Enhanced Raman Scattering Detection 40
2.5 Health Diagnostic Applications of Microfluidic Paper-Based Analytical Device 44
2.5.1 Urinalysis 44
2.5.2 Blood Analysis 47
2.5.3 Virus Analysis 49
2.5.4 Saliva Analysis 52

CHAPTER 3: METHODOLOGY 56
3.1 Fabrication of Microfluidic Paper-Based Analytical Device 57
3.1.1 Optimisation of Heating Time and Temperature 58
3.1.2 Optimisation of Sample Volume and Colour Development Time 58
3.2 Colourimetric Assay Procedure on Microfluidic Paper-Based Analytical Device 59
3.2.1 Conjugation of Nanoparticles with Detecting Antibodies 64

University of Malaya

3.2.2 Characterisation of Colourimetric Conjugates 67

3.2.3 Qualitative Colourimetric Analysis 67

3.2.4 Semi-Quantitative Colourimetric Analysis 67

3.2.5 Quantitative Colourimetric Analysis 68

3.3 SERS Assay Procedure on Microfluidic Paper-Based Analytical Device 69

3.3.1 Conjugation of SERS Probe with Detecting Antibodies 71

3.4 Characterisation of SERS Conjugates 73

3.4.1 Quantitative SERS Analysis 74

3.5 Analytical Performance of Microfluidic Paper-Based Analytical Device for Colourimetric and SERS Assay 75

3.5.1 Optimisation of Blocking Reagents 75

3.5.2 Reproducibility Studies 76

3.5.3 Intra-and Inter-day Precision Studies 77

3.5.4 Stability Studies 77

3.5.5 Cross-reactivity Studies 78

3.5.6 Clinical Sample Analysis 78

3.5.7 Method Comparison 79

3.6 Multivariate Statistical Analysis 80

3.6.1 Principal Component Analysis 80

3.6.2 Partial Least Square Regression 81

CHAPTER 4: RESULTS AND DISCUSSION 83

4.1 Fabrication Parameters of Microfluidic Paper-Based Analytical Device 83

4.1.1 Optimisation of Heating Time and Temperature 83

4.1.2 Optimisation of Sample Volume and Colour Development Time 86

4.2 Microfluidic Paper-Based Analytical Device for Colourimetric Assay 89

University of Malaya

4.2.1 Conjugation of Nanoparticles with Detecting Antibodies 89
4.2.2 Characterisation of Colourimetric Conjugates 94
4.2.2.1 Ultraviolet-Visible Spectroscopy 94
4.2.2.2 Dynamic Light Scattering and Zeta Potential 97
4.2.3 Assay Cutoff for Qualitative Colourimetric Assay 99
4.2.4 Qualitative Colourimetric Assay 100
4.2.5 Semi-Quantitative Colourimetric Assay 102
4.2.6 Quantitative Colourimetric Assay 105
4.3 Microfluidic Paper-Based Analytical Device for SERS Assay 109
4.3.1 Conjugation of SERS Probe with Detecting Antibodies 109
4.3.2 Characterisation of Raman SERS Probe Conjugates 111
4.3.2.1 Ultraviolet-Visible Spectroscopy 111
4.3.2.2 Fourier-Transform Infrared Spectroscopy 114
4.3.2.3 Raman Spectroscopy 117
4.3.3 Quantitative SERS Assay 120
4.4 Analytical Performance of Microfluidic Paper-Based Analytical Device for Colourimetric and SERS assay 124
4.4.1 Optimisation of Blocking Reagents 124
4.4.2 Reproducibility Studies 128
4.4.3 Intra-and Inter-day Precision Studies 131
4.4.4 Stability Studies 137
4.4.5 Cross-reactivity Studies 141
4.4.6 Clinical Sample Analysis 144
4.4.7 Comparison of Methods 147
4.4.7.1 Correlation and Regression Analysis 147
4.4.7.2 Bland–Altman Plot Difference 149

University of Malaya

4.4.7.3 Independent T−test (Two−Tailed) 152

4.5 Multivariate Analysis..... 155

4.5.1 Principal Component Analysis 155

4.5.2 Partial Least Squares Regression..... 159

CHAPTER 5: CONCLUSIONS AND FUTURE PERSPECTIVES 168

5.1 Conclusions 168

5.2 Future Perspectives..... 169

5.3 Recommendations..... 171

REFERENCES..... 174

LIST OF PUBLICATIONS..... 191

APPENDICES 195

University of Malaya

LIST OF FIGURES

Figure 2.1 : Algorithm for the evaluation of patients with chest pain. 9

Figure 2.2 : Characteristics of the ideal cardiac biomarkers for AMI diagnosis. 11

Figure 2.3 : Release of cardiac troponins into bloodstream following ischemic induced myocardial injury. 13

Figure 2.4 : Photolithography procedure for SU8-photoresist patterning onto paper substrate. 19

Figure 2.5 : Polydimethylsiloxane plotting technique by printing hydrophobic PDMS to define hydrophilic channels on paper. 20

Figure 2.6 : Fabrication process of microfluidic multi-analyte chemical sensing paper by using the inkjet-printed technique. 21

Figure 2.7 : A µPAD patterned with the AKD and exposed to plasma treatment. 22

Figure 2.8 : Fabrication process of wax printing and dipping method. (i) Patterning hydrophobic barriers in paper by wax printing using a wax printer. (ii) Patterning paper by wax dipping using an assembled mold. 23

Figure 2.9 : Flexographic printing of polystyrene to define hydrophobic region on paper substrate. 24

Figure 2.10 : Cutting techniques. (i) Paper device is prepared by manually cutting. (ii) Paper device is cut by using the knife plotter. (iii) µPAD is fabricated by one-step laser cutting method with hollow microstructures as hydrophobic barriers. (iv) Laminated paper-based analytical device is fabricated by simple craft-cutting and lamination. 26

Figure 2.11 : Stamping techniques. (i) Fabrication process of µPADs based on handheld stamping. (ii) Fabrication process of µPAD using flash foam stamp lithograph. 27

Figure 2.12 : Fabrication of 3D-µPAD for multiplex detection based on the principles of origami. (i) Layers of patterned papers are stacked with double-sided adhesive tape based on origami principle. (ii) The µPAD is simply folded into multiple layers without using a tape. 28

Figure 2.13 : Colourimetric detection in µPAD using a smartphone for image processing. 35

Figure 2.14 : Figure 2.14: Electrochemical detection in three electrode µPAD. 37

Figure 2.15 : Chemiluminescence detection in µPAD, where CL signal was measured using a computerised ultra-weak luminescence analyser. 38

University of Malaya

Figure 2.16 : Electrochemiluminescence detection in µPAD. 39

Figure 2.17 : Surface enhanced Raman scattering (SERS) nanotags based LFA. .. 41

Figure 2.18 : µPADs for protein and glucose detection in urine sample, (i) Photoresist-patterned tree-shaped µPAD. (ii) Tree-shaped µPAD with multi-branches. (iii) Wax-patterned 3D-µPAD with principles of origami. 46

Figure 2.19 : µPAD for separating blood plasma from red blood cells (RBCs). (i) using red blood cell (RBC) agglutination. (ii) using different types of paper. 49

Figure 2.20 : µPAD for virus analysis. (i) 3D-µPAD for detection of HBsAg. (ii) Paper-based electrochemical sensor for detection of Hepatitis B virus DNA. (iii) Electrochemical µPAD for simultaneous detection of HIV and HCV. 52

Figure 2.21 : µPAD used for saliva analysis. (i) µPAD for the detection of salivary nitrite for diagnosing hemodialysis. (iii) µPAD for simultaneous determination of pH and nitrite. (iii) µPAD for the detection of salivary nitrite for diagnosing periodontitis disease.. 55

Figure 3.1 : Flow chart of research work. 56

Figure 3.2 : Design and dimensions of the fabricated µPAD used for multiplex detection of cardiac biomarkers. 57

Figure 3.3 : Images of (i) µPAD before heating and (ii) µPAD after heating. 58

Figure 3.4 : Schematic illustration of multiplex colourimetric detection of cardiac biomarkers at respective reaction zone(s), G for GPBB, M for CK−MB, and T for cTnT on µPAD 63

Figure 3.5 : The measurement procedure of colour intensity in Image J. 64

Figure 3.6 : Preparation of colourimetric conjugates−nanoparticles-labeled detecting antibody. 66

Figure 3.7 : Schematic illustration of multiplex SERS detection of cardiac biomarkers at respective reaction zone(s), G for GPBB, M for CK−MB, and T for cTnT on µPAD. 70

Figure 3.8 : Preparation of Raman SERS probe conjugated with detecting antibodies for Raman SERS assay. 71

Figure 3.9 : Structural equation showing the SERS probe's thorough synthesis mechanism conjugates with the detecting antibodies. 73

Figure 4.1 : Optimisation of heating time and temperature for µPAD fabrication. 84

University of Malaya

Figure 4.2 : Result interpretation on μPAD at reaction zone (~30 mm diameter) instead of 50 mm diameter (44 nm diameter after heating). 85

Figure 4.3 : Optimisation of (a) sample volume and (b) colour development time for an assay. 88

Figure 4.4 : λmax of nanoparticles—Gold, Silver and Gold-urchin. 91

Figure 4.5 : pH optimisation of nanoparticles ─ (a) silver, (b) gold-urchin and (c) gold. 92

Figure 4.6 : Concentration optimisation of detecting antibody ─ (a) GPBB, (b) CK−MB and (c) cTnT 93

Figure 4.7 : Absorption spectrum of nanoparticles (a) silver; (b) gold-urchin and (c) gold, before and after conjugating with detecting antibody. 96

Figure 4.8 : The assay cutoff for qualitative detection of cardiac biomarkers. 99

Figure 4.9 : Qualitative test result for multiplex detection of cardiac biomarkers on the fabricated μPAD. 101

Figure 4.10 : The calibration curve for quantitative colourimetric detection of multiplex cardiac biomarkers using (▲) smartphone-based camera, (●) desktop scanner. (a)(i) Signal intensity of test zone G measured versus concentrations of GPBB. Dynamic range obtained via (i) smartphone-based camera and (ii) desktop scanner. (b)(i) Signal intensity of test zone M measured versus concentrations of CK−MB. Dynamic range obtained via (i) smartphone-based camera and (ii) desktop scanner. (c) Signal intensity of test zone T measured versus concentrations of cTnT. Dynamic range obtained via (i) smartphone-based camera and (ii) desktop scanner. 108

Figure 4.11 : The binding interaction stage of SERS probes. (a) Gold SERS probe conjugated anti-cTnT detecting antibody; (b) Silver SERS probe conjugated anti-GPBB detecting antibody; (c) Gold-urchin SERS probe conjugated anti-CK−MB detecting antibody 110

Figure 4.12 : UV−Visible absorption spectra of the SERS nanoparticles (a) silver, (b) gold−urchin and (c) gold, before and after silica coating. 113

Figure 4.13 : FTIR spectra for SERS Probes─ (a) silver, (b) gold−urchin and (c) gold. SERS probe functionalised with glycine-glutaldehyde reaction (orange line) and carbonyl group-functionalised SERS Probe conjugated with detecting antibody (blue line). 116

University of Malaya

Figure 4.14 : The peak frequencies and assignment of the fingerprints of Raman molecules (a) 4-nitroanilline, (b) tert-Butylhydroquinone and (c) methyl red in SERS probe on silicon slide and NC membrane. 119

Figure 4.15 : Calibration plots of quantitative analysis of multiplex cardiac biomarkers ─ (a) GPBB, (b) CK−MB and (c) cTnT on SERS-based μPAD. 123

Figure 4.16 : The signal to background ratio versus blocking reagents ─ (a) smartphone-based camera, (b) desktop scanner, and (c) Renishaw InVia Raman Microscope 127

Figure 4.17 : Reproducibility tests using a (a) smartphone-based camera, (b) desktop scanner, and (c) Renishaw InVia Raman Microscope 130

Figure 4.18 : Intra-day precision tests using a (a) smartphone-based camera, (b) desktop scanner, and (c) Renishaw InVia Raman Microscope ... 133

Figure 4.19 : Inter-day precision tests using a (a) smartphone-based camera, (b) desktop scanner, and (c) Renishaw InVia Raman Microscope ... 135

Figure 4.20 : Stability test was conducted where the obtained images/spectra captured using ─ (a) smartphone-based camera, (b) desktop scanner, and (c) Renishaw InVia Raman Microscope 139

Figure 4.21 : Stability test conducted for detecting three cardiac biomarkers (GPBB, CK-MB and cTnT) based on three detection methods (smartphone-based camera, desktop scanner and Renishaw InVia Raman Microscope) from Day 1 ─ Day 28..... 140

Figure 4.22 : Cross-reactivity tests were conducted where the obtained images/spectra were captured using ─ (a) smartphone-based camera, (b) desktop scanner, and (c) Renishaw InVia Raman Microscope 143

Figure 4.23 : Calibration curve for levels of CK−MB protein in the human serum samples measured by (▲) smartphone-based camera; (●) desktop scanner and (■) Renishaw InVia Raman Microscope. The concentrations of three unknown human serum samples containing CK−MB were marked as 1, 2 and 3. 146

Figure 4.24 : The linear regression analysis measured by (▲) smartphone-based camera; (●) desktop scanner and (■) Renishaw InVia Raman Microscope 148

Figure 4.25 : Bland–Altman analysis of cardiac CK−MB for 12 serum samples, measured by (a) smartphone-based camera; (b) desktop scanner and (c) Renishaw InVia Raman Microscope. Solid line represents mean (bias), upper dashed line indicates the mean +1.96 SD (upper limit of agreement), and lower dashed line

University of Malaya

indicates mean -1.96 SD (lower limit of agreement)..... 151

Figure 4.26 : Principle component score plot in the (a, b) PC1−PC2 and (c, d) PC3–PC4 plane. Sample indicated as ○ for GPBB, × for cTnT and ◊ for CK−MB. 157

Figure 4.27 : PCA - *k*-NN prediction. Sample indicated in group: (1) GPBB. (2) cTnT and (3) CK−MB. 158

Figure 4.28 : Raman spectra data of three cardiac biomarkers (700 – 2000 cm^{-1}) ─ (a) GPBB (concentration: 0.001−100 ng mL^{-1}), (b) CK−MB (concentration: 0.001−100 ng mL^{-1}), and (c) cTnT (concentration: 0.001−200 ng mL^{-1}). 160

Figure 4.29 : Percentage of variance explained in concentration of three cardiac biomarkers across the first 20 PLS components (Method 1: the optimal PLS components are chosen based on the largest increase of the percent variance). 161

Figure 4.30 : Estimated root mean square prediction of three cardiac biomarkers across the first 20 PLS components (Option 2: the optimal PLS components was chosen based on the lowest root mean square prediction value). 162

Figure 4.31 : Goodness-of-fit of three cardiac biomarkers ─ (a) GPBB, (b) CK−MB and (c) cTnT. 164

Figure 4.32 : Model parsimony of three cardiac biomarkers ─ (a) GPBB, (b) CK−MB and (c) cTnT. 166

University of Malaya

LIST OF TABLES

Table 2.1 : Time of release of biomarkers during myocardial infarction. 16

Table 2.2 : Various fabrication techniques and pattern for 2D-and 3D-μPAD. 29

Table 2.3 : Comparison of the detection methods of μPAD..... 42

Table 3.1 : Total time taken for sandwich formation on μPAD. 62

Table 3.2 : Upper reference limit for three cardiac marker ─ GPBB, CK−MB and cTnT categorized as low risk, moderate risk (within borderline), and high risk..... 68

Table 4.1 : Hydrodynamic size and zeta potential for monodisperse nanoparticles—silver, gold-urchin and gold before and after conjugation. 98

Table 4.2 : The semi-quantitative reference chart based on the levels of multiple cardiac biomarkers, (a) GPBB; (b) CK−MB and (c) cTnT..... 104

Table 4.3 Comparison of methods of measurement on CK−MB levels (a) I versus II, (b) I versus III and (c) I versus IV. 153

University of Malaya

LIST OF SYMBOLS AND ABBREVIATIONS

%	:	Percent
μg mL^{-1}	:	Micrograms per Milliliter
μL	:	Microliter
2D	:	2-Dimensional
3D	:	3-Dimensional
copies/mL	:	Copies per Milliliter
CV	:	Coefficient Variation
IU/mL	:	International Units per Milliliter
mm	:	Milimeter
mV	:	Millivolts
ng mL^{-1}	:	Nanograms per Milliliter
nm	:	Nanometer
º	:	Degree
ºC	:	Degree Celsius
pM	:	picometer
v/w	:	Weight per Volume
λmax	:	Wavelength of Maximum Absorption
μPAD	:	Microfluidic Paper-Based Analytical Device
ACS	:	Acute Coronary Syndrome
Ag	:	Silver
AgNPs	:	Silver Nanoparticles
AKD	:	Alkyl ketene Dimer
AMI	:	Acute Myocardial Infarction
ASV	:	Anodic Stripping Voltammetry

University of Malaya

Au	:	Gold
BSA	:	Bovine Serum Albumin
CK	:	Creatine Kinase
CK−MB	:	Creatine Kinase MB
CL	:	Chemiluminescence
CMOS	:	Complementary Metal-Oxide Semiconductor
cTnI	:	Troponin I
cTnT	:	Troponin T
Cu	:	Copper
CV	:	Coefficient of Variation
CVD	:	Cardiovascular Disease
CVF	:	Charge to Voltage Factor
D/A	:	Digital-to-Anolog Converter
DBAE	:	2-(dibutylamino) Ehtanol
DLS	:	Dynamic Light Scattering
DNA	:	Deoxyribonucleic Acid
DPV	:	Differential Pulse Voltammetry
ECG	:	Electrocardiogram
ECL	:	Electrochemiluminescence
ELISA		Enzyme-Linked Immunosorbent Assays
FTIR	:	Fourier-Transform Infrared Spectroscopy
GERTs		Gap-Enhanced Raman Tags
GP	:	Glycogen Phosphorylase
GPBB	:	Glycogen Phosphorylase Isoenzyme BB
H_2O_2	:	Hydrogen Peroxide
HBsAg	:	Hepatitis B Surface Antigen

University of Malaya

HBV	:	Hepatitis B Virus
HCV	:	Hepatitis C Virus
HIV	:	Human Immunodeficiency Virus
HRP	:	Horseradish Peroxidase
k-NN	:	k-Nearest Neighbours' Algorithm
LFAs	:	Lateral Flow Assays
LOD	:	Limit of Detection
LOO	:	Leave-One-Out
LSPR	:	Localized Surface Plasmon Resonance
MµB	:	Magnetic Microbeads
MI	:	Myocardial Infarction
NaCl	:	Sodium Chloride
NADH	:	Nicotinamide Adenine Dinucleotide
NC	:	Nitrocellulose
NH_4OH	:	Ammonium Hydroxide
NSTEMI	:	Non-ST-segment Elevation Myocardial Infarction
OTS	:	Octadecyltrichlorosilane
Pb	:	Lead
PC	:	Principe Components
PCA	:	Principal Component Analysis
PCR	:	Polymerase Chain Reaction
PDMS	:	Polydimethylsiloxane
PGMEA	:	Propylene Glycol Mono-Methyl Ether Acetate
PLS	:	Partial Least Square
POCT	:	Point-of-Care Testing
PVP	:	Polyvinylpyrrolidone

University of Malaya

RBC	:	Red Blood Cell
RSD	:	Relative Standard Deviation
SERS	:	Surface Enhanced Raman Scattering
STEMI	:	ST-segment Elevation Myocardial Infraction
TEOS	:	Tetraethyl Orthosilicate
UA	:	Unstable Angina
UV-Vis	:	Ultraviolet-Visible Spectroscopy
WBR	:	Western Blocking Reagent
WHO	:	World Health Organization
Zn	:	Zinc

University of Malaya

LIST OF APPENDICES

Appendix A : Supporting Information for SERS Assay 195

University of Malaya

CHAPTER 1: INTRODUCTION

World Health Organization (WHO) estimated that 17.9 million people died from cardiovascular disease (CVD) in 2016, representing 31% of global deaths. Of these deaths, 85% are due to heart attack and stroke. Acute myocardial infarction (AMI) is the medical name for a heart attack, one of the most severe ischemic events in CVD that leads to all the causes of mortality worldwide, which increased from 7.96 million deaths in 2006 to 9.48 million deaths in 2016 (Roth et al., 2017). In Malaysia, the mortality rate of AMI as reported in the latest WHO data is around 150 per 100,000 people in a year, approximately 23.10% of total death, which is ranked 33rd in the world (Abdullah et al., 2017).

A heart attack, or myocardial infarction (MI), is permanent damage to the heart muscle. According to WHO criteria, MI is defined when the presence of any two of three characteristics including (i) chest pain symptom, (ii) detection of a rise or fall of cardiac biomarker values and (iii) electrocardiogram (ECG) pattern changes involving the development of Q waves (Bernard, 1979). Patients with chest pain and suspected acute coronary syndrome (ACS) are usually referred urgently to the emergency department to undergo ECG monitoring to aid in risk stratification (Lang et al., 2000). However, ECG findings can be misleading as it is accounts for > 30% of misdiagnosed MI cases (Chacko et al., 2017; Kontos et al., 2010).

Therefore, serial cardiac biomarkers sampling is crucial for the diagnosis of AMI in patient with non-diagnostic ECGs or chest discomfort symptom. The traditional cardiac biomarkers include troponins (I or T), the creatine kinase MB isoenzyme (CK−MB), and myoglobin play an important role in the diagnosis, risk stratification and management of AMI (Al-Hadi & Fox, 2009; De Winter et al., 1995). However, early diagnosis of AMI is difficult because troponins and CK−MB tend to rise beyond the

University of Malaya

reference range at least 6 hours after the onset of symptoms. Even though myoglobin is detectable within the first 3 hours of chest pain onset, but it is found to be more specific for skeletal muscle injury than myocardial injury. Thus, glycogen phosphorylase isoenzyme BB (GPBB), which can diagnose ischemia as well as myocardial injury, was introduced as a reliable early marker to replace myoglobin for detection of myocardial injury (Bozkurt et al., 2011; Cubranic et al., 2012). The release of GPBB in blood circulation is much earlier compared to those traditional cardiac biomarkers as there is an increase in glycogen degradation during myocardial ischemia.

The conventional laboratory methods of diagnosis for AMI rely on immunoassay methods conducted in central laboratories. However, laboratory tests usually require high sample volumes (approximately 200 μL), long turnaround time (60─90 minutes) from the blood collection site to the laboratory, and a skillful technician to handle the instrument.

In the past decades, a portable point-of-care testing (POCT) device ─ lateral flow assays (LFAs) was proposed with the purpose of miniaturising the immunoassay procedures presently done at the central laboratory, and to minimise the waiting time for emergency room patients. There are several commercialised LFAs available from a variety of manufacturers for cardiac biomarkers measurement in single and multiplex strategy for qualitative and/or quantitative detection with a portable reader (Amundson & Apple, 2015). All the important cardiac biomarkers, i.e., troponin (T or I), CK−MB and myoglobin can be read qualitatively based on the colour change and are quantified individually and/or simultaneously with a reader with approximately 10−20 minutes after addition of the sample to POCT device. However, a dedicated reader is required for quantification of the colourimetric signal.

University of Malaya

On the other hand, the LFAs are limited in terms of design flexibility and detection sensitivity for multi-analytes on single test strip. Owing to limited space on a single lateral test strip, a flexible design such as comprising several separate reaction zones on strip is challenging. Hence, most of the cases for multiplexed LFAs are designed with the additional test lines over a single strip or overlap few strips together at the sides of the sample pad. Next, the number and types of biomarkers that can be detected in a LFA multiplex assay is limited. The use of a large amount of capture and labeled-detecting antibodies is required for detecting different types of biomarkers on a single test strip. Hence, this increased the possibility of false positivity and reduced the detection sensitivity due to non-specific binding with non-target analytes during the lateral flow. Notwithstanding, there are many LFAs manufacturers who are currently available, but they require a proper readout device for highly sensitive and quantitative analysis during clinical diagnostic testing.

For this reason, a portable detection device with high multiplexing capability and flexibility in the assay design is demanded. Paper-based device is a good approach because any design could be easily adapted to paper substrate by various fabrication techniques (Abe et al., 2008; Cassano & Fan, 2013; Dungchai et al., 2011; He et al., 2014; Lu et al., 2009b; Martinez et al., 2008b; Martinez et al., 2010b; Songjaroen et al., 2011). To further enhance the detection sensitivity of multiplex assay, the analyte can be detected in separate detection zone to avoid the problem of non-specific binding with their specific detecting labels. Besides that, the nanoparticles could be an option of detecting label because it offers distinct advantages such as allowing for easy visual colour distinction, resistance to photobleaching, and high binding efficiencies with a relatively low usage of antibody during bio-conjugation.

University of Malaya

Therefore, this Ph.D. study is aimed to develop a microfluidic paper-based device (μPAD) with multi-markers for early diagnosis and prognosis of AMI. Multiple cardiac biomarkers strategy is recommended to be a better option to ameliorate diagnostic and prognostic accuracy. The wax printing fabrication technique was employed to fabricate the μPAD. Two optical detection methods (colourimetric and surface enhanced Raman scattering (SERS) were performed for quantification analysis.

1.1 Aim and Objectives

1.1.1 Aim

The aim of this Ph.D. study is to develop an inexpensive, portable and user-friendly μPAD as a point-of-care device for early diagnosis and prognosis of AMI. Considering the fact that none of the single markers has exhibited sufficient diagnosis accuracy for AMI, a novel combination of three specific cardiac biomarkers was incorporated into the μPAD. These specific cardiac biomarkers comprised of GPBB for early diagnosis (within the first 4 hours); cTnT and CK−MB for late after symptom onset (> 6 hours) and prognosis of AMI (7−14 days).

1.1.2 Research Objectives

i. To fabricate μPAD for simultaneous multiplex detection of cardiac biomarkers ─ glycogen phosphorylase isoenzyme BB, creatine kinase MB and troponin T for early diagnosis and prognosis of AMI.
ii. To study and optimise the analytical performance of μPAD for qualitative, semi-quantitative and quantitative colourimetric detection of multiple cardiac biomarker.
iii. To study and optimise the analytical performance of μPAD for quantitative SERS detection of multiple cardiac biomarkers.

University of Malaya

iv. To compare both colourimetric and SERS detection techniques and validate the developed diagnostic tools such as phone camera, desktop scanner and Renishaw Invia Raman Microscope with Siemens Centaur XPT Immunoassay System (a standard laboratory method used at the University Malaya Medical Center) for multiple cardiac biomarkers measurements.

v. To extend the analysis on μPAD into clinical analysis with colourimetric and SERS technique for early diagnosis and prognosis of AMI.

1.2 Organisation of Thesis

This thesis is divided into five chapters; each chapter is then subdivided into sections and subsections. The arrangements of the chapters are as follow:

Chapter 1 features the introduction which mainly discusses the research motivations, aim and objectives of the study.

Chapter 2 contains the literature review which provides an overview of acute coronary syndromes, ideal cardiac biomarkers, fabrication and detection techniques, and biomedical applications for μPAD.

Chapter 3 provides the methods employed in this project. All the experimental procedures for colourimetric and SERS assays are described in detail and a flow chart summarising the entire research work is presented.

Chapter 4 contains the results and discussion. Results of colourimetric assay are discussed at section 4.1−4.2 whereas the results of SERS assay are discussed at section 4.3. The analytical performance of μPAD using diagnostic tool, i.e., Siemens Centaur XPT Immunoassay System (I), smartphone-based camera (II), desktop scanner (III) and Renishaw InVia Raman Microscope (IV) are discussed at section 4.4. Moreover,

University of Malaya

multivariate analysis (i.e. principal component analysis and partial least squares regression) for SERS assay is conferred at section 4.5.

Chapter 5 contains the conclusion and future perspectives. The main findings of the study are highlighted and suggestions for future works are made.

University of Malaya

CHAPTER 2: LITERATURE REVIEW

2.1 Acute Coronary Syndrome

Acute coronary syndrome (ACS) is an umbrella term for situations where the blood supplied to the heart muscle is suddenly blocked, which represents a spectrum of cardiac events ranging from unstable angina to MI (heart attack) (Overbaugh, 2009). The term ACS is applied to patients in when there is a suspicion or confirmation of myocardial ischemia. However, ACS is divided into three distinct clinical patterns. Two of the patterns represent different forms of MI such as ST-segment elevation myocardial infarction (STEMI) and non-ST-segment elevation myocardial infarction (NSTEMI), whereas one represents a particularly severe form of angina termed as unstable angina (UA) (Kumar & Cannon, 2009a, 2009b; Thygesen & Alpert, 2001).

The treatment algorithm for the evaluation of patients with chest pain was displayed in **Figure 2.1**. Doctor should first take a careful look at the previous medical history and conduct a physical examination on the patient with chest discomfort when the patient arrives in the emergency department complaining of chest pain. If the doctor suspects an ACS, a few other tests are usually performed such as measuring the heart's electrical activity that is associated with ECG changes (ST-elevation or depression or T-inversion) and blood tests with cardiac biomarkers which can show evidence that heart muscles are dying so as to distinguish patient of having true MI (STEMI or NSTEMI) or UA. As the ECG may show that an AMI has occurred or is in progress whereas blood tests measure the biomarkers that has released into the blood where heart muscle has been damaged by an acute MI. At the same time, the patient who is designated as non-bearers of ACS will be discharged from the emergency room with the recommendation of undergoing a follow-up exercise test (Apple et al., 2005b; Nagesh & Roy, 2010; Thygesen & Alpert, 2001).

University of Malaya

AMI are commonly known as heart attack, STEMI and NSTEMI, in which there is complete occlusion of a major coronary artery caused by atherosclerosis. The blockage of blood supply to the heart muscle has caused intense changes to take place in the heart muscle, leading to irreversible changes and death of myocardial cells. However, STEMI is a more severe type of heart attack compared to NSTEMI in which a full thickness damage of heart muscle develops. The ultimate ECG findings of STEMI are ST-elevation with Q-wave formation. Normally, the ST-elevation indicates a full thickness cardiac muscle injury; Q-wave indicates muscle necrosis; and T-wave inversion indicates muscle ischemia. For STEMI, ST-elevation and tall T-waves in the first few hours are the earliest shifts in the ECG. Within 24 hours the T-waves invert and the ST-elevation resolves; Q wave changes can occur within 24 hours or severely (Deshpande & Birnbaum, 2014; O'Gara et al., 2013).

On the other hand, NSTEMI is defined as a development of heart muscle necrosis without the ECG change of ST-elevation, resulting from partial thickness injury of heart muscles. Therefore, it is confirmed by measuring the elevation of cardiac biomarkers when the ECG changes show ST-depression or T-wave inversion (Amsterdam et al., 2014; Bertrand et al., 2000). A diagnosis of NSTEMI can be made when the ischemia is sufficiently severe to cause myocardial damage that results in the release of biomarkers of myocardial injury into the blood circulation, for example like troponin (T or I) and/or CK-MB (Al-Hadi & Fox, 2009). Moreover, UA is defined as angina pectoris, a chest pain caused by ischemia that lasts longer than 20 minutes, with no elevation in cardiac markers of myocardial necrosis, with or without ECG changes, (ST-depression or T-inversion) indicative of ischemia. The difference between NSTEMI and UA is based on the presence or absence of a rise in cardiac biomarkers level in bloodstream (Braunwald et al., 2000).

University of Malaya

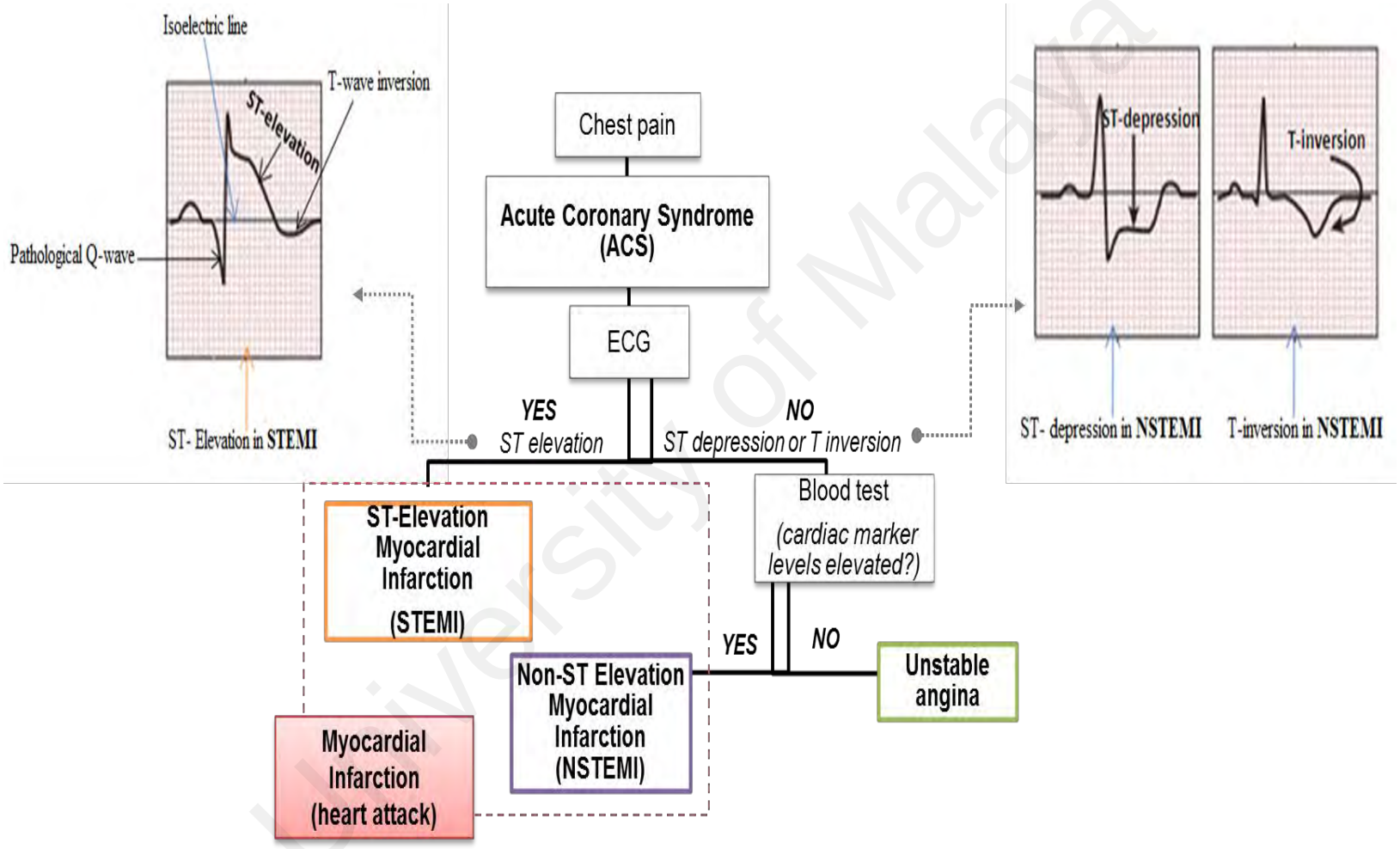

Figure 2.1: Algorithm for the evaluation of patients with chest pain.

University of Malaya

2.2 Cardiac Biomarkers

This section addresses the possible medical use of cardiac biomarkers including troponins (T and I), creatine kinase MB (CK−MB), myoglobin and glycogen phosphorylase isoenzyme BB (GPBB) for the identification of ACS patients. These biomarkers are defined as biological analytes that are detectable in the blood circulation at elevated level during damage or death of cardiac myocytes. As shown in **Figure 2.2**, the ideal characteristics of a biomarker of myocardial injury must fulfil some factors such as (i) high specificity; (ii) high sensitivity; (iii) rapid release; (iv) long half-life; (v) short turnaround time; and (vi) ability to provide valuable clinical information (Ahmad & Sharma, 2012; Kemp et al., 2004).

It should be concentrated in the myocardium and absent in non-myocardial tissues for the ideal characteristics of a cardiac marker. This gives it a high specificity for myocardial injury and reduces the false positive outcome. In contrast, it should also be elevated in myocardium but weak or undetectable in the blood in the absence of disease. This gives it a high sensitivity in order to quickly detect small quantities of releases, reducing the rate of false negative results. Once myocardial injury occurs, the biomarker should be released rapidly in the bloodstream to allow early detection of injury, while it should have a long half-life and be able to remain in circulation to provide a convenient diagnostic window for late diagnosis. In addition, the diagnostic assay must have a short turnaround time so that the test results could be obtained fast enough to influence therapy and aid doctor in decision making (de Tarso Garcia et al., 2014; Thygesen & Alpert, 2001). Overall, these biomarkers can provide an earlier evaluation of the overall patient risk, aid in identifying the suitable diagnostic and therapeutic management for ACS patients and allow for prevention of severe cardiac events.

University of Malaya

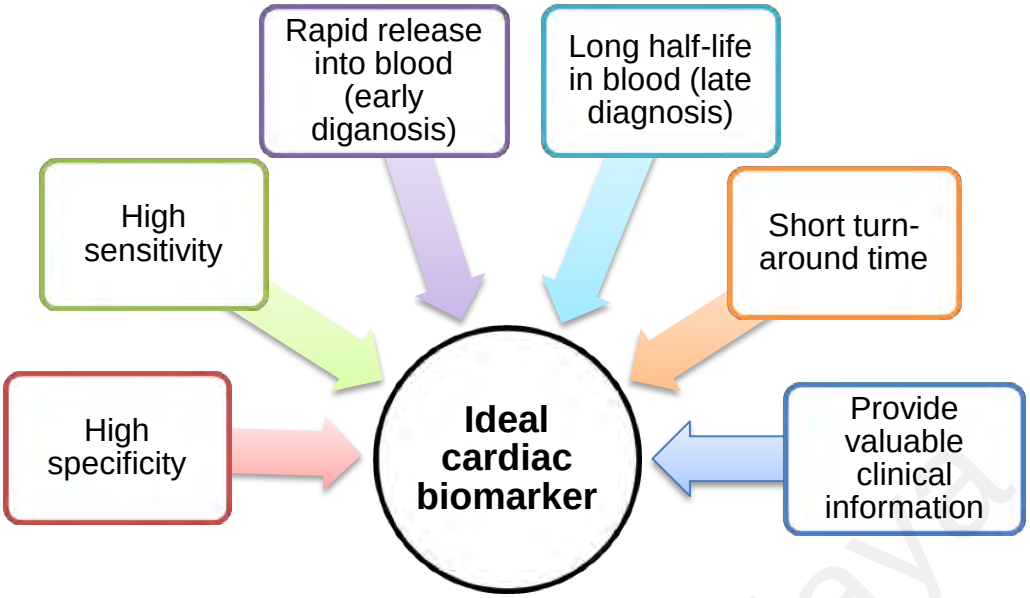

Figure 2.2: Characteristics of the ideal cardiac biomarkers for AMI diagnosis.

2.2.1 Troponin

Troponin complex is made up of three subunits—T (TnT), I (TnI), and C (TnC) which together control calcium mediated interaction of actin and myosin which leads to the contraction and relaxation of striated muscle (**Figure 2.3**) (de Lemos, 2013). A separate gene encodes each troponin subunit. TnI and TnT exist as specific cardiac muscle isoform, with differing amino acid sequences and immunological activity. The European Society of Cardiology and the American College of Cardiology Consensus group recommended the diagnostic usefulness of troponins as gold standard biomarkers for AMI due to its superior sensitivity and specificity for myocardial damage (Dickstein, 2008; Hamm et al., 2011). Troponin subunits are detectable in the circulation where the damage to the cardiac myocyte leading to the release of free cytoplasmic troponin, accounts for 3% to 5% of cTnI and 6% to 8% of cTnT levels (Bhayana & Henderson, 1995; Wu & Feng, 1998).

University of Malaya

Myocardial injury typically requires 2─4 hours to occur in the setting of ischemia hence they can only be detected at least 4─6 hours after AMI onset. Consequently, troponins are detectable only after this latency period following the onset of injury. Furthermore, serial measurements are recommended to be drawn at presentation and again after 6─9 hours later as the earlier blood samples are likely to be negative (Daubert & Jeremias, 2010; de Tarso Garcia et al., 2014; MacRae et al., 2006). It remains elevated for up to days (4–7 days for cTnI and 10–14 days for cTnT) following the onset of infarction (Jaffe et al., 2006). Although troponin elevation persists for days, troponins are unable to yield early diagnosis (< 6 hours after symptoms onset) as it is unable to detect myocardial ischemia in the absence of injury. Despite that, it also emerged as a powerful predictor of prognosis in patients with ACS but it limits the diagnosis of re-infarction (Nagesh & Roy, 2010). Also, it might have found elevation of troponins in chronic renal failure patients without significant myocardial damage (Diris et al., 2004; Freda et al., 2002). However, troponins are more specific and sensitive than other traditional cardiac enzymes, such as creatine kinase (CK) and its isoenzyme MB (CK−MB) and myoglobin. For the analytical performance for troponin assays, the optimal precision of coefficient variation at a 99th percentile cut-off point should be ≤ 10% (Apple et al., 2005a; Panteghini et al., 2004).

University of Malaya

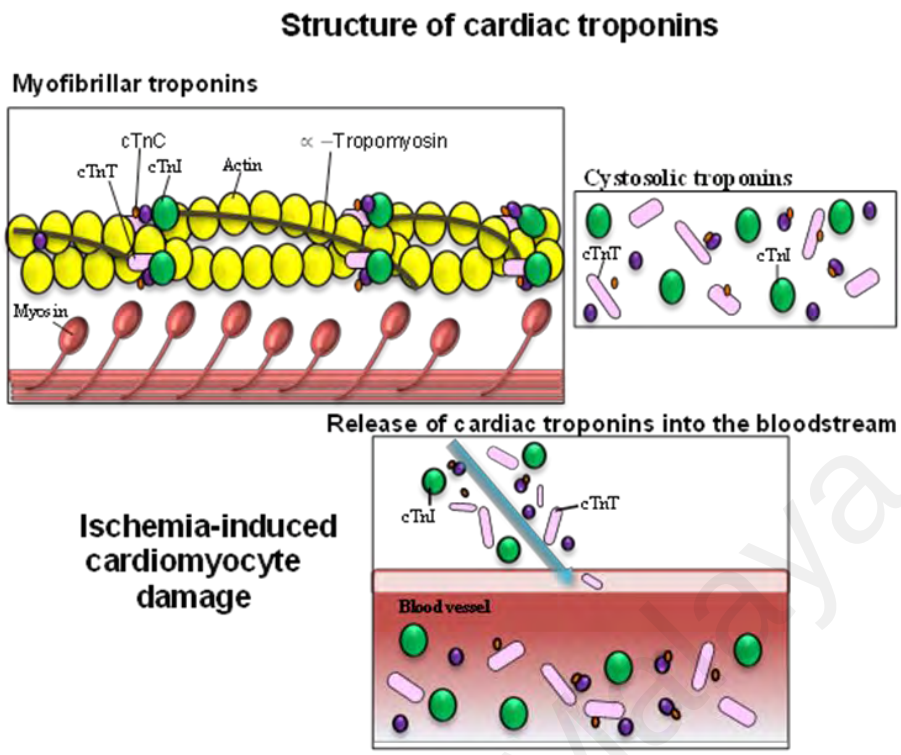

Figure 2.3: Release of cardiac troponins into bloodstream following ischemic induced myocardial injury. Adapted from de Lemos (2013).

2.2.2 Creatine Kinase−MB

The best alternative biomarker for diagnosis of myocardial injury is CK−MB mass assay when a troponins assay is not available. Creatine Kinase (CK) isoenzymes is made up by two dimer — B and M. CK−BB is mainly found in the brain; whereas CK−MM is found in skeletal muscle and CK–MB found in the cardiac and skeletal muscles. CK–MB is a CK isoenzyme which is predominantly found in the myocardium and its elevation occurs 4─6 hours after the injury, reaching peak serum concentration after 12─24 hours and returning to baseline after 2─3 days. CK−MB mass assay is used for the diagnosis of the AMI by measuring the protein mass in serum or plasma using specific antibodies against the M, B or MB subunits. The reference ranges for CK−MB mass is 5─10 ng mL^{-1} (Al-Hadi & Fox, 2009; Alpert et al., 2000; Kemp et al., 2004). However, CK−MB is more specific than myoglobin, but it is less sensitive (as similar to troponins) in the first 6 hours after chest pain onset for early diagnosis of AMI. Hence,

the sensitivity of CK−MB mass for AMI is only 50% when it is measured early at the time of presentation. Besides that, CK−MB also presents about 1%─3% in skeletal muscles and a small fraction in the muscle of the urinary bladder, which then leads to the rise in CK−MB level in patients with trauma and renal failure (Bozbas et al., 2006; Daubert & Jeremias, 2010; Odum & Wakwe, 2017).

2.2.3 Glycogen Phosphorylase Isoenzyme BB

Glycogen phosphorylase (GP) is a glycolytic enzyme that plays an important role in regulating carbohydrate metabolism by mobilisation of glycogen. GP isoenzyme is composed of two identical subunits such as BB (brain and heart); MM (skeletal muscle); and LL (liver). In a human heart, the isoenzyme BB and MM found but GPBB is the predominant isoenzyme in myocardium. GPMM is only contained in the skeletal muscle whereas GPLL is the predominant isoenzyme in the human liver. GPBB is converted from a structurally bound form to a soluble form and is free to move around in the cytoplasm after glycogenolysis with the onset of tissue hypoxia, and then to diffuse out the cell through the damaged cell membrane. Its molecular weight as a monomer is approximately 94 kD. GPBB was found to be a sensitive marker for the detection of ischemic myocardial damage as it is detectable at the first 4 hours after the onset and peaks of chest pain before CK−MB and cTnT. As it increases between 2─4 hours after the onset of chest pain, then peaks at 6─20 hours after chest pain onset; it returns to normal within 1 to 2 days of damage occurring (Apple et al., 2005b; Mair et al., 1994; Rabitzsch et al., 1995).

2.2.4 Myoglobin

Myoglobin is a small globular oxygen-carrying protein found in the heart and striated skeletal muscle. Its concentration is elevated within 1─3 hours in the setting of

University of Malaya

myocardial injury, which usually peaks within 6─9 hours, and may become normal in 2─3 days (Kemp et al., 2004). The National Academy of Clinical Biochemistry, and the Joint European Society of Cardiology (ESC)/ American College of Cardiology (ACC) Committee for the Redefinition of myocardial infarction both have recommended myoglobin as early markers for myocardial damage within 3 hours after the onset of chest pain because of its relatively low molecular weight (17 kDa) and high cytoplasmic content (Alpert et al., 2000). The reference range of myoglobin is about 20─80 ng mL^{-1}. However, the myoglobin was also reported as a non-cardiac specific biomarker for myocardial injury as the amino acid sequence of myoglobin is identical in both skeletal and cardiac muscle. Hence, its specificity is compromised in the presence of skeletal muscle damage (De Winter et al., 1995; Kemp et al., 2004). Additionally, elevated plasma myoglobin concentration is also found in patients with renal insufficiency which resulted from failure of clearance of myoglobin from the circulation (Al-Hadi & Fox, 2009; Bozbas et al., 2006; Kemp et al., 2004).

By definition, the elevation of one or more of the mentioned markers is detected in all ACS patients at various time courses (**Table 2.1**). In comparison to other cardiac biomarkers, troponins (T or I) with its high specificity and sensitivity are the preferred biomarkers for the diagnosis of a myocardial injury 6 hours after the onset of symptoms. Besides that, troponins also can be a useful prognostic indicator for patients with ACS as it remains elevated in the blood up to several days. Furthermore, GPBB has also been proposed to be an early cardiac biomarker for diagnosis of ischemia myocardial injury at the first 4 hours after the onset of chest pain. To date, current clinical diagnosis for AMI depends on troponins, CK−MB and myoglobin. However, many other potential biomarkers have arisen and are under intensive research.

University of Malaya

Table 2.1: Time of release of biomarkers during myocardial infarction (Cubranic et al., 2012; Kemp et al., 2004; Mohammed & Desmulliez, 2011).

Cardiac Biomarkers	Molecular weight	Initial elevation	Time to peak	Return to normal	Advantages	Limitation
Troponin T (cTnT)	37 kDa	• 4 to 6 hours	• 12 to 24 hours	• 7 to 10 days	• High specificity and sensitivity for myocardial injury. • Useful prognostic indicator in patients with ACS. • Only one source currently marketed with well-established standards in terms of reference range, detection limits, and clinical cut-off concentrations.	• Poor sensitivity to diagnose ischemia in the absence of infraction. • Require specimen collection at patient presentation, 6−9 hours later and earlier results (< 6 hours) are negative. • Elevated concentration of cTnT in patients with renal failure.
Troponin I (cTnI)	26 kDa	• 4 to 6 hours	• 12 to 24 hours	• 6 to 8 days	• High specificity and sensitivity for myocardial injury. • Useful prognostic indicator in patients with ACS.	• Poor sensitivity to diagnose ischemia in the absence of infraction. • Require specimen collection at patient presentation, 6−9 hours later and earlier results (< 6 hours) are negative.
Creatine Kinase-MB (CK–MB)	85 kDa	• 4 to 6 hours	• 12 to 24 hours	• 24 to 48 hours	• Modest sensitivity and specificity for ACS. • Alternative marker for myocardial injury if troponin is not available. • Ability to detect early re-infarction.	• Low sensitivity during very early MI (< 6 hours after symptoms onset) or later after symptom onset (> 36 hours). • False positive elevation occurs in trauma, heavy exertion and myopathies. • Less sensitive than Troponin (T and I) as presence in skeletal muscle injury.

University of Malaya

Table 2.1, continued

Cardiac Biomarkers	Molecular weight	Initial elevation	Time to peak	Return to normal	Advantages	Limitation
Glycogen phosphorylase isoenzyme BB (GPBB)	94 kDa	• 2 to 4 hours	• 8 to 12 hours	• 24 to 36 hours	• Sensitive early markers for myocardial ischemia and injury.	• Increased GPBB in patients with trauma or significant damage to central nervous system.
Myoglobin	17 kDa	• 1 to 3 hours	• 6 to 12 hours	• 24 to 48 hours	• Earliest markers for myocardial injury.	• Non-specific markers for myocardial injury. • Limited specificity for myocardial injury in patients with renal insufficiency and skeletal muscle trauma. • The specificity of myoglobin measurement is increased when combined with other diagnostic methods like ECG or more specific cardiac markers like CK−MB and troponins.

University of Malaya

2.3 Fabrication Techniques of Microfluidic Paper-Based Analytical Device

Various fabrication techniques have been developed for the design of two dimensional (2D) and three dimensional (3D) μPADs such as photolithography, polydimethylsiloxane (PDMS) plotting, inkjet printing, plasma etching, wax printing, flexographic printing, cutting, stamping and origami. Along with the number of fabrication techniques utilised, there are a wide variety of hydrophobic substances available (e.g., photoresist, polymer or wax) for creating fluidic channel network on hydrophilic paper, each with its own advantages and disadvantages. The comparison of the fabrication techniques of μPAD was detailed in **Table 2.2**. Also, there are different types of paper substrates, such as filter paper, chromatography paper, glossy paper which can be used for μPAD fabrication because of its specific capabilities. The choice of the fabrication is determined by factors which include cost, fabrication speed, ideal material substrate and accessibility of inexpensive technologies and equipment, based on respective application required (Fiorini & Chiu, 2005).

2.3.1 Photolithography

In 2007, Whitesides and his team first successfully developed a tree pattern design in cellulose paper as microfluidic platform using photolithography technique (**Figure 2.4**), for colourimetric detection of glucose and BSA protein in artificial urine (Martinez et al., 2007). This novel development led to the rise of a new research of patterning paper as an inexpensive, portable microfluidic platform for biological, chemical and medical applications (Martinez et al., 2008a). In the lithography process, the chromatography paper was immersed in a negative photoresist (SU-8 2010) solution and then been baked at 95°C for 5 minutes to remove the cyclopentanone in the SU-8 formula. The paper was then exposed to ultraviolet (UV) light through a photomask to create hydrophilic–hydrophobic areas using a mask aligner. After UV exposure, the paper was baked for a

second time at 95°C for 5 minutes to cross-link the exposed portion of resist. The un-polymerised photoresist was removed by soaking in propylene glycol mono-methyl ether acetate (PGMEA) and then the pattern was rinsed with acetone and isopropyl alcohol. This technique was able to create high-resolution channels on the paper, but the complex fabrication process requires a lithography instrument, expensive photoresist, and a clean room. It also requires an extra washing step to remove un-crosslinked polymer on paper substrate. Additional drawbacks of this method are the risks of damage to the flexibility of paper by bending and folding after exposure to organic solvents. Herein, lots of improved methods are proposed to reduce the fabrication cost and increase its flexibility. Some hydrophobic materials such as epoxy negative photoresist (Martinez et al., 2008c), SC photoresist (Carrilho et al., 2009b) and octadecyltrichlorosilane (OTS) (He et al., 2013) are used to substitute SU-8 2010 photoresist to reduce cost. Likewise, UV lamp and a hotplate are also found to be an alternative way to solidify photoresist on the paper to avoid use of costly lithography machine.

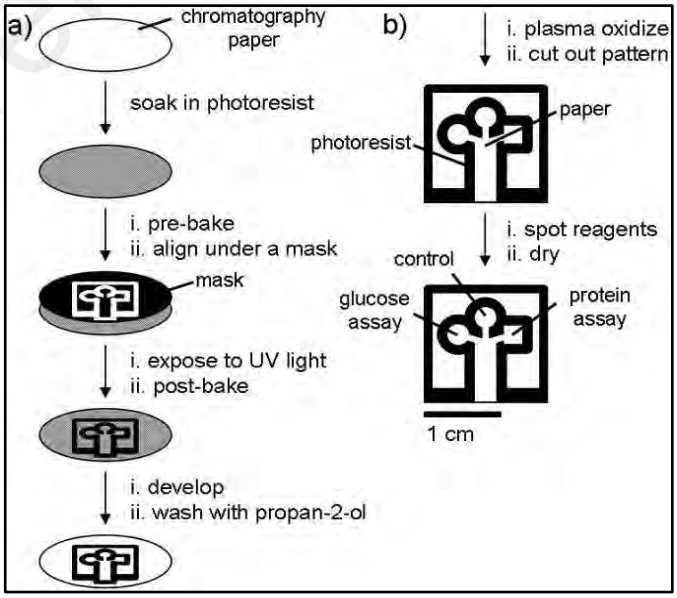

Figure 2.4: Photolithography procedure for SU8-photoresist patterning onto paper substrate. Reprinted with permission from Martinez et al. (2007). Copyright 2007 WILEY - VCH Verlag GmbH & Co. KGaA, Weinheim.

2.3.2 Polydimethylsiloxane Plotting

Bruzewicz et al. (2008) presented polydimethylsiloxane (PDMS) plotting with a customised plotter to generate hydrophobic channels on filter paper (**Figure 2.5**). The customised plotter is filled with hydrophobic materials — PDMS dissolved in hexanes was used as a drawing pen for the rapid hand-held prototyping based on paper (Bruzewicz et al., 2008). The solid hydrophobic barrier was formed on a paper after 1 hour curing. The advantage of PDMS is found to be much cheaper and elastic than photoresist; the paper is more flexible and could be folded after curing. However, the dispersion of PDMS is hard to be well controlled during drawing because of low surface tension of solvent used. Therefore, this method might just be recommended for prototype fabrication in laboratory but not for mass production due to low reproducible as it requires long duration for PDMS curing.

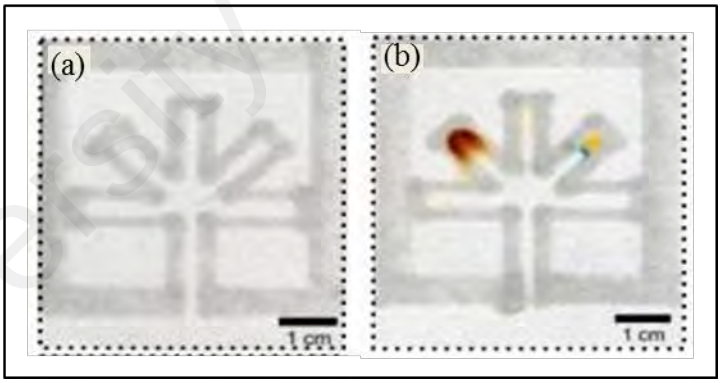

Figure 2.5: Polydimethylsiloxane plotting technique by printing hydrophobic PDMS to define hydrophilic channels on paper. Reprinted with permission from Bruzewicz et al. (2008). Copyright 2008, American Chemical Society.

2.3.3 Inkjet Printing

To enhance the reproducibility in patterning µPADs, an automotive and reproducible inkjet printing technique (**Figure 2.6)** was introduced by Abe et al. (2008), to design hydrophilic channels and distribute chemical reagents to the test zones by printing. This

University of Malaya

method offers advantages of using several print heads to allow direct patterning on paper substrates and the parallel dispensing of multiple chemical reagents (Abe et al., 2008). For patterning hydrophilic channel, the filter paper was first immersed in 1% solution of polystyrene in toluene for 2 hours prior; then etched the channels by printing toluene to dissolve hydrophobic polymer on the paper with multiple cycle of toluene printing. In addition, different types of the chemical reagents can be deposited on the paper at one time with uniform amount by multiple printing cycles. The weakness of inkjet printing is that it requires several printing cycles in etching hydrophilic pattern and reagents distribution in paper (Li et al., 2010a). However, the colour changes when sensing the area lacks of colour uniformity thus making it difficult in visual judgement. Hence, more fabrication time is needed due to the increased printing cycles required to enhance colour intensity.

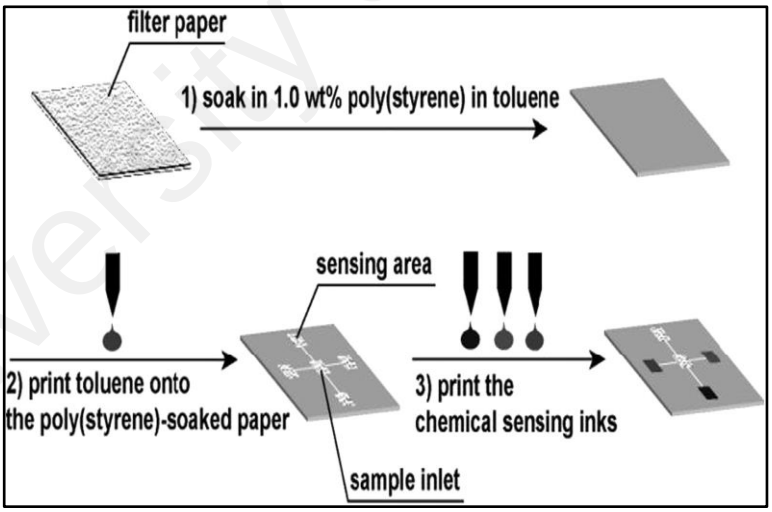

Figure 2.6: Fabrication process of microfluidic multi-analyte chemical sensing paper by using the inkjet-printed technique. Reprinted with permission from Abe et al. (2008). Copyright 2008, American Chemical Society.

University of Malaya

2.3.4 Plasma Etching

Plasma etching (**Figure 2.7**) is used to define the hydrophilic channels by removing the coated hydrophobic material (alkyl ketene dimer, AKD) on a paper using a vacuum plasma reactor (Li et al., 2008; Li et al., 2010a). This fabrication process is simpler and more rapid than inkjet printing. It also retains the original flexibility of the paper and leaves no visible channel marks on the paper. In addition, this chemical modification technique results to proper solvent resistance since the chemical agents are effectively coupled with hydroxyl groups on the cellulose fibre in a chromatography paper through covalent bonding. However, this technique requires a longer heat treatment for curing and the defined channel on paper is visible only after the fluid is applied to the paper due to a colourless hydrophobic material was used.

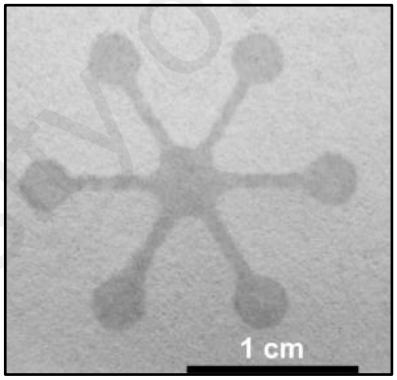

Figure 2.7: A μPAD patterned with the AKD and exposed to plasma treatment. Reprinted with permission from Li et al. (2010b). Copyright 2009, Springer-Verlag.

2.3.5 Wax Printing and Wax Dipping

Fabrication with wax is to allow wax diffusion to penetrate throughout the paper depth to form the barrier for microfluidic channels (**Figure 2.8**). This technique gives a cheaper and more convenient alternative than conventional patterning of photoresist SU-8 or PDMS onto the paper substrate. Wax printing is a simple and inexpensive technique for fabricating μPAD with a wax printer and a hot plate or oven (Carrilho et

University of Malaya

al., 2009a; Lu et al., 2009a; Lu et al., 2009b). This fabrication process only requires 2 steps ─ printing and heating, which takes about 5 to 10 minutes to complete. However, the resolution of wax priming on paper is coarse and not sharp. The spreading of melted wax could alter the intended size of the channel and block certain parts of the hydrophilic channel at too high melting temperature. The blockage restricts the fluid flow on the desired region of µPADs during an assay.

Furthermore, wax dipping can also be used to pattern the hydrophobic–hydrophilic area onto the paper where a wax printer is unavailable (Songjaroen et al., 2012; Songjaroen et al., 2011). For wax dipping, it only requires a hot plate and molten beeswax for less than 1 minute's fabrication process. The paper is dipped into an assembled iron mold (produced using a magnet, a glass slide, paper and an iron mold) with the molten beeswax to create a hydrophilic channel. The penetration of molten beeswax into the paper is reportedly well controlled by melting time and temperature; as well the resolution is not coarse compared to wax printing.

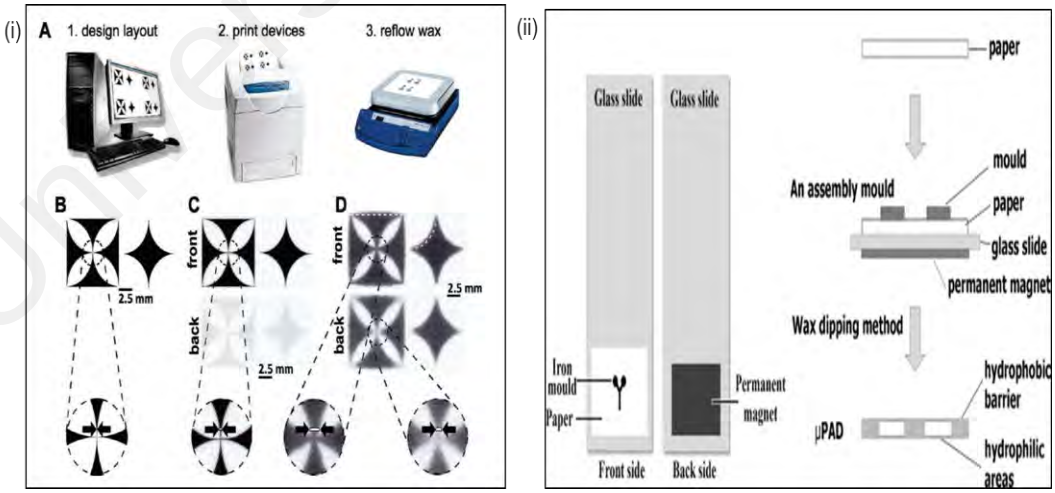

Figure 2.8: Fabrication process of wax printing and dipping method. (i) Patterning hydrophobic barriers in paper by wax printing using a wax printer, is reprinted with permission from Carrilho et al. (2009a). Copyright 2009, American Chemical Society. (ii) Patterning paper by wax dipping using an assembled mold, is reprinted with permission from Songjaroen et al. (2011). Copyright 2011, Elsevier B.V.

University of Malaya

2.3.6 Flexographic Printing

Flexographic printing (**Figure 2.9**) is a direct roll-to-roll production of patterned polystyrene (hydrophobic material) boundaries onto a paper (Olkkonen et al., 2010). This method is advantageous in fabricating thinner channel (about 1 mm) which reduces the consumptions of sample volume required for multi-analyte analysis. Moreover, the pressure between the plate roll and the impression roll, including the viscosity of the ink must be optimised well to obtain sufficient ink penetration into the paper during patterning process. However, high viscosity ink decreases the penetration due to the slower movement of ink as the polystyrene used in this method acts as hydrophobic agent and render the paper surface to be only hydrophobic, thus the applied liquid (sample/reagent) with lower surface tension can escape from the channel easily.

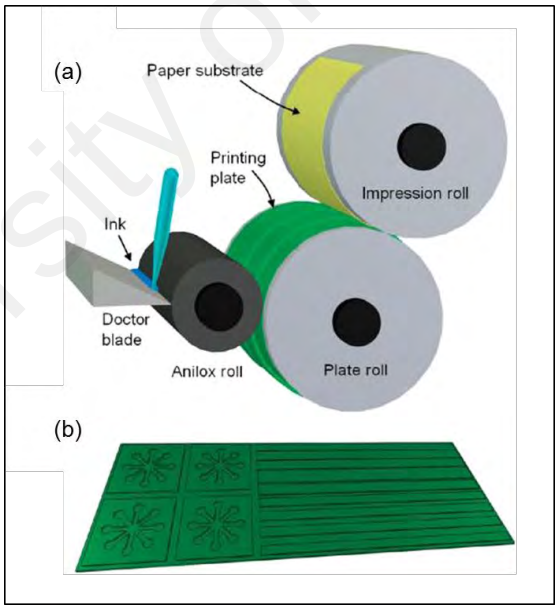

Figure 2.9: Flexographic printing of polystyrene to define hydrophobic region on paper substrate. Reprinted with permission from Olkkonen et al. (2010). Copyright 2010, American Chemical Society.

University of Malaya

2.3.7 Cutting

Cutting techniques (**Figure 2.10**) include manual cutting (Wang et al., 2010), computer-controlled X-Y knife plotter (Fenton et al., 2008), laser cutting (Nie et al., 2013), and craft-cutting and lamination (Cassano & Fan, 2013). To omit the usage of chemical (e.g., hydrophobic agent) during fabrication, a simple manual cutting method was proposed by Wang et al. (2010). Nevertheless, this method can cause irregular multiple branches to form by careless cutting when performed manually. In a more defined approach, computer controlled X−Y knife plotter is used (Fenton et al., 2008). The knife plotter programmed by a computer, functions as a pen and rotates freely on a turret to cut multiple shapes on a paper sheet. Thus, the operator error is reduced and mass production can be assured.

In addition, Nie et al. (2013) also presented one-step laser cutting technique that uses a laser to cut the paper according to the pattern designed with computer software. Hence, it can provide better resolution than a knife plotter. However, the critical parameter for channel patterning is the applied current and cutting rate of the laser, because the heat produced by the laser will burn the paper through its thickness when the pre-designed width is too narrow. On the other hand, craft-cutting and lamination techniques are useful for preventing leakage which requires heat for lamination as the craft cutter is used to cut for generating a physical boundary of paper and then laminate (Cassano & Fan, 2013). For an exact design of μPAD patterns, specific computer software is required for designing pattern before proceeding to the cutting process, in order to prevent any problems involved in manual cutting.

University of Malaya

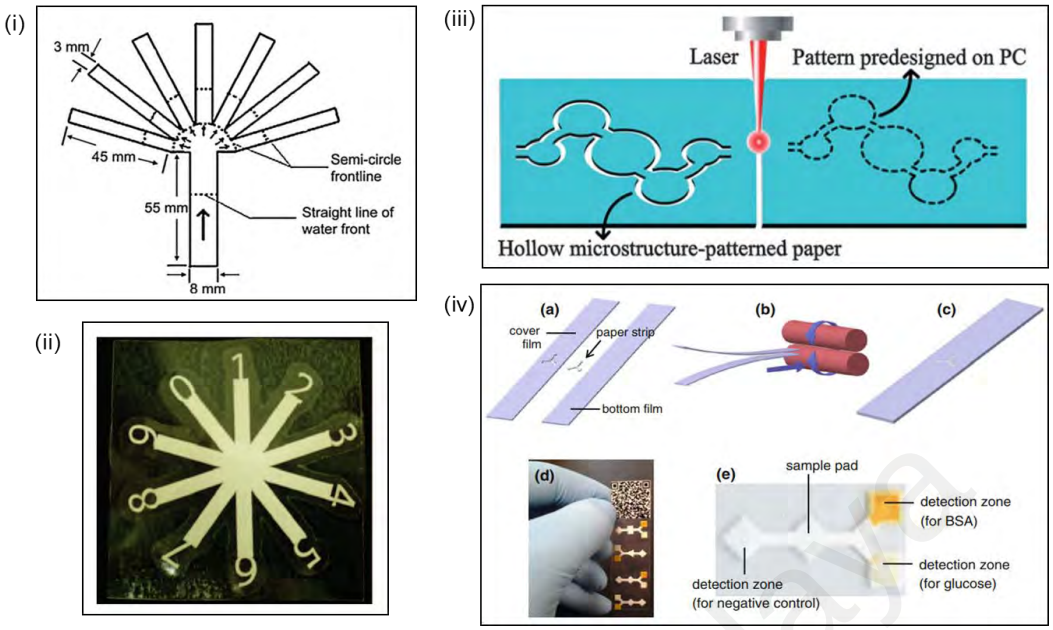

Figure 2.10: Cutting techniques. (i) Paper device is prepared by manually cutting, is reprinted with permission from Wang et al. (2010). Copyright 2010 Elsevier B.V. (ii) Paper device is cut by using the knife plotter. Reprinted with permission from Fenton et al. (2008). Copyright 2008, American Chemical Society. (iii) µPAD is fabricated by one-step laser cutting method with hollow microstructures as hydrophobic barriers. Reprinted with permission from Nie et al. (2013). Copyright 2013, The Royal Society of Chemistry. (iv) Laminated paper-based analytical device is fabricated by simple craft-cutting and lamination. Reprinted with permission from Cassano and Fan (2013) . Copyright 2013, Springer-Verlag Berlin Heidelberg.

2.3.8 Stamping

Stamping (**Figure 2.11**) such as handheld stamping (de Tarso Garcia et al., 2014) and flash foam stamp lithography (He et al., 2014) are also introduced for fabricating µPAD. In handheld stamping, paraffin is used as the hydrophobic material with a metal stamp; heat pressing is required to impregnate the melted paraffin on the surface of a filter paper. This method is simple and rapid, but manually sampling and mistakes in sampling time could affect the pattern resolution on paper.

In flash foam stamp lithography, two-step process involves the fabrication of the flash foam stamp and requires stamping with polymer (He et al., 2014). To fabricate the flash foam stamp, mask and flash foam are exposed together to an intense UV light to transfer the pattern from the mask on to the flash foam. PDMS ink is then stamped on

the paper as the hydrophobic barrier to define the channel. With this method, the expensive flash stamp machine is required for fabricating the flash foam stamp.

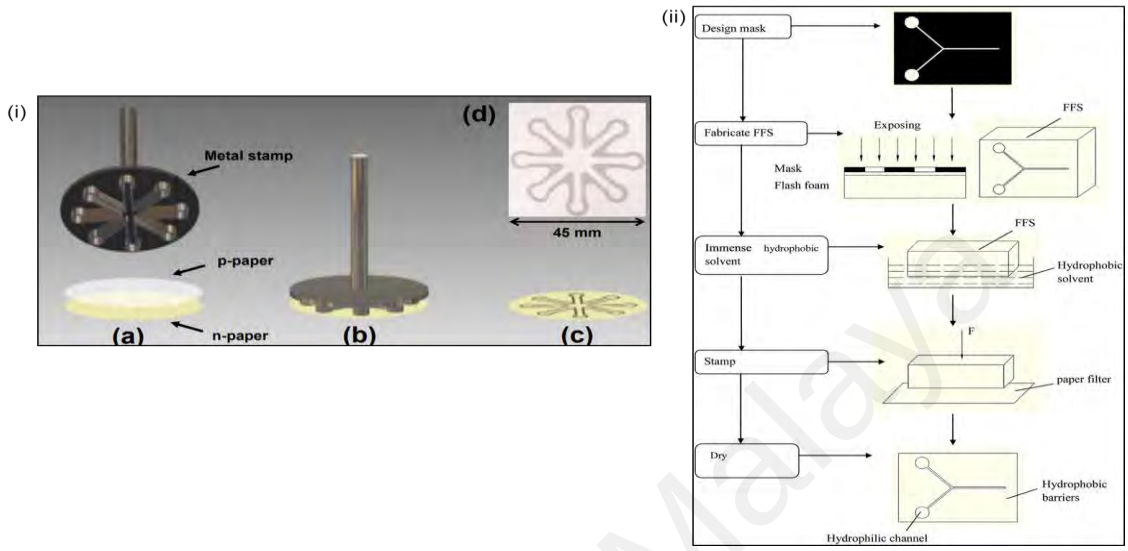

Figure 2.11: Stamping techniques. (i) Fabrication process of µPADs based on handheld stamping. Reprinted with permission from de Tarso Garcia et al. (2014). Copyright 2014, The Royal Society of Chemistry. (ii) Fabrication process of µPAD using flash foam stamp lithograph. Reprinted with permission from He et al. (2014). Copyright 2014, The Royal Society of Chemistry.

2.3.9 Origami

By using the 3D origami techniques (**Figure 2.12**), the µPAD can be created by folding it into a 3D shape with multiple layers. 3D-µPAD is patterned by photolithography and then stacked the layers of patterned papers such as sample inlet and zone of spot detection with double-sided adhesive tape based on the origami principle for multiplex detection (Liu et al., 2011; Martinez et al., 2010a; Martinez et al., 2008b). Hence, it can deliver samples from a single inlet on the top layer of a device into the reaction zones at the bottom layer. The holes are punched in the tape using a laser cutter, and the resulting holes that connect the adjacent layers of the paper are then filled with cellulose powder to allow fluid distribution in complex assays. The fluid may wick between the paper layers if cellulose power is not used. However, the doubled-

University of Malaya

sided tape was used to attach the paper layers in contact, which may cause contamination of patterned paper and non-specific absorption of reagents and analytes from the adjacent paper surface during fluid transportation from layer by layer.

To avoid the use of cellulose powder and doubled-sided, Liu and Crooks (2011) developed a 3D-µPAD by using photolithography and origami technique. The µPAD can be simply folded into multiple layers without using a tape as in previous designs. Moreover, avoiding tape also speeds the assembly of the device and eliminates the need for laser cutting. Like photolithography with origami, Sechi et al. (2013) also proposed wax printing with origami folding technique to fabricate 3D-µPAD. As wax printing only requires a wax printer is a simple and inexpensive technique compared to photolithography that requires costly reagent and a clean room. Moreover, the layer in the 3D-µPAD can be made using different papers and the multiple functionalities provided by the different types of paper can therefore be combined into a single device (Martinez et al., 2010b; Xia et al., 2016).

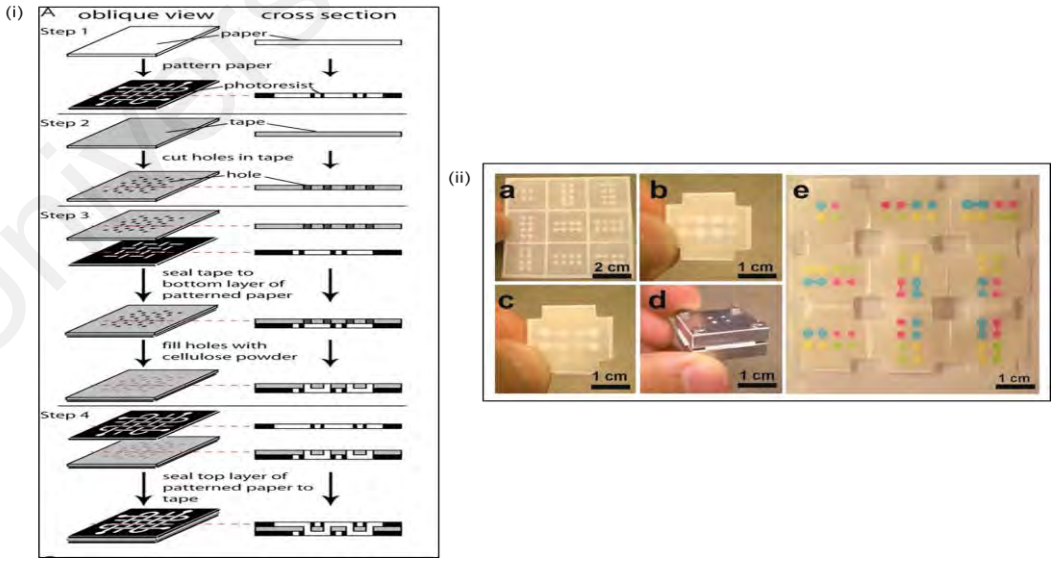

Figure 2.12: Fabrication of 3D-µPAD for multiplex detection based on the principles of origami. (i) Layers of patterned papers are stacked with double-sided adhesive tape based on origami principle. Reprinted with permission from Martinez et al. (2008b). Copyright 2008, The National Academy of Sciences of the USA. (ii) The µPAD is simply folded into multiple layers without using a tape. Reprinted with permission from Liu and Crooks (2011). Copyright 2011, American Chemical Society.

Table 2.2: Various fabrication techniques and pattern for 2D-and 3D-µPAD.

Fabrication technique and material used	Advantages	Disadvantages	Limitations	Reference
a) Photolithography with su-8 photoresist (2D)	• Provides sharp channel resolution.	• Complex fabrication step (Baking and UV exposure is required). • High cost for mass production. • Flexibility of paper can be damaged when exposed to organic solvent and photoresist because the paper hardens after heat curing. • Easily damaged by bending and folding.	• Requires expensive photoresist, lithography equipment, and a clean room.	(Carrilho et al., 2009b; Martinez et al., 2007; Martinez et al., 2008c)
b) PDMS plotting	• Can be folded without destroying the channel or flexibility of the paper.	• High cost for mass production. • Reduction in the resolution of the channel due to slight lateral spread of PDMS. • Solution with higher viscosity does not penetrate the paper.	• Requires a modified plotter. • Amount of PDMS used is difficult to control due to continuous line drawing.	(Bruzewicz et al., 2008)
c) Inkjet printing with a solution of polystyrene in toluene	• Low cost in fabrication. • No risk of substrate damage. • Offers control of the amount of liquid deposition.	• Complex fabrication step (multiple printing step). • Reduction in the reproducibility of device fabrication because multiple printing steps are required to align the microfluidic paper-based device.	• Requires an inkjet printer to deposit reagents in the test zones.	(Abe et al., 2008)

University of Malaya

Table 2.2, continued.

Fabrication technique and material used	Advantages	Disadvantages	Limitations	Reference
d) Plasma etching with an alkyl ketene dimer (AKD)—heptane solution	• Removes hydrophobic paper coating via plasma oxidation. • Retains original flexibility and leaves no visible mark on the paper.	• Over-etching may cause the treated pattern to be slightly bigger than the metal mask.	• Requires a customised metal mask and vacuum plasma reactor for patterning. • Heat treatment for curing AKD is required.	(Li et al., 2008; Li et al., 2010a)
e) Wax printing with a wax printer	• Wax is cheaper material than photoresist and PDMS. • Simple fabrication step and mass fabrication. • Requires only a wax printer.	• Channel resolution is reduced due to lateral spreading.	• Unstable at high melting temperature (>200°C).	(Carrilho et al., 2009a; Lu et al., 2009a; Lu et al., 2009b)
f) Wax dipping with white beeswax	• Native paper surface is preserved. • No requirement for expensive instrument or exposure organic solvent.	• Penetration of wax into the paper can be affected by melting temperature and dipping duration.	• Requires an iron mold and permanent magnet in the patterning step. • High temperature and longer dipping time can boil the paper and spread excessive wax onto the paper substrate.	(Songjaroen et al., 2012; Songjaroen et al., 2011)

University of Malaya

Table 2.2, continued.

Fabrication technique and material used	Advantages	Disadvantages	Limitations	Reference
g) Flexographic printing with a solution of polystyrene in xylene	• Forms very thin fluidic channels on paper	• Low-surface-tension liquids (reagent/sample) can escape from a channel • High viscosity of ink may decrease penetration owing to slower ink movement	• A unit of RK Flexiproof 100 is required for printing • Requires pressure for the plate roll and impression roll during printing to ensure sufficient ink penetration into paper	(Olkkonen et al., 2010)
h) Cutting with computer controlled X-Y knife plotter	• No chemicals are needed in the fabrication process • The knife plotter can be programmed to cut complex shapes	• Requires specific software to design the pattern of µPADs (e.g., AutoCAD)	• Requires a Graphtec FC7000-100 plotter for patterning	(Fenton et al., 2008)
i) Laser cutting	• One step laser cutting	• The heat produced by the laser will burn the paper across the thickness of paper if predesigned width of channel is too narrow (e.g., 0.2−0.6 mm)	• Requires a mini type CO_2 laser cutting/engraving machine	(Nie et al., 2013)

University of Malaya

Table 2.2, continued.

Fabrication technique and material used	Advantages	Disadvantages	Limitations	Reference
j) Craft-cutting and lamination	• No viscous adhesive material is required • Physical edge of laminated strip can stop the excessive absorption of sample/ reagent	• Heat is required to fuse a lamination film with paper strip	• Requires a craft cutter and a laminator	(Cassano & Fan, 2013)
k) Handheld stamping on chemically modified paper	• Paraffin is used as the hydrophobic material	• Low reproducibility due to manually stamping in deviation of stamping time. • Pressure is required for thermal transfer paraffin on a filter paper surface	• Requires a metal stamp for stamping	(de Tarso Garcia et al., 2014)
l) Flash foam stamp lithography (FFSL)	• Two step for fabrication • Require no toxic substances (e.g., PDMS as stamping ink)	• Require UV exposure for fabricating FFS stamping	• Requires a flash stamp machine for FFS fabrication	(He et al., 2014)
m) Photolithography with photoresist (3D)	• Consists of multiple detection zones and a sample inlet	• Requires doubled-sided tape to attach the paper layers together	• Requires cellulose powder to fill the holes between adjacent layers of paper	(Liu et al., 2011; Martinez et al., 2010a; Martinez et al., 2008b)

University of Malaya

Table 2.2, continued.

Fabrication technique and material used	Advantages	Disadvantages	Limitations	Reference
n) Photolithography with photoresist (3D) and simple paper folding (origami)	• Does not require adhesive tape and is a powder-free device • Device is unfolded to read the results on the paper layers	• Requires an aluminum housing to support the 3D paper microfluidic system	• Requires an additional photolithographic patterning step according to the desired number of layers	(Liu & Crooks, 2011)
o) Wax printing (3D) with origami	• Requires a wax printer only • Allows combination assay of several analyte	• Heat is required for wax melting • Channel resolution is reduced due to lateral spreading	• Unstable at high melting temperature (>200ºC)	(Scida et al., 2013; Sechi et al., 2013)

University of Malaya

2.4 Detection Methods of Microfluidic Paper-Based Analytical Device

Several detection methods such as colourimetric, electrochemical, electrochemiluminescence and surface-enhanced Raman scattering (SERS) have been successfully applied to µPAD for health diagnostics. The comparison of the detection methods of µPAD was detailed in **Table 2.3**.

2.4.1 Colourimetric Detection

Among all detection methods, colourimetric method based on the detectable colour reaction between analytes and colourimetric reagent (e.g., enzymes, acid–base indicators or dyes), is the most widely used with µPAD as they are simple and easy-to-use. For colourimetric assay, the chemical reagent was spotted in the detection zones and prepared for chemical reaction to take place with the target analyte in the sample. After the reaction occurs, the colour change in the detection zone can be visualised with the naked eye or with a reflectance detector, as presented in **Figure 2.13** (Lopez-Ruiz et al., 2014; Martinez et al., 2008a; Martinez et al., 2010b).

The concentration of an analyte can be determined qualitatively and semi-quantitatively via colourimetry using only the naked eye. For quantitative analysis by µPADs based on colourimetry requires no special apparatus as it only needs a reflectance detector (e.g., digital camera, smartphone or scanner) to capture images and a computer with image software for image processing (Martinez et al., 2008a). Then the intensity is converted to a number of pixel based on RGB (red, green, and blue) colour or grayscale for colourimetric image analysis (Jalal et al., 2017; Kaneta et al., 2019).

A calibration plot can be generated based on the obtained values which can then be used for any quantitative analyte measurement. The combination of µPAD and image analysis is a suitable technique for point of care testing and applications in resource-

University of Malaya

limited settings. However, the major drawback of colourimetric detection is low detection sensitivity as the colour intensity data obtained with reflector may differ depending on ambient lighting conditions and personal judgment or observations (Papautsky et al., 2016). In order to prove the concept of the patterned paper can be derived for biological assays by adding the appropriate reagents to the test zones, the most common conventional colourimetric μPAD was demonstrated for simultaneous detection of glucose and bovine serum albumin (BSA) protein in the urine sample. In general, the colour reagents were used as colour indicator to catalyse the reaction between analyte, such as glucose oxidase/peroxidase reagent and tetrabromophenol blue, respectively (Martinez et al., 2007; Martinez et al., 2008b; Martinez et al., 2010b). This is because the significant change in colouration on the paper substrate with white background is easily observed visually, for instance changing from brown to light brown for glucose assay whereas yellow to blue for BSA assay. The colour intensity is correlated to the concentrations of glucose and BSA.

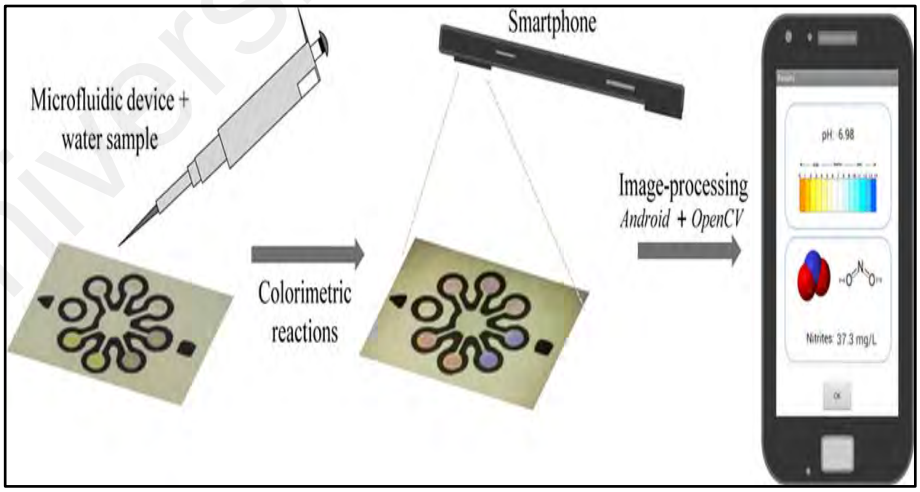

Figure 2.13: Colourimetric detection in μPAD using a smartphone for image processing. Reprinted with permission from Lopez-Ruiz et al. (2014). Copyright 2014, American Chemical Society

University of Malaya

2.4.2 Electrochemical Detection

Colourimetric detection is more widely used than electrochemical detection as the sensitivity of the former is lower than the latter. Compared to colourimetric detection, the electrochemical detection in μPAD is more sensitive and offers easily obtainable quantitative test results using simple electronic (e.g., potentiostat). An electrochemical μPAD typically replicates a three-electrode system which is similar to the conventional electrochemical cell, which comprised of counter electrode, working electrode and reference electrode on paper (**Figure 2.14**). The common fabrication process for electrochemical μPAD is the deposition of electrodes in the form of conductive ink. Silver ink is usually used for the reference electrode, whereas carbon inks are used for working and counter electrode (Yetisen et al., 2013). The conductive electrode pads are screen-printed in the hydrophilic region of the paper in which the sample and reagent are subsequently spotted. Henry and co-workers was the first team who demonstrated the feasibility of using paper microfluidic devices for diagnosis purposes, for example glucose, lactate, and uric acid (Dungchai et al., 2009).

The detection occurs in the hydrophilic region in which conductive ink are deposited on the paper as electrodes and connected to a potentiostat that interfaces with the computer. Followed this, the electrochemical reading can be obtained in term of peak current. The signal circuits are generated where a digital-to-analog (D/A) converter converts the computer generated number into voltages. The strength of this method is that it allows reproducible conformal contact, which also refers to the interactions between the printed electrodes and the paper channels. Moreover, the paper containing the analytes could inhibit the convective movement of solutions after the wetting of the paper channel with fluids, thereby increasing the accuracy for time-dependent measurement (Nie et al., 2010a; Nie et al., 2010b; Oh & Chow, 2015). Hence, the electrochemical detection is perceived to be more sensitive and accurate compared to

the colourimetric detection, but it still requires an expensive Autolab potentiostat and skillful operator to operate.

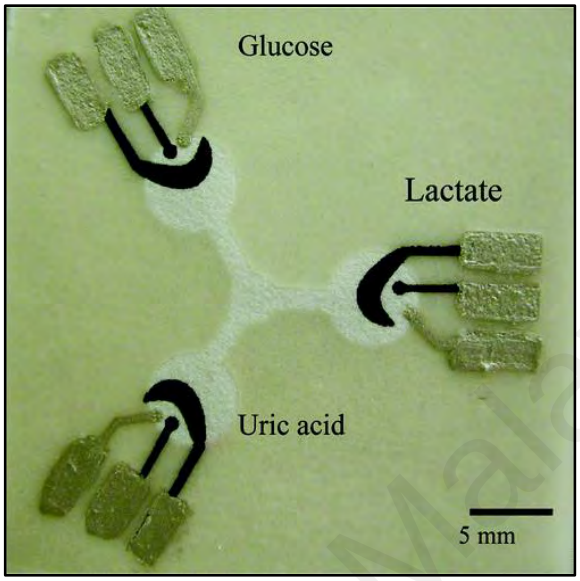

Figure 2.14: Electrochemical detection in three electrode µPAD. Reprinted with permission from Dungchai et al. (2009). Copyright 2009, American Chemical Society.

2.4.3 Chemiluminescence Detection

Chemiluminescence (CL) is a term that refers to light emitted as a product of chemical reactions. The luminescence in CL detection is initiated and controlled by the mixing of fluid flow reagent. For the CL assay on µPAD, the CL reagents are immobilised on a paper substrate via physical absorption, and then the target analyte is allowed to interact with the immobilised reagent by fluid transport. The sample is migrated through the bioactive channel towards the CL detection area to obtain a CL signal, which is produced from the interaction between the rhodamine derivative and hydrogen peroxide from the sample solution in an acidic medium. At last, the concentration of the sample is quantified by the peak height of the CL signal (Yu et al., 2011).

University of Malaya

The strength of the CL method is that it requires only a single light detector (e.g., photomultiplier tube), which is highly sensitive when incorporated with computerised ultra-weak luminesce analyser in order to detect light emission from CL-analyte reaction (**Figure 2.15**). However, the large variance in CL signal may occur because the CL signal is dynamic, temporary, and fades exponentially over time. Thus, multiple exposures are typically required to capture optimal signal and avoid signal saturation.

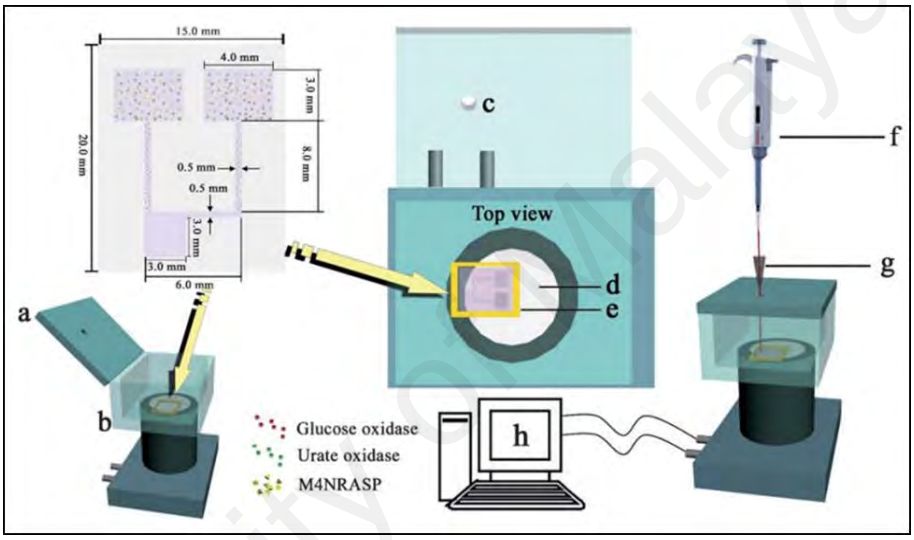

Figure 2.15: Chemiluminescence detection in µPAD, where CL signal was measured using a computerised ultra-weak luminescence analyser. Reprinted with permission from Yu et al. (2011). Copyright 2011, The Royal Society of Chemistry.

2.4.4 Electrochemiluminescence Detection

Electrochemiluminescence (ECL) is luminescence generated at an electrode surface during electrochemical reaction in solution. It is an attractive detection method that combines CL reactions and electrochemical technique via screen-printed electrodes. ECL can improve the sensitivity, selectivity and imaging analysis of ECL detection. Besides that, it allows better control over the emission position, which is closer to the electrode surface. Moreover, ECL is more useful than CL because the unstable CL reagents can also be electrogenerated *in situ*.

University of Malaya

ECL occurs which resulted from high-energy electron transfer reactions either the electro−oxidised or electro−reduced species. A luminophore is oxidised simultaneously at an electrode with a co−reactant, and then the oxidised luminophore and co−reactant will react to produce photons. The two most commonly utilised ECL luminophore are ruthenium complex [tris (2,2−bipyridyl)ruthenium(II)] and luminol whereas the ECL co−reactant are 2-(dibutylamino) ehtanol (DBAE) and nicotinamide adenine dinucleotide (NADH) (Gross et al., 2017; Marquette & Blum, 2006).

However, ECL−based µPAD was first demonstrated by Delaney et al. (2011). The hydrophobic channel was printed on the paper with inkjet printing and then laminated onto screen-printed electrodes (**Figure 2.16**). The reactants for luminescence are produced near the electrode surface when an appropriate potential is applied. Following this, the ECL emission signal was captured with a smartphone-based camera and analysed using imaging application (Delaney et al., 2011). Additionally, there are also other paper-based device which have detected a wide variety of analytes using ECL technique (Liu et al., 2016; Liu et al., 2015; Zhang et al., 2013).

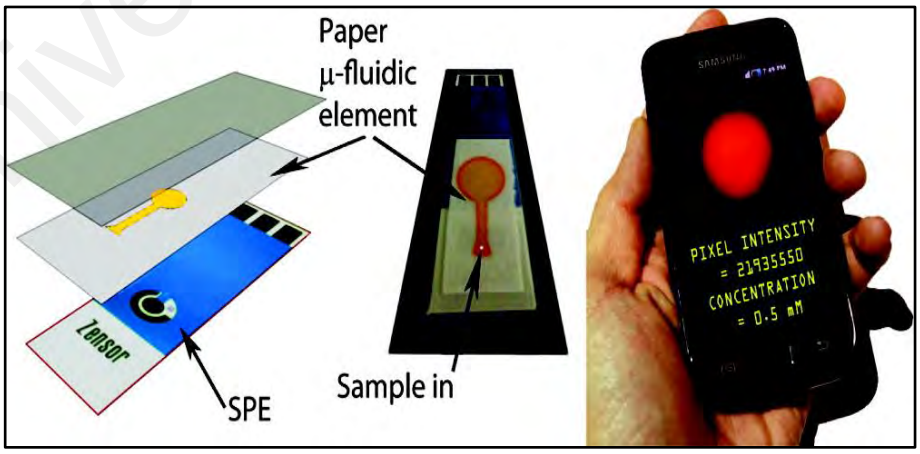

Figure 2.16: Electrochemiluminescence detection in µPAD. Reprinted with permission from Delaney et al. (2011). Copyright 2011, American Chemical Society.

University of Malaya

2.4.5 Surface Enhanced Raman Scattering Detection

This SERS technique relies on the enhancement of Raman scattering intensity where Raman molecules are adsorbed on and/or embedded between metal surfaces. This is because nanostructures function as the optical enhancing agent that has a high enhancement effect to the Raman signal of molecules. The main advantages of Raman SERS based techniques are their ability to enhance the signal and sensitivity by providing sharp molecularly specific spectra ("fingerprint" information of chemical structure of molecules) from the 'reporter' molecules, which can be very helpful to the diagnosis of clinical biomarkers, compared to other optical detections (Zhang et al., 2010).

There is no SERS method being employed in μPADs; however several literatures have recently reported the incorporation of SERS into LFAs for health diagnostics using a variety of SERS tags based on colloidal gold, gold@silver nanoparticles and nanostars. For instance, Gao et al. (2017) have developed LFA with SERS probes in which the Raman reporter molecules are sandwiched between a gold nanostar and a thin silica shell (nanoparticles@Raman reporter molecules@silica). The silica coating layer could prevent the Raman reporter molecules from leaking out, provides a platform for bio-conjugation, and also makes the SERS probe stable in aqueous solutions with high ionic strength while bare nanoparticles tend to aggregate under the same condition.

In addition, Zhang et al. (2018a) have developed both the multiplexed and single LFA used bimetallic particles as SERS tags to enhance the assay sensitivity, which embedded Raman reporters inside a core/shell nanoparticle, including tags with a nanorod core (**Figure 2.17**) (Zhang et al., 2018a; Zhang et al., 2018b). Also, Khlebtsov et al. (2019) proposed gap-enhanced Raman tags (GERTs) which embedded the Raman reporters into a 1 nm gap between gold core and gold shell. In this system, gold

nanorods were used as cores instead of spherical nanoparticles to improve the SERS intensity of GERT; but time consuming and laborious fabrication procedures are required. For quantification, the concentration of target analyte was quantified via the characteristics peak of the Raman reporter molecules.

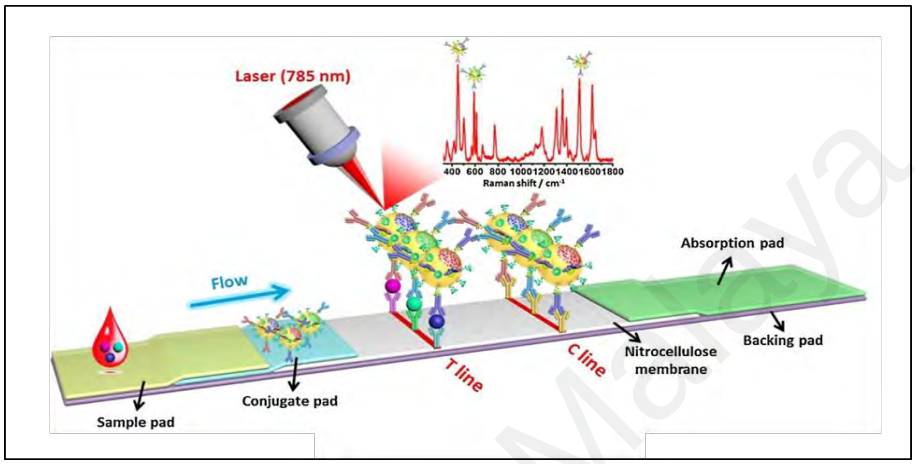

Figure 2.17: Surface enhanced Raman scattering (SERS) nanotags based LFA, is reprinted with permission from Zhang et al. (2018b). Copyright 2018, Elsevier B.V.

University of Malaya

Table 2.3: Comparison of the detection methods of µPAD (Lim et al., 2017).

Types of detection	Description	Advantages	Disadvantages	Limitations
a) Colourimetric	• Determines the concentration of analytes with the aid of colour reagents (Klasner et al., 2010; Martinez et al., 2007).	• Fast and simple. • Direct analyses visualised by naked eye via colour change of reagents.	• Errors due to personal judgment/ observation and differences in ambient illumination.	• Colour intensity data obtained from cameras differ under different ambient lighting condition.
b) Electrochemical	• Typically requires a reference electrode, a counter and a working electrode screen-printed on paper platform (Grieshaber et al., 2008).	• High sensitivity and selectivity.	• Expensive instrument required (e.g., Autolab potentiostat) • Tedious electrodes deposition (conductive ink) on paper.	• Fabrication of electrodes (conductive ink) on paper cannot be avoided.
c) Chemiluminescence	• Detects analyte light emission during a chemical reaction involved a highly oxidised species such as peroxide (Yu et al., 2011).	• High sensitivity and selectivity. • Offers a more reproducible response, independent of ambient light compared to colourimetric detection.	• Large variance due to dynamic and temporary chemiluminescence signal.	• Light measurement must be performed in dark and detected with a light detector (e.g., photomultiplier tube)
d) Electro-chemiluminescence	• Combines chemiluminescence reaction and electrochemical techniques.	• High sensitivity and selectivity. • Better control over emission position and electrogenerated in situ the unstable chemiluminescence reagent and intermediates.	• Emission much weaker than chemiluminescence.	• Electrochemical setup and frequent renewal of the electrode surface is required (Hu & Xu, 2010).

University of Malaya

Table 2.3, continued.

Types of detection	Description	Advantages	Disadvantages	Limitations
e) **Surface Enhanced Raman Scattering (SERS)**	• Surface technique that enhances Raman scattering by molecules adsorbed on metal surfaces or by nanostructures (e.g., nanoparticles) (Prochazka, 2016).	• High sensitivity and selectivity. • Capable to provide Raman peaks at different Raman shift for different molecule structures.	• Expensive Raman spectroscopy required for signal measurement.	• Different types of SERS nanotag may affect the sensitivity of assay.

University of Malaya

2.5 Health Diagnostic Applications of Microfluidic Paper-Based Analytical Device

Microfluidic paper-based device had been developed and used for various health diagnostic applications to test urine, blood and saliva samples in respective assays such as urinalysis, virus analysis, blood analysis, and saliva analysis. These applications are discussed in the following sections.

2.5.1 Urinalysis

In past decades, urine can be colourimetrically tested with the well-known commercial dipstick assay (e.g., urine test strips) for several parameters simultaneously, involving pH, specific gravity, presence of leucocytes, nitrite, urobilinogen, proteins, hemoglobin, ketone, bilirubin and glucose. However, this kind of test strips is only capable of providing qualitative result via colour change. To resolve this drawback, many research groups have worked to develop more advanced colourimetric paper-based assay to provide rapid result in qualitative and semi-quantitative analysis for multiple analytes, such as glucose and BSA protein in urine sample (Martinez et al., 2007; Sechi et al., 2013; Wang et al., 2010). The reason is that the urinary glucose and BSA have been widely used as important markers used in urinalysis for determining the patients risk with kidney disease (Cowart & Stachura, 1990).

Since 2007, Whitesides and co-worker developed the first μPAD for determination of BSA protein and glucose levels in artificial urine sample (Martinez et al., 2007). As shown in **Figure 2.18 (i)**, the μPAD was photoresist patterned in three separate test areas on chromatography paper by photolithography method. In the patterned paper, 0.3 μL of reagents was spotted in each specific region: the square region on the right was for protein test; the circular region on the left was for glucose test while the circular region at the top was a control well. For glucose assay, the presence of glucose resulted

University of Malaya

in a colour change from clear to brown as a result of the enzymatic oxidation of iodide to iodine (Yuen & McNeill, 2000). For BSA protein assay, the changes from yellow to blue when tetrabromophenol blue ionised and bound to proteins (Mogensen, 1984). The amount of glucose and BSA protein in the artificial urine can be determined semi-quantitatively on μPAD via the colour change of the reagent in the reaction zones. The detection ranges of glucose and protein levels were 0—500 mM and 0—75 μM respectively (Martinez et al., 2007), which cover the clinical relevant range such as 2.5—500 mM for glucose and 0.38—75 μM for BSA protein.

Besides this, Wang et al. (2010) designed a tree-shaped μPAD with micro-flows in different branches by the cutting method for simultaneous calibration and semi-quantitative determination of concentration of BSA in artificial urine, as presented in **Figure 2.18 (ii)** (Wang et al., 2010). Hence, a series of BSA solution included standard solutions and an unknown sample, as well as the protein reagent (bromophenol blue) was spotted on the paper. For protein assay, the formation of stable blue complex resulted from the binding of bromophenol blue with BSA protein via a combination of electrostatic and hydrophobic interaction. The advantage of this μPAD was able to provide a direct assessment by measuring various sample concentration in parallel, with the standard reference without requiring trained personnel or specialised equipment. Despite the fact that, the precise measurement of the sample volume for this method can be omitted as different volumes of samples with the same concentration was ascertained, it could generate same colour intensity on μPAD. The detection range for BSA was 0—5 mg mL^{-1}, as low as 0.08 mg mL^{-1} can be detected visually with the naked eye (Wang et al., 2010).

In addition, a wax-patterned 3D-μPAD was created with origami technique and used for glucose and protein detection, as shown in **Figure 2.18 (iii)** (Sechi et al., 2013). The

advantage of this 3D-µPAD with nine-layer platform along with the flexible reservoirs and channels allow for detection of several analyte, in their respective assays. Herein, the reagents used for detecting protein and glucose were brilliant blue G dye and glucose oxidase/peroxidase reagent, respectively (Chial & Splittgerber, 1993; Free et al., 1957) When mixed with urine, the glucose assay changed from clear to brown, while the protein assay changed from brown to a lighter shade of brown. The amounts of glucose and protein presented to the 3D-µPAD were proportional to the colour change of each assay. For semi-quantitative analysis, all the colourimetric result of urinalysis was obtained by capturing the image of µPAD and analysed with the image software (e.g., Adobe Photosoft or Quality one) (Martinez et al., 2008a; Martinez et al., 2010b).

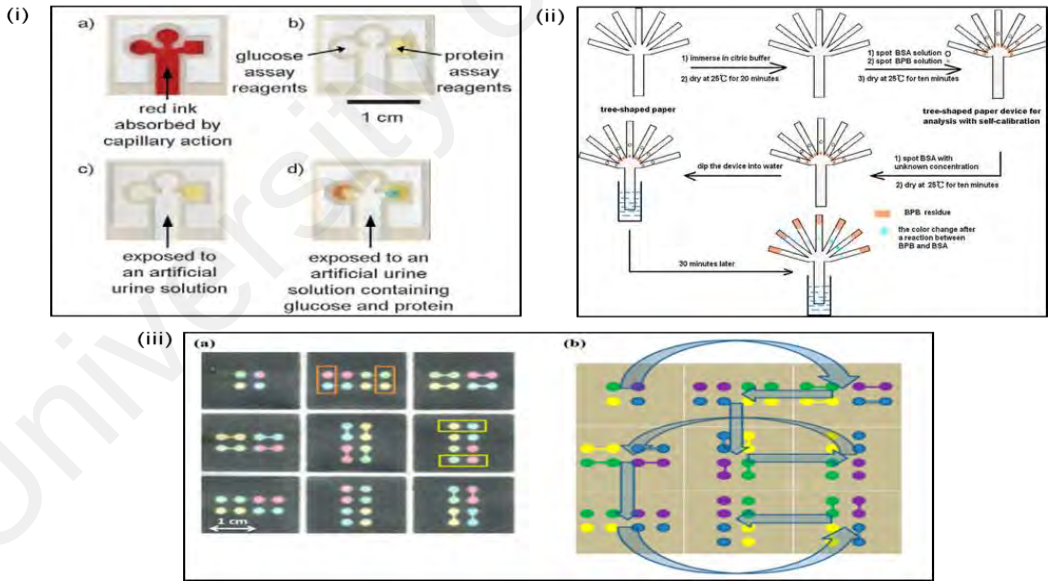

Figure 2.18: µPADs for protein and glucose detection in urine sample, (i) Photoresist-patterned tree-shaped µPAD is reprinted with permission from Martinez et al. (2007). Copyright 2007 WILEY - VCH Verlag GmbH & Co. KGaA, Weinheim. (ii) Tree-shaped µPAD with multi-branches, is reprinted with permission from Wang et al. (2010). Copyright 2010, American Chemical Society. (iii) Wax-patterned 3D-µPAD with principles of origami, is reprinted with permission from Sechi et al. (2013). Copyright 2013, American Chemical Society.

University of Malaya

2.5.2 Blood Analysis

Blood tests are extensively used in clinical laboratory diagnostics; however to detect analytes in whole blood is difficult due to the chemical complexity of the matrix. Therefore, biochemical blood tests are normally performed on blood serum or plasma, the liquid portion of blood without cells. Hence, most of the biological samples require additional steps to remove cells that often interfere with the analytical measurement (Crowley & Pizziconi, 2005). In a conventional laboratory setting, the separation of plasma from whole blood for diagnostics is commonly achieved using centrifuge that requires dedicated instrumentation, a skilled operator and typically involves drawing a few mL blood sample from a patient by venipuncture. To reduce the turnaround time and sample preparation steps needed for clinical assay from hours to minutes; several research groups struggled for direct separate plasma from whole blood using μPADs, with two approaches as presented in **Figure 2.19** such as **(i)** using red blood cell (RBC) agglutination (Yang et al., 2012) and **(ii)** using different types of paper, e.g. blood separation membrane and filter paper (Songjaroen et al., 2012; Vella et al., 2012).

Yang et al. (2012) developed a μPAD to separate blood plasma from whole blood using RBC agglutination for colourimetric detection of plasma glucose. As shown in **Figure 2.19(i)**, the device is fabricated on chromatography paper by patterning the hydrophobic barrier with a wax printer to define a plasma separation zone and four test readout zones. To perform the assay, a drop of whole blood (~7 μL) was placed onto the plasma separation zone of a μPAD and deposited with agglutinating antibodies (anti-AB), which lead to agglutination of RBC in the sample and separation of plasma. Because of agglutination, RBCs formed large multi-cellular aggregates that could be filtered out from chromatography paper with the size of pores larger than 2.5 μm, and thus produce purified plasma at a much higher volumetric flow rate. Subsequently, the plasma was transported laterally to the test readout zones of the device by capillary

action where glucose in plasma reacted with the colourimetric reagents (glucose oxidase) to produce a visible colour change. This is because of glucose oxidase catalyses oxidation of glucose present in the plasma to produce hydrogen peroxide (H_2O_2). Horseradish peroxidase then catalyses the reaction of H_2O_2 with potassium iodide, by oxidising iodide to iodine which resulted in brown colour. The intensity of the colour change was proportional to the amount of H_2O_2 produced, and thus to the amount of glucose present in plasma. The colour change was then digitised using a portable scanner and the average colour intensity in the test readout zones of the µPAD was converted to glucose concentration levels using a calibration curve. The detection range of glucose concentration in blood plasma samples was 50—200 mg dL^{-1} (Yang et al., 2012). However, the drawback of this separation strategy that used anti-AB antibodies to induce RBC agglutination in whole blood samples is only applicable for patient with blood type A, B or AB only and would not apply to those with blood type O.

In addition, a µPAD was also developed with melted white beeswax on filter paper by wax-dipping method then overlapped with blood separation membrane to quantify plasma BSA protein (Songjaroen et al., 2012). As shown in **Figure 2.19 (ii),** this approach used different types of paper (e.g., blood separation membrane and filter paper) to separate blood plasma from whole blood without requiring additional agglutinating antibodies to aggregate RBC. For blood separation, the blood separation membrane was used to receive the whole blood sample and trapping the blood cells (both red and white), to isolate the pure plasma from the whole blood sample to flow to the detection zone by capillary force. The colour was developed after the binding of BSA protein to bromocresol green reagents in the detection zone. Subsequently, the images of the detection zones were captured using a digital camera and the colour intensity was analysed as protein concentration in plasma samples. The detection range

of protein concentration in the blood plasma sample was 1.6 —5.3 g dL^{-1} (Songjaroen et al., 2012). Because of its simplicity, this method of plasma separation could be readily integrated into µPADs to enable the operation of these devices on whole blood samples for point-of-care diagnostics, especially in resource limited settings.

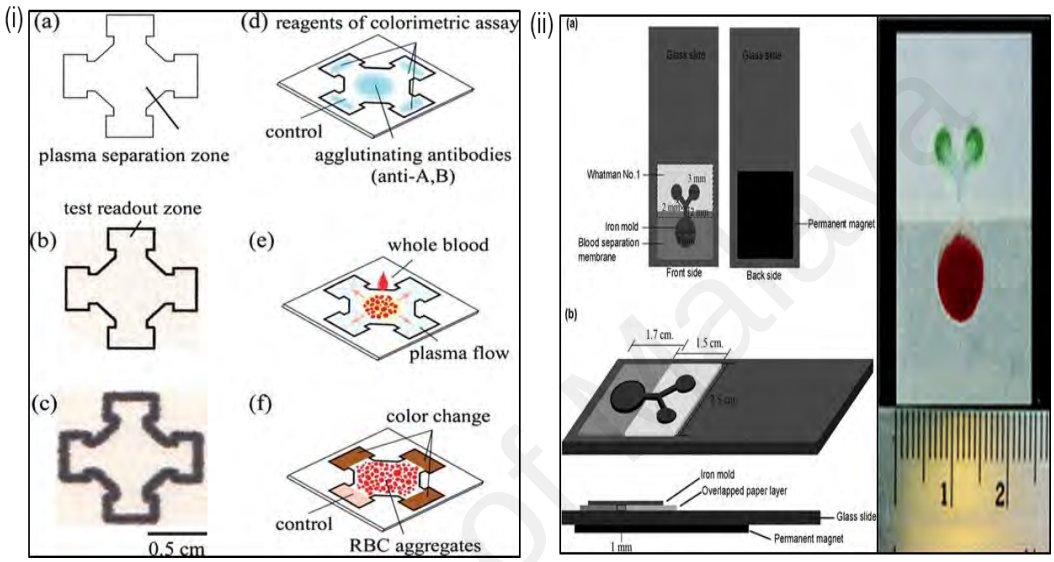

Figure 2.19: µPAD for separating blood plasma from red blood cells (RBCs). (i) using red blood cell (RBC) agglutination, is reprinted from Yang et al. (2012) with permission. Copyright 2012, Royal Society of Chemistry. (ii) using different types of paper, is reprinted from Songjaroen et al. (2012) with the permission. Copyright 2012, Royal Society of Chemistry.

2.5.3 Virus Analysis

There are several µPAD which have been developed for virus analysis such as detection of hepatitis B surface antigen (HBsAg) in serum (Chen et al., 2018; Li et al., 2015; Liu et al., 2011); human immunodeficiency virus (HIV) and hepatitis C virus (HCV) in serum (Zhao & Liu, 2016). Indeed, hepatitis B is a life-threatening liver infection caused by the hepatitis B virus (HBV). It occurs when HBV attacks the liver cells which lead to liver failure and liver cancer (Inoue & Tanaka, 2016; Lee, 1997). In virus-infected liver cells, HBsAg was produced in excess and secreted into the blood, where it serves as a marker for active infection for infected patients. On the other hand,

University of Malaya

co-infection with HBV or HCV is common among HIV-positive patients due to their similar blood transmission routes. Despite the fact that HIV-positive, individuals with chronic hepatitis caused by either HBV or HCV have greater liver mortality than those infected with HIV alone (Utsumi & Lusida, 2015).

A 3D-µPAD used as portable enzyme-linked immunosorbent assays (ELISA) for detection of HBsAg was demonstrated by Liu et al. (2011). The device was fabricated by stacking layers of wax-patterned paper and adhering them together with water-impermeable double-sided adhesive tape, as presented in **Figure 2.20 (i)**. One of the paper layers was patterned as reagent storage zones that stored all reagents in dry form comprising primary antibody and alkaline phosphate conjugated detecting antibody, and then dissolved in the buffer and delivered to the test zones during the assay to detect HBsAg in serum samples. The images of the test zones were captured using a photo scanner with 600 dpi resolution, and the colourimetric signal was quantified as concentration of HBsAg using the Image J software. This 3D-µPAD provides fast analysis (43 minutes per assay) for an assay than the conventional ELISA (>3 hours per assay) that requires a skillful operator in pipetting and removing a series of reagents and buffer.

On the other hand, deoxyribonucleic acid (DNA) from HBV is the essential biomarker for HBV infection. Clinically, HBV DNA test is usually performed by using polymerase chain reaction (PCR) to generate HBV DNA fragments so that they can be measured in copies per milliliter (copies/mL) or international units per milliliter (IU/mL). During acute HBV infection, the level of HBV DNA was as high as 10^{10} copies/mL or range from ten of thousands up to billions IU/mL (Whalley et al., 2001). However, these PCR assays are usually performed in centralised laboratory settings due to the specialised nature of the required equipment and personnel. To simplify the assay

procedure, Li et al. (2015) presented a paper-based electrochemical sensor for detecting HBV DNA, as shown in **Figure 2.20 (ii)**. This paper-based electrochemical sensor was fabricated based on paper folding. It is capable of detecting a 30-base nucleotide sequence characteristic of DNA from the HBV with a detection limit of 85 pM, without using any enzymes or antibodies in the assay. The superior of the μPAD was with its two-stage amplification that made it possible to detect HBV DNA target levels at pico-molar. Twenty (20) nm silver nanoparticle labels provide a maximum amplification factor of 250 000 and magnetic microbeads concentrated at the detection electrode, provide an additional 25-fold amplification. For quantification, the charge under the anodic stripping voltammetry (ASV) peaks as a function of the concentration of HBV DNA. The ASV signal changed linearly with the HBV DNA concentrations ranging from 0 to 500 pM. In comparison to conventional electrochemical cell, the current was ~25 times higher in the paper device due to the presence of small rare-earth magnet situated above the working electrode, which is capable of capturing directly the DNA sandwich (MμB-bound AgNP labels) at the working electrode. However, this device is not desirable for POC application as the DNA sandwich must be prepared ex-situ.

In addition, Zhao and Liu (2016) presented a portable μPAD platform for multiplexed electrochemical detection of antibody markers of HIV and HCV in serum samples, as shown in **Figure 2.20 (iii)**. The principle of indirect ELISA was employed on electrochemical μPAD for diagnosing HIV/HCV co-infection. The μPAD was developed with eight electrochemical immunosensor with a handheld-multi-channel potentiostat, which is capable to perform simultaneous detection of HIV and HCV antibody markers for eight types of serum samples (four immunosensors for each marker) within 20 minutes. Moreover, this unique integration of electrochemical μPAD with wireless communication is very useful for healthcare data collection as the multiple measurement data of HIV and HCV markers from a single run can be transmitted to a

remote site (e.g., hospital or laboratory) via internet network or Bluetooth by computer or smartphone. On the other hand, the limit of detection for HIV p24 core antigen was 300 pg mL^{-1} and HCV core antigen was 750 pg mL^{-1} in mouse serum, which is lower than the present ELISA tests for HIV antibody at 1 ng mL^{-1} (Bhimji et al., 2013) and HCV core antibody at 5 ng mL^{-1} (Moradpour et al., 1996).

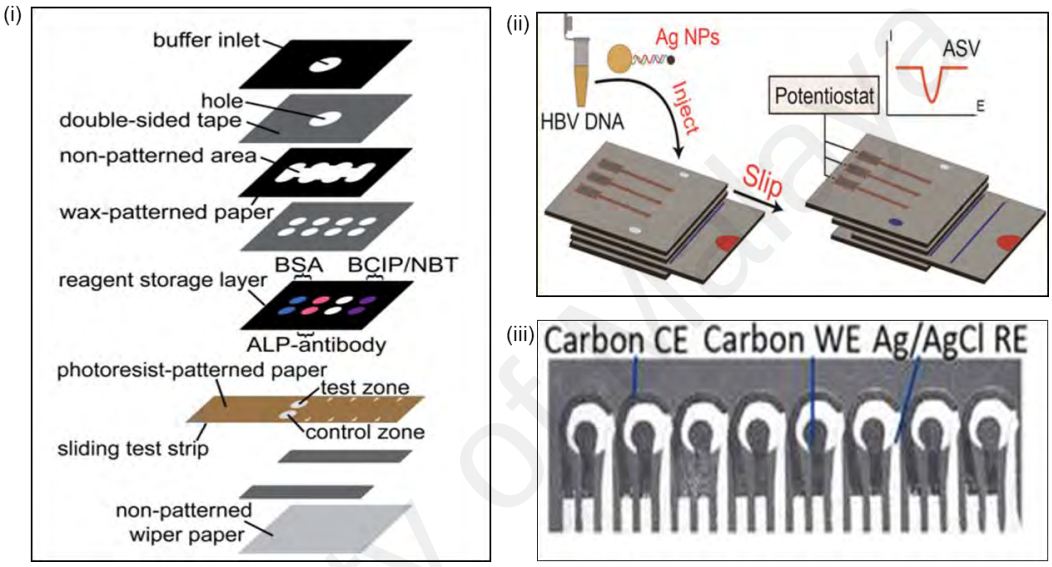

Figure 2.20: µPAD for virus analysis. (i) 3D-µPAD for detection of HBsAg, is reprinted with permission from Liu et al. (2011). Copyright 2011, American Chemical Society. (ii) Paper-based electrochemical sensor for detection of Hepatitis B virus DNA, is reprinted with permission from Li et al. (2015). Copyright 2011, IEEE. (iii) Electrochemical µPAD for simultaneous detection of HIV and HCV. Reprinted from Zhao and Liu (2016), with the permission of AIP Publishing.

2.5.4 Saliva Analysis

Saliva is composed of 99.5% water, 0.3% proteins and 0.2% inorganic markers and trace substances. It contains many types of health-related biomarkers including glycoproteins, immunoglobulins, blood type substances, enzymes, electrolytes and hormones. Of late, saliva as a sample matrix is rapidly gaining interest for diagnosing diseases and point-of-care assays because the ease and non-invasiveness of collection, thus intensely diminishes the discomfort associated with blood collection and privacy issues associated with urine collection (Lee & Wong, 2009).

Hemodialysis is the most common treatment for patients with kidney failure. During hemodialysis, nitrite and other waste produce are filtered from the blood. The significant decrease in blood nitrite levels after dialysis is reflected in the patient's saliva (Kawasaki, 1990). Since 2008, the measurement of saliva markers, nitrite was developed as an alternative to blood tests for monitoring the progression of hemodialysis on patients with end-stage renal disease. Saliva contains 20% of the proteins found in blood (Blicharz et al., 2008; Nagler, 2008). However, the spectrophotometric method based on Griess test (Sun et al., 2003) is commonly used for the quantification of nitrite; but it requires a large volume of reagent and sample. Thus, the spectrophotometric method is employed on μPAD for the determination of salivary nitrite in rapid and simple way.

As reported in the previous method, the Griess reagent was prepared by sulfanilamide, citric acid, and n-(1-napthyl)-ethylenediamine as the detection reagent for nitrite determination on μPAD (Klasner et al., 2010; Li et al., 2010b). As the occurrence of the reaction is based on nitrite reacting with a primary aromatic amine (e.g., sulfanilamide) under acidic conditions (e.g., citric acid), a diazonium salt was formed which further reacted with an aromatic compound containing an amino group (e.g., N-(1-naphthyl)-ethylenediamine) to form an intense coloured azo dye (Jayawardane et al., 2014). In 2010, a μPAD was developed by Klasner et al. (2010) with photolithography technique for colourimetric detection of salivary nitrite, as presented in **Figure 2.21 (i)**. In this device, a detection solution, Griess reagent was reacted with the nitrite present in the artificial saliva sample on the paper. The μPAD images were converted to CMYK format in Adobe Photoshop CS4, and the colour intensity measurements were measured using the magenta channel. A semi-quantitative result was obtained via colour intensity measurement and produced a linear response over a wide range of 25—250 μM on μPAD.

University of Malaya

Additionally, Bhakta et al. (2014) developed a μPAD for the detection of nitrite in saliva for diagnosing periodontitis disease, as shown in **Figure 2.21 (ii)**. The traditional methods for diagnosis of periodontitis include probing the gingival tissues for bleeding and suppuration, inspecting for biofilm deposits, and taking X-rays to evaluate the teeth and bone (Cutler et al., 2000; Lang et al., 1986) which require a specialist for evaluation. On the other hand, the concentration of nitrite was reported that it is possible to be used as an indicator for the progression of the periodontitis disease. For indication of the progression of periodontitis, the Griess reagent will lead to the formation of a magenta azo compound in the presence of nitrite. Thus, the colour intensity can be related to the concentration of nitrite present in the sample. Compared to other traditional method, the analysis of the saliva samples using the μPADs is simpler just by analysis using an office-grade scanner; however the result obtained was found to have larger errors than the previous method (Bhakta et al., 2014).

Furthermore, Noiphung et al. (2018) also developed a μPAD for simultaneous determination of pH and nitrite for monitoring oral cancer periodontal disease (**Figure 2.21 (iii)**). Herein, three different pH indicators such as chlorophenol red, phenol red and phenolphthalein were used for the measurement of salivary pH from 5.0 to 10.0 on μPAD, whereas the nitrite level determination was performed using the Griess reaction that covers a detection range from 0.1 to 2.4 mg dL^{-1}. To identify a pH colour scale, cholorphenol red changes colour from yellow to violet in the pH range of 4.8 to 6.7; phenol red changes from a yellow to red colour in the pH range of 6.8 to 8.2; and phenolphthalein changes from colourless to a red colour in the pH range of 8.0 of 10.0. Similarly, the salivary pH can be used as useful prognostic indicator for oral cancer as the salivary pH value in oral cancer patient was found to have shifted toward acidic pH due to the tumor cell producing the lactic acid by anaerobic metabolism (Ramya et al., 2015).

In the past decade, salivary diagnostic approaches have been developed to monitor oral and systemic diseases. Nowadays, there are several numbers of assays that have been established using saliva to monitor diseases such as detection of illicit drug use (Cone, 1993; Kidwell et al., 1998); immune response to viral infection (Chaita et al., 1995; Ochnio et al., 1997), HIV infection (Emmons, 1997; Malamud, 1997) and myocardial infarction (Foo et al., 2012; Mirzaii-Dizgah & Jafari-Sabet, 2011; Mirzaii-Dizgah & Riahi, 2013; Out et al., 2012). Hence, salivary biomarkers are promising to be used for future clinical and diagnostic utilities (Arunkumar et al., 2014; Kaufman & Lamster, 2002; Wei & Wong, 2012). In the near future, µPAD is possible to be developed as an alternative point-of-care platform for salivary diagnostics to provide, rapid and simple measurement of biomarkers in order to enable the early detection of disease and routine health monitoring.

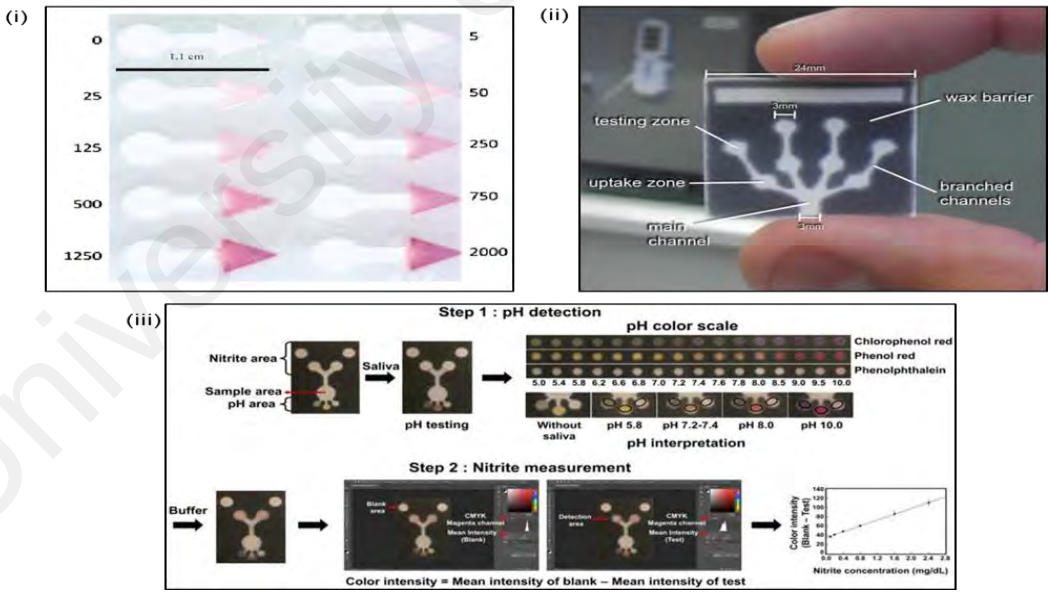

Figure 2.21: µPAD used for saliva analysis. (i) µPAD for the detection of salivary nitrite for diagnosing hemodialysis. Reprinted with permission from Klasner et al. (2010). Copyright 2010, Springer-Verlag. (iii) µPAD for simultaneous determination of pH and nitrite. Reprinted with permission from Bhakta et al. (2014). Copyright 2013 Elsevier (iii) µPAD for the detection of salivary nitrite for diagnosing periodontitis disease. Reprinted with the permission from Noiphung et al. (2018). Copyright 2018 Ivyspring International Publisher.

University of Malaya

CHAPTER 3: METHODOLOGY

In this chapter, µPAD was fabricated using a wax-printing technique for simultaneous multiplex detection of cardiac biomarkers–GPBB, CK–MB and cTnT, using colourimetric method (detected using reflectance detector–smartphone-based camera and desktop scanner) and SERS method (detected using Renishaw InVia Raman Microscope). The research works was conducted according to the flow chart **Figure 3.1** and all the experimental procedures for colourimetric and SERS assays were also detailed in the following section.

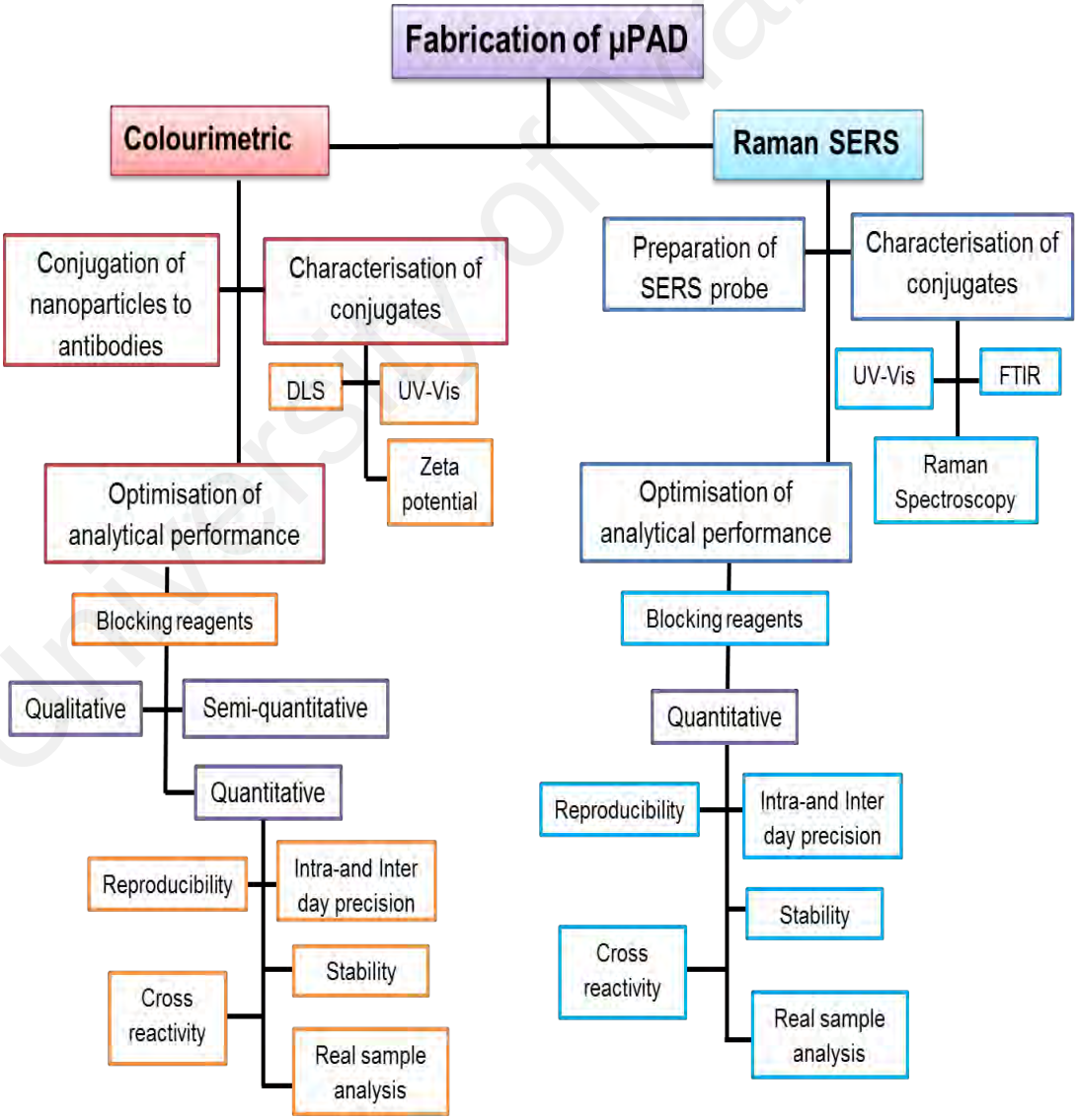

Figure 3.1: Flow chart of research work.

University of Malaya

3.1 Fabrication of Microfluidic Paper-Based Analytical Device

The wax-printing method as described by Carrilho et al. (2009a) was chosen to fabricate a µPAD. The µPAD pattern was designed using AutoCAD software 2015 and printed on a Hi-Flow Plus 135 nitrocellulose (NC) membrane card of 60 mm × 301 mm using a wax printer ─ Fuji Xeror ColorQube 8870. The printed wax was then melted in an oven at 100° C for 5 minutes to allow the melted wax to penetrate into the membrane to form a well-defined microchannel. After that, the patterned paper was allowed to cool at room temperature (25°C) before continuing with further procedure.

As shown in **Figure 3.2**, the black area was printed as the hydrophobic barrier, whereas the white area remained as the hydrophilic area for an assay. The paper-based device was designed with three reaction zones ─ G for GPBB, M for CK−MB and T for cTnT with a diameter of 50 mm and connected by 30 mm microchannel at an angle of 120° from the sample zone, C. The sample zone was designed at the centre of the paper-based device with 60 mm diameter. Moreover, two precaution steps were taken. First, the NC membrane card was attached with a backing polyester film, which prevents fluid from leaking away from the backside of a paper-based device during an assay. Second, WhatmanTM Chromatography paper Grade 1 was stacked on the boundary of the membrane and used as absorbent pad to absorb any excessive fluid flowing out from the open channel.

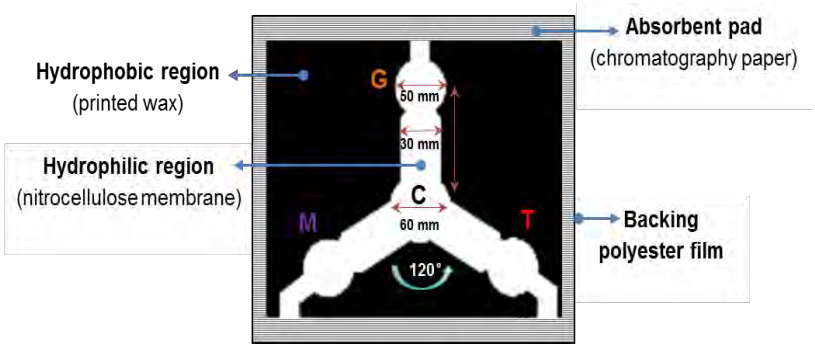

Figure 3.2: Design and dimensions of the fabricated µPAD used for multiplex detection of cardiac biomarkers.

3.1.1 Optimisation of Heating Time and Temperature

The wax spreading ratio and colour of the printed wax on µPAD were used as indicators to determine the optimal heating time and temperatures. The ratio of wax spreading was calculated by dividing the measured width of the channel by the desired width of channel on the fabricated µPAD. The width of the channel was measured using the microstructure measurement software. Besides that, the colour of the printed wax on µPAD was observed before (black) and after heating (grey) to confirm that the wax has melted and penetrated into the membrane to form a hydrophobic barrier as shown in **Figure 3.3**. In this study, the time and temperature ranges were varied at 50°C, 100°C, 150°C at 3 minutes, 5 minutes, 10 minutes and 15 minutes time interval.

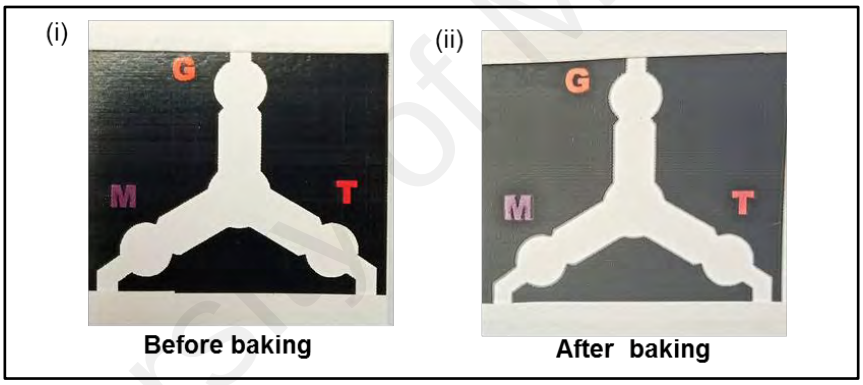

Figure 3.3: Images of (i) µPAD before heating and (ii) µPAD after heating.

3.1.2 Optimisation of Sample Volume and Colour Development Time

The ideal sample volume for an assay was selected depending on the minimal sample volume required to completely wet the µPAD with multiplex reaction zones. Therefore, a series of sample volumes ─ blue dye solutions (3 µL, 5 µL, 10 µL and 15 µL) were tested on µPAD. The best analysis time for an assay was determined based on the retention time required for colour development on µPAD, which indicated the formation of sandwich complex after the addition of nanoparticle-labeled detecting antibody. Hence, different retention time (1 minute, 3 minutes, 5 minutes, and 10 minutes) were

University of Malaya

tested in developing colour signal on μPAD. The image of colourimetric result of the μPAD was captured using smartphone-based camera and transmitted to a computer programmed with Image J software program (NIH, Bethesda, MD, USA) for result interpretation.

3.2 Colourimetric Assay Procedure on Microfluidic Paper-Based Analytical Device

Figure 3.4 is a schematic illustration of a direct sandwich assay for colourimetric detection of multiple cardiac biomarkers — GPBB, CK–MB and cTnT on μPAD. The colourimetric analysis was performed to determine the concentration of the cardiac biomarkers (target analytes) on the μPAD with the aid of the colour indicator (nanoparticles-labeled detecting antibody). The use of three nanoparticles (e.g., 40 nm silver nanoparticles, 50 nm gold-urchin nanoparticles and 40 nm gold nanoparticles) as labels were designed to allow a visual analysis of various colour signals for the detection of multiplex cardiac biomarkers on μPAD. The hydrophilic region (sample area) in the centre of the μPAD wicks sample simultaneously in the three separate test zones (G, M, T) where independent sandwich detection takes place.

The sandwich immunoassay was performed on μPAD based on four basic steps: **(1)** 1 μL of 1 mg mL^{-1} monoclonal capturing antibody was immobilised initially on each reaction zone(s). For instance, monoclonal anti-GPBB antibody at reaction zone G, monoclonal anti-CK–MB antibody at reaction zone M and monoclonal anti-cTnT antibody at reaction T, respectively. Physical adsorption method offers the simplest attachment pathway due to the specific hydrophobic and electrostatic interaction between the domains of antibody (protein) and nitrocellulose. For μPAD, the capture antibody was immobilised by direct adsorption to porous nitrocellulose substrates in a fixed geometry area (30 mm at each reaction zone) for sandwich immunoassay via a

combination of intermolecular forces (electrostatic, hydrogen and hydrophobic forces from NC derivatives (e.g., cellulose nitrate)), thereby making simple spotting effective for antibody immobilisation. (2) Subsequently, the non-specific region on NC membrane was blocked with 1% (w/v) Western Blocking Reagents (WBR) for 1 hour to inhibit non-specific absorption of proteins. (3) Next, 10 μL of the desired concentration of sample (human serum diluted with dilution factor 1:2 or purified protein diluted at the desired concentration by 0.01 M phosphate buffer, pH 7.4) was applied at the central sample zone (C) of membrane. The pH of the phosphate buffer was adjusted to pH 7.4 to correspond to the normal physiological pH range between 7.35 and 7.45 in human blood (Huang et al., 2013). The sample was allowed to flow spontaneously from the central sample zone to all three reaction zones by capillary action, and this process requires two minutes. **(4)** Lastly, the nanoparticles-conjugated detecting antibodies (colourimetric conjugates) such as silver nanoparticles-conjugated polyclonal anti-GPBB detecting antibody (yellow colour); gold-urchin nanoparticles-conjugated monoclonal anti-CK–MB detecting antibody (M1709CKMB1) (purple colour) and gold nanoparticles-conjugated polyclonal anti-cTnT detecting antibody (red colour), was deposited at the respective reaction zone(s) – G for GPBB, M for CK−MB, T for cTnT and left for three minutes to allow the formation of sandwich immuno-complex which could be identified as a coloured dot on the membrane. Herein, several dilution factors (such as 1: 2, 1: 5, and 1:10) were studied, and the dilution factor of 1: 2 was selected for assay because it is well enough to allow the human serum sample to flow smoothly to each reaction zone(s) on the membrane. Moreover, 1 hour incubation time of WBR blocking reagent was selected according to the recommendations of the Sigma Aldrich's product sheet (Cat. No. 11 921 673 001) to obtain best analytical performance on μPAD. In this study, all the washing process was performed using 3% (v/v) Tween 20 as the washing buffer to remove the background staining caused by excess unbound

nanoparticles-labeled detecting antibodies, which took two minutes. The monoclonal antibody was used as a capture antibody to specifically capture antigen in a monoclonal-polyclonal sandwich detection of cardiac biomarkers (e.g., GPBB and cTnT), whereas the polyclonal antibody was used as a detection antibody (conjugated with nanoparticles as a detection label) to sensitively "sandwich" antigen between two separate antibodies. Except for the CK−MB assay, two monoclonal antibodies from different cell lines have been selected to bind and detect CK−MB biomarkers because there is no polyclonal CK−MB antibody on the market.

Additionally, the image of colourimetric result of the μPAD was captured using a Xiaomi Mi4i smartphone camera (13 megapixel) and scanned with a portable scanner PIXMA E610 series scanner (Canon, Tokyo, Japan). Then, images were transmitted to a computer programmed with Image J software programme (NIH, Bethesda, MD, USA) for result interpretation. The process was very simple and took approximately three minutes. To minimise bias from changing the ambient light, μPAD images are taken under a desk lamp (in dark) by a smartphone camera. The length between μPAD and light source (desk lamp) has been set (in 30 cm) to monitor sample positioning and provide constant object illumination. By selecting the area of each test region, G, M and T (with a circle of width and height in 200) in a digital image of the μPAD that was either captured by a scanner or a smartphone-based camera, the mean intensity for each data point was obtained using the histogram function in Image J (Image J: Analyze → Measure → Results). The blank image was taken as reference and subtracted to obtain the final mean intensity. **Figure 3.5** displays the colour intensity measurement process using Image J. Overall, the total analysis time required for completing the entire assay and interpreting the data only takes about 10 minutes (**Table 3.1**).

University of Malaya

Table 3.1: Total time taken for sandwich formation on μPAD.

Analysis Process	Time taken (minutes)
1. Sample flow to each reaction zone(s) from central sample zone	2
2. Colour development for formation of sandwich immuno-complex after applying nanoparticles-labeled detecting antibodies	3
3. Washing off excess unbound nanoparticles-labeled detecting antibodies from reaction zone(s)	2
4. Analysing reflectance detection of colour intensity using a smartphone-based camera or a desktop scanner	3
Total time	10

University of Malaya

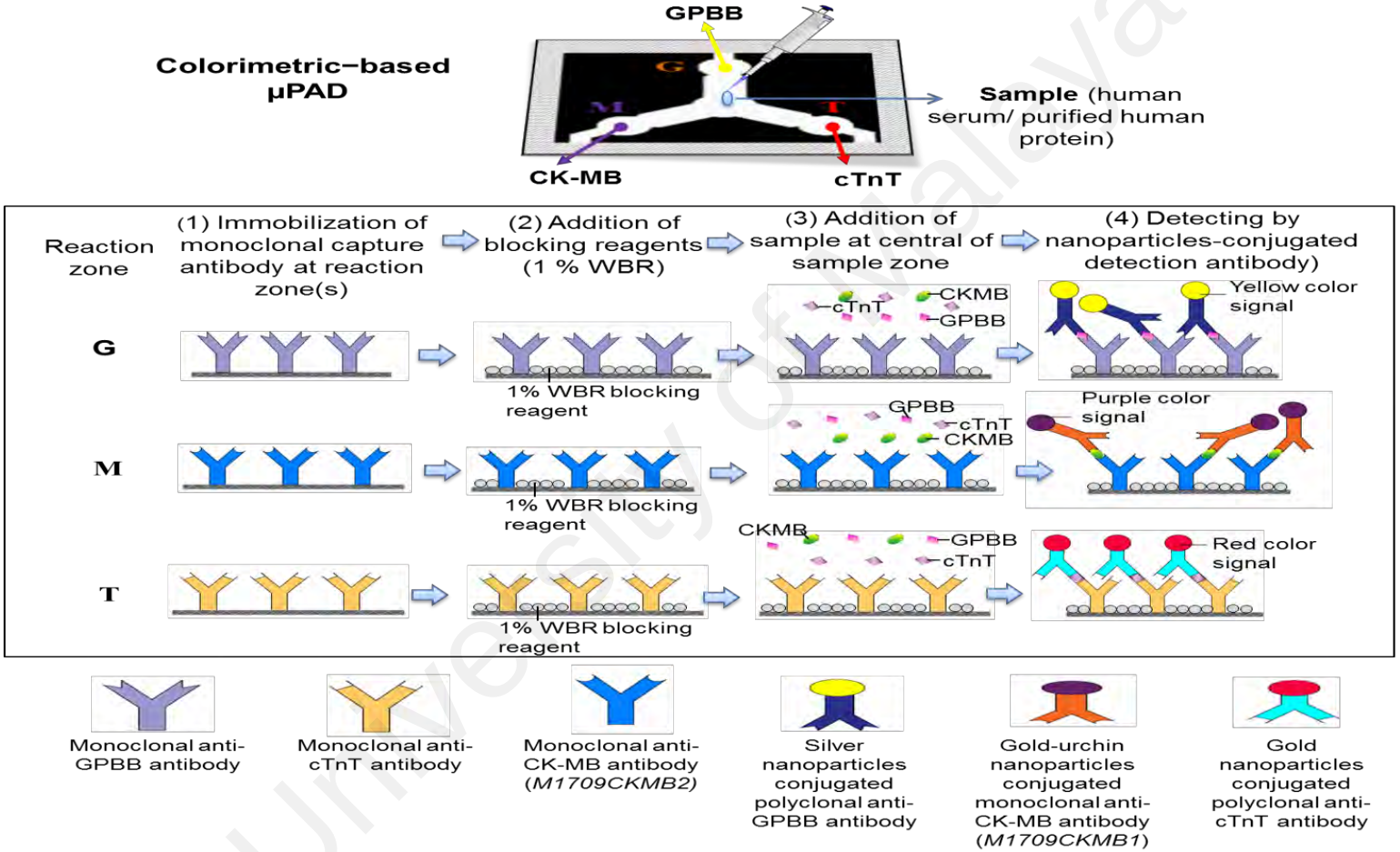

Figure 3.4: Schematic illustration of multiplex colourimetric detection of cardiac biomarkers at respective reaction zone(s), G for GPBB, M for CK−MB, and T for cTnT on µPAD.

University of Malaya

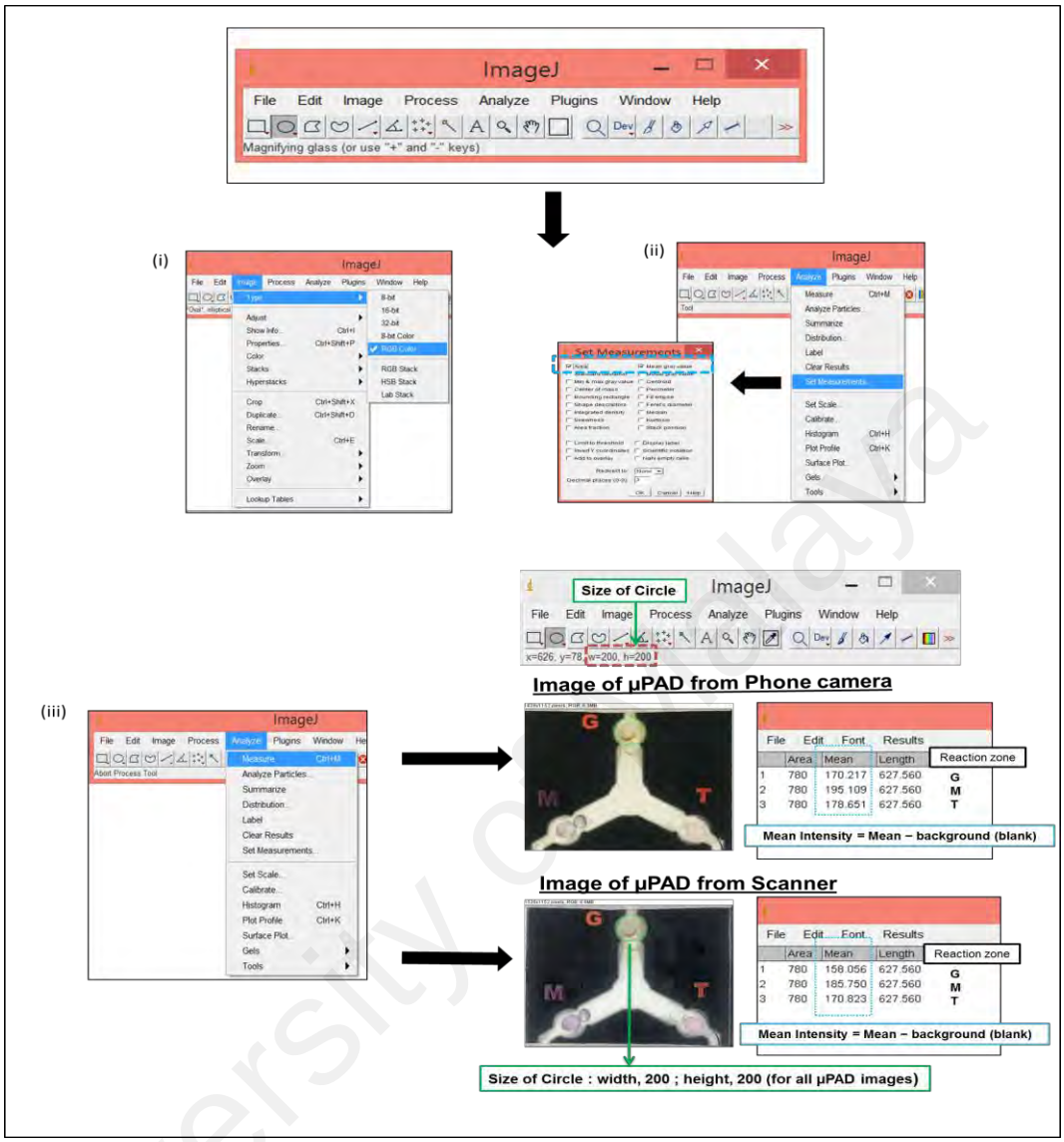

Figure 3.5: The measurement procedure of colour intensity in Image J.

3.2.1 Conjugation of Nanoparticles with Detecting Antibodies

For colourimetric assay, the flocculation assay was performed as described by Thobhani et al. (2010) in order to determine the ideal condition for conjugation of nanoparticles with detecting antibodies. Hence, the ideal pH and concentration of antibody loaded onto the nanoparticles required to stabilise those colourimetric conjugates were studied. Three types of colourimetric conjugates were prepared for multiplex detection of cardiac biomarkers, comprising silver gold nanoparticles-

University of Malaya

conjugated polyclonal anti-GPBB detecting antibody (yellow colour); gold urchin nanoparticles-conjugated polyclonal anti-CK−MB detecting antibody (purple colour); and gold nanoparticles-conjugated polyclonal anti-Troponin T detecting antibody (red colour).

For ideal pH determination, each type of nanoparticles (e.g., 40 nm diameter silver nanoparticle, 50 nm diameter gold-urchin nanoparticles and 40 nm diameter 50 nm avg. part. size gold nanoparticles) was adjusted to a pH range of 5.0 to 9.0 by 0.2 M K_2CO_3, under a constant antibody concentration of 10 μg mL^{-1}. Next, 10% sodium chloride (NaCl) was added into each well and colour change resulting to the collapse and aggregation of nanoparticles was observed after 10 minutes. An Infinite® M200 PRO microplate reader (Tecan Group Ltd, Männedorf, Switzerland) was used to measure the difference in absorbance before and after treatment of 10% NaCl at their respective wavelength — silver nanoparticles were measured at 412 nm; gold-urchin nanoparticles were measured at 557 nm; and gold nanoparticles were measured at 523 nm. For determination of optimal concentration of antibody which is required to stabilise the conjugates; the ideal pH adjusted metal nanoparticles were then titrated with different range of antibody concentrations at 1 μg mL^{-1}, 3 μg mL^{-1}, 5 μg mL^{-1}, 10 μg mL^{-1}, 30 μg mL^{-1}, and 40 μg mL^{-1}. The stability of the conjugates across the antibody concentration range was assessed as described above.

With the ideal concentration of antibody and pH were determined, the conjugates were conjugated on a large scale for assay as shown in **Figure 3.6**, where **(i)** Silver conjugate was prepared with 2 mL colloidal silver nanoparticles adjusted to pH 7.0 and polyclonal anti-GPBB detecting antibody at final concentration of 10 μg mL^{-1}. **(ii)** Gold-urchin conjugate was prepared with 2 mL colloidal gold-urchin nanoparticles adjusted to pH 8.0 and monoclonal anti-CK−MB detecting antibody at final

concentration of 10 µg mL^{-1}. **(iii)** Gold conjugate was prepared with 2 mL colloidal gold nanoparticles adjusted to pH 7.0 and polyclonal anti-Troponin T detecting antibody at final concentration of 10 µg mL^{-1}. All conjugates were incubated and shaken on an orbital shaker at 100 RPM for 1 hour at room temperature (25°C). After incubation for 1 hour at room temperature (25°C), 1% (w/v) BSA was added to each conjugate for stabilising of the nanoparticles-antibodies complex and the mixture was shaken for another 1 hour. All conjugates were centrifuged at 10000 RPM for 30 minutes at 4°C to obtain a soft pellet. Most of the supernatant was removed and the pellet re-suspended into 0.01 M phosphate buffer containing 1% (w/v) BSA. Lastly, all the prepared conjugates were stored at 4°C and ready for use.

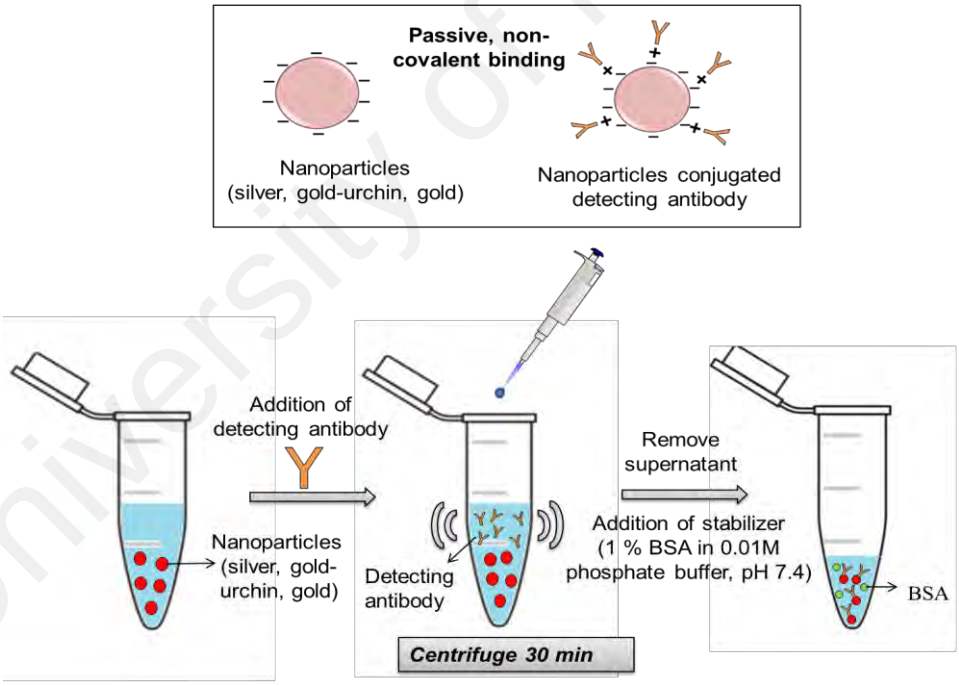

Figure 3.6: Preparation of colourimetric conjugates–nanoparticles-labeled detecting antibody.

University of Malaya

3.2.2 Characterisation of Colourimetric Conjugates

The successful conjugations for three nanoparticles were confirmed with the UV−Visible absorption spectra using an Infinite® M200 PRO microplate reader (Tecan Group Ltd, Männedorf, Switzerland). The absorbance values of each colourimetric conjugates were recorded at wavelength which ranged from 300 to 800 cm^{-1}. In addition, the size and surface charge characterisation of nanoparticles (before conjugation) and conjugates (after conjugation) were assessed by dynamic light scattering and zeta potential respectively, using a Zetasizer Nano ZS (Malvern Instruments Ltd, Malvern, UK). Measurements were performed before and after conjugation and recorded as the average of the three test runs.

3.2.3 Qualitative Colourimetric Analysis

The ideal cutoff level of each cardiac marker used for qualitative analysis (for naked eye judgment) was determined. A serial of concentration of each cardiac biomarker was tested at 5 ng mL^{-1}, 10 ng mL^{-1} and 20 ng mL^{-1} for GPBB; 1 ng mL^{-1}, 5 ng mL^{-1}, and 10 ng mL^{-1} for CK−MB; while 0.05 ng mL^{-1}, 0.1 ng mL^{-1} and 1 ng mL^{-1} for cTnT. The determined ideal cutoff level was then used as the guidelines for qualitative analysis. For qualitative analysis, the presence or absence of cardiac markers in a sample was detected as negative (undetectable below the cutoff level at concentration of 1 ng mL^{-1} for GPBB and CK−MB and 0.05 ng mL^{-1} for cTnT) or positive (detectable at or above the cutoff level at the concentration at 10 ng mL^{-1} for GPBB, CK−MB and cTnT).

3.2.4 Semi-Quantitative Colourimetric Analysis

On the other hand, the risk stratification of heart condition was categorised as low risk, moderate (within borderline) and high risk based on the 99th upper reference limit (URL) for each cardiac marker ─ GPBB, CK−MB and cTnT (**Table 3.2**). For

semi−quantitative analysis, the risk levels tabulated as a reference chart based on the signal intensity of each cardiac marker ─ GPBB, CK−MB and cTnT and, which is proportional to the concentration of each cardiac marker.

Table 3.2: Upper reference limit for three cardiac markers ─ GPBB, CK−MB and cTnT categorised as low risk, moderate risk (within borderline), and high risk.

Cardiac Markers	Condition		
	Low Risk	**Moderate**	**High Risk**
GPBB	< 8 ng mL^{-1}	8 to 12 ng mL^{-1}	≥ 15 ng mL^{-1}
CK−MB	< 5 ng mL^{-1}	5 to 10 ng mL^{-1}	≥ 10 ng mL^{-1}
cTnT	< 0.1 ng mL^{-1}	1 to 10 ng mL^{-1}	≥ 100 ng mL^{-1}

3.2.5 Quantitative Colourimetric Analysis

For quantitative analysis, calibration curves for reflectance detection was created by eight purified samples with human protein GPBB, CK−MB and cTnT in the following concentration ranges: 0─100 ng mL^{-1} for GPBB and CK−MB; 0─200 ng mL^{-1} for cTnT, respectively. The limits of detection (*LOD*) for each cardiac biomarker was determined based on the degree of visibility on μPAD in the calibration plot. The procedure of sandwich colourimetric assay was conducted on the fabricated μPAD as described in Section 3.2. For quantification of colour intensity on μPAD, the μPAD images were scanned using a PIXMA E610 series scanner (Canon, Tokyo, Japan). Each image was saved as a tiff file with 600 dpi resolution whereas images captured by a Xiaomi Mi 4i smartphone camera (13 megapixels) were saved as a JPEG file. The Image J software programme was used to measure the mean value of RGB colour of the image. Parameters such as area and mean intensity were selected. The mean intensity for each data point was obtained using the histogram function in Image J by circling the

University of Malaya

area of each test zone, G, M, and T in a digital image of the μPAD that which was obtained using a desktop scanner and smartphone-based camera.

3.3 SERS Assay Procedure on Microfluidic Paper-Based Analytical Device

Figure 3.7 is a schematic that illustrates SERS multiplex detection of cardiac biomarkers on μPAD. The general principle of SERS immunoassay is similar to colourimetric immunoassay as described in Section 3.2. The main difference was that readout signal is SERS instead of colourimetric signal detected with SERS probes. For instance, silver SERS probe conjugated polyclonal anti-GPBB detecting antibody, gold−urchin SERS probe conjugated polyclonal anti-CK−MB detecting antibody, gold SERS probe conjugated polyclonal anti-cTnT detecting antibody was added at their respective reaction zones. Then, a sandwich immuno-complex was formed via antibody-antigen interaction on the NC membrane. For quantification, the amount of captured biomarkers (target analytes) on membrane was reflected in the intensity of the SERS signals, a SERS spectrum ─ which is a "fingerprint" profile that is unique to the Raman reporter molecules. The characteristic peak of each Raman reporter molecule was determined, i.e., 4−nitroanilline at 1387 cm^{-1} for GPBB; tert-Butylhydroquinone at 1450 cm^{-1} for CK−MB; and methyl red at 1400 cm^{-1} for cTnT. The limit of detection (*LOD*) for cardiac biomarker quantitative SERS measurement was determined using the following Equation (3.1).

$$Limit\ of\ Detection\ (LOD) = \frac{3 \times standard\ deviation\ of\ blank}{mean\ of\ blank} \quad (3.1)$$

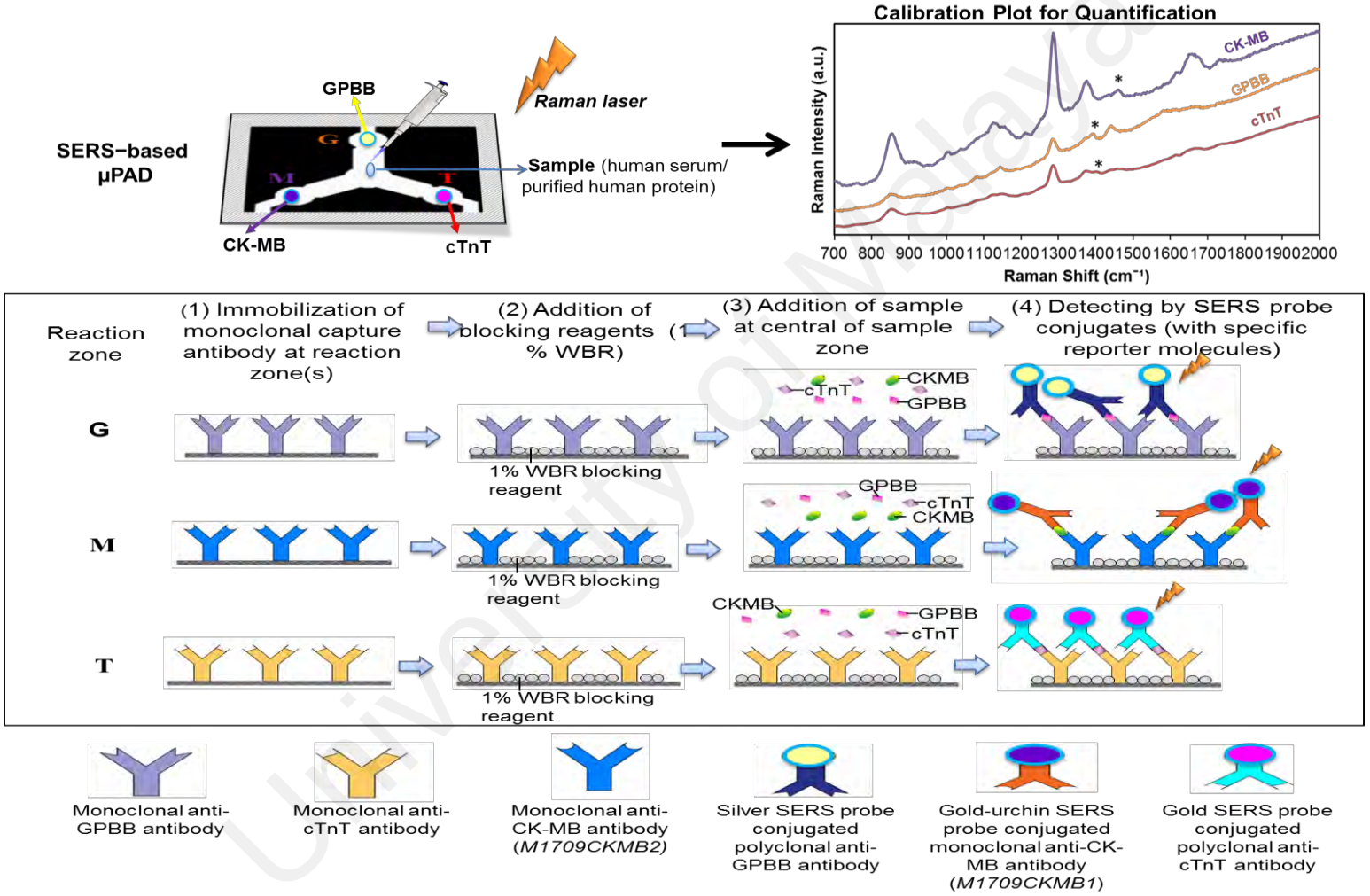

Figure 3.7: Schematic illustration of multiplex SERS detection of cardiac biomarkers at respective reaction zone(s), G for GPBB, M for CK−MB, and T for cTnT on μPAD.

3.3.1 Conjugation of SERS Probe with Detecting Antibodies

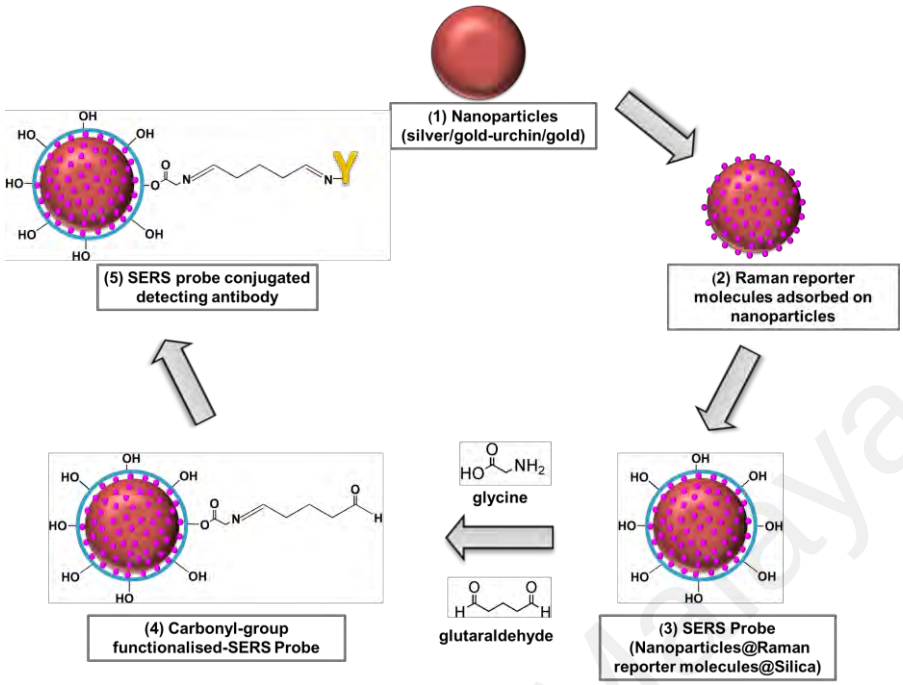

SERS Probe	Nanoparticles	Raman reporter molecules	Analyte detection
Silver SERS Probe	Silver	4-nitroanilline	GPBB
Gold-urchin SERS Probe	Gold-urchin	tert-Butylhydroquinone	CK-MB
Gold SERS Probe	Gold	Methyl Red	cTnT

Figure 3.8: Preparation of Raman SERS probe conjugated with detecting antibodies for Raman SERS assay.

For Raman SERS assay, SERS probe was prepared as the alternative indicator for quantification. The SERS tag was prepared via absorption of the Raman active molecule (used as Raman reporter) on the surface of nanoparticles (act as signal enhancer). In this study, three types of SERS probe (nanoparticles@Raman reporter molecule@silica) were prepared as described by Gao et al. (2017), with slight modification. As shown in **Figure 3.8**, the Raman reporter molecules such as 4-nitroanilline, tert-Butylhydroquinone, methyl red were attached to the surface of each type of nanoparticles—silver, gold-urchin, and gold particularly and then encapsulated with a silica shell to form a unique SERS probe. For instance, silver nanoparticles@4-

University of Malaya

nitroaniline@silica; gold-urchin nanoparticles@tert-Butylhydroquinone@silica; and gold nanoparticles@methyl red@silica.

For preparation of SERS probes, 10 µL of 1.0 mM Raman reporter molecules (i.e., 4-nitroanilline/tert-Butylhydroquinone/methyl red) was added into 500 µL colloid nanoparticles (silver/gold-urchin/gold) under continuous shaking at 100 RPM for 1 hours. Then, 5 µL each of tetraethyl orthosilicate and ammonium solution were added into the mixture in sequence for silica coating. After the SERS probes were formed, the resulting solutions were centrifuged and re-suspended in 500 µL of 10% ethanol solution. First, to functionalise the SERS-probes, the hydroxyl (−OH) groups on the surfaces of the probes were modified into primary amine functional groups with the addition of a 1 M glycine solution followed by the addition of 1% glutaraldehyde to induce a primary amine-aldehyde (glutaraldehyde) chemical reaction and form imine. At this point, the carbonyl (aldehyde) functionalised-SERS probe was successfully synthesised. Thereafter, 10 µL of 1 mg mL^{-1} detecting antibody (i.e., polyclonal anti-GPBB detecting antibody, monoclonal anti-CKMB detecting antibody and polyclonal anti-cTnT detecting antibody) was added and incubated overnight with respective carbonyl-functionalised-SERS probe to prepare the SERS conjugates via an aldehyde-primary amine reaction. After being centrifuged, the final SERS probes were obtained and stored in an eluent buffer (0.01 M phosphate buffer containing 1% BSA) for further use. **Figure 3.9** shows a clear structural equation that indicates the SERS probe's comprehensive synthesis process in conjugation with the detecting antibodies.

University of Malaya

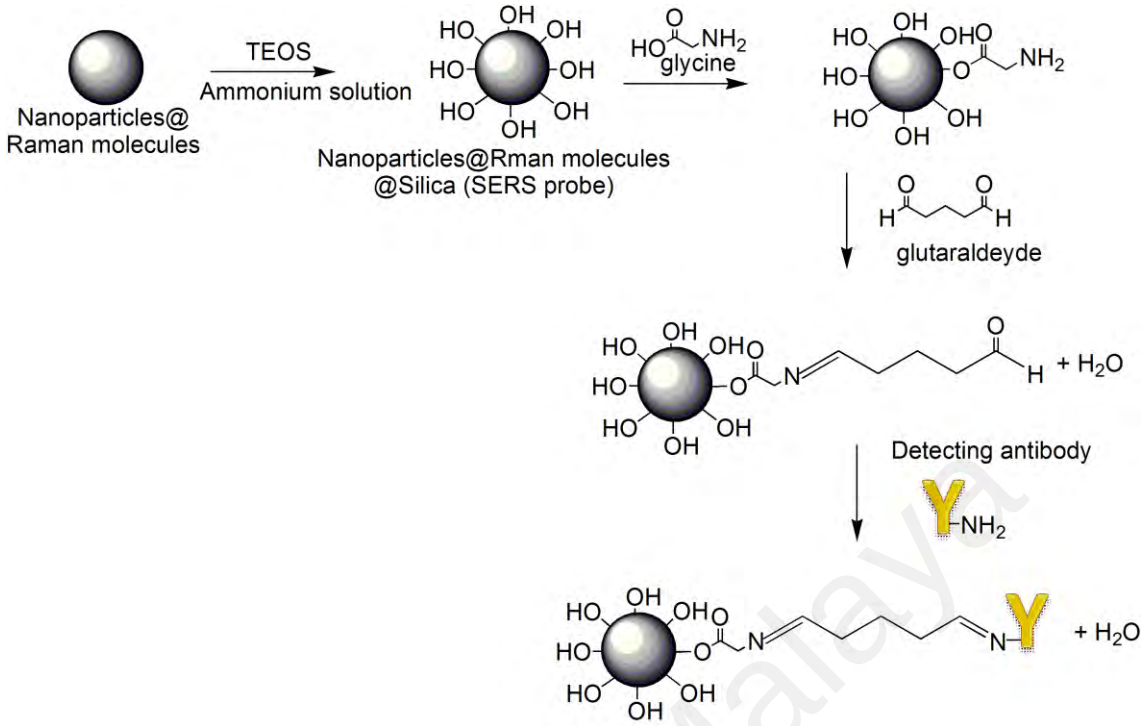

Figure 3.9: Structural equation showing the SERS probe's thorough synthesis mechanism conjugates with the detecting antibodies.

3.4 Characterisation of SERS Conjugates

Three types of SERS nanoparticles (i.e., silver, gold-urchin and gold) that were coated with silica at outer surface were further confirmed by the UV-Visible absorption spectra. The UV-visible absorption spectra of these SERS nanoparticles were measured at wavelength ranging from 300 to 800 nm using UV-2600 UV-Vis Spectrophotometer (Shimadzu, US). Subsequently, Fourier transform infrared (FTIR) spectra were measured from 400 to 4000 cm^{-1} at a resolution of 4 cm^{-1} using Spectrum™ 400 (Perkin Elmer, USA), to ensure that the SERS probe was well-functionalised with carbonyl group and well-conjugated with detecting antibody.

Moreover, Raman spectroscopy was used for confirmation in each stage of Raman SERS Probe during conjugation and to determine the characteristics peak of each Raman probe on a NC membrane. In each SERS probe, the adsorbed Raman reporter molecules used to detect GPBB, CK−MB and cTnT were 4-nitroaniline, tert-

University of Malaya

Butylhdyroquinone and methyl red, respectively. For confirmation of each conjugation stage of SERS probe, 1 μL of prepared solution was dropped and dried on a silicone slide. The SERS signal was then determined from each Raman reporter molecule that has absorbed on the surface of nanoparticles. For instance, (i) Raman reporter molecules; (ii) nanoparticles@ Raman reporter molecule; (iii) nanoparticles@ Raman reporter molecules@silica (SERS Probe); and (iv) SERS Probe conjugated detecting antibody (SERS probe conjugate). The readout signal was produced as a SERS spectrum ─ which is a "fingerprint" profile that is unique to the Raman reporter molecules. Thus, the Raman spectrum of SERS probe obtained on silicon slide was used as a reference throughout this study and then compared with the peak of SERS probe obtained on NC membrane (paper substrate). The samples were analysed under a Renishaw InVia Raman microscope with the 514 nm laser excitation wavelength under a 20× objective lens focused on a μPAD. The laser power was adjusted to 10% at an acquisition time of 10 s at 700 to 2000 cm^{-1}.

3.4.1 Quantitative SERS Analysis

To generate a calibration plot for quantitative SERS analysis, various concentration of cardiac biomarkers was tested, 0─100 ng mL^{-1} for GPBB and CK−MB; 0─200 ng mL^{-1} for cTnT. The SERS probe conjugates were used as an indicator for quantitative assays. The SERS signals on SERS-based μPAD were measured using Renishaw InVia Raman microscope and identified via their peak characteristic of each Raman reporter such as 4-nitroanilline at 1387 cm^{-1} for GPBB assay; tert-Butylhydroquinone at 1450 cm^{-1} for CK−MB assay and methyl red at 1400 cm^{-1} for cTnT assay. The mean of Raman intensity of each Raman reporter molecules was measured with three replicate measurements. Error bars represented the standard deviation of triplicates for each data point.

3.5 Analytical Performance of Microfluidic Paper-Based Analytical Device for Colourimetric and SERS Assay

The analytical performance of μPAD comprised optimisation of blocking reagent, reproducibility test, long-term stability test (28 days), intra-day (within same day) and inter-day (consecutive 3 days) precision assay, cross-reactivity test, clinical sample analysis (for CK−MB only) was studied for both colourimetric assay and SERS assay in this section. For colourimetric-based μPAD, the nanoparticles (i.e., silver, gold-urchin and gold) were used as the colourimetric indicator for multiplex detection of cardiac biomarkers such as yellow colour for GPBB, purple colour for CK−MB and red colour for cTnT. Then, colourimetric signals were measured by the Image J colour image analysis software (NIH, Bethesda, MD, USA). In contrast, for SERS-based μPAD, the SERS probe (nanoparticles@Raman reporter molecules@silica) was used as Raman nanotags for quantification of multiple cardiac biomarkers. In other words, the different nanoparticles were used as the signal enhancer to increase the enhancement factor of the Raman reporter molecules on the probe for triggering high SERS signals. The SERS intensity signals were measured by using Renishaw InVia Raman Microscope.

3.5.1 Optimisation of Blocking Reagents

The vital role of blocking is to block the unoccupied binding surfaces on the membrane so as to reduce background interference, improved signal-to-noise ratio, and minimal non-specific binding. To select the suitable blocking reagents for μPAD, several blocking reagents (protein, polymer and non-ionic detergent) including western blocking reagent (WBR) containing casein; bovine serum albumin (BSA); polyvinylpyrrolidone (PVP); and Tween 20 were tested for blocking non-specific sites on NC membrane. In this study, positive μPAD (tested with 10 μg mL^{-1} purified protein) and negative μPAD (blank) (tested with 0.01 M phosphate buffer) were

conducted on the fabricated μPAD. The colourimetric signals generated on μPAD was photographed by the smartphone-based camera and scanner, then analysed using computer programmed with Image J software programme (NIH, Bethesda, MD, USA). Alternatively, SERS signals generated on μPAD were measured using Renishaw InVia Raman Microscope. The signal-to-background ratio was calculated by dividing the signal produced on positive μPAD with the background (signal on negative μPAD) for both colourimetric and Raman SERS assays.

3.5.2 Reproducibility Studies

The reproducibility of fabricated μPAD was assessed by examining five fabricated μPAD. For detection, 1 μL of sample (purified human protein diluted with 0.01 M phosphate buffer, pH 7.4) with concentration 10 ng mL^{-1} of GPBB, CK−MB and cTnT was applied on the central sample zone on fabricated μPAD. The fluids were travelled to the reaction zones by capillary action and direct sandwich reaction was induced by adding respectively the colourimetric conjugates for colourimetric assay or SERS probe conjugates for Raman SERS assay. Colourimetric signals were measured by the Image J colour image analysis software (NIH, Bethesda, MD, USA) whereas SERS signals were measured by using Renishaw InVia Raman Microscope. The mean intensity of each biomarker was determined and the relative standard deviation (*RSD*) was calculated for the total of five tested fabricated μPAD by dividing the standard deviation of the data by means of the data set, expressed as a percentage using the following Equation (3.2).

$$Relative\ Standard\ Deviation\ (RSD) = \frac{standard\ deviation}{mean} \times 100 \qquad (3.2)$$

University of Malaya

3.5.3 Intra-and Inter-day Precision Studies

The intra and inter-day assays were assessed to evaluate the precision of an assay on both colourimetric-based µPAD and SERS-based µPAD. For intra-day precision test, three fabricated µPAD were examined using GPBB, CK−MB and cTnT specimen levels at 10 ng mL^{-1}, 50 ng mL^{-1} and 100 ng mL^{-1} within the same day. For inter-day precision test, a further three fabricated PAD were examined using GPBB, CK−MB and cTnT specimen levels at 10 ng mL^{-1}, 50 ng mL^{-1} and 100 ng mL^{-1} on three consecutive days. Colourimetric signals were measured by the Image J colour image analysis software (NIH, Bethesda, MD, USA) whereas SERS signals were measured by using Renishaw InVia Raman Microscope. The mean intensity of the produced colourimetric and Raman SERS signals was determined for each biomarker and then the coefficient of variation (*CV*) percent was calculated as the ratio of the standard deviation of the sample to the mean of the sample, expressed as a percentage using Equation 3.3.

$$Coeffient\ of\ Variation\ (CV) = \frac{standard\ deviation}{mean} \times 100 \qquad (3.3)$$

3.5.4 Stability Studies

Six silica gel-filled aluminum pouches, each with three µPADs have immobilised their respective capture antibodies. They were then packed for 28 days in a 4 °C refrigerator. For stability test, three µPADs (kept inside a pouche) were tested on day 1, 3, 7, 14, 21, and 28 with the sample (containing purified human protein GPBB, CK−MB and cTnT at 10 ng mL^{-1}) diluted with 0.01 M phosphate buffer, pH 7.4 all the way through the study. Colourimetric signals were measured by the Image J colour image analysis software (NIH, Bethesda, MD, USA) whereas SERS signals were measured by using Renishaw InVia Raman Microscope. The mean intensity of generated colourimetric and Raman SERS signals for each biomarker was measured and then the

coefficient of variation (*CV*) % was calculated using Equation (3.3). The stability of the μPAD was evaluated on the basis of the minimum signal loss over 28 days.

3.5.5 Cross-reactivity Studies

The cross-reactivity test was performed to ensure that the assay performed on the μPAD is accurate and reliable in clinical applications, as well as to minimise the risk of misinterpretation of results due to false positive signal. For colourimetric assay, a non-spiked sample (containing three cardiac biomarkers only) and three spiked samples (separately spiked with three different endogenous substances) were examined for cross-reactivity test. The cross-reactant was then spiked in human serum containing cardiac biomarkers with certain concentration such as 100 μg mL^{-1} uric acid, 100 μg mL^{-1} ascorbic acid, and 100 mg mL^{-1} human serum albumin. The colourimetric signals generated on μPAD were captured by a smartphone-based camera or scanner and then quantified by the Image J colour image analysis software (NIH, Bethesda, MD, USA). Conversely, the SERS assay was quantified sensitively than colourimetric assay, even when there was no colour seen with the naked eyes on μPAD. For SERS assay, a sample (containing three cardiac biomarkers only) and three individual cross-reactants were tested directly on μPAD. The SERS signals were measured by using Renishaw InVia Raman Microscope.

3.5.6 Clinical Sample Analysis

A series of different sera concentration of CK−MB in the range of 1.2 to 12.18 ng mL^{-1} were collected from University Malaya Medical Center (UMMC). A clinical sample analysis was conducted to evaluate the utility of the μPAD for clinical usage. In UMMC, the standard cardiac biomarkers for ruling out AMI are Troponin I (in plasma) and CK−MB (in serum) using Siemens Centaur XPT Immunoassay System. However,

only CK−MB biomarker was matched with this work, therefore cTnT and GPBB were excluded in this section. 10 µL human serum sample was dispensed directly at the central sample zone on NC membrane, then the fluid was moved forward by capillary action to reaction zone(s) – G for GPBB, M for CK−MB and T for cTnT. The desired analyte was captured by immobilised capturing antibody at each reaction zone(s), and then sandwiched by their conjugates using a colourimetric (nanoparticle-labeled detecting antibody) or SERS assay (SERS probe conjugated detecting antibody). Lastly, the generated colour dot signal for colourimetric or SERS sandwich assay on the µPAD was observed. To obtain the quantitative colourimetric results, the image of µPADs was captured using a desktop scanner and smartphone-based camera, then imported into Image J software and the intensity of each signal was quantified. On the other hand, the quantitative SERS signals were obtained using the Renishaw InVia Raman Microscope.

3.5.7 Method Comparison

First of all, the CK−MB levels in 12 human sera were assessed by Siemens Centaur XPT Immunoassay System (as the standard reference method) in UMMC. For method validation, the results values on proposed µPAD obtained from smartphone-based camera, desktop scanner, and Renishaw InVia Raman Microscope were compared with the results value obtained from Siemens Centaur XPT Immunoassay System (reference method). The correlation and regression analysis and Batman and Altman plot was performed for comparing these three methods such as Siemens Centaur XPT Immunoassay System (labeled as I), fabricated µPAD captured using smartphone-based camera (labeled as II); fabricated µPAD captured using desktop scanner (labeled as III) and Renishaw InVia Raman Microscope (labeled as IV). Moreover, independent T-test was performed to investigate the significant differences observed between these two methods in pair of I and II or I and III or I and IV, respectively.

University of Malaya

3.6 Multivariate Statistical Analysis

Multivariate analysis is a set of statistical analysis to understand the relationship between variables (Raman spectra of cardiac biomarkers) and the relevance of the variables with the problem (concentrations of relevant cardiac biomarkers) being studied. These variables may be correlated with each other, and their statistical dependence is often taken into account when analysing such data. Two multivariate statistical techniques, principal component analysis (PCA) and partial least square (PLS) regression were performed using MATLAB R2018b (MathWorks, Inc., Natrick, MA) in this study for SERS-based μPAD only . The Raman spectra in the range of 700 cm^{-1} to 2000 cm^{-1} have been used to investigate the vibrational modes of three different Raman reporter molecules that represents each respective cardiac biomarker: such as 4-nitroanilline for GPBB biomarkers, tert-Butylhydroquinone for CK−MB biomarkers and methyl red for cTnT biomarkers.

3.6.1 Principal Component Analysis

Principal component analysis (PCA) is a technique employed to reduce the dimensionality of a set of variables while retaining the maximum variability in terms of variance-covariance structure. By reducing the dimension of data, it will help us to visualise the data better. For example, a principal component (PC) model transforms a set of ten variables into a new set of two-dimensional PC model, while preserving as much information contained in the data as possible. In this study, the ultimate goal of PCA is to separate all the obtained data into three main groups (i.e., GPBB, CK−MB and cTnT) by using the optimal number of PCs. The optimal number of PCs with the most discriminatory power could successfully discriminate between different groups of cardiac biomarkers via their characteristics Raman spectral.

University of Malaya

In this study, Raman spectra (consisted 550 wavelength number) of three different groups of cardiac biomarkers ─ GPBB, CK−MB and cTnT were presented to PCA algorithm. Then, the data split with 81% of the dataset (100 Raman spectra) were identified as training sets and the remaining 19% (23 Raman spectra) were identified as testing sets. Testing sets are important in order to validate the PCA model. The score plot is a projection of data onto two-dimensional diagram. It is used to display the two PCs newly computed variable from PCA. Coefficients computed from PCA model based on training sets were then tested with testing sets and the *k*-nearest neighbours' algorithm (*k*-NN) was employed for the classification of the cardiac biomarkers. The accuracy of the PCA-k-NN algorithm for predicting respective cardiac biomarkers among the three groups was determined.

However, the number of Raman spectra used for PCA study is different for three groups of cardiac biomarkers, such as 27 Raman spectra for GPBB (9 standard concentration ranged from 0.01 ng mL^{-1} ─ 100 ng mL^{-1}); 63 Raman spectra for CK−MB, which included nine different standard concentration of cardiac biomarkers ranged from 0.01 ng mL^{-1} ─ 100 ng mL^{-1} (27 Raman spectra) and twelve clinical sample with concentration range from 1.2 ng mL^{-1} ─ 12.18 ng mL^{-1} (36 Raman spectra); and 33 Raman spectra for cTnT (11 standard concentration ranged from 0.001 ng mL^{-1} ─ 200 ng mL^{-1}).

3.6.2 Partial Least Square Regression

Partial Least Squares (PLS) is a widely used technique in chemometrics, especially in the case where the number of independent variables is significantly larger than the number of data points. It finds a linear regression model by projecting the predicted variables (i.e., independent variable (predicted concentration of cardiac biomarkers)) and the observable variables (i.e., dependent variable (known concentration of cardiac

biomarkers)) to a new space. In this study, leave-one-out (LOO) was used as the cross-validation technique for PLS due to the reason of the limited number of sample in the dataset. In LOO analysis, one sample is left out of the calibration set at a time. Then, the PLS model is developed using the remaining data and then applied to the singular sample. To build up a set of validation result, the process is repeated by leaving each sample out, one at a time. The predicted concentration of this sample is then compared to the actual concentration and is used to evaluate the quality of the model. LOO cross-validation enables validation of a new technique even in a relatively small dataset. In addition, the prediction error in the calibration and validation sets was determined by calculating the root mean square error of prediction using the Equation (3.4), where *conc* represents the actual concentration of a sample, *pred* represents the predicted concentration for that sample, and *n* is the total number of samples. Moreover, the optimal number of components (also termed as latent variable) used for PLS calibration was determined by selecting the minimum error revealed in the root mean square prediction plot.

$$Root\ mean\ square\ prediction = \sqrt{\frac{(conc_1 - pred_1)^2 + (conc_2 - pred_2)^2 + \cdots + (conc_n - pred_n)^2}{n}} \quad (3.4)$$

University of Malaya

CHAPTER 4: RESULTS AND DISCUSSION

4.1 Fabrication Parameters of Microfluidic Paper-Based Analytical Device

4.1.1 Optimisation of Heating Time and Temperature

For the fabrication of μPAD, the heating time and heating temperature were optimised to control the extent of wax spreading and penetration into the membrane to form a hydrophobic barrier through heating using an oven. The black colour of the printed wax turned grey after baking, indicating that the wax has melted and penetrated into the membrane. The heating time and temperature have led to a change in the channel width due to the wax spreading. The higher the heating temperature, the melted wax not only spread faster into the paper substrate but also narrowed the width of the channel. In this case, the optimal heating time and temperature were determined by the ratio of wax spreading, which is measured by dividing the measured width of channel with the desired width of channel (50 mm). The printed μPADs were tested for viability upon varying the heating temperature (50°C, 100°C, 120°C) and heating time (3 minutes, 5 minutes, 10 minutes and 15 minutes) after the desired channel width was measured.

As shown in **Figure 4.1**, the wax spreading ratio of 0.99 over 1 did not vary with the heating time from 3 minutes to 15 minutes at heating temperature, 50°C. In addition, the colour of the printed wax on μPAD also did not show any changes. The optimum baking time and temperature for the fabrication process was proposed at 100°C with 5 minutes heating time. The width of the desired channel was designed with 50 mm diameter; however it was reduced to 44 mm after baking at optimum condition as mentioned above. The wax spreading ratio of 0.87 over 1 was determined. The reduced width channel indicated that wax has melted and penetrated into the membrane and formed a hydrophobic barrier. A similar result was also found by baking at 120°C for 3 minutes, but the NC membrane card began to bend due to the high heating temperature.

University of Malaya

Thus, the heating temperature was recommended to be not more than 120°C with heating time around 5 minutes. Other conditions that are not suitable to be used for fabricating because of wax spreading ratio of 0.42 to 0.8 over 1 was determined, which indicates too much melted wax have spread and narrowed the hydrophilic channel.

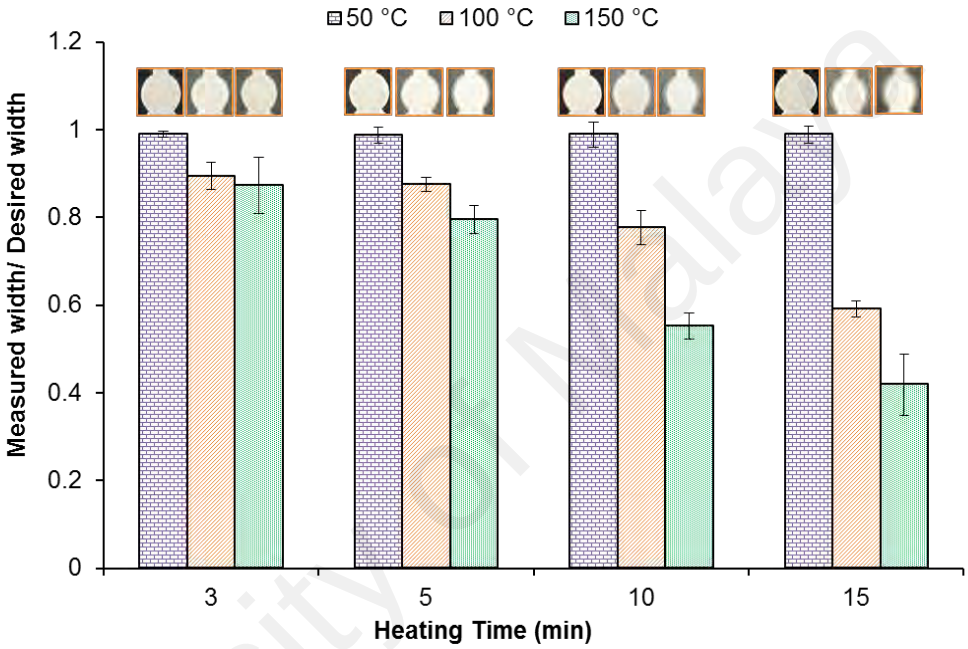

Figure 4.1: Optimisation of heating time and temperature for µPAD fabrication.

Indeed, the width of hydrophilic channel and reaction zones on paper substrate could be selected depending on the application required. Most of the previous report on µPAD was designed with a smaller width (µm to mm) using various wax printing methods, which are dependent on their pattern design (Carrilho et al., 2009a; Dungchai et al., 2011; Lu et al., 2009a; Lu et al., 2009b; Songjaroen et al., 2011). For instance, Songjaroen et al. (2011) designed a Y shape paper device that composed of two test zones with 3 mm width of circular shape for the simultaneous detection of glucose and protein. After the wax dipping process, the width of reaction zone obtained was 3.91 ± 0.06 mm using 3 mm width of the iron mold (1 mm thick). This is because the total

width of the hydrophilic channel as well as the reaction zone will also include the thickness width of the designed mold. For wax printing, Lu et al. (2009a) also reported that the melted wax penetrated into the paper after heating, resulting to the reduction of the channels width from 1 mm to about 0.5 mm after heating.

In this work, the fabricated µPAD was used for the colourimetric detection of three cardiac biomarkers (GPBB, CK−MB and cTnT), with three different colours of nanoparticles used as the colour indicator. The colour signal of this fabricated µPAD was quantified based on the colour intensity provided by nanomaterials, instead of from colour change from colour reagents (e.g., glucose oxidase and horseradish peroxidase (HRP) as reported in other paper-based devices). Hence, the original idea of my design is to interpret the result on µPAD at the colour dot reaction zone (diameter ~30 mm) instead of 50 mm diameter (note: 44 nm diameter after heating) as shown in **Figure 4.2**. This is because when 1 µL of the capturing antibody was immobilised at each reaction zone, it will occupy approximately 30 mm diameter after dried on the membrane. The main advantage of this design allows the end user to easily discern a positive result from a false positive result which might be due to the colour stain which resulted from the nanoparticles conjugates that got remained near the boundary of the reaction zone if the washing step was incomplete (**Figure 4.2**).

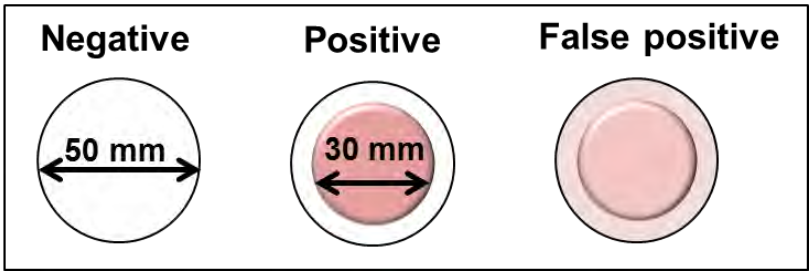

Figure 4.2: Result interpretation on µPAD at reaction zone (~30 mm diameter) instead of 50 mm diameter (44 nm diameter after heating).

University of Malaya

In short, the optimal heating time (5 minutes) and temperature (100°C) were selected for this μPAD fabrication process as these settings showed a minimal wax spreading ratio (0.87 over 1) and the melted wax was able to penetrate completely to the membrane (black colour wax being changed to grey colour).

4.1.2 Optimisation of Sample Volume and Colour Development Time

For selecting the ideal sample volume for μPAD, different volumes of blue dye solution includes 1 μL, 3 μL, 5 μL, 10 μL and 15 μL were tested onto the μPAD and allowed to travel along the hydrophilic channels from sample zone to each reaction zone(s). The travelled distance of fluid was observed in order to evaluate the minimal sample volume required to completely wet the μPAD. In **Figure 4.3a**, the result displayed that a volume of 10 μL and 15 μL can completely wet the μPAD with all three reaction zones ─ G, M and T. In other words, the sample volume 10 μL was sufficient to fully wet the multiple reaction zones. On the other hand, the experiment also revealed that too little sample volumes such as 1 μL, 3 μL and 5 μL lead to the incomplete wetting of reaction zones with significant difference in the flow distance, which did not entirely wet all the three detection zones.

In addition, the optimal time for colour development on μPAD was determined, which indicated the successful formation of sandwich between the capturing antibody and nanoparticles-labeled detecting antibody (colourimetric conjugates). The retention time of colourimetric conjugates at each reaction zone(s) was tested at 1 minute, 3 minutes, 5 minutes, and 10 minutes. The result as shown in **Figure 4.3b** was a slight increase in the colour signal produced on μPAD at the retention time of 1 minute, 3 minutes and also 10 minutes; however, the colour intensity decreased at 5 minutes. Herein, the retention time of 3 minutes was optimal for colour development because the colour signal measured at each reaction zone(s) of μPAD was obviously higher for the

University of Malaya

respective cardiac biomarkers. The extended retention time for colour development at 10 minutes was much better for CK−MB and cTnT assay; however, the colour development on μPAD was not recommended. This is because the high intensity was not caused by the development of the immune-complex sandwich; vice versa, as it was caused by unbound colourimetric conjugates which remained too long on the membrane, then it was completely dried and difficult to wash out of the reaction area, based on the observation during the experiment. On the other hand, the decrease in intensity during the 5-minute retention period was also caused by a similar problem that the colour stain caused by unbound colourimetric conjugates persisted in the test area after a long retention period; therefore, repeated washing was applied during the experiment to remove the dried colour stain from the membrane, causing the colour intensity to fall. In this case, it is not advisable to pick the μPAD retention time of 5 minutes and 10 minutes to avoid false positive results induced by stubborn colour stain. Finally, a retention period of 3 minutes was selected for an μPAD test to meet the requirement of rapid analytical time for AMI detection.

The sample volume required for an assay is dependent on the distinct pattern of μPAD. The optimal sample volume was decided by using a minimal amount of sample required to wet the entire pattern of μPAD. Additionally, the colour development time for a colourimetric assay was based on the change of colour reagent due to an enzymatic or chemical interaction between spotted reagents and the analyte. Usually, it requires extra time for the colour to fully develop. For instance, as reported previously by Martinez et al. (2007), a tree patterned μPAD with three separate test zones needed 5 μL sample solution for the determination of glucose and protein. The study reported that the assay required about 10−11 minutes for the paper to dry and for the colour to fully develop. Next, the square-patterned regions of μPAD developed by Yang et al. (2012) for determination of blood plasma glucose, required 7 μL of sample volume to obtain

the same performance. The assay was then allowed to develop for 5 minutes to produce colour change upon reaction with enzyme reagent.

In contrast, based on our experimental result, 10 µL was chosen as the optimal sample volume for this designed µPAD as the fluid is sufficient to reliably fill all three reaction zones. The suitable retention time for colour development was selected at 3 minutes because it showed the significant high colour intensity than other retention time. This indicates that the analytes were successfully sandwiched by capturing antibody and colourimetric conjugates with 3 minutes retention time. In short, my developed colourimetric-based µPAD allows for more rapid analysis as compared to other colourimetric assays (Martinez et al., 2007; Martinez et al., 2010b; Yang et al., 2012).

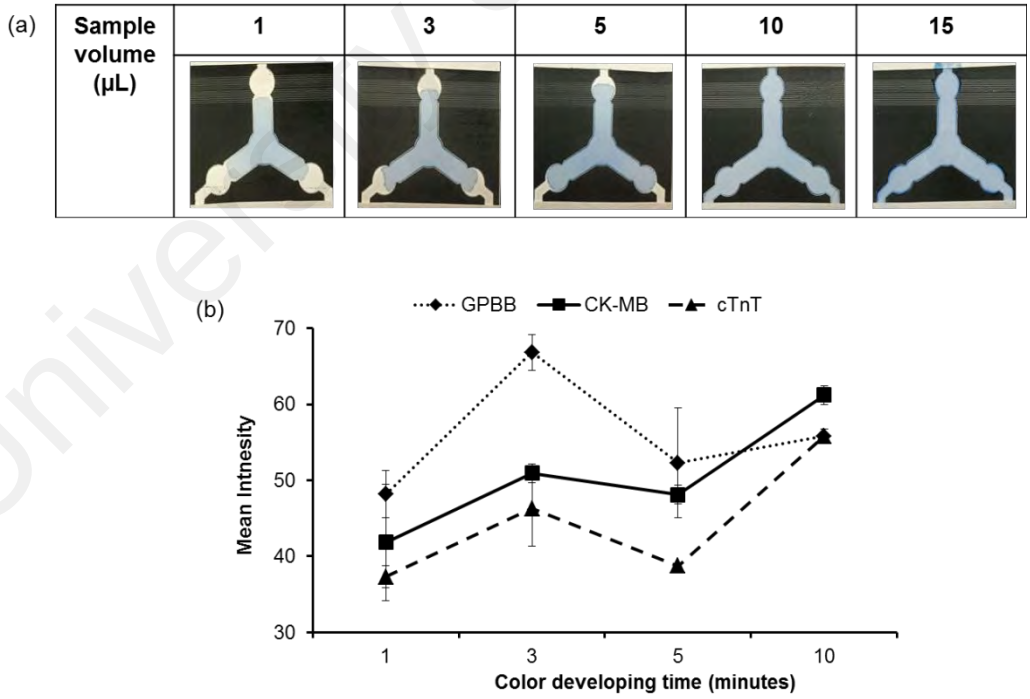

Figure 4.3: Optimisation of (a) sample volume and (b) colour development time for an assay.

University of Malaya

4.2 Microfluidic Paper-Based Analytical Device for Colourimetric Assay

4.2.1 Conjugation of Nanoparticles with Detecting Antibodies

Nanoparticles are conjugated to antibodies that recognise the antigen of interest, and the strong optical absorption of nanoparticles enables the colourimetric detection with the naked eye. Passive adsorption relies primarily on hydrophobic attractions and electrostatic interactions between the antibody and the nanoparticle (Jazayeri et al., 2016). For conjugation of antibodies to the nanoparticles, ionic interactions are formed between positively charged groups in antibodies and the negatively charged surface of the nanoparticles (Zaret et al., 1984). The optimisation steps include antibody titration to ensure the surface of the particle is fully covered, as well as identification of suitable pH for conjugation. Hence, a flocculation assay was performed at different pH of nanoparticles solution and a dilution series with different antibody concentration in order to determine the optimal pH and detecting antibody concentration to produce a stable conjugate.

As shown in **Figure 4.4**, the wavelength of maximum absorption (λmax) of each nanoparticle was scanned beforehand by using Infinite® M200 PRO microplate reader (Tecan Group Ltd, Männedorf, Switzerland). The λmax means that at a certain wavelength more lights are absorbed. The wavelength of the light from a certain region of the spectrum is absorbed by a material, as the reflected light appears to be a complementary colour of the absorbed light. For instance, the silver nanoparticles are in yellow absorbed violet light with a wavelength of 412 nm, gold-urchin nanoparticles in violet (purple) colour absorbed yellow light with a wavelength of 557 nm, while gold nanoparticles in red absorbed green light with a wavelength of 527 nm. Therefore, λmax was identified as 412 nm, 557 nm and 527 nm for silver (yellow), gold (purple) and gold (red) nanoparticles, respectively.

University of Malaya

In the flocculation assay, the smallest absorbance decreases before and after treatment of 10% NaCl in their respective wavelength — 412 nm (silver nanoparticles), 557 nm (gold–urchin nanoparticles), and 527 nm (gold nanoparticles), indicates that the higher the stability in conjugation of proteins onto the surface of nanoparticles by electrostatic attraction. Based on the results obtained for the three types of nanoparticles — silver, gold-urchin and gold, the optimal pH and antibody concentration for the conjugation of polyclonal anti-GPBB detecting antibody with 40 nm silver nanoparticles was identified at pH 7 (**Figure 4.5a**) and at 10 μg mL^{-1} (**Figure 4.6a**). Next, the optimal antibody concentration for conjugating the monoclonal anti-CK−MB detecting antibody with 50 nm gold-urchin was found to be ideal at pH 8 (**Figure 4.5b**) and at 10 μg mL^{-1} (**Figure 4.6b**). The ideal condition for 40 nm gold nanoparticles to be conjugated with the polyclonal anti-cTnT detecting antibody was at pH 7 (**Figure 4.5c**) and at a concentration of 10 μg mL^{-1} (**Figure 4.6c**). Under their optimal conditions, the nanoparticles were very stable for use in the preparation of conjugates on a large scale as nanoparticle-conjugated detecting antibody to allow the cardiac biomarkers detection on μPAD.

For nanoparticles−antibody conjugation, the citrate-capped nanoparticles (i.e., silver, gold and gold-urchin) were used. This is because the citrate layer was reported to be quite loosely bound to the nanoparticle surface, which is useful for further bio-conjugation (Daniel & Astruc, 2004). In a flocculation assay, NaCl (as electrolytes) masked the charges on the nanoparticles and this has led to disruption in the attraction and repulsive forces, resulting in the collapse and aggregation of nanoparticles that showed a visual change in colour. Indeed, the particle aggregation would occur when there is an increase in ionic strength in the surrounding solution that leads to the displacement of the capping citrate layer and absence of repulsive charge to counteract the attraction forces. Therefore, the nanoparticles can be prevented from aggregating

with the addition of protein that is absorbed onto the surface of nanoparticles (Ljungblad, 2009; Schmid, 2011). Herein, the smaller the difference in absorbance before and after an addition of 10% NaCl indicates that the conjugation of protein on the surface of nanoparticles by electrostatic attraction is better and more stable. Based on our experimental result, the ideal conditions such as optimal pH and concentration was carefully selected with the purpose for generating three stable colourimetric conjugates for multiplex detection of cardiac biomarkers, for instance pH 7 and 10 µg mL^{-1} for GPBB; pH 8 and 10 µg mL^{-1} for CK−MB; and pH 7 and 10 µg mL^{-1} for cTnT.

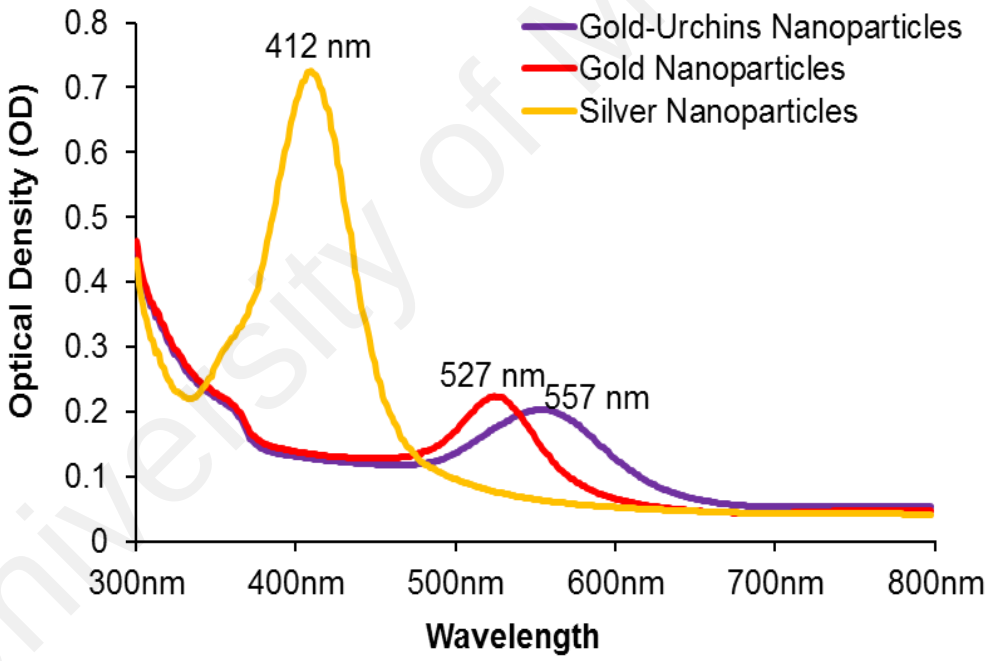

Figure 4.4: λmax of nanoparticles–Gold, Silver and Gold-urchin.

University of Malaya

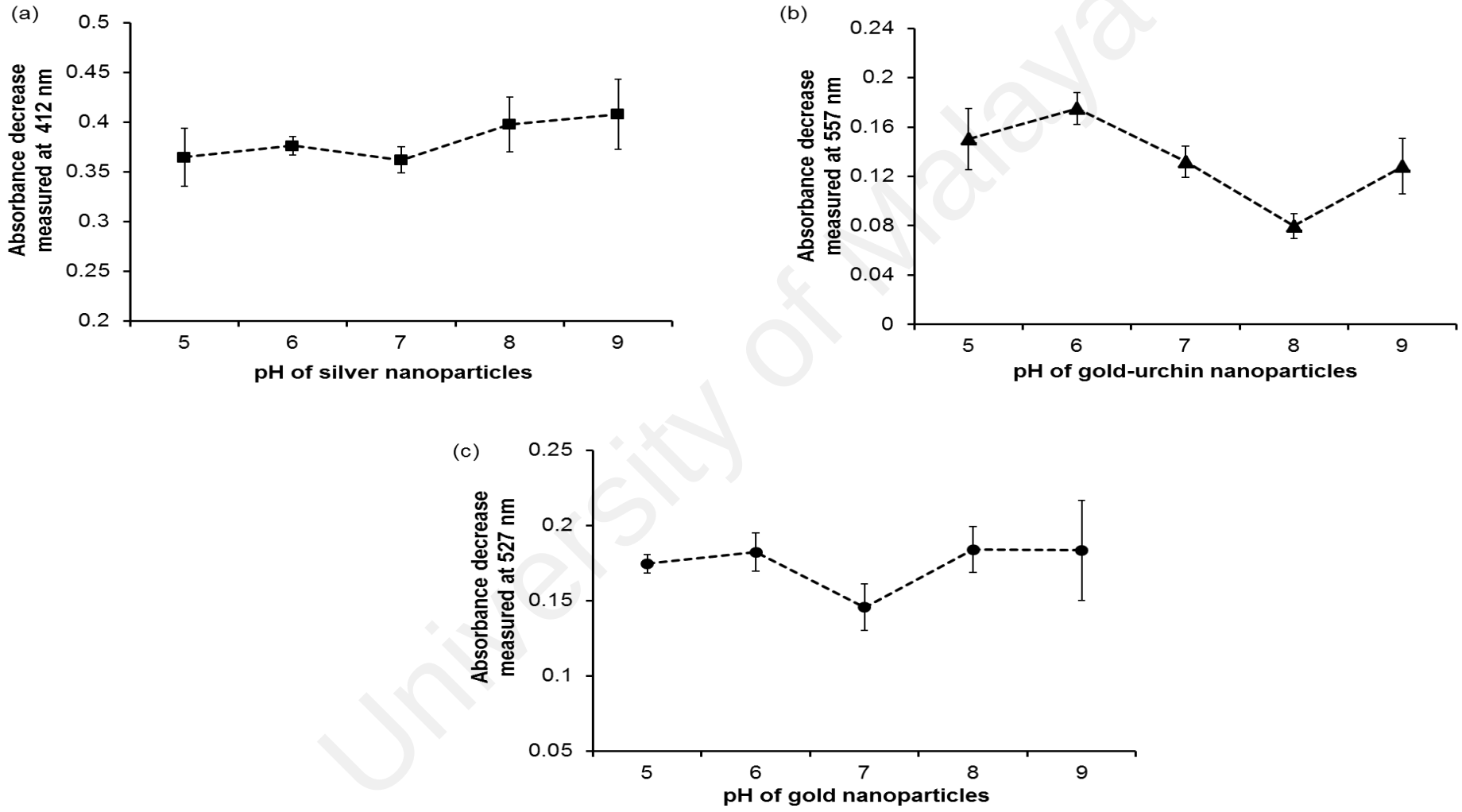

Figure 4.5: pH optimisation of nanoparticles ─ (a) silver, (b) gold-urchin and (c) gold.

University of Malaya

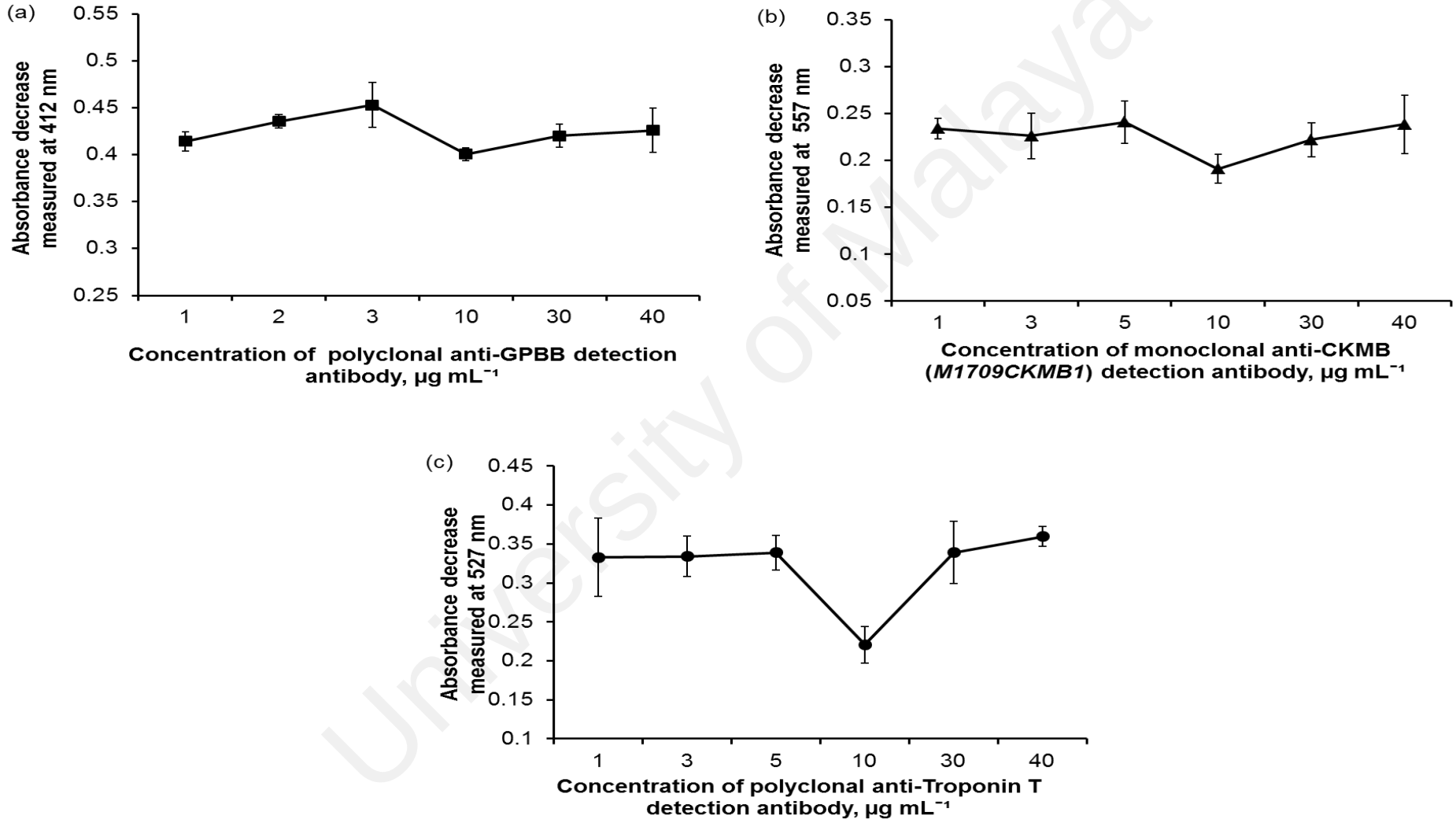

Figure 4.6: Concentration optimisation of detecting antibody ─ (a) GPBB, (b) CK−MB and (c) cTn

University of Malaya

4.2.2 Characterisation of Colourimetric Conjugates

4.2.2.1 Ultraviolet-Visible Spectroscopy

Nanoparticles exhibit a distinct optical feature commonly referred to as localised surface plasmon resonance (LSPR), that is, the collective oscillation of electrons in the conducting band of nanoparticles in resonance with a specific wavelength of incident light, which can be measured by UV−Vis spectroscopy (Ghosh & Pal, 2007; Noginov et al., 2007). Theoretically, LSPR of spherical gold nanoparticles results in a strong absorbance band in the visible region of 500 nm to 600 nm; whereas the absorption peak of spherical silver nanoparticles are primarily in the range of 400 nm to 500 nm. Besides that, the spiky uneven surface of gold-urchin nanoparticles causes larger enhancement of the electromagnetic field resulting to absorption peak in the range of 500 nm to 700 nm. Herein, the nanoparticle solutions were examined at a spectra range 300 to 800 nm for silver nanoparticles whereas gold and gold-urchin nanoparticles were examined between 400 nm to 800 nm, respectively. In an experimental study, the λmax was determined at 412 nm, 557 nm, and 527 nm for bare silver, gold-urchin and gold nanoparticles, respectively.

UV-Vis spectroscopy is a simple and reliable method for monitoring the stability of nanoparticle solutions. The characterisation of citrate stabilised nanoparticles before and after conjugation was done by observing their absorption peaks and absorption curve appearances. **Figure 4.7(a-c)** shows the spectrum which revealed that the λmax was shifted (red-shift) by a few nanometers from left to right, **(a)** silver nanoparticles shifted from 412 nm to 416 nm; **(b)** gold-urchin nanoparticles shifted from 557 nm to 563 nm; and **(c)** gold nanoparticles increased from 527 nm to 531 nm because the relative particle size got bigger which indicated the successful binding of antibodies to the surface of nanoparticles for passive conjugation. The spectrum of absorption for all the samples was shifted to longer wavelengths due to the effect of the quantum size

attributed to the increasing in particle size. In fact, the nanoparticles have distinctive characteristics because they are small enough to confine their electrons and produce quantum size effects (Daniel & Astruc, 2004; Mittal & Banerjee, 2016).

The UV−Vis spectrum is an important tool for understanding the stability and conjugation state of particles. It is very useful in conjugate optimisation as the stable conjugates can provide high quality and consistent result for an assay. From the result, three citrate-capped nanoparticles (before conjugation) and three nanoparticle-antibody conjugates (after conjugation) were recognised in a stable state and not in an aggregated condition. These citrate-crapped nanoparticles are retaining their narrow SPR peak even before and after conjugation. On the other hand, the destabilised particles can be determined where the optical density decreases due to the depletion of stable nanoparticles and resulting to the presence of broad spectral peak. Moreover, the formation of aggregates can be determined when a secondary peak is formed at longer wavelength. (Ljungblad, 2009). In this study, these reported changes did not appear in the graph for these three citrate-capped nanoparticles and three colourimetric conjugates.

University of Malaya

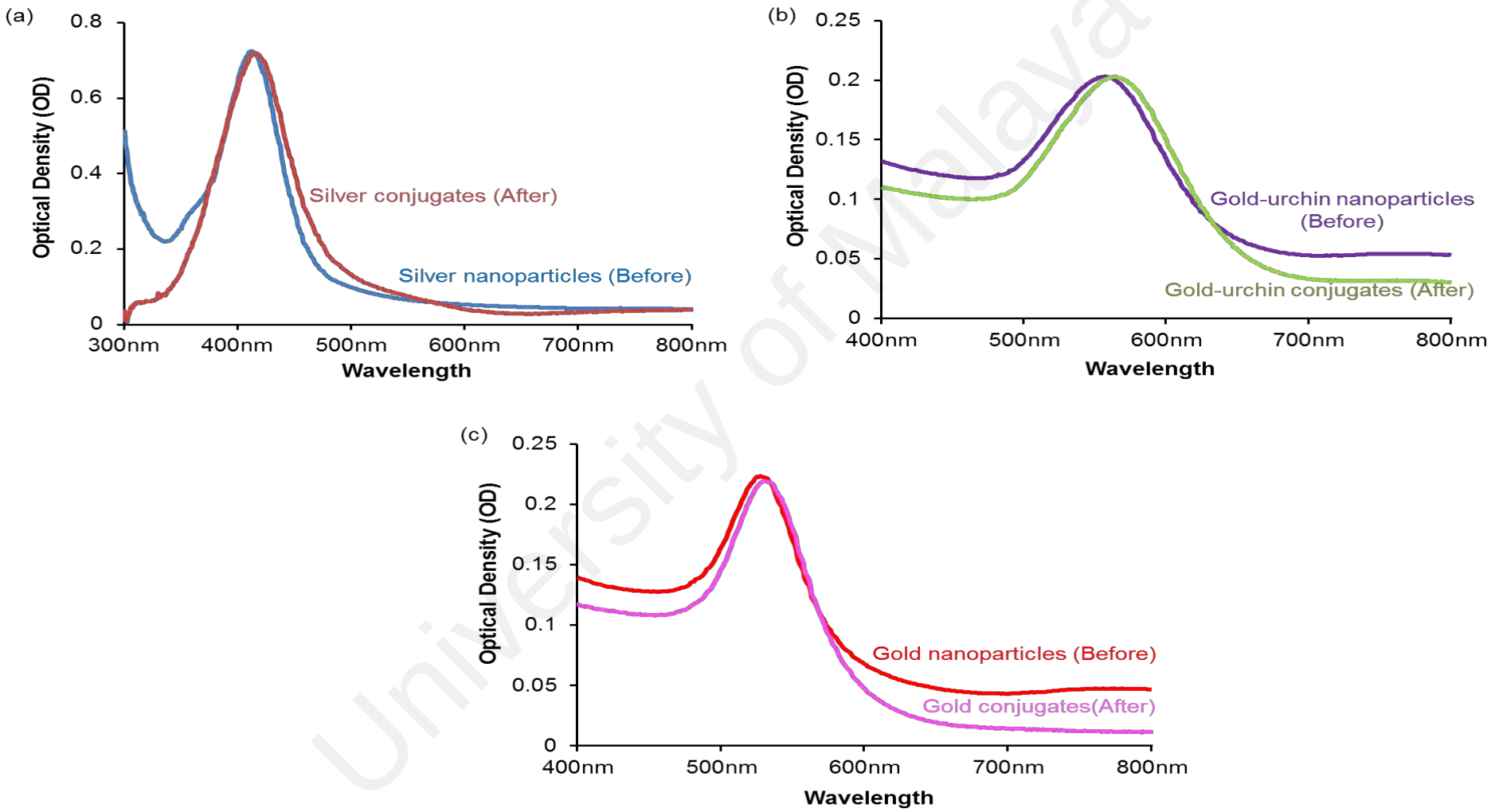

Figure 4.7: Absorption spectrum of nanoparticles (a) silver; (b) gold-urchin and (c) gold, before and after conjugating with detecting antibody.

University of Malaya

4.2.2.2 Dynamic Light Scattering and Zeta Potential

Dynamic Light Scattering (DLS) method is useful to determine the hydrodynamic diameter of nanoparticles in solution and provides information on the aggregation state of nanoparticles in solution, by measuring the random changes in the intensity of light scattered from a suspension or solution (Brar & Verma, 2011; Clayton et al., 2016). In theory, the hydrodynamic size of nanoparticles was increased after the antibody attachment to the surface of nanoparticles (Bhattacharjee, 2016; Tam et al., 2017). Herein, the hydrodynamic size of the three nanoparticles such as gold, silver and gold-urchin before and after the antibody conjugation was measured by Zetasizer Nano ZS (Malvern Instruments Ltd, UK). As displayed in **Table 4.1**, 40 nm silver nanoparticles have increased in hydrodynamic diameter from 57.7 nm to 72.5 nm upon antibody conjugation. With antibody conjugation, 50 nm gold-urchin nanoparticles have also increased in hydrodynamic diameter from 59.4 nm to 78.0 nm; and for 40 nm gold nanoparticles, have increased from 44.7 nm to 76.7 nm.

In addition, the surface charge of the nanoparticles before and after conjugation was measured using the zeta potential mode of the Zetasizer Nano ZS (Malvern Instruments Ltd, UK). The magnitude of the zeta potential is predictive of the colloidal stability, with particles with higher magnitude zeta potentials exhibiting increased stability due to a larger electrostatic repulsion between particles. As reported, citrate-capped nanoparticles dispersions with zeta potential values that are greater than 30 mV or less than -30 mV are classified as having high degrees of stability (Bhattacharjee, 2016). In **Table 4.1**, zeta potential measurement showed that all nanoparticles-antibody conjugates were negatively charged. Originally, citrate-capped silver nanoparticles, gold-urchin nanoparticles, and gold nanoparticles have a zeta potential of -37.9 mV, -39.4 mV, and -33.1 mV, respectively which are more negative than -30 mV and hence they were considered stable. However, the value of zeta potential of citrate-capped

nanoparticles is negative due to the presence of negative charge on the surface. However, after antibody conjugation, the zeta potential of conjugates has increased (become less negative). This is due to the binding of positively charged antibody onto the surface of the negatively charged nanoparticles. As result, the zeta potential of nanoparticles has become less negative from -37.9 mV to -22.8 mV; -39.4 mv to -23.4v mV; and -33.1 mV to -20.5 mV for silver conjugates, gold-urchin conjugates and gold conjugates, respectively after passive conjugation. This change in zeta potential between the bare nanoparticles and the other three conjugates indicates that the entire detecting antibody was successfully attached to the surface of nanoparticles and was found to be stable in solution.

The determination of particle size (hydrodynamic diameter) and surface charge of nanoparticles are indispensable for the characterisation of nanoparticles. The magnitude of the zeta potential is predictive of the colloidal stability. In general, the surface of citrate-capped nanoparticles is negatively charged due to the citrate ion used as capping as well as stabilising agent (Zhao et al., 2013). The decrease in the negative zeta potential of the nanoparticles was reflected as an ionic interaction between the positively charged antibody and the negatively charged nanoparticles. In this, the successfully attachment of antibody to the nanoparticles' surface was confirmed; thereby three stable colourimetric conjugates were formed.

Table 4.1: Hydrodynamic size and zeta potential for monodisperse nanoparticles—silver, gold-urchin and gold before and after conjugation.

Characterisation	**Hydrodynamic Size (nm)**		**Zeta potential (mV)**	
Conjugation stage	**Before**	**After**	**Before**	**After**
Silver nanoparticles	57.7	72.5	-37.9	-22.8
Gold-urchin nanoparticles	59.4	78.0	-39.4	-23.4
Gold nanoparticles	44.7	76.7	-33.1	-20.5

University of Malaya

4.2.3 Assay Cutoff for Qualitative Colourimetric Assay

There are numerous qualitative point-of-care testing devices with single strategy and multiplex strategy for cardiac biomarkers detection which were commercialised in the current market with their specific cutoff level. For qualitative detection, the established cutoff level for the cTnT was 0.1 ng mL^{-1} (Kilickap et al., 2005; Peacock IV et al., 2008); CK−MB was 5 ng mL^{-1} (Rao et al., 1999); myoglobin was 80 ng mL^{-1} whereas GPBB was 10 ng mL^{-1} based on the ELISA method (Stejskal et al., 2007). In this study, the fabricated µPAD was developed as paper-based platform for colourimetric detection of multiple cardiac biomarkers. Hence, the assay cutoff for each biomarker was tested on fabricated µPADs based on the reported clinical cutoff levels for point-of-care testing devices. In **Figure 4.8**, the ideal cutoff concentrations for each cardiac biomarker on fabricated µPAD (N = 5) were determined at 10 ng mL^{-1} for GPBB, 5 ng mL^{-1} for CK−MB and 0.1 ng mL^{-1} for cTnT. Hence, it is promising that the fabricated µPADs are able to achieve the same cutoff levels as established qualitative point-of-care testing devices for clinical assay.

Cardiac markers	Prepared concentration of analyte (ng mL^{-1})	Color intensity		Test result		Cutoff level (ng mL^{-1})
		Phone camera	Scanner	Negative (N)	Positive (N)	
GPBB	5			4/5	1/5	
	10			0/5	5/5	√
	20			0/5	5/5	
CK-MB	1			3/5	2/5	
	5			0/5	5/5	√
	10			0/5	5/5	
cTnT	0.05			3/5	2/5	
	0.1			0/5	5/5	√
	1			0/5	5/5	

Figure 4.8: The assay cutoff for qualitative detection of cardiac biomarkers.

4.2.4 Qualitative Colourimetric Assay

In healthcare, qualitative analysis has become increasingly important to provide immediate results for detecting the presence or absence of biomarkers in the sample to diagnose patients suspected with AMI. For qualitative assay, the presence and absence of the analytes can be observed from the fabricated μPAD with naked eyes. Qualitative test results can aid clinicians in decision making at the critical moment for admitting a patient with myocardial infarction. The incorporation of nanoparticles, such as gold, silver, and gold urchin, as labels allows a visual examination of the colour signal at the reaction zone(s), resulting in qualitative (Yes/No).

As shown in **Figure 4.9**, a coloured dot displayed at the respective test zone(s) indicated a positive result (presence of analytes) whereas without a coloured dot displayed at the respective test zone (s) indicated a negative result (absence of analytes) for qualitative assay. The intensity of the colour dot in the test zones, G for GPBB, M for CK−MB, and T for cTnT varies depending on the concentration of respective target analytes present in the given sample. Hence, any shade of colour displayed in the test zone(s) should be considered as positive. For the fabricated μPAD, the cutoff levels for each cardiac biomarker were determined at 10 ng mL^{-1} for GPBB, 5 ng mL^{-1} for CK−MB, and 0.1 ng mL^{-1} for cTnT (**Figure 4.8**). Moreover, the user can observe the colourimetric result easily with the naked eye based on their distinct colours which appeared on the μPAD as the qualitative test method requires no measurement instruments. The concentration above the cutoff level is considered as a positive result whereas the concentration lower than the cutoff level is considered as a negative result.

University of Malaya

Cardiac biomarker			Qualitative test result on fabricated µPAD	
GPBB	CK-MB	cTnT	Phone camera	Scanner
N	N	N		
P	N	N		
N	P	N		
N	N	P		
P	P	P	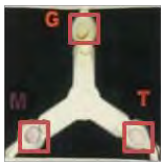	

Note: N represents Negative (absence of cardiac biomarkers) and P represent Positive (presence of cardiac biomarkers)

Figure 4.9: Qualitative test result for multiplex detection of cardiac biomarkers on the fabricated µPAD.

University of Malaya

4.2.5 Semi-Quantitative Colourimetric Assay

Semi-quantitative tests are used as a screening tool to assess the existence and to measure the estimated concentrations of certain cardiac biomarkers. A reference chart displayed in **Table 4.2** was made based on the levels of multiple cardiac biomarkers, G for GPBB; M for CK−MB and T for cTnT on the fabricated µPAD. The levels of the biomarkers were categorised into three risk categories; higher levels were associated with increased damage (high risk), lower levels with less damage (moderate), and levels in a patient suspected with unstable angina (low risk), are based on the 99th percentile upper reference limit in which the 99th percentile of a normal, healthy reference population is the decision level for the diagnosis of myocardial infarction, as described in **Table 3.2**.

The semi-quantitative results on each reaction zone showed a significantly different colour intensity that was proportional to the concentrations of the cardiac biomarkers. As shown in **Table 4.2**, the signal intensity on the fabricated µPADs gradually got intensed with the increase in the levels of the respective cardiac biomarkers from left to right and also the degree of visibility of the colour dot in each test zone. Hence, a darker intensity of the colour dot on the fabricated µPAD indicated high seriousness of heart injury. As reported in literature, the normal level of GPBB is < 7 ng mL^{-1} and peaks at 50 ng mL^{-1} after AMI (Kaski & Holt, 2013). In fact, in the current research, GPPB was identified as a "new cardiac marker" that could enhance the early diagnosis of ACS but was not systematically used in clinical settings. In this study, the concentration of < 5 ng mL^{-1} was classified as low (normal) risk for GPBB assay as it has approximately the same colour signals for 5 ng mL and 7 ng mL. To avoid delaying early screening, ≥ 5 ng mL^{-1} is classified as a moderate risk to alert patients with suspected ischemic myocardial injury to receive appropriate treatment at an early stage. For CK−MB, the concentration is 1 ng mL^{-1} and increases to 5─20-times on incident of AMI (Gupta et

al., 2008; Qureshi et al., 2012). Elevated troponin T level, which is 3–4-times higher than the normal level 0.1 ng mL^{-1}, is associated with a high mortality rate to MI (Ohman et al., 1996). However, many literature have reported that the negative Troponin T level is lower than 0.01 ng mL^{-1} (or < 0.03 ng/mL with the standard cTnT assay), which indicates that troponin T was not being detected in the blood (Giannitsis et al., 2010; Nilsen et al., 2015).

Based on semi-quantitative detection, the distinct colour exhibited on the fabricated μPAD can be used to predict the extent of heart muscle damage. For instance, the presence of only the yellow colour in the reaction zone of G for GPBB indicates patients are suspected with ischemic myocardial injury at an early stage. The presence of purple colour at the reaction zone of M for CK−MB and red colour at the reaction zone of T for cTnT on the fabricated μPAD (absence of ischemia-specific marker, GPBB) indicate that patient are suspected with myocardial injury and they are encouraged to be admitted to hospital to receive immediate treatment to avoid infarction incidence (heart attack). In the current clinical setting, there is no semi-quantitative detection assays available as cardiac biomarker measurements, thus typically requires laboratory quantitative analysis in a hospital to obtain accurate results before admission of the patient .

Therefore, the semi-quantitative analysis is demanded in the current clinical setting to assist medical doctors when deciding to admit of ACS patients with moderate and high risk of myocardial injury and to provide them with immediate treatment to save their live without waiting for laborious laboratory results. Therefore, ACS patients with low risk can be treated as an unstable angina patient, and cardiac evaluation should be conducted to prevent heart damage and infarction after prolonged ischemia.

University of Malaya

Table 4.2: The semi-quantitative reference chart based on the levels of multiple cardiac biomarkers, (a) GPBB; (b) CK−MB and (c) cTnT.

(a)	Concentration of GPBB (ng mL^{-1})	0	0.5	1	3	5	10	30	50	100
	(i) Phone camera									
	(ii) Scanner									
	Risk levels	Negative	Low			Moderate		High		
(b)	Concentration of CK-MB (ng mL^{-1})	0	0.5	1	3	5	10	30	50	100
	(i) Phone camera									
	(ii) Scanner									
	Risk levels	Negative	Low			Moderate		High		
(c)	Concentration of cTnT (ng mL^{-1})	0	0.05	0.1	1	5	10	50	100	200
	(i) Phone camera									
	(ii) Scanner									
	Risk levels	Negative	Low		Moderate			High		

University of Malaya

4.2.6 Quantitative Colourimetric Assay

Quantitative colourimetric detection of multiplex cardiac biomarkers, GPBB, CK−MB, and cTnT, were performed by determining the reflectance of colour intensity developed in the three test zone(s) of G, M, and T on the μPAD, respectively. The mean of colour intensity for each data point was measured using the Image J software by selecting the area of the test zones G, M, and T for each assay based on a digital image of the μPAD that was captured using the proposed reflectance detectors, smartphone-based camera and desktop scanner. The calibration curve for reflectance detection of the colour signal intensity of cardiac biomarkers — GPBB, CK−MB and cTnT on the μPAD was plotted as shown in **Figure 4.10.** Then, the concentration of the unknown analytes was quantified by comparing the intensity in the test zones of G, M, and T to the plotted calibration curve. The calibration curves for reflectance detection usually follow the non-linear function of concentration (Teasdale et al., 1999).

In this study, non-linearity in wide dynamic range is caused by two factors, such as complementary metal-oxide semiconductor (CMOS) image sensors embedded in phone camera, which detect and convey information used to make an image (Wang & Theuwissen, 2017) or the limited sensitivity at higher concentrations of analyte due to signal (colour) saturation (Carrilho et al., 2009b; Martinez et al., 2010b). Measurements using cameras and scanners (reflection mode) are based on light reflectance, which illuminates the sample with a light source, and the light reflected from the surface of the sample is then captured by a photodetector. The CMOS image sensor that is embedded in the phone camera will convert the voltage output of sensor back to the corresponding number of electrons that were detected in a pixel, known as the Charge to Voltage Factor (CVF), which has a non-linear relationship with the signal (Soman et al., 2015). In this study, the μPAD was captured by a smartphone-based camera under a fixed light source (e.g. desk lamp) in dark to avoid the effect of ambient light. Since a consistent

experimental lighting condition was maintained as a constant variable, the light intensity that affects the saturation in CMOS can be excluded. In addition, the non-linear relationship can also be interpreted as an intensity measurement that is very sensitive at low concentrations and less sensitive at high concentrations. Therefore, the non-linearity is most likely to be caused by saturation of bio-recognition molecules instead of the CMOS saturation.

Dynamic range is defined as the highest detectable cardiac biomarkers level to the lowest detectable cardiac biomarkers level. From the result obtained, the dynamic range of the GPBB obtained via smartphone-based camera was y = 3.2317 x + 43.855 with R^2 = 0.78 and desktop scanner was y = 3.0149 x + 15.414 with R^2 = 0.96 (**Figure 4.10a**). Dynamic range of the CK─MB obtained via smartphone-based camera was y = 5.1863 x + 10.422 with R^2 = 0.94 and desktop scanner was y = 5.2072 x + 4.9382 with R^2 = 0.99 (**Figure 4.10b**). Dynamic range of the cTnT obtained via smartphone-based camera was y = 2.4741 x + 35.555 with R^2 = 0.90 and desktop scanner was y = 2.2937 x + 14.012 with R^2 = 0.97 (**Figure 4.10c**). As a result, the colourimetric-based µPAD was found to be very sensitive in detecting a lower concentration of cardiac biomarkers 0─10 ng mL^{-1}. This is very crucial for early diagnosis of AMI, especially at low clinical cutoff value (e.g., GPBB, < 7 ng mL^{-1}), hence a linear function is used. In addition, the *LOD* of the developed µPADs for GPBB, CK−MB, and cTnT were 0.5 ng mL^{-1}, 0.5 ng mL^{-1}, and 0.05 ng mL^{-1}, respectively, which was determined by the degree of visibility of the colour signal observed in the test zones G, M, and T, respectively on the fabricated µPAD. For the most part, the colourimetric-based µPAD achieved a clinically significant visual *LOD* compared to the established quantitative POCT devices for the CK−MB assay (cutoff 4─7 ng mL^{-1}) and cTnT assay (cutoff 0.01─0.05 ng mL^{-1}). On the other hand, the cut-off values varied in accordance with the manufacturers' recommendations.

For quantification of cardiac biomarkers, the portable lateral flow strip reader is much more convenient and user-friendly compared to a bench-top analyser in the central laboratory, which is still unaffordable for medical centres in developing countries. For example, a bench-top immunoassay analyser costs approximately 50, 000 £, whereas a portable reader costs almost 5, 000 £, and easily available smartphone-based cameras and a scanner only cost ≤ 100 £. Moreover, a scanner has been reported to provide reproducible results in previous studies because the focus, image, and lighting condition are constant (Carrilho et al., 2009b; Martinez et al., 2008a; Martinez et al., 2010b). However the low quality of the images scanned from a scanner due to low resolution may have an impact when processed with the image analyser software programmed into a computer.

Based on the experimental result displayed in **Figure 4.10**, the non-linearity at elevated quantities of analytes from the image captured by a smartphone-based camera was found to be higher than that captured by a scanner. Perhaps, it was because the smartphone-based camera could capture good quality (resolution) images with better pixels than that of a scanner. Second, the colour chosen for the colourimetric indicator could also be another important factor. Herein, the intensity obtained from desktop scanner and smartphone-based camera showed a slightly difference for GPBB and cTnT assay. This may possibly be due to the red colour signal for cTnT assay and yellow colour signal for GPBB assay which are considered as warm colour when compared to the cold colour of purple colour signal for CK−MB assay. Therefore, both detection systems for CK−MB assay did not show much difference as like cTnT and GPBB assay. Moreover, the colourimetric intensity measured using smartphone-based camera is much better than desktop scanner for this work. Of late, almost everybody has a smartphone, and if the resolution of the phone camera is sufficiently high, a

University of Malaya

smartphone-based camera can possibly function as an effective and accurate diagnostic tool for reflectance detection of the semi-quantitative and quantitative data evaluation.

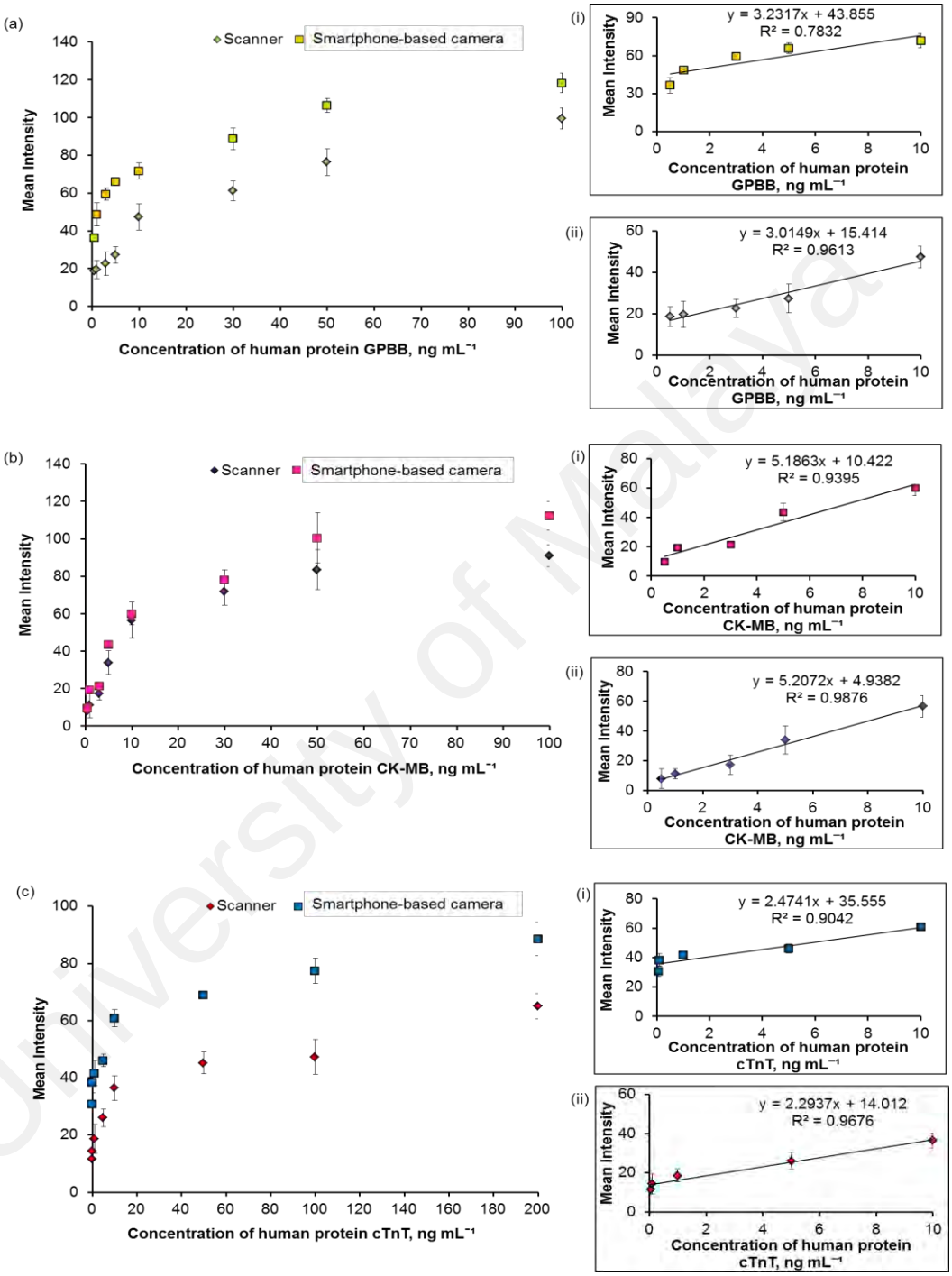

Figure 4.10: The calibration curve for quantitative colourimetric detection of multiplex cardiac biomarkers using (▲) smartphone-based camera, (●) desktop scanner. (a)(i) Signal intensity of test zone G measured versus concentrations of GPBB. Dynamic range obtained via (i) smartphone-based camera and (ii) desktop scanner. (b)(i) Signal intensity of test zone M measured versus concentrations of CK−MB. Dynamic range obtained via (i) smartphone-based camera and (ii) desktop scanner. (c) Signal intensity of test zone T measured versus concentrations of cTnT. Dynamic range obtained via (i) smartphone-based camera and (ii) desktop scanner.

University of Malaya

4.3 Microfluidic Paper-Based Analytical Device for SERS Assay

4.3.1 Conjugation of SERS Probe with Detecting Antibodies

The SERS probe was prepared with some modification from the protocol described by Gao et al. (2017). In the SERS method, the nanoparticles acted as the signal enhancer, the Raman active molecules were excited to provide a significant increase in the intensity of the Raman scattering, which resulted in a detectable Raman signature. Herein, the SERS probe was prepared by the adsorption of Raman reporter molecules (i.e., 4-nitroanilline, tert-Butylhydroquinone and methyl red) on the nanoparticles (i.e., silver, gold-urchin and gold), before being encapsulated in a silica shell. Subsequently, three different SERS probes (also known as nanotags) were conjugated with the detecting antibodies to actively target the interest antigen for multiplex detection of cardiac biomarkers.

Figure 4.11 showed that the SERS intensity gradually increased in each stage of the binding interaction indicating the successful attachment of the molecules onto the surface of the nanoparticles. For instance, the Raman reporter molecules (*green line*); absorption of Raman reporter molecules on the surface of nanoparticles (*red line*); silica coating enclosed nanoparticles' surface (SERS probe formation) (*blue line*); and conjugation SERS probe with detecting antibody (*orange line*). In each binding interaction stage, the characteristics peak of spectra (marked using an asterisk (*)) was identical, such as 1387 cm^{-1} for 4-nitroanilline (**Figure 4.11a**); 1450 cm^{-1} for tert-Butylhydroquinone (**Figure 4.11b**) and 1400 cm^{-1} for methyl red (**Figure 4.11c**). Based on the experimental result, the Raman reporter molecules confirmed that they were effectively bound to the SERS probe and were still detectable after a few stages of binding interactions. Thus, the SERS probe conjugates ascertained can be used as the specific SERS indicator for the detection of cardiac biomarkers (GPBB, CK−MB, cTnT) on μPAD.

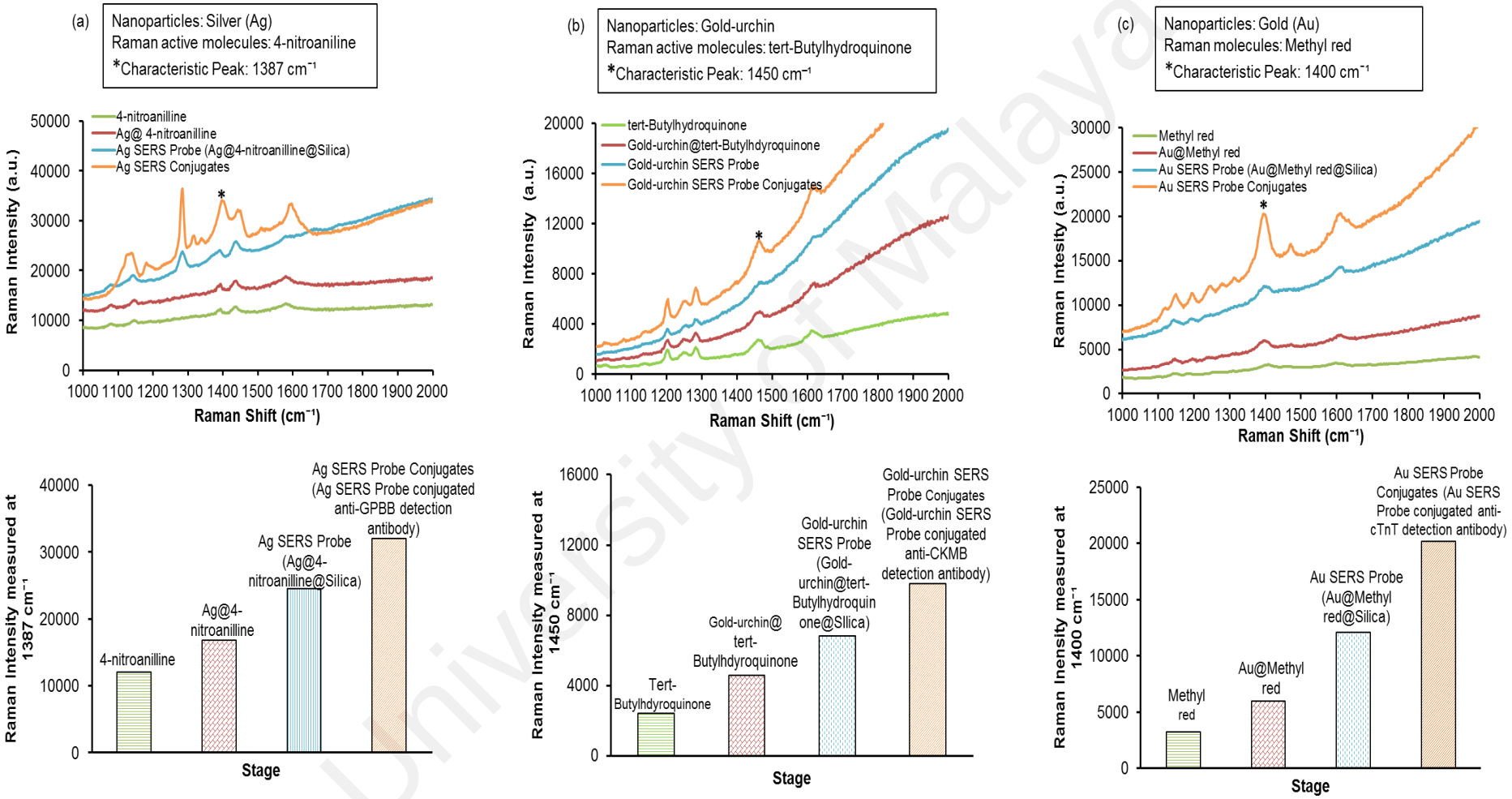

Figure 4.11: The binding interaction stage of SERS probes. (a) Gold SERS probe conjugated anti-cTnT detecting antibody; (b) Silver SERS probe conjugated anti-GPBB detecting antibody; (c) Gold-urchin SERS probe conjugated anti-CK−MB detecting antibody

University of Malaya

4.3.2 Characterisation of Raman SERS Probe Conjugates

4.3.2.1 Ultraviolet-Visible Spectroscopy

Three prepared Raman SERS Probes were characterised using UV-Visible spectroscopy in order to confirm the presence of silica shell encapsulated on the surface of nanoparticles. To further study the observed plasmonic shift of the three nanoparticles after coated with silica, a UV-Vis analysis of nanoparticles (gold/ silver/ gold-urchin) and nanoparticle encapsulated with silica shell (gold nanoparticles@silica/ silver nanoparticles@silica /gold-urchin nanoparticles@silica) was conducted.

From the results, the silver nanoparticles encapsulated with a silica shell present quite a broad absorption peak and shifted from 416 nm to 429 nm (**Figure 4.12a**). Gold-urchin nanoparticles were shifted from 564 nm to 584 nm (**Figure 4.12b**). Gold nanoparticles were shifted from 524 nm to 544 nm after its surface was encapsulated with a silica shell **(Figure 4.12c)**. The spectrum from each of the nanoparticles was red-shifted to a longer wavelength after silica coating.

According to earlier literatures, numerous studies have been performed on the coating of metal nanoparticles with silica shells (Do Kim & Kim, 2002; Kobayashi et al., 2005; Shah, 2018). The main advantage of the bare nanoparticles covered with an outer silica shell is to enhance the colloidal stability. The silica shell can provide effective steric-hindrance and electrostatic protection on the nanoparticles to provide electrostatically stable colloids. Therefore, nanoparticles that get encapsulated with silica shell can be more biocompatible and allow for further bio-conjugation with other functional groups. Herein, the nanoparticles encapsulated with silica shell exhibited the red-shift of the absorption spectra; that can be ascribed to the increase of local refractive index due to silica coating. The silica-coated nanoparticles are larger than bare

University of Malaya

nanoparticles and have peaks that stretch and move to longer wavelengths as shown in **Figure 4.12**.

University of Malaya

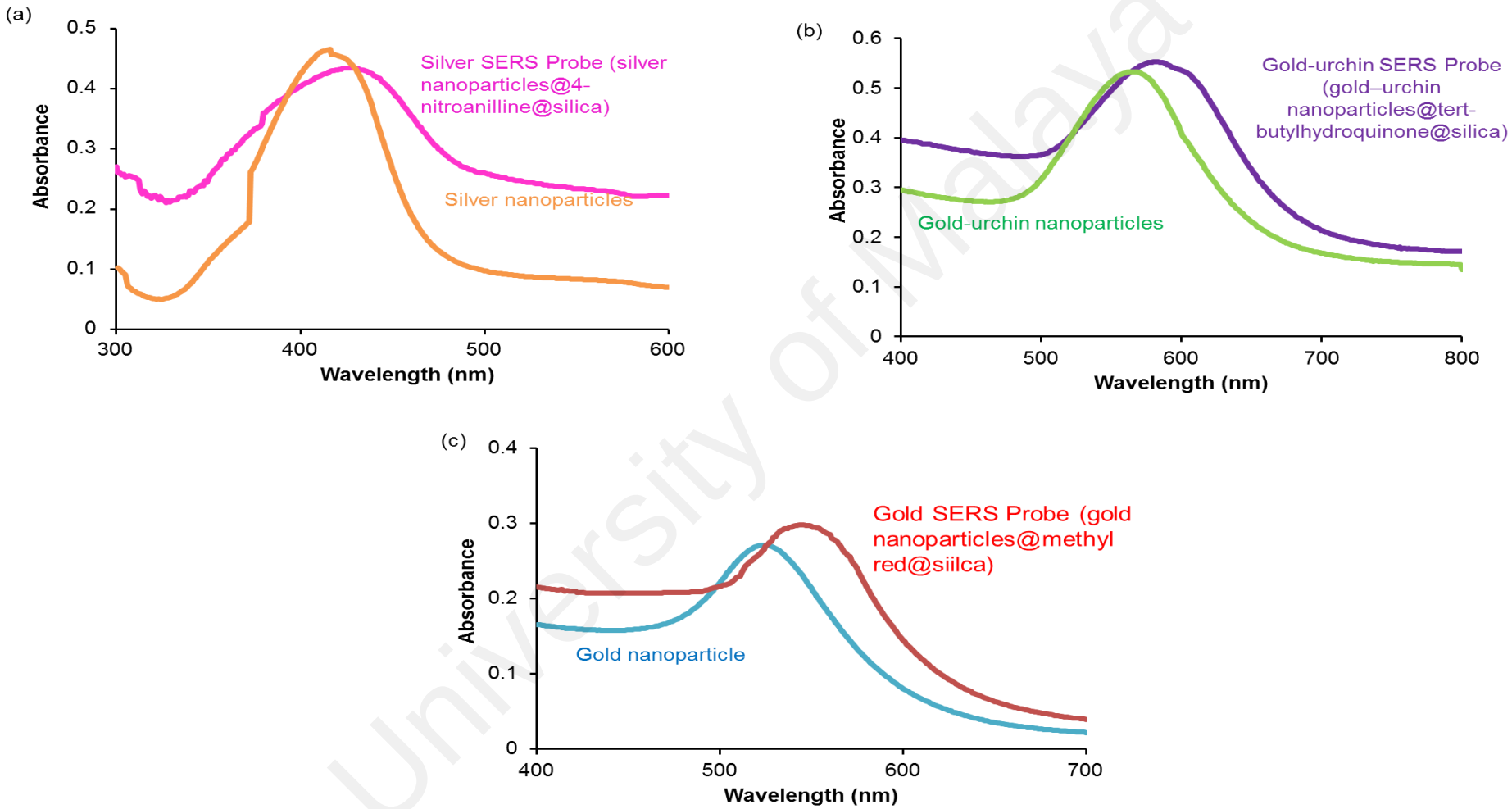

Figure 4.12: UV−Visible absorption spectra of the SERS nanoparticles (a) silver, (b) gold−urchin and (c) gold, before and after silica coating.

University of Malaya

4.3.2.2 Fourier-Transform Infrared Spectroscopy

Indeed, the silica shell is able to provide physical robustness, signal stability and protection in biochemical environment (e.g., high ionic strength solution), and also provide a platform for bio-conjugation (Hamblin et al., 2016). After being encapsulated by silica shell, the SERS probe was functionalised with carbonyl group via glycine-glutaraldehyde reaction to form imine. The carbonyl (aldehyde) functionalised-SERS probe was then conjugated with the respective detecting antibody. The aldehyde terminated SERS probe reacts with the primary amine groups of detecting antibody to form a SERS indicator (SERS nanotags) as presented in **Figure 3.9**. Subsequently, the carbonyl group functionalisation and conjugation with detecting antibody onto the surface of SERS nanoparticles was confirmed by FTIR.

In **Figure 4.13**, the results obtained show that the presence of silica shell encapsulated the SERS nanoparticles (i.e., silver, gold and gold−urchin). This can be observed from the characteristic bands that appeared at spectra 891 cm^{-1} and 914 cm^{-1} for Si−OH absorption band whereas 1039 cm^{-1} and 1110 cm^{-1} correspond to Si-O-Si stretching. For the functionalised silver SERS probe, two absorption peaks which appeared at 1596 cm^{-1}, 1511 cm^{-1} were referred to C=O (acetyl group) of secondary amide and NH_2 of primary amine. Two absorption peaks that appeared at 1406 cm^{-1}, and 1332 cm^{-1} were attributed to the C−H bending. After conjugation, the amide functional group of detecting antibody was found at 3790 cm^{-1}, 3246 cm^{-1}, and 3169 cm^{-1} for N−H bending modes. This indicated a successful binding of SERS probe with detecting antibody (**Figure 4.13a**). Noticeably, gold-urchin SERS probe also shows that 1595 cm^{-1}, and 1510 cm^{-1} correspond to C=O whereas 1406 cm^{-1}, 1331 cm^{-1} associated to C−H bending of glycine, respectively. These bands at 3790 cm^{-1}, 3701 cm^{-1}, 3159 cm^{-1} appeared in the SERS probe conjugates, which represent the presence of amide group of detecting antibody **(Figure 4.13b).** For gold SERS probe, two

absorption peaks at 1593cm^{-1} and 1510 cm^{-1} correspond to C=O (acetyl group) and another two absorption peaks at 1406 cm^{-1} and 1331 cm^{-1} were credited to the C−H bending. After conjugation, the FTIR spectra of the attachment of detecting antibody on the functionalised SERS probe showed the peak at 3790 cm^{-1}, 3250 cm^{-1} and 3178 cm^{-1} for N−H bending modes (**Figure 4.13c).**

Herein, the presence of silica shell encapsulating the SERS nanoparticles were confirmed from the characteristic bands which appeared at a spectra range of 800 to 1100 cm^{-1}. The strong Si−OH absorption band was located between 910 cm^{-1} and 830 cm^{-1} whereas the Si-O-Si stretching in 1000–1300 cm^{-1} ranges, was reported by Ke and Stroeve (2005) and Rubio et al. (1998). Moreover, the SERS nanoparticles were proven to be well-functionalised via glycine−glutaldehyde reaction and well-conjugated with the detecting antibody of GPBB, CK−MB and cTnT on the surface of SERS probe. This is due to the bands being designated to vibrational modes of glycine-glutaldehyde such as C−N stretching was found to have appeared at 1030 cm^{-1} whereas to C=O stretching mode, it was detected in the range of 1400 cm^{-1} − 1600 cm^{-1}, which were observed from these SERS nanoparticles. Additionally, the band appeared for N−H stretching was also detected at the range of 3100 cm^{-1} − 3500 cm^{-1}, and N−H bending was observed at the range of 1600 cm^{-1} − 1700 cm^{-1}, which were assigned to the amide group of antibody that were reported by many authors (Kong & Yu, 2007).

University of Malaya

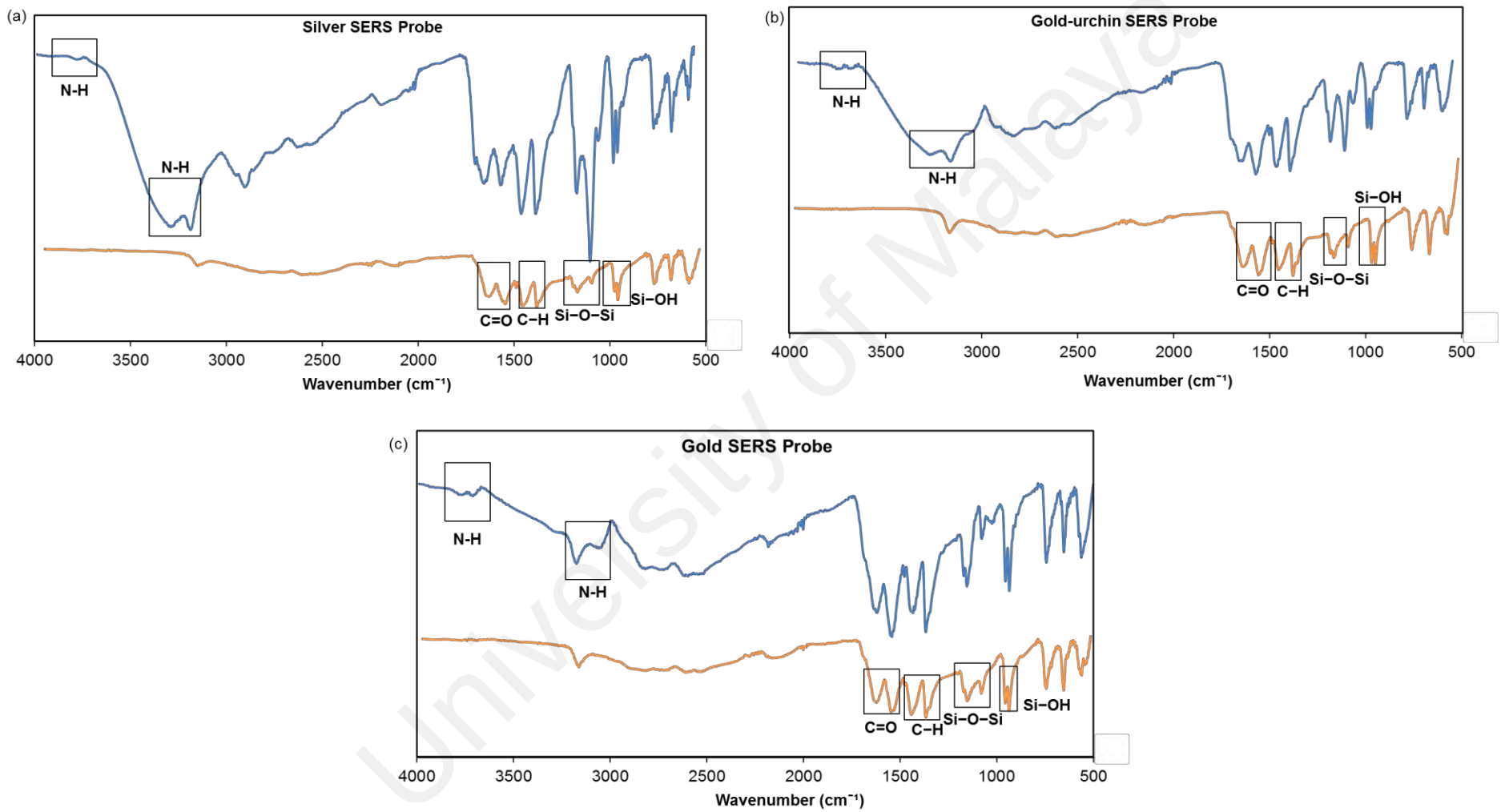

Figure 4.13: FTIR spectra for SERS Probes─ (a) silver, (b) gold−urchin and (c) gold. SERS probe functionalised with glycine-glutaldehyde reaction (*orange line*) and carbonyl group-functionalised SERS Probe conjugated with detecting antibody (*blue line*).

University of Malaya

4.3.2.3 Raman Spectroscopy

In addition, the Raman active molecules enclosed in the SERS probe were examined by Renishaw InVia Raman Microscope to confirm the characteristics peak. The SERS spectra of three prepared SERS probes on silicon and paper substrates were examined, and the peak frequencies and assignment of major SERS peaks was displayed in **Figure 4.14**.

Moreover, the NC membrane made up by nitro-cellulose was used as the platform of μPAD for a multiplex detection of cardiac biomarkers. Hence those bands at 852 cm^{-1} and 1284 cm^{-1} were observed in the spectra of SERS probe on NC membrane which correspond to the nitro-group. For GPBB detection, 4-nitroanilline was used as the specific Raman reporter adsorbed on the surface of silver nanoparticles. The SERS peak located at 1387 cm^{-1}, was assigned as the symmetric bending and stretching modes of the NO_2 group. The most intense SERS band observed at about 1450 cm^{-1} and 1580 cm^{-1}, was due to the aromatic ring C=C stretching mode (**Figure 4.14a**).

For CK−MB detection, Raman reporter molecule of interest, tert-Butylhydroquinone was absorbed onto the surface of gold-urchin nanoparticles. The Raman spectrum of tert-Butylhydroquinone which showed the peak at 932 cm^{-1} and 1204 cm^{-1} were assigned to rocking vibrations of CH_3 and C-C stretching mode of tert-butyl groups. The peak at about 1287 cm^{-1} was attributed to C-O stretching mode of C-OH vibrations whereas C–C aromatic ring chain vibration was detected at 1450 cm^{-1} and 1616 cm^{-1} (**Figure 4.14b**). For cTnT detection, Methyl red was used as the particular Raman reporter that adsorbed onto the surface of gold nanoparticles. The Raman peak appeared at 1400 cm^{-1} in the spectra of Methyl red was assigned to N=N stretching vibration of the azo group. The C–C band was observed at 1370 cm^{-1} whereas the aromatic ring of C=C vibration was observed at 1600 cm^{-1} (**Figure 4.14c**). Although the assignments

may vary according to the different literature sources (Castro et al., 2012; Dereli et al., 2012; Moore & McGrane, 2003; Subramanian et al., 2011), nevertheless, all observed modes were unequivocally related to these Raman molecules used in this study.

From the result, each Raman reporter produces a molecularly specific spectrum that contains a characteristics peak which can be used to identify the target cardiac biomarkers present in the sample. In short, the multiplex detection of cardiac biomarkers on SERS−based μPAD, the characteristics peak was selected at 1387 cm^{-1} for 4-nitroanilline (for GPBB); 1450 cm^{-1} for tert-Butylhydroquinone (for CK─MB) and 1400 cm^{-1} for methyl red (for cTnT).

University of Malaya

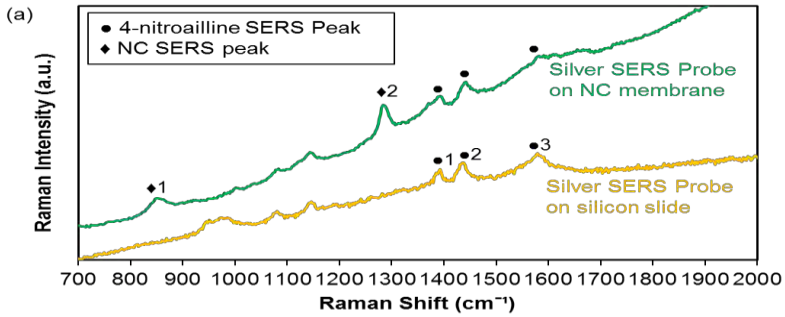

	Peak position (cm^{-1})	Assignment
♦1	852	N-O
♦2	1284	N-O_2
●1	1387	C-NO_2 & NO_2 stretching
●2	1450	C-C aromatic ring chain vibrations
●3	1580	C-C aromatic ring chain vibrations

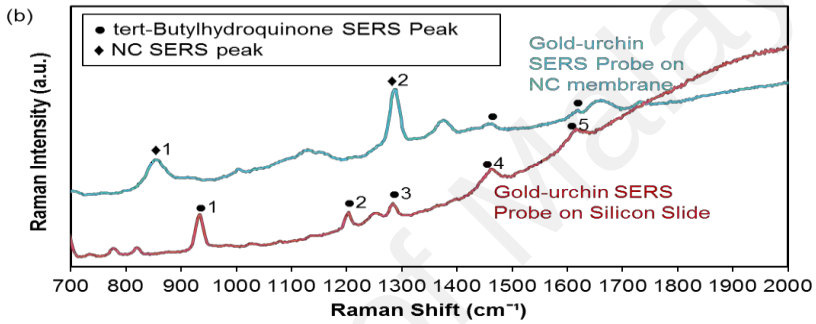

	Peak position (cm^{-1})	Assignment
♦1	852	N-O
♦2	1284	N-O_2
●1	932	CH_3 rocking vibration
●2	1204	CH_3 rocking vibration
●3	1287	C-O stretching mode of C-OH vibration
●4	1450	C-C aromatic ring chain vibrations
●5	1616	C-C aromatic ring chain vibrations

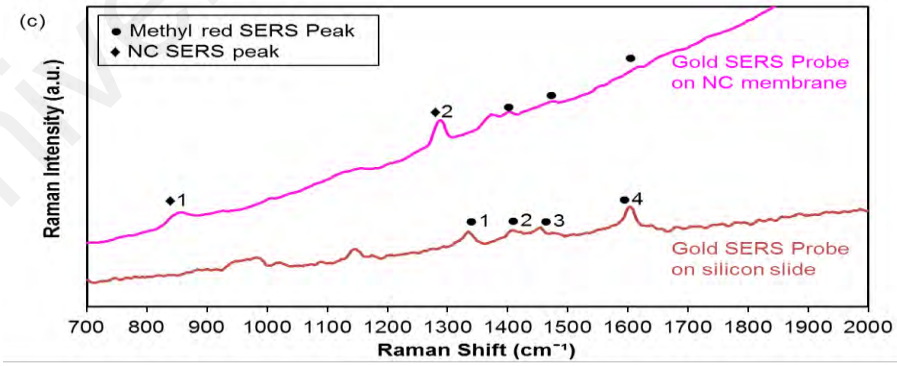

	Peak position (cm^{-1})	Assignment
♦1	852	N-O
♦2	1284	N-O_2
●1	1370	Aromatic C-N bonds vibration
●2	1400	N=N aromatic stretching
●3	1450	C-C aromatic ring chain vibrations
●4	1600	C-C aromatic ring chain vibrations

Figure 4.14: The peak frequencies and assignment of the fingerprints of Raman molecules (a) 4-nitroanilline, (b) tert-Butylhydroquinone and (c) methyl red in SERS probe on silicon slide and NC membrane.

University of Malaya

4.3.3 Quantitative SERS Assay

Surface enhanced Raman scattering (SERS) is an advanced technique that when combined with nanoparticles enables a highly accurate target detection. As shown in **Figure 4.15**, the calibration plot was generated for quantitative SERS assay for GPBB, CK−MB and cTnT. For SERS assay, the SERS probe was used as indicator, which was prepared by absorption of Raman reporter molecules on the surface of nanoparticles. The amount of analytes was directly proportional to the amount of SERS probe being captured at each reaction zone. Hence, the quantitative values of the respective biomarker were determined based on the characteristic peak of specific Raman reporter. To enhance the sensitivity at low concentration (0.01 ng mL^{-1} or even lower), the working range of the biomarkers was tested at 0.01 to 100 ng mL^{-1} for GPBB; 0.01 to 100 ng mL^{-1} for CK−MB; and 0.001 to 200 ng mL^{-1} for cTnT; respectively.

For quantitative analysis, the calibration curve for the quantification of cardiac biomarker levels was generated from the characteristics peak of each Raman reporter molecules. For instance, the peak of 4-nitroaniline was measured at 1387 cm^{-1}; the peak of tert-Butylhydroquinone was at 1450 cm^{-1} while the peak of methyl red was at 1400 cm^{-1}. All these frequencies were used for quantifying biomarkers cTnT, GPBB and CK−MB, respectively. To widen the detection range of the calibration curve, the measurement of biomarker cTnT was prepared in the range of 0.001 ng mL^{-1} to 200 ng mL^{-1}, whereas for biomarkers GPBB and CK−MB, the concentrations were prepared from 0.01 ng $mL^{-1}$to 100 ng mL^{-1} in order to develop a reliable and quantitative SERS-based μPAD for the detection of cardiac biomarkers that would lead to early and accurate diagnosis of AMI.

University of Malaya

There are two linear dynamic ranges displayed in **Figure 4.15(a-c)** for the measurement of respective cardiac biomarker at ≤ 1 ng mL^{-1} or ≥ 5 ng mL^{-1}. For GPBB assay, the regression line equation was shown as y = 356.13 x + 22695 with R^2 = 0.96 for 5 ng mL^{-1} – 100 ng mL^{-1} whereas y = 7938.9 x + 9943.5 with R^2 = 0.88 for 0.01ng mL^{-1} – 1 ng mL^{-1}. For CK−MB, the regression line equation was revealed as y = 229.7 x + 21478 with R^2 = 0.97 for 5 ng mL^{-1} – 100 ng mL^{-1} whereas y = 10389 x + 7766.4 with R^2 = 0.98 for 0.01 ng mL^{-1} – 1 ng mL^{-1}. For cTnT assay, the calibration curve was plotted with the regression line equation, y = 156.06 x + 15749 with R^2 = 0.98 for 5 ng mL^{-1} – 200 ng mL^{-1} whereas y = 6152.6 x + 5487.1 with R^2 = 0.74 for 0.001 ng mL^{-1} – 1 ng mL^{-1}. The limit of detection was determined from the slope of the calibration curve using the standard deviation of y-intercepts (blank) of regression lines as the standard deviation, was defined as $LOD = 3 \times \text{SD of blank/mean of blank}$ (Equation 3.1). The *LOD* for SERS measurement of GPBB, CK−MB and cTnT was calculated to be 8 pg mL^{-1}, 10 pg mL^{-1}, 1 pg mL^{-1}, respectively.

With this SERS-based μPAD, the detection range of GPBB, CK−MB and cTnT was achieved at 0.01 to 100 ng0 mL^{-1}, 0.01 to 100 ng mL^{-1}, and 0.001 to 200 ng mL^{-1}, respectively. These detection ranges covered the clinical range of CK−MB and cTnT in the human body. Despite that, GPPB has not yet been used for clinical test but it is still a potential biomarker for early diagnosis of AMI. Moreover, this SERS-based μPAD with wider detection range is more reliable in aiding an early diagnosis at lower concentration levels and prognosis at higher concentration levels of cardiac biomarkers. This study showed that the SERS-based μPAD could be used for a quantitative measurement of cardiac biomarkers at very low concentration, which was below their clinical cutoff values (i.e., GPBB at 10 ng mL^{-1}; CK−MB at 5 ng mL^{-1} and cTnT at 0.01 ng mL^{-1}). By using this SERS-based μPAD, the *LOD* for GPBB, CK−MB and cTnT was calculated at 8 pg mL^{-1}, 10 pg mL^{-1}, 1 pg mL^{-1} respectively; but the values

are higher than the previously reported values tested on LFAs. Previous study reported the *LOD* for cTnI at 0.44 pg mL^{-1} and CK-MB at 0.55 pg mL^{-1}, with multiple lines of SERS-LFA (Zhang et al., 2018a), whereas the *LOD* with single line of SERS-LFA for CK−MB, cTnI was reported as 0.93 and 0.89 pg mL^{-1}, respectively (Zhang et al., 2018b). The author also reported that the linear dynamic range for CK−MB and cTnI was 0.02 ─ 90 ng mL^{-1}, 0.01 ─ 50 ng mL^{-1}. In other words, the effect of *LOD* might result from the SERS nanotag when using different shape of nanoparticles to maximise enhancement factors. This is because the efficiencies of device can be increased with the nanotag in the following order: spherical or cubes, bimetallic nanorods, nanostars, gold (core)/silver (shell), as reported by Khlebtsov et al. (2019).

In a nutshell, this SERS-based μPAD with multiplex cardiac biomarkers at multi reaction zone was the first attempt for AMI detection. The *LOD* achieved through this proposed SERS-based μPAD was slightly higher than the others reported as SERS-LFAs. However, the *LOD* of SERS-based μPAD in pg mL^{-1} was substantial enough to be used for clinical early diagnosis, as they are well below the clinical cutoff values in ng mL^{-1}.

University of Malaya

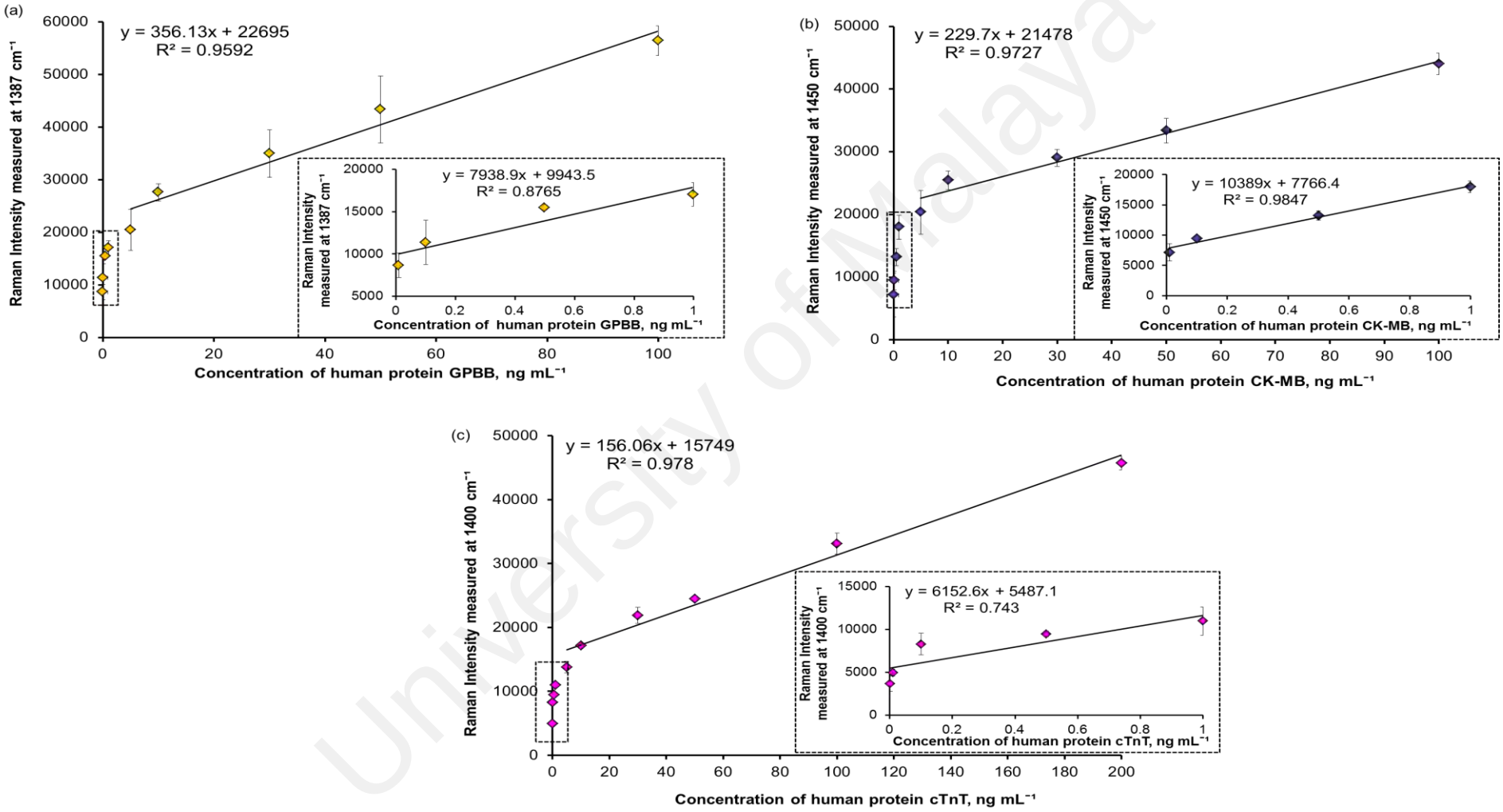

Figure 4.15: Calibration plots of quantitative analysis of multiplex cardiac biomarkers ─ (a) GPBB, (b) CK−MB and (c) cTnT on SERS-based μPAD.

University of Malaya

4.4 Analytical Performance of Microfluidic Paper-Based Analytical Device for Colourimetric and SERS assay

4.4.1 Optimisation of Blocking Reagents

The role of blocking reagent in immunoassay was to block the free surface area to abrogate the high background signals due to non-specific interaction (Gibbs & Kennebunk, 2001). To select the ideal blocking reagent for µPADs, several blocking reagents were tested such as polymer blocker (PVP), non-ionic detergents blocker (Tween 20) and protein blocker (WBR and BSA). For optimisation of blocking reagent, the negative µPAD (phosphate buffer without target analyte) was used as blank and then compared with positive µPAD (phosphate buffer with target analyte). This ensure that the colour signal generated on the µPAD originates from the target analytes in sandwich assay, and not due to the non-specific signal (background) caused by the nanoparticles-conjugated detecting antibody) that was non-specifically absorbed onto the NC membrane without the presence of cardiac biomarkers. In this study, the signal to background ratio versus blocking reagents was measured by smartphone-based camera, desktop scanner and Renishaw InVia Raman Microscope. The high signal to background ratio reflected the optimal blocking performance on NC membrane for an assay. Subsequently, appropriate blocking reagent was used to block the NC membrane after the incubation with primary capturing antibody.

Based on the optimisation results obtained from the colourimetric and SERS assays (**Figure 4.16**), 1% WBR was able to block the unwanted non-specific signal efficiently. Little to no background signal was observed on the negative µPAD (blank), which was tested with phosphate buffer in substitution of purified cardiac biomarkers. Thus, the signal generated from the fabricated µPADs blocked with 1% WBR could confirm that the signal obtained originated from the sandwich assay between capturing antibody and detecting antibody for the respective cardiac biomarker (target analyte). On the other

University of Malaya

hand, the unblocked μPADs and those blocked with other blocking reagents such as 1% BSA, 1% Tween 20, and 1% PVP had generated a high background signal in negative μPAD (blank). This was caused by the nanoparticles-conjugated detecting antibody which was non-specifically absorbed onto the NC membrane without the presence of cardiac biomarkers. Hence, the signal observed on its positive μPADs (tested with cardiac biomarkers) did not necessarily originate from the binding of the interest antigen.

In most of the reported immunoassay studies, the use of BSA as a blocking reagent had been proven to be a good blocker of non-specific protein-surface binding. It was a widely used blocking agent for LFAs (Choi et al., 2010; Lee et al., 2013) and ELISA studies (Ahirwar et al., 2015; Xiao & Isaacs, 2012). However, it did not show similar performance as what had been studied in this study. The μPAD blocked with 1% BSA unexpectedly has yielded a high background signal in negative μPAD, which pointed to the significant non-specific binding of excessive BSA (protein molecules) to immobilised capture antibody on the NC membrane, then attracting and causing non-specific adsorption of detecting antibody onto the NC membrane. As a consequence, this condition has increased the background signal.

Hence, the non-specific binding of BSA proteins has led to a high background signal generated on NC without the presence of target analyte. As reported in earlier studies, Tween 20 was used as a blocking agent in the immunological detection of proteins transferred to nitrocellulose membranes (Batteiger & Jones, 1982) and ELISA (Steinitz, 2000). However, Tween 20 (a non-ionic detergent blocker) showed its weak blocking ability in this study as the μPAD blocked with 1% Tween 20 generated a high background signal in negative μPAD. This could be caused by non-specific absorption of colour nanoparticles-labeled detecting conjugates at unblocked sites on NC

membrane. Similar to the reported literature, Tween 20 is usually incorporated in a washing buffer instead of using it as a blocking reagent for immunoassay. As it is easily removed by washing with aqueous buffer and leaving behind all unblocked sites, hence there is a high probability in generating non-specific signal (Bird et al., 1988). Moreover, 1% PVP is a water-soluble polymer that readily binds to NC membrane of µPAD, but the speed of fluid flow (sample) on the membrane was significantly reduced during assay, thus it might be due to its high viscosity (high molecular weight, 40,000) which is not really suitable for blocking on NC membrane of µPAD. In short, BSA and other blocking reagents did not block the protein-binding sites on the µPAD sufficiently whereas 1% WBR was the best blocking reagent for the reaction zones on µPAD.

University of Malaya

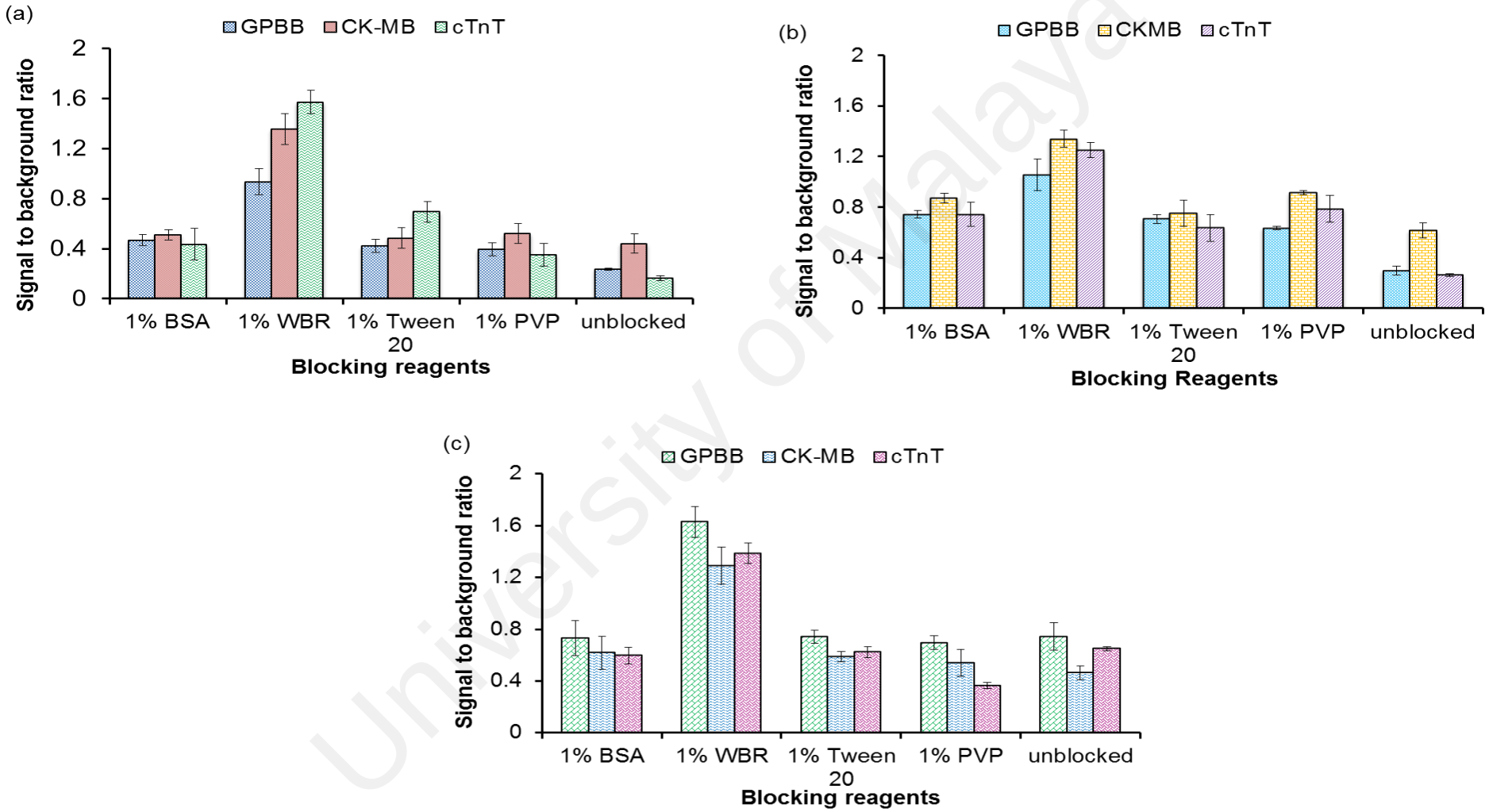

Figure 4.16: The signal to background ratio versus blocking reagents ─ (a) smartphone-based camera, (b) desktop scanner, and (c) Renishaw InVia Raman Microscope.

University of Malaya

4.4.2 Reproducibility Studies

Reproducibility test is a very important parameter for the performance analysis in practical applications as it is a significant and challenging favour to commercial mass production. Thus, the reproducibility of the fabricated μPAD for multiplex colourimetric and SERS assay was evaluated with five equivalent replicates with 10 ng mL^{-1} of standard (containing purified human protein GPBB, CK−MB and cTnT) prepared in 0.01 M phosphate buffer, pH 7.4.

In this study, the relative standard deviation (*RSD*) value is a measure of reproducibility and is used to express the precision of the average of obtained results (mean intensity) by using Equation (3.2). The responses of the sample for 5 times (N = 5) were measured and verified *RSD* in percentage. As shown in **Figure 4.17**, the obtained *RSD* from smartphone-based camera and desktop scanner was 10.6%, 7.0%, 9.8% and 12.2%, 10.2%, 8.5% for GPBB, CK−MB and cTnT, respectively with N = 5. The fabricated μPADs showed a good reproducibility on the colourimetric results as the *RSD* were calculated to be ± 10% for five replicates of multi-cardiac biomarkers measurements. On the other hand, the fabricated μPADs also showed good reproducibility for multiplex SERS assay as the *RSD* obtained from Renishaw InVia Raman Microscope was 5.5%, 4.6%, 5.6% for GPBB, CK−MB and cTnT, respectively with N = 5. The SERS-based μPAD attained the *RSD* at < 10% from five replicates of multi-cardiac biomarkers measurements compared to the colourimetric-based μPAD.

The smaller the *RSD* value means the less difference between the repetitions of an experiment, the better the sensing performance of μPAD. A *RSD* < 10% is considered good reproducibility for an assay (Cazes, 2004; Jaffe et al., 2010). Thus, the signals generated from the μPADs with the constant concentration of cardiac biomarkers were found sensibly consistent with *RSD* ≤ 10%. This indicated that the multiplex detection

of cardiac biomarkers was a reproducible technique using the fabricated μPAD with the proposed colourimetric and also SERS assay procedures as described in Section 3.2 and Section 3.3, respectively.

University of Malaya

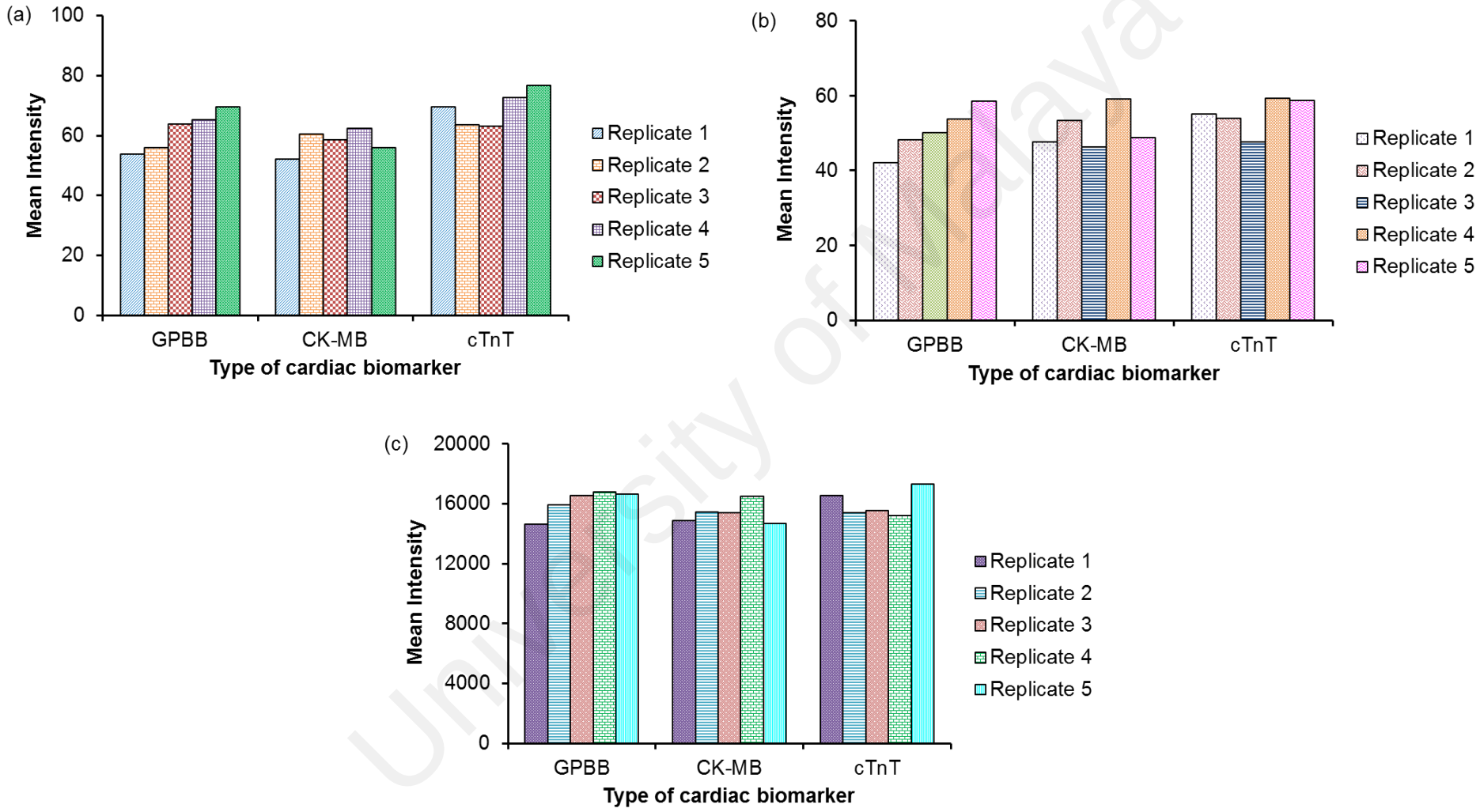

Figure 4.17: Reproducibility tests using (a) smartphone-based camera, (b) desktop scanner, and (c) Renishaw InVia Raman Microscope.

University of Malaya

4.4.3 Intra-and Inter-day Precision Studies

Measurement of the precision is usually expressed numerically as an imprecision-coefficient of variation (*CV*). The *CV* is a measure of relative variability, which is defined as the ratio of the standard deviation to the mean. Prior to ensuring that the fabricated μPAD met the clinical specifications, the results obtained from the precision studies were evaluated. Indeed, the lower the imprecision reflects the better reproducibility of the device. Moreover, the μPAD was intended to be used over a large concentration range; hence precision was estimated at three concentration levels (low, medium and high) across the working range.

As shown in **Figure 4.18**, the precision tests of μPAD were examined in colourimetric using smartphone-based camera and desktop scanner whereas in SERS assay using Renishaw InVia Raman Microscope. For intra-day precision in colourimetric and SERS assay, each cardiac biomarkers, GPBB, CK−MB and cTnT concentrations of 10 ng mL^{-1}, 50 ng mL^{-1} and 100 ng mL^{-1} were carried out within the same day with three replicates and *CV* % was calculated using Equation (3.3). For GPBB, CK−MB and cTnT detection using smartphone-based camera, the CVs of concentrations 10 ng mL^{-1} were calculated as 0.9%, 4.8% and 6.9% respectively. The CVs of 50 ng mL^{-1} concentrations were calculated as 3.7%, 3.5% and 9.1%, respectively. Next, the CVs of 100 ng mL^{-1} concentrations were calculated as 3.9%, 3.2% and 5.2%, respectively (**Figure 4.18a**). For GPBB, CK−MB and cTnT detection using a desktop scanner, the CVs of concentrations 10 ng mL^{-1} were calculated as 3.9%, 11.2% and 10.4% respectively. The CVs of concentrations 50 ng mL^{-1} were determined as 16.8%, 9.1% and 10.3%, respectively Accordingly, the CVs of 100 ng mL^{-1} were determined as 8.5%, 6.7% and 6.0%, respectively (**Figure 4.18b**). For GPBB, CK−MB and cTnT detection using Renishaw InVia Raman Microscope, the CVs of concentrations 10 ng mL^{-1} were calculated as 6.6%, 9.4% and 7.1%

respectively. The CVs of concentrations 50 ng mL^{-1} were calculated as 9.3%, 7.8% and 4.7%, respectively. Next, the CVs of 100 ng mL^{-1} were calculated as 1.2%, 9.0% and 3.9%, respectively (**Figure 4.18c**).

University of Malaya

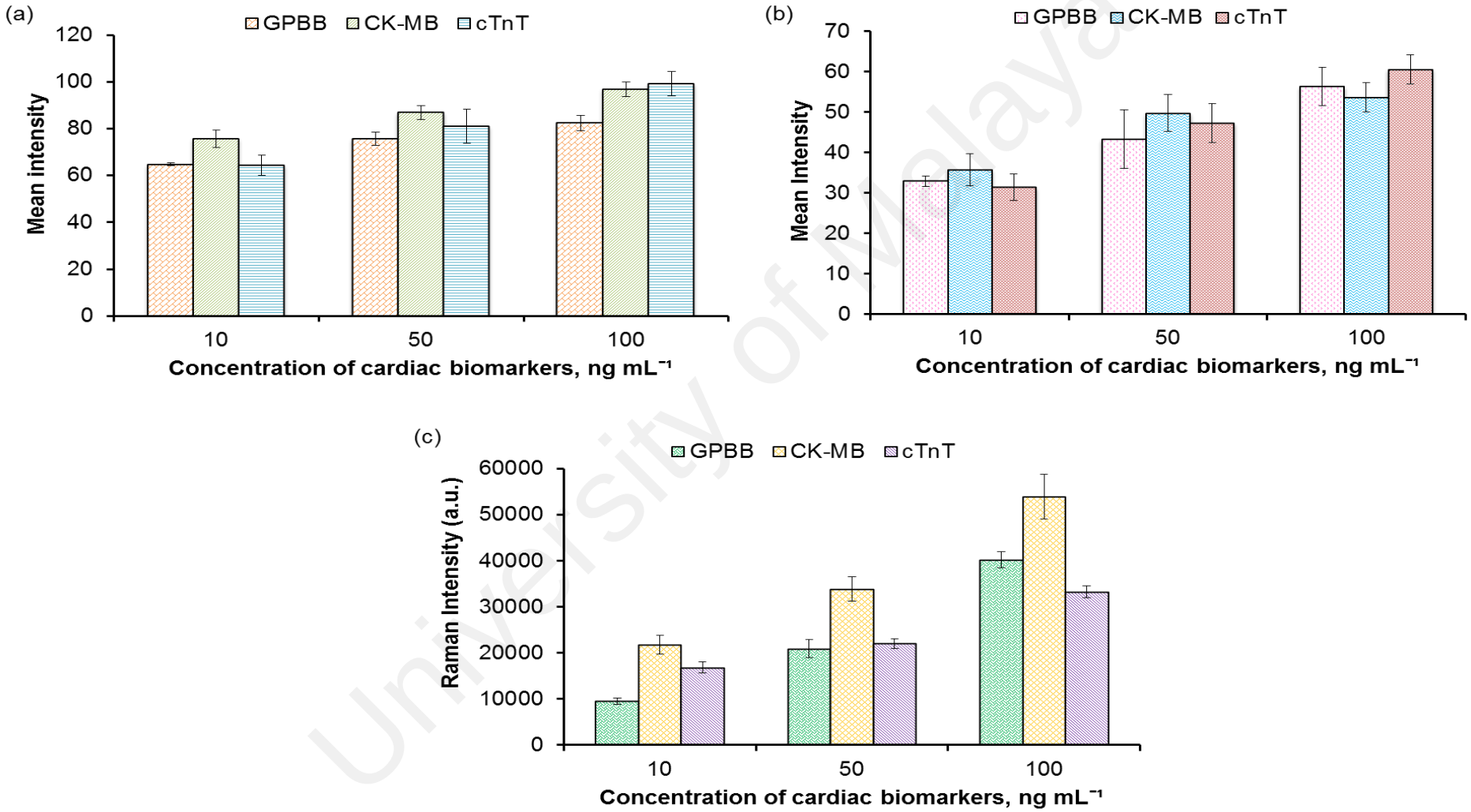

Figure 4.18: Intra-day precision tests using a (a) smartphone-based camera, (b) desktop scanner, and (c) Renishaw InVia Raman Microscope.

University of Malaya

For inter−day precision in colourimetric and SERS assay, the detection of each cardiac biomarker, GPBB, CK−MB and cTnT for concentrations of 10 ng mL^{-1}, 50 ng mL^{-1} and 100 ng mL^{-1} were performed as 3 repetitive measurements on three consecutive days. By using smartphone-based camera in the detection of GPBB, CK−MB and cTnT for three consecutive days, the CVs of 10 ng mL^{-1} concentrations were determined as 5.5%, 6.4% and 6.9%, respectively. In addition, the CVs of 50 ng mL^{-1} concentrations were determined as 8.7%, 3.7% and 3.7%, respectively and the CVs of 100 ng mL^{-1} concentrations were determined as 6.0%, 5.3% and 4.0%, respectively (**Figure 4.19a**). By using a desktop scanner in the detection of GPBB, CK−MB and cTnT for three consecutive days, the CVs of 10 ng mL^{-1} concentrations were determined as 4.6%, 6.1% and 7.0%, respectively The CVs of 50 ng mL^{-1} concentrations were determined as 4.3%, 3.8% and 7.0%, respectively. The CVs for 100 ng mL^{-1} concentrations were determined as 4.9%, 4.3% and 4.6%, respectively (**Figure 4.19b**). On the other hand, by using Renishwa InVia Raman Microscope, the CVs of 10 ng mL^{-1} concentrations of GPBB, CK-MB and cTnT were determined as 7.2%, 7.5% and 4.1%, respectively. The CVs of 50 ng mL^{-1} concentrations were determined as 5.4%, 4.8% and 5.0%, respectively. The CVs for 100 ng mL^{-1} concentrations were determined as 8.5%, 8.4 % and 3.5%, respectively (**Figure 4.19c**).

University of Malaya

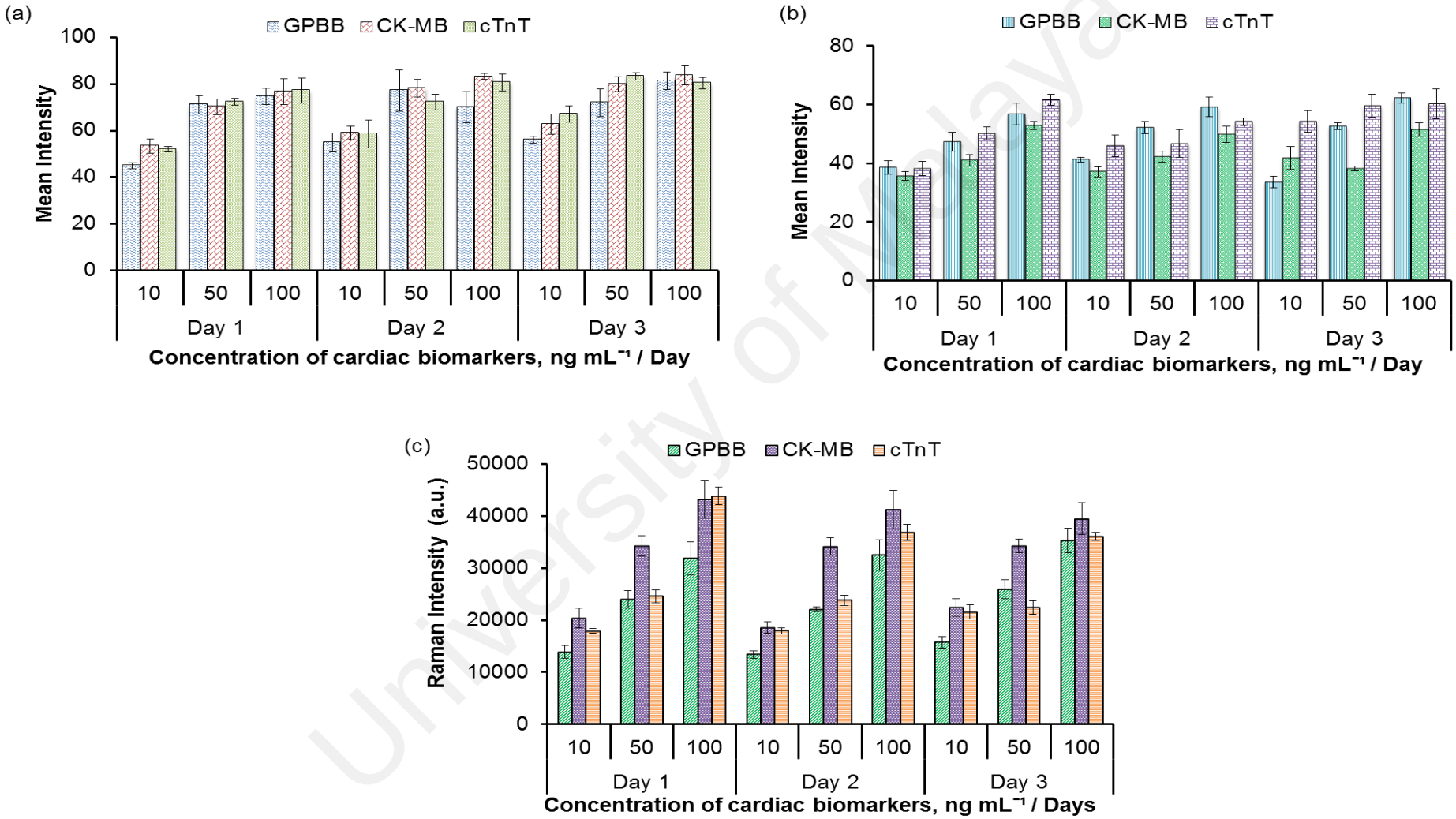

Figure 4.19: Inter-day precision tests using a (a)smartphone-based camera, (b) desktop scanner, and (c) Renishaw InVia Raman Microscope

University of Malaya

It is essential to employ well-characterised and fully validated analytical methods to yield reliable results which can be satisfactorily interpreted. As described by Apple et al. (2005a), the optimal precision for a sensitive clinical assay is considered when *CV* is 10% or lower. However, *CV* with more than 10% is still acceptable if it does not lead to any false positive result. Moreover, the Joint European Society of Cardiology/American College of Cardiology Foundation/ American Heart Association/ World Heart Federation task force for the definition of myocardial infarction has allowed imprecision to be less than 20% *CV* at the 99th percentile concentration. This will preclude the use of assay that do not achieve a level of 10% *CV* imprecision at 99th percentile concentration as it is not rationale (Jaffe et al., 2010). However, assays with *CV* more than 20% at the 99th percentile concentration are not recommended because there is no available data regarding the effect of assay imprecision on clinical accuracy (Apple et al., 2005a; Shah et al., 1992).

Based on the experimental result of intra−day precision at all three concentration tested (10 ng mL^{-1}, 50 ng mL^{-1}, 100 ng mL^{-1}), the results of CVs that were obtained from the colourimetric−based µPAD fall within 0.9% to 9.1% for smartphone-based camera; whereas for desktop scanner, the CVs fall within 3.9% to 16.8%. On the other hand, SERS-based µPAD yielded the CVs from 1.2% to 9.4 %. For inter−day precision, the CVs for three concentrations were found to be less than 10% with optimal precision; that were in the range of 3.7% to 8.7% using smartphone-based camera; 4.3% to 7.3% using desktop scanner; and 3.5% to 8.5% using Renishaw InVia Raman Microscope. To conclude, this fabricated µPAD achieved the intra− and inter−day precision in colourimetric within an acceptable range which is less than 20%; whereas in SERS assay, the CVs fall below 10% (at all three concentrations tested) for all three cardiac biomarker measurements. In comparison, the intra-and inter-day precision of µPAD using SERS assay were found to be more consistent than using colourimetric assay in

detecting multi-cardiac biomarkers. However, both assays are still fulfilling the analytical criteria for clinical use.

4.4.4 Stability Studies

For stability test, the fabricated µPAD surface was stable and retained at 91.2% (G), 85.5% (M), 93.3% (T); 86.2% (G), 78.1% (M), 89.9% (T); 94.5% (G), 92.5% (M), 95.1% (T) of its detection ability after being stored up to 28 days (N = 3). This was calculated using a smartphone-based camera, desktop scanner and Renishaw InVia Raman Microscope, respectively as shown in **Figure 4.20 (a-c)**. In **Figure 4.21**, the results evidently showed that the signal obtained on µPAD slightly changed about 10% to 20% (measured by smartphone-based camera, desktop scanner and Renishaw InVia Raman Microscope) after being stored for 1 week. Despite that, the pair T-test was conducted and the results showed that there was no significant difference in multiplex cardiac biomarker at day 1 with day 28 ($p = 0.451$). Therefore, the overall results were considered stable for both colourimetric and SERS signals as the µPAD can still maintain its detection ability after long period of storage (28 days), which is equivalent to the result obtained on day 1.

As compared to other porous paper substrate (e.g., cellulose filter paper and chromatography paper), the NC membrane has a relatively high protein-binding capacity and is suitable for use in the immunoassay procedure (Holstein et al., 2016). The µPAD with immobilised capturing antibody was tested in different days. The result showed that the immobilised capturing antibody bound well on the membrane and remained active on the membrane to capture the interest antigen (target biomarkers) under 4ºC storage for 28 days: GPBB at 86.1%─94.5%; CKMB at 78.1%─92.5%; and cTnT 89.9%─95.1%. Hence, this accounts that about 90% of the immobilised capturing

monoclonal antibodies on membrane are accessible by target biomarker (analyte) over a period of 28 days, for both colourimetric and SERS assay.

University of Malaya

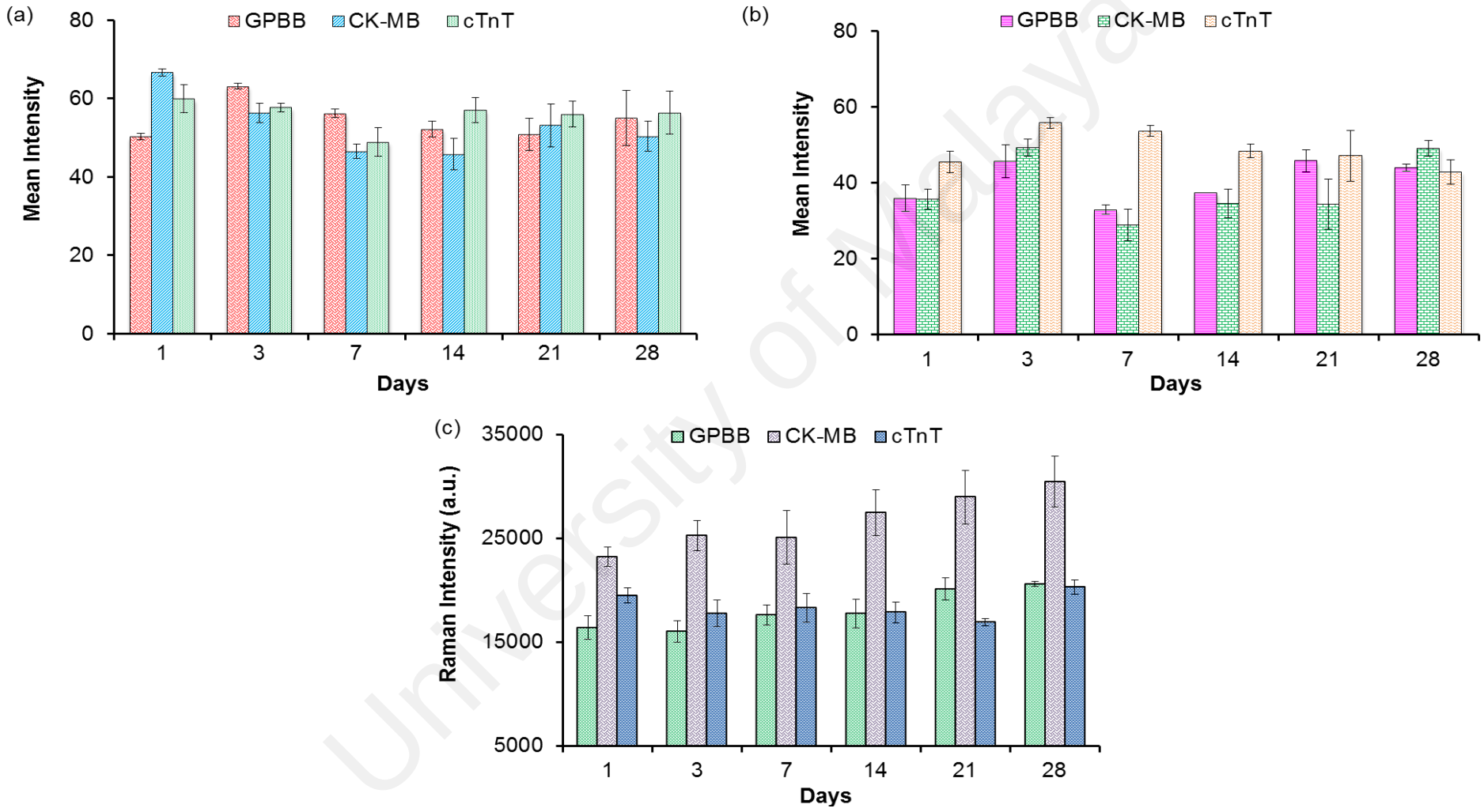

Figure 4.20: Stability test was conducted where the obtained images/spectra captured using ─ (a) smartphone-based camera, (b) desktop scanner, and (c) Renishaw InVia Raman Microscope.

University of Malaya

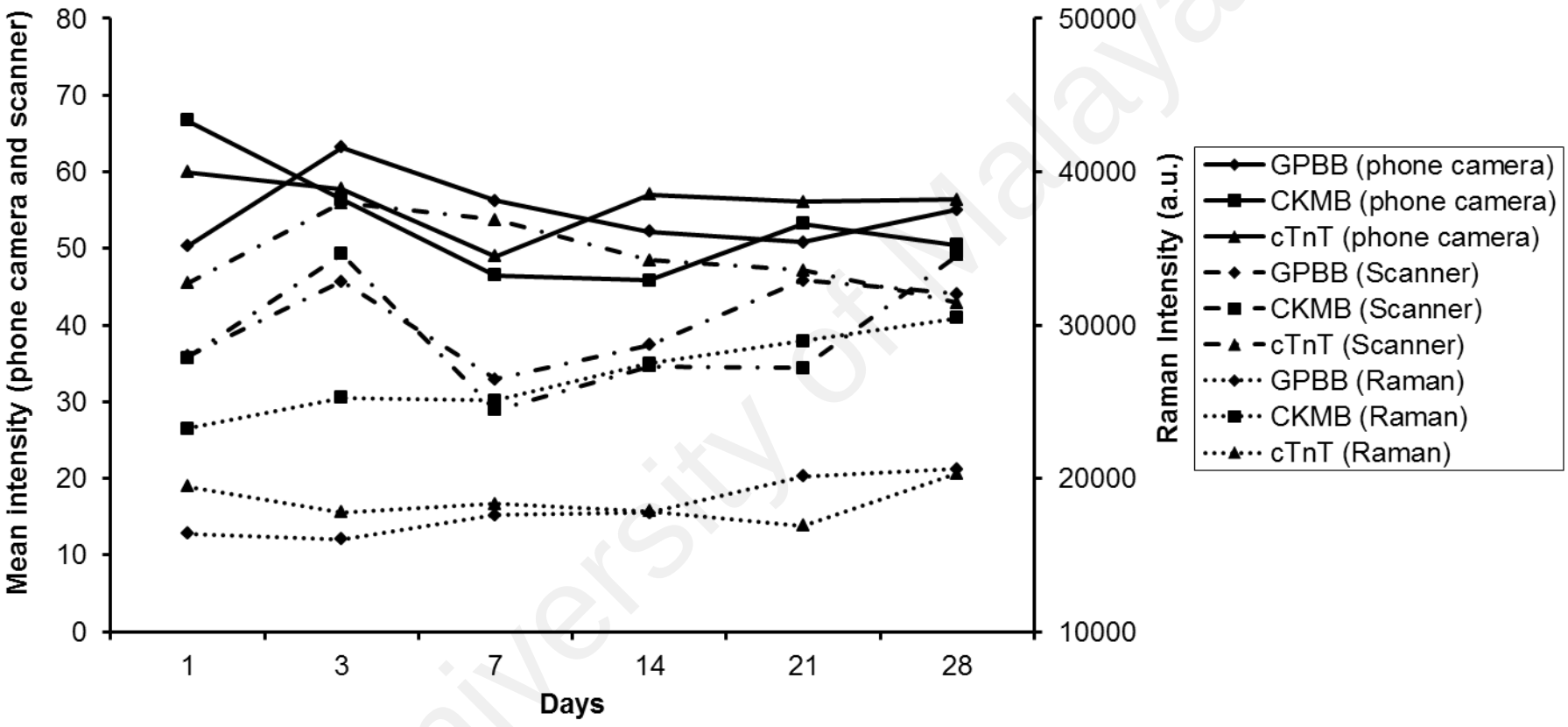

Figure 4.21: Stability test conducted for detecting three cardiac biomarkers (GPBB, CK-MB and cTnT) based on three detection methods (smartphone-based camera, desktop scanner and Renishaw InVia Raman Microscope) from Day 1 ─ Day 28.

University of Malaya

4.4.5 Cross-reactivity Studies

For colourimetric and SERS assay, the cross-reactivity test of human endogenous substances in human serum was assessed, because it might lead to higher background and non-specific binding with the immobilised capturing antibody on the fabricated μPAD. For colourimetric assay, the result was interpreted via the colour change on μPAD hence the cross-reactivity of endogenous substance was spiked in the samples containing cardiac biomarkers. In **Figure 4.22(a-b)**, the colourimetric result obtained for the cross-reactant spiked samples and non-spiked samples (with cardiac biomarker only) did not show any significant difference. This indicates that the immobilised capturing antibody at each reaction zone of μPAD showed high selectivity to their respective cardiac biomarker (GPBB, CK−MB and cTnT), therefore it did not cross-react with the high levels of endogenous substances, including 100 mg mL^{-1} human serum albumin, 100 μg mL^{-1} uric acid and 100 μg mL^{-1} ascorbic acid in human serum containing cardiac biomarkers. In addition, an independent T-test was performed to investigate the significance of the signal intensity differences observed between the three groups of non-spiked samples and cross-reactant spiked sample. Evidently, the result revealed that there was no significant difference in the measurement of multiple cardiac biomarkers between non-spiked samples and spiked sample with each type of cross-reactant such as human serum albumin (p-value = 0.98), uric acid (p-value = 1.00) and ascorbic acid (p-value = 0.99).

For SERS assay, the result was interpreted based on the amount of captured Raman reporter molecules in the SERS probe on μPAD, then being quantified with their respective peak characteristic instead from colour change. Hence, the cross-reactivity of endogenous substance was conducted directly with three cross-reactants and the sample containing cardiac biomarkers. In **Figure 4.22c**, the result showed that the immobilised capturing antibody at each reaction zones was highly selective to their specific cardiac

biomarkers (target analyte). This is because only the sample containing cardiac biomarkers was presented with high SERS intensity signal on SERS-based μPAD instead of three respective cross-reactants.

University of Malaya

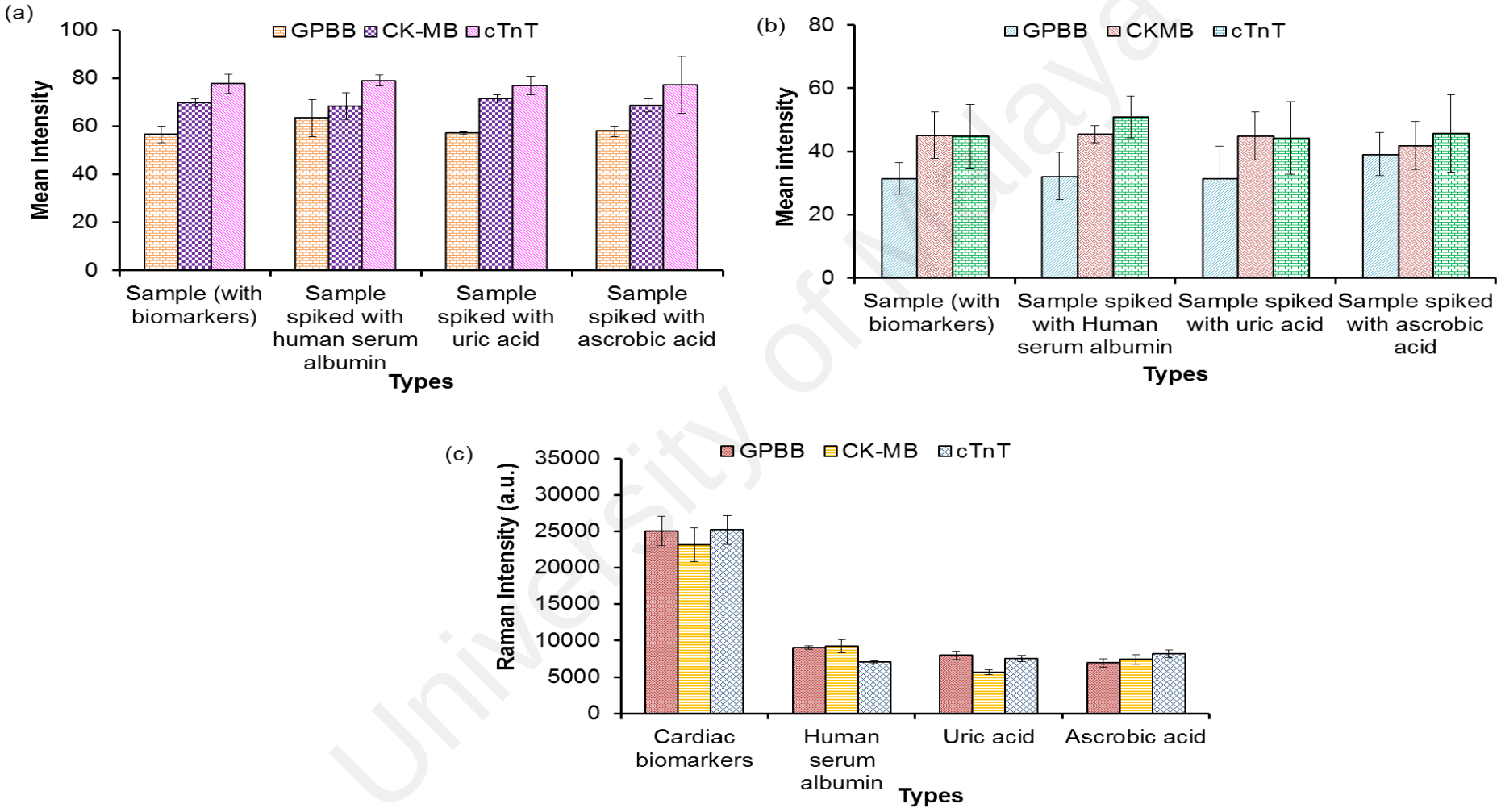

Figure 4.22: Cross-reactivity tests were conducted where the obtained images/spectra were captured using — (a) smartphone-based camera, (b) desktop scanner, and (c) Renishaw InVia Raman Microscope.

University of Malaya

4.4.6 Clinical Sample Analysis

At the University Malaya Medical Center, the Siemens Centaur XPT immunoassay system was used to measure the levels of cardiac biomarkers, CK−MB and Troponin I (cTnI) for ruling out AMI patients. However, GPBB and cTnT assays were not conducted and discussed in this section as only CK−MB human serum was matched with this work.

To ensure the applicability of μPAD in the sample analyses and to overcome matrix interference in human serum, a new calibration curve was plotted using the actual human serum samples containing CK−MB with a known concentration supplied by University Malaya Medical Center. For the colourimetric method, the calibration plot is developed based on the colour signal obtained from smartphone-based camera (**Figure 4.23a**) and desktop scanner (**Figure 4.23b)** which displayed a good linear regression with R^2 =0.96, y= 3.1195 x + 30.545 and with R^2 =0.94, y = 2.3762 x + 14.681, respectively. For the SERS method, the calibration plot is developed based on the SERS signal obtained from Renishaw InVia Raman Microscope (**Figure 4.23c**) which also displayed a good linear regression with R^2 = 0.97, y = 868.39 x + 14083.

As shown in **Figure 4.23**, the points circled and marked as 1, 2 and 3 were the CK−MB levels determined from three unknown human sera samples for both colourimetric and SERS assay. Using these calibration plots, the CK−MB levels in the three unknown human serum samples were calculated and the reliability and accuracy of obtained results were validated using levels measured by Siemens Centaur XPT Immunoassay System (laboratory standard method) used at the University Malaya Medical Center. The results obtained for unknown samples 1, 2 and 3 from the laboratory method using Siemens Centaur XPT Immunoassay System was 2.06 ng mL^{-1}, 2.61 ng $mL^{-1}$and 7.00 ng mL^{-1}, respectively. On the other hand, the colourimetric

result obtained from smartphone-based camera (**Figure 4.23a**) were 1.83 ng mL^{-1}, 2.89 ng mL^{-1} and 8.29 ng mL^{-1} whereas the colourimetric result obtained from the scanner (**Figure 4.23b**) were 2.63 ng mL^{-1}, 2.88 ng mL^{-1} and 8.32 ng mL^{-1} for unknown sample 1, 2 and 3, respectively. In addition, the SERS results obtained from Renishaw InVia Raman Microscope (**Figure 4.23c**) were 1.62 ng mL^{-1}, 2.41 ng mL^{-1} and 7.03 ng mL^{-1} for unknown sample 1, 2 and 3, respectively. From the findings, both the colourimetric and SERS methods were applicable as a promising diagnostic tool for clinical sample analysis.

University of Malaya

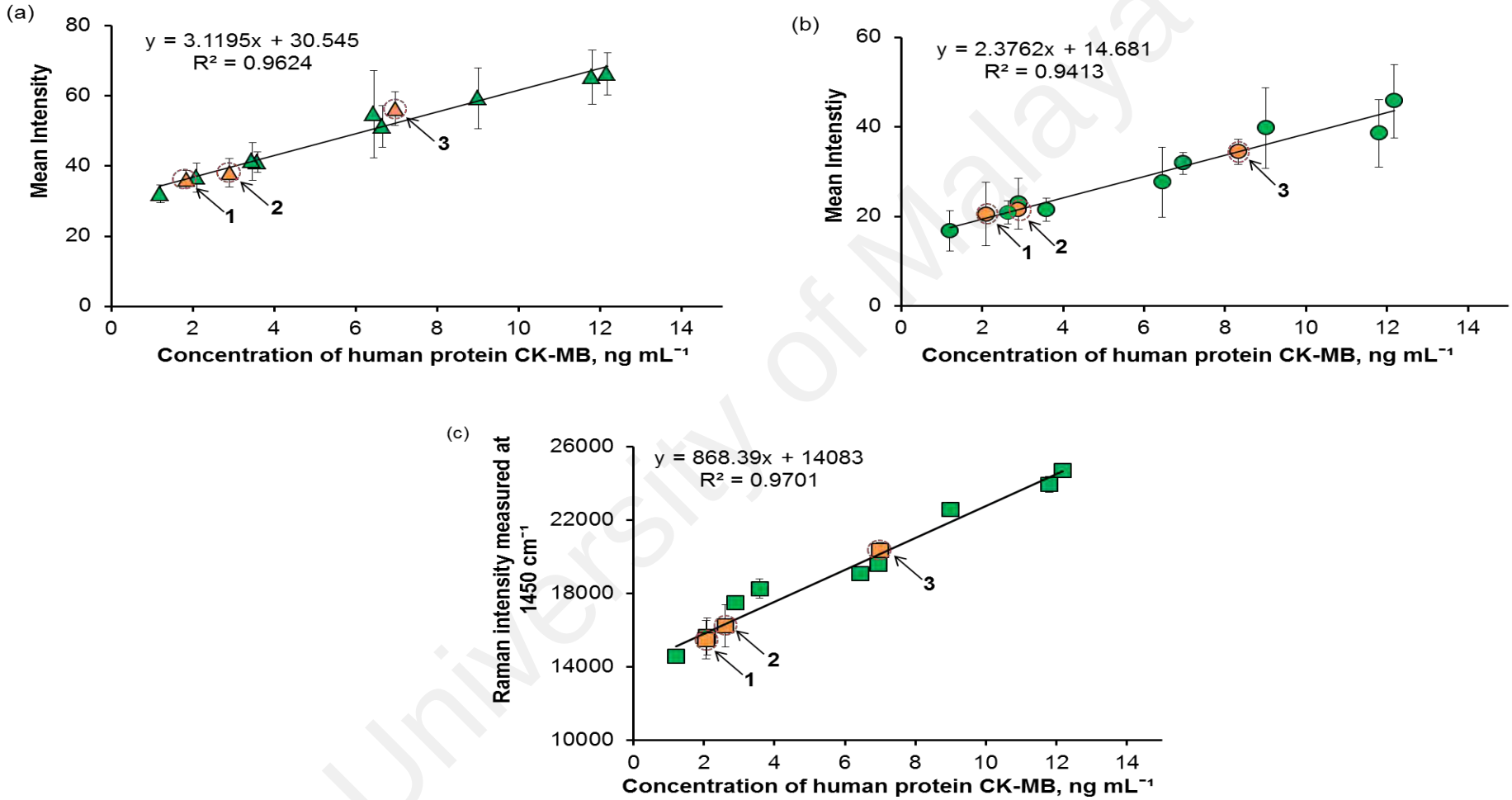

Figure 4.23: Calibration curve for levels of CK−MB protein in the human serum samples measured by (▲) smartphone-based camera; (●) desktop scanner and (■) Renishaw InVia Raman Microscope. The concentrations of three unknown human serum samples containing CK−MB were marked as 1, 2 and 3.

University of Malaya

4.4.7 Comparison of Methods

4.4.7.1 Correlation and Regression Analysis

The Method validation was performed for a total of 12 human serums samples between standard laboratory method— Siemens Centaur XPT Immunoassay System (labeled as I) with these three proposed methods on the fabricated μPAD such as smartphone-based camera (labeled as II); desktop scanner (labeled as III) and Renishaw InVia Raman Microscope (labeled as IV). Therefore, linear regression analysis; Bland–Altman plots and paired sample T-test were discussed in the following section for method comparison studies.

Correlation and linear regression are the common techniques for investigating the relationships between two quantitative variables by fitting a liner equation to observed data obtained from the fabricated μPAD (colourimetric and SERS method) with standard laboratory method (Siemens Centaur XPT Immunoassay System) used in the University Malaya Medical Center, for instance I and II, I and III, and I and IV. Correlation quantifies the strength of the linear relationship between a pair of variables, whereas regression expresses the relationship in the form of an equation.

As shown in **Figure 4.24(a),** there is an excellent correlation between I and II with R^2 of 0.96, y = 0.9759 x + 0.114; **Figure 4.24(b)** showed an excellent correlation was observed between I and III with R^2 of 0.94, y = 1 x + 0.219; and **Figure 4.24(c)** also revealed that an excellent correlation was also observed between I and IV with R^2 of 0.97, y = 1 x − 0.004, respectively. Overall, the proposed methods II (R^2 = 0.96); III (R^2 = 0.94) and IV (R^2 = 0.97) for CK−MB detection promises practical reliability as they exhibited a good fit and strong linear relationship with R^2 close to 1 (Schneider et al., 2010), with 96.3% , 94.1% and 97.1% variance of the observed values that fall within the regression line.

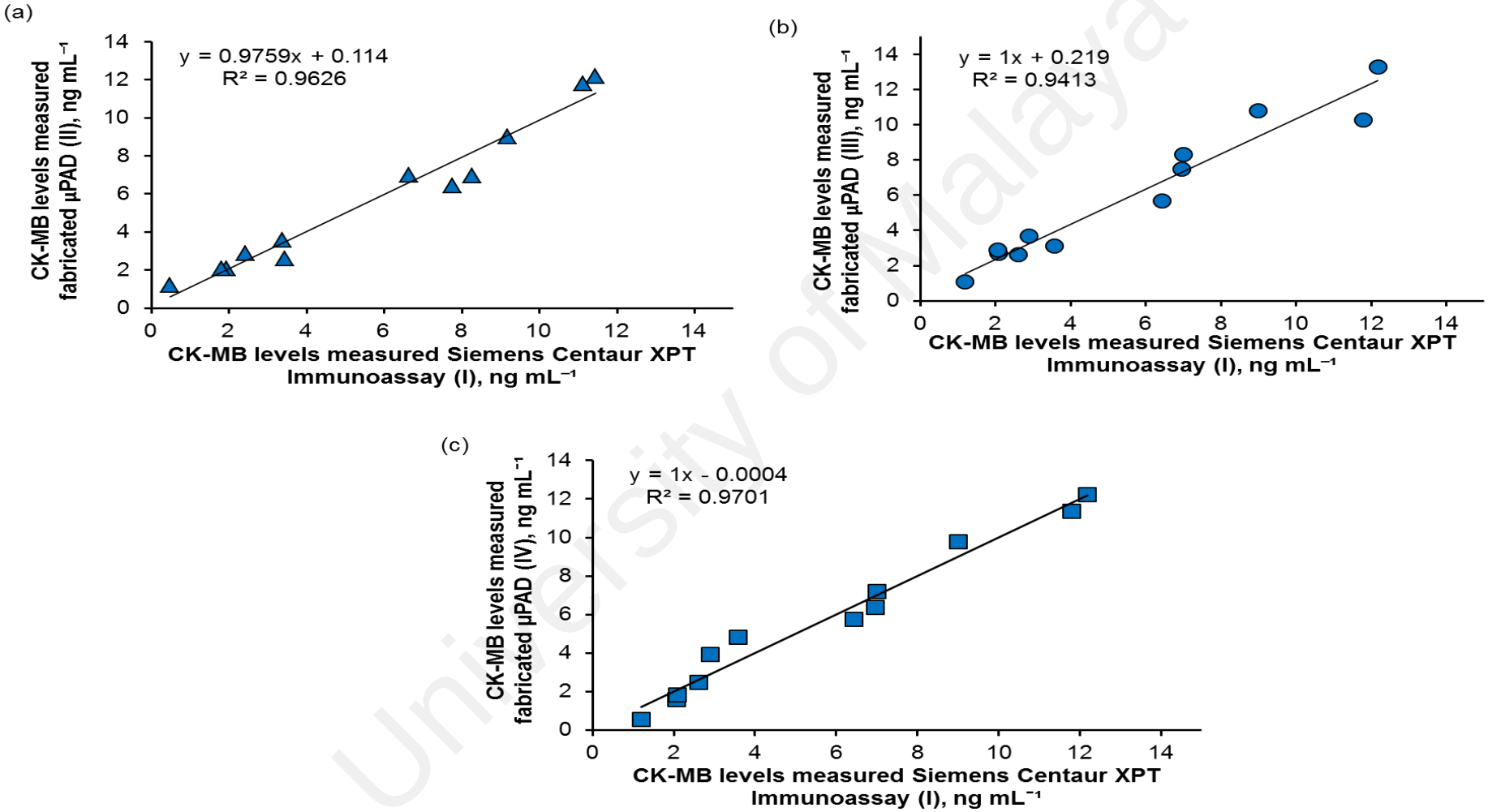

Figure 4.24: The linear regression analysis measured by (▲) smartphone-based camera; (●) desktop scanner and (■) Renishaw InVia Raman Microscope.

University of Malaya

4.4.7.2 Bland–Altman Plot Difference

In clinical measurement, the comparison of a new proposed measurement technique with an established technique is requisite to assess two methods of measurement, the agreement of which are sufficiently close. The Bland–Altman plot difference was schemed to describe the average bias (mean) relative to the reference method and the limits of agreement (95% of the differences) (Altman & Bland, 1983). The resulting graph was a scatter plot, in which the difference of the two paired measurements was plotted against the mean of the two measurements. The mean difference should lie within 95% limit of agreement (mean bias $\pm$ 1.96 SD) (Giavarina, 2015). In this study, the Bland-Altman plot was used to analyse the agreement between the standard laboratory method (I) and proposed µPADs (II, III and IV).

Based on the Bland–Altman plot, **Figure 4.25(a)** shows that the bias (difference between the means I and II) was -0.060, and for the 95% limit of agreement was calculated between -1.499 and 1.379; **Figure 4.25(b)** shows that the bias (difference between the means I and III) was -0.344, and the 95% limit of agreement was between -2.357 and 1.668; and **Figure 4.25(c)** shows that the bias (difference between means I and IV) was 0.00045 and the 95% limit of agreement fell between 1.321 and -1.321. In the limit of agreement, the two methods are defined by a 95% confidence interval of a particular value of the difference. Hence, the value of 1.96 is based on the fact that 95% of the area of a normal distribution is within 1.96 standard deviations of the mean. From the result obtained, all differences were within the mean of -1.96 SD (lower limit of agreement) and mean of +1.96 SD (upper limit of agreement). This indicates that the difference between the two methods (i.e. I and II; I and III and I and IV) were practically significant.

University of Malaya

Moreover, these scatter plots also allow us to investigate any possible relationship between the measurement error and the true value (Giavarina, 2015). The mean of difference equals to zero indicates that exactly the same results were obtained in the measurements from the two methods, but any measurement of variables always involves some degree of error. Compared to I, the mean bias of II (-0.060) and IV (0.00045) was closer to zero than that of III (-0.344), indicating the good agreement between the methods I and II and/or I and IV as they systematically produced equivalent results. Despite this, IV showed the narrowest limits of agreement (between 1.321 and -1.321) and II also showed narrower limit of agreement (between -1.499 and 1.379) than III (between -2.357 and 1.668), indicating that II and IV were reasonably comparable with I, whereas III showed a wider limit range, reflecting less precision and ambiguous results. Therefore, the colourimetric method using smartphone-based camera (II) and SERS method using Renishaw InVia Raman Microscope spectroscopy (IV) are sensibly comparable with the laboratory method (I) used at University Malaya Medical Center for clinical sample analysis.

University of Malaya

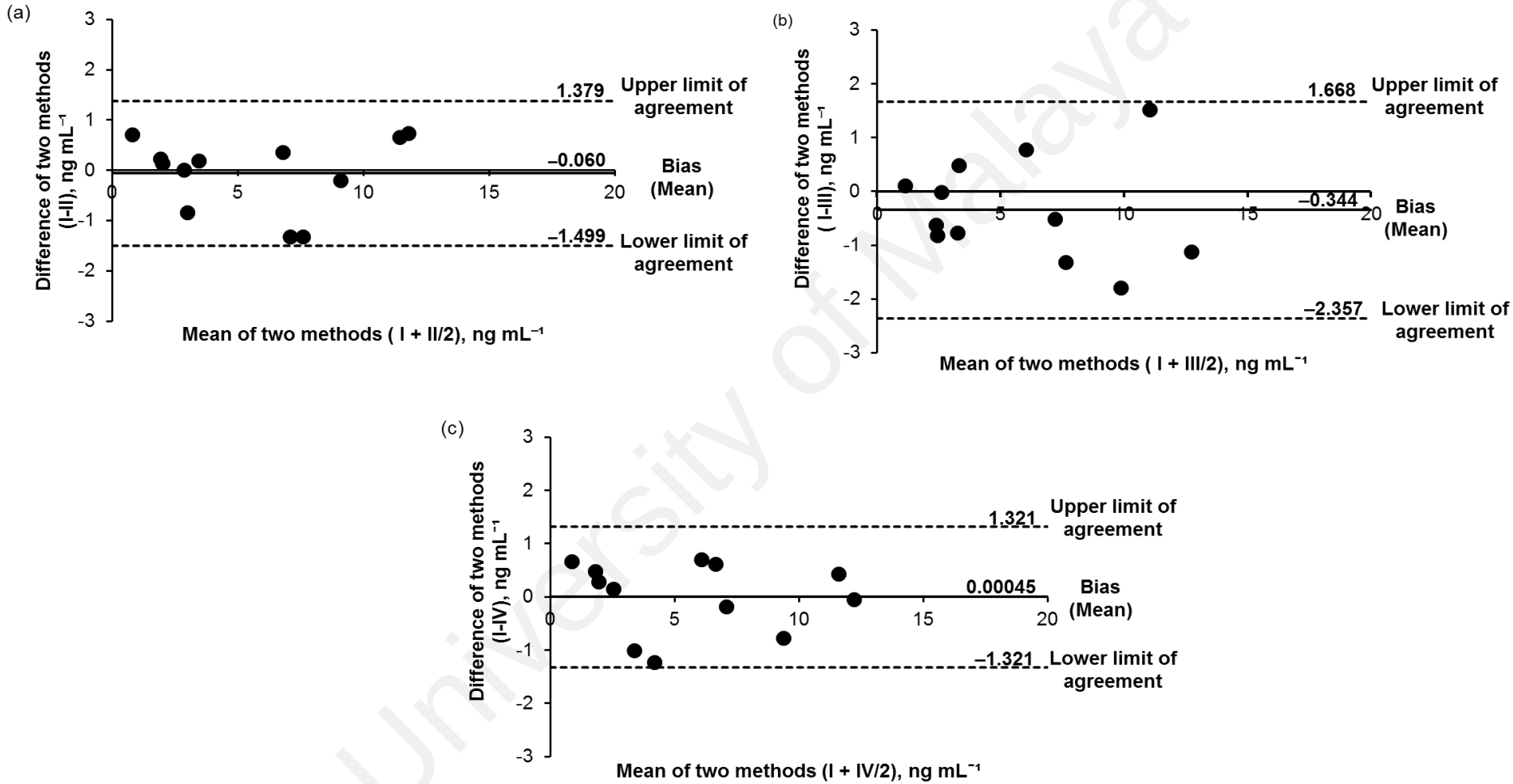

Figure 4.25: Bland–Altman analysis of cardiac CK−MB for 12 serum samples, measured by (a) smartphone-based camera; (b) desktop scanner and (c) Renishaw InVia Raman Microscope. Solid line represents mean (bias), upper dashed line indicates the mean +1.96 SD (upper limit of agreement), and lower dashed line indicates mean -1.96 SD (lower limit of agreement).

University of Malaya

4.4.7.3 Independent T−test (Two−Tailed)

Independent T-test is a statistical method to find out whether there is any significant difference between the two groups. In this study, T-test was employed to compare the differences of methods of measurements on CK−MB levels. Twelve human serum samples were measured using laboratory method (i.e., Siemens Centaur XPT Immunoassay System, (I)). Then, three proposed diagnostic tools (i.e., smartphone-based camera (II), desktop scanner (III) and Renishaw InVia Raman Microscope (IV)) were used and a comparison was made between I and II, I and III, and I and IV. As shown in **Table 4.3**, none of the proposed diagnostic tools were found to be significantly different with the standard laboratory method ($p = 0.970$ for I versus II; $p = 0.830$ for I versus III; and $p = 0.997$ for I versus IV) as only p-value below 0.05 will be considered as significantly different. Taken together, the fabricated μPAD showed an excellent concordance with the calibration and reference method in CK−MB colourimetric and SERS assay.

For acquiring colourimetric quantitative data, the results revealed that a smartphone-based camera is nearly as effective as Siemens Centaur XPT Immunoassay System (laboratory method). Hence, all type of smartphone-based cameras can be used but using a high pixel model of camera (not less than 13 megapixels) is recommended to capture high-resolution images for interpretation, which is similar to this study. Additionally, SERS method can also be an alternative way for attaining SERS quantitative data with high detection sensitivity by using Renishaw InVia Raman Microscope. It is useful for quantitative analysis by determining the fingerprint for particular molecules and their Raman intensity; however the drawback of this SERS method is that it requires the pricey benchtop instrument for quantification of SERS signal on SERS-based μPAD compared to colourimetric method that utilised smartphone-based camera and/or scanner as the diagnostic tool for quantification.

University of Malaya

Table 4.3: Comparison of methods of measurement on CK−MB levels (a) I versus II, (b) I versus III and (c) I versus IV.

(a)	**Siemens Centaur XPT Immunoassay System (I)**	**µPAD with smartphone-based camera (II)**
Mean	5.650833333	5.710700299
Variance	14.75971742	14.66934367
Observations	12	12
Hypothesised Mean Difference	0	
df	22	
t Stat	-0.038228712	
P(T<=t) one-tail	0.484925057	
t Critical one-tail	1.717144374	
P(T<=t) two-tail	**0.969850113**	
t Critical two-tail	2.073873068	

(b)	**Siemens Centaur XPT Immunoassay System (I)**	**µPAD with desktop scanner (III)**
Mean	5.650833	5.995111
Variance	14.75972	15.64409
Observations	12	12
Hypothesised Mean Difference	0	
df	22	
t Stat	-0.21629	
P(T<=t) one-tail	0.415377	
t Critical one-tail	1.717144	
P(T<=t) two-tail	**0.830755**	
t Critical two-tail	2.073873	

University of Malaya

Table 4.3., continued

(c)	**Siemens Centaur XPT Immunoassay System (I)**	**µPAD with Renishaw InVia Raman Microscope spectroscopy (IV)**
Mean	5.650833	5.644415
Variance	14.75972	15.19011
Observations	12	12
Hypothesised Mean Difference	0	
df	22	
t Stat	0.004063	
P(T<=t) one-tail	0.498397	
t Critical one-tail	1.717144	
P(T<=t) two-tail	**0.996795**	
t Critical two-tail	2.073873	

University of Malaya

4.5 Multivariate Analysis

4.5.1 Principal Component Analysis

The PCA is a variable reduction technique used to simplify the structure of compositional data by reducing a large set of variables to a small set of variables while retaining most of the information, which makes it much easier to analyse and interpret (Karamizadeh et al., 2013). It is a mathematical procedure that transforms a number of possibly correlated variables into a smaller number of uncorrelated variables called principle component (PC). When many variables correlate with one another, these variables will contribute strongly to the same PC. Then, each PC sums up a certain percentage of the total variation in the dataset. The first PC always accounts for as much of the variability in the data as possible, and each succeeding component accounts for as much of the remaining variability as possible. By adding more PCs, it should be able to summarise more of the original dataset and estimate the total dataset more accurately, however, it also caused it to be more unwieldy. Therefore, it is always aimed to explain as much of the variance as possible using the minimum number of PCs (Wölcken & Papadopoulos, 2015). The goal of our study is to transform the original multivariate data into a new representative dataset, and to discriminate the three types of cardiac biomarkers.

In this study, 27 Raman spectra of GPBB, 63 Raman spectra of CK−MB and 33 Raman spectra of cTnT making a total of 123 Raman spectra were presented to PCA algorithm. The number of Raman spectra used for PCA study is different for the three groups of cardiac biomarkers, due to their distinct concentrations tested, as mentioned in section 3.5.1. As aforementioned, the training and testing sets are required. With the rules of 80:20, 100 Raman spectra (81% of the total datasets) were randomly selected into the training sets (**Figure 4.26a, c**). The rest of the 23 Raman spectra were automatically classed as testing sets. Based on the experiment results, it shows that the

percentage accounted for the first four PCs were 60.87% for PC1 and 78.27% for PC2, PC3 and PC4. The percentage was rather stabilised after PC4, thus no further PC was examined after PC4. In the PCA score plot, it will also show the distribution of our models. In **Figure 4.26 (b, d)**, the two−dimensional score plot for the two specified PCs were shown. The score plot for PC1 and PC2 showed that most of their scores were not well separated. This indicated that PC1 and PC2 contained most of the common variables of the three cardiac biomarkers; therefore they were incapable of discriminating samples from different classes. Conversely, the score plot for PC3 and PC4 were more helpful to make finer distinction as these two components could discriminate the datasets better and at the same time summarise more variation in the datasets than any other pair of components. Three clusters of cardiac biomarkers in the testing sets can be clearly discriminated by plotting the graph based on PC3 and PC4 (**Figure 4.26d**). Thus, the PCA supports the previous finding (**Figure 4.14**) in which successful identification and discrimination between the three cardiac biomarkers in the multiplex can be made via three unique Raman spectra of each Raman reporter molecules components.

University of Malaya

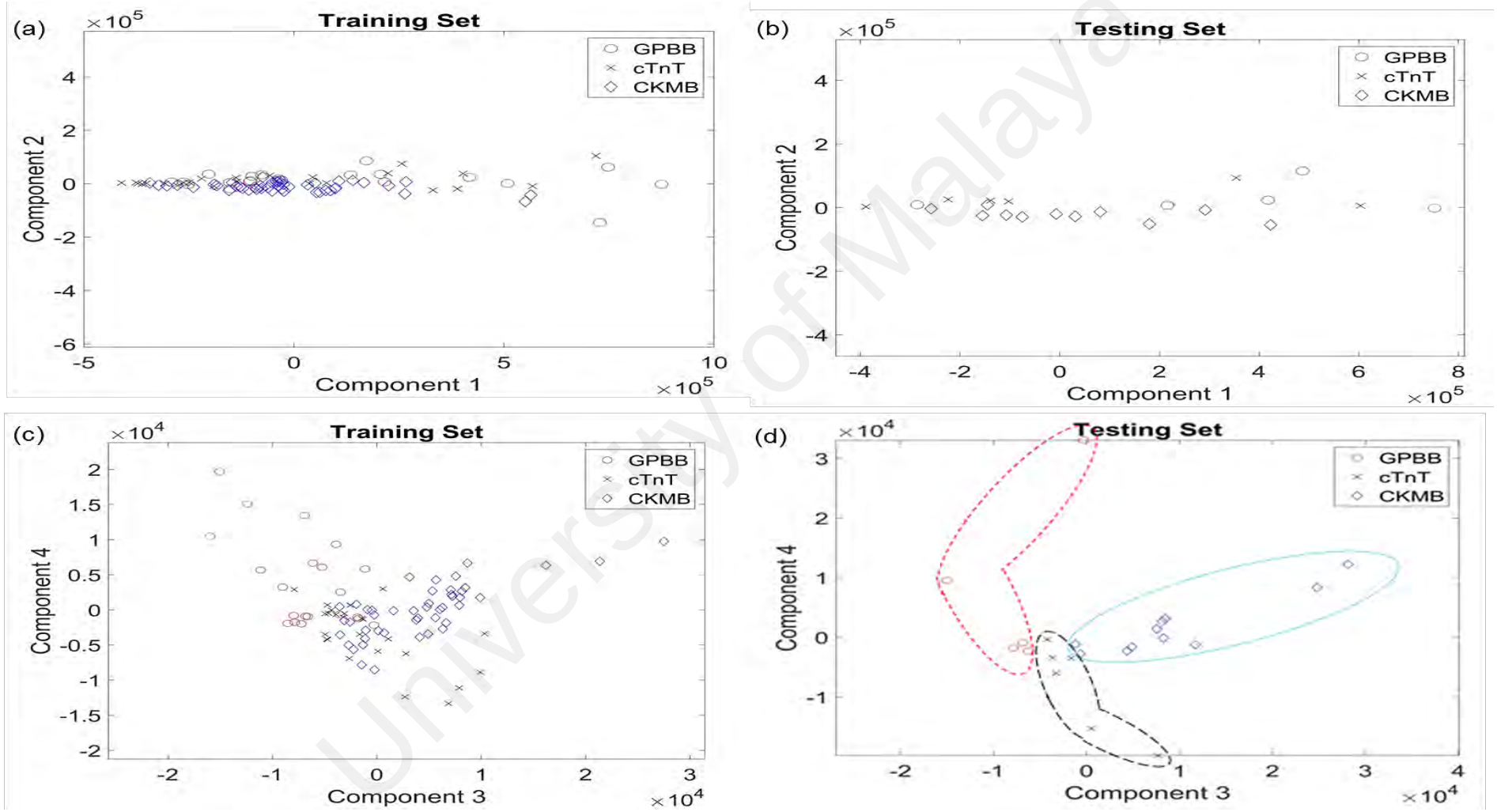

Figure 4.26: Principle component score plot in the (a, b) PC1−PC2 and (c, d) PC3–PC4 plane. Sample indicated as ○ for GPBB, × for cTnT and ◊ for CK−MB.

University of Malaya

In addition, *k*-NN algorithm was implemented to classify the scores plotted with PC3 and PC4 into three groups instead of just by visualising it. The *k*-NN algorithm is a non-parametric method that classifies the cases based on a similarity measure (e.g., distance function). By implementing *k*-NN algorithm in our PCA models, it provides a better confidence that the PCA model was well developed. **Figure 4.27** shows the PCA-*k*-NN prediction, that the data of 18 out of 23 testing sets were predicted correctly. For instance, 5 out of 5 for GPBB (group 1); 4 out of 6 for cTnT (group 2); and 9 out of 12 for CK─MB (group 3) were accurately predicted. In a nutshell, this PCA-*k*-NN algorithm can predict respective cardiac biomarkers (i.e., GPBB, CK−MB and cTnT) from groups accurately with 78.3% accuracy.

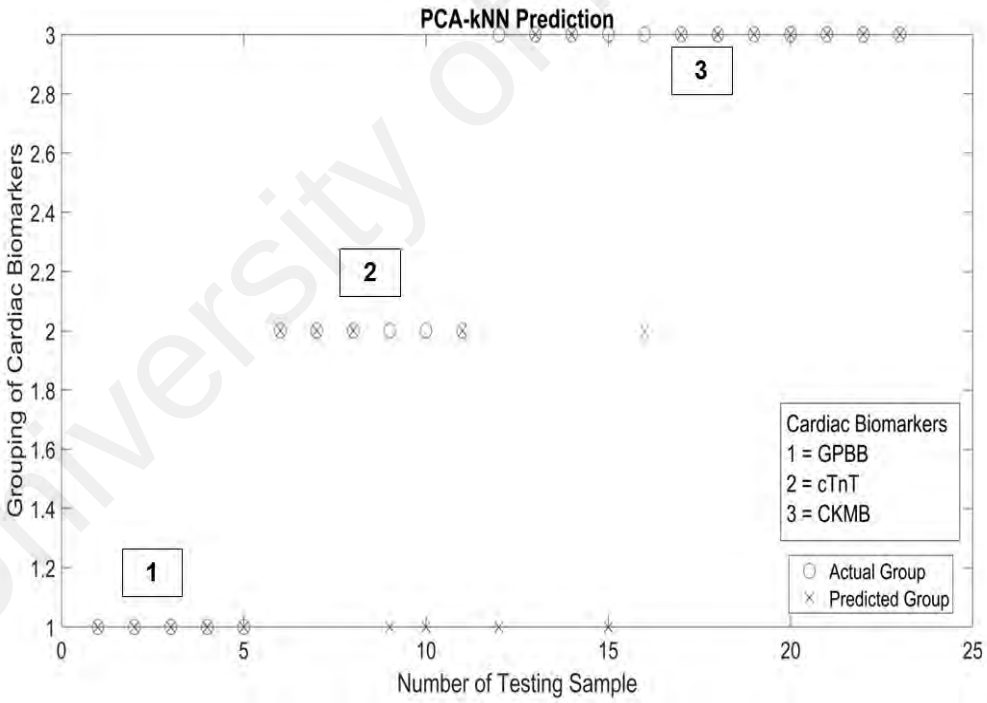

Figure 4.27: PCA - *k*-NN prediction. Sample indicated in group: (1) GPBB. (2) cTnT and (3) CK−MB.

University of Malaya

4.5.2 Partial Least Squares Regression

Partial least squares regression is typically used for a predictive model construction for spectral response as a function of the target variable. In this study, PLS models were developed to examine the relationships of the cardiac biomarkers concentration levels based on the Raman spectral data obtained in the quantitative analysis. Each spectrum is comprised of measurements at 550 different frequencies (from 700 cm^{-1}– 2000 cm^{-1}).

Before developing the PLS models, all the respective spectral data of cardiac biomarkers with their respective concentration were plotted in a 3D plot, as shown in **Figure 4.28**. There were 27 spectra of GPBB assay and 33 spectra of cTnT assay prepared with standard concentrations at 0.01 ng mL^{-1} – 100 ng mL^{-1} and 0.001 ng mL^{-1} – 200 ng mL^{-1}, respectively. On the other hand, in CK−MB assay, it contains a total of 63 spectra: 27 spectra of standard concentrations (0.01 ng mL^{-1} – 100 ng mL^{-1}) and 36 spectra are from clinical samples with random concentrations (between 1.2 ng mL^{-1} – 12.18 ng mL^{-1}).

University of Malaya

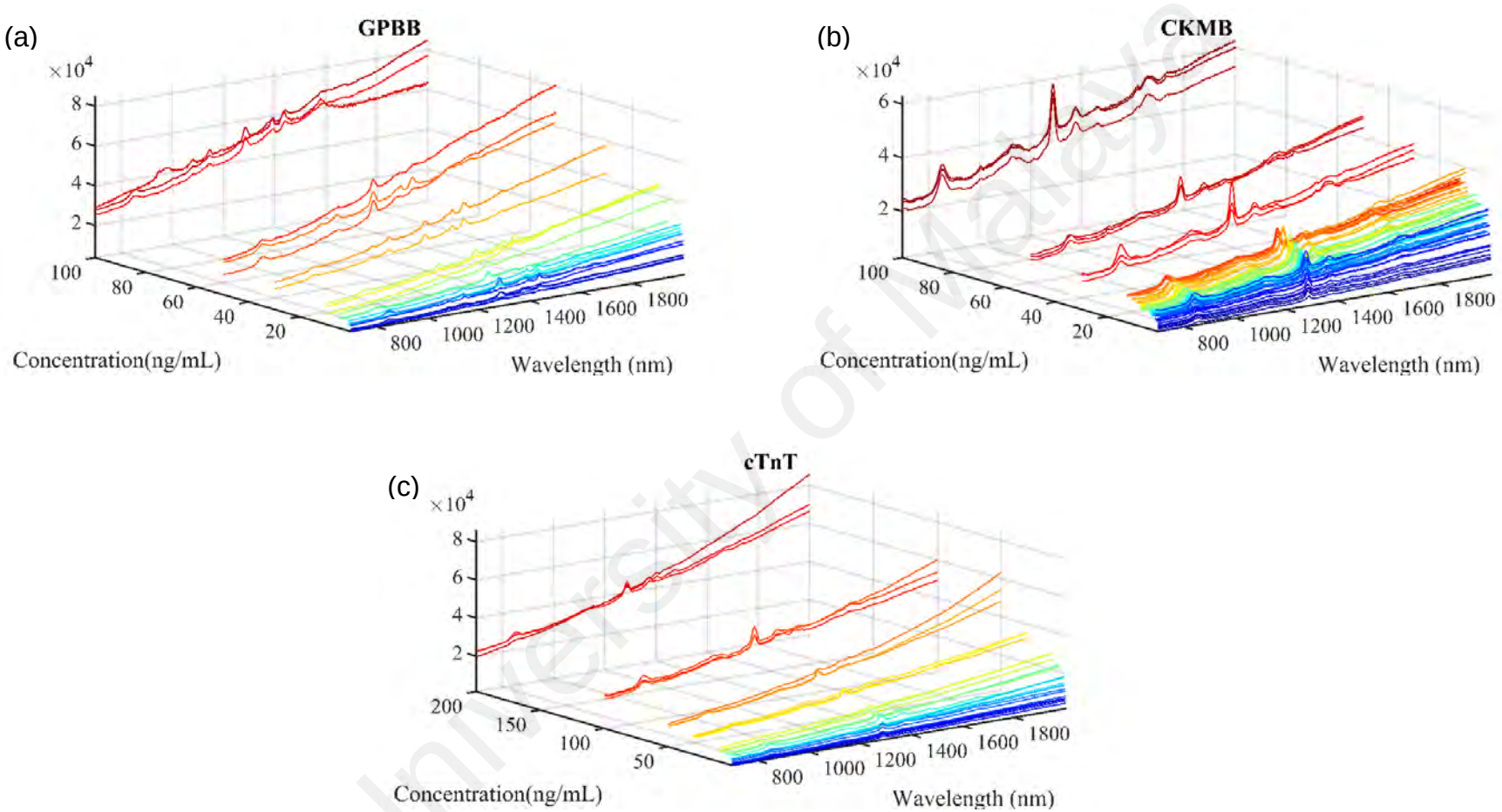

Figure 4.28: Raman spectra data of three cardiac biomarkers (700 – 2000 cm^{-1}) — (a) GPBB (concentration: 0.001−100 ng mL^{-1}), (b) CK−MB (concentration: 0.001−100 ng mL^{-1}), and (c) cTnT (concentration: 0.001−200 ng mL^{-1}).

University of Malaya

There were two options in selecting the best PLS model across the first 20 PLS components. The first option was by measuring the largest increase of percentage of concentration variance by increasing the number of PLS components, as shown in **Figure 4.29**. Based on this selection option, the optimal PLS components were identified: 2 components for GPBB assay, 5 components for CK−MB assay and 7 components for cTnT assay. The larger increase of variance for GPBB was 6% from 83% to 89% at 2 components; CK−MB assay was increased 9% at 5 components from 83% to 92% and cTnT was increased 5% at 7 components from 92% to 97%. These indicated that specific components made significant contributions for the indication of respective cardiac biomarkers concentration as it was explained that there is more variance in the original dataset. The larger the percentage of variance being explained in y-axis (response variable) represents that more information is explained from the original dataset.

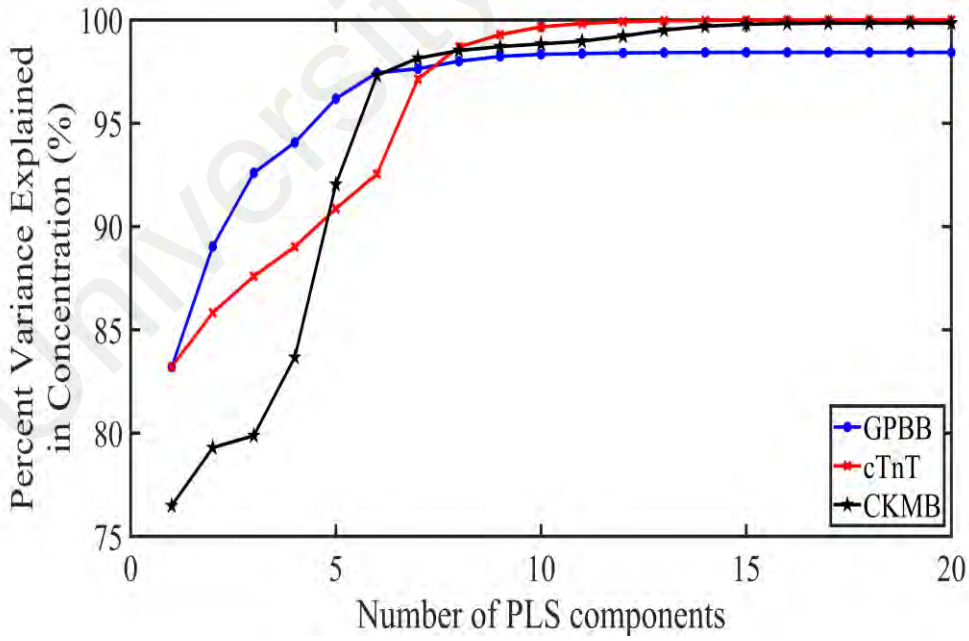

Figure 4.29: Percentage of variance explained in concentration of three cardiac biomarkers across the first 20 PLS components (Method 1: the optimal PLS components are chosen based on the largest increase of the percent variance).

University of Malaya

A second option is to measure the lowest root mean square prediction in LOO cross-validation test. By taking the lowest predictive error will help to preserve a better accuracy for new cardiac biomarker concentration prediction. As shown in **Figure 4.30**, the optimal PLS component was identified at 4 components for GPBB assay (predictive error = 12%), 3 components for CK−MB assay (predictive error = 11%) and 2 components for cTnT assay (predictive error = 27%).

In short, the first option is the quickest way to choose the number of component through the largest increase in variance. However, this can be inaccurate; because of the main purpose of my designed PLS model which was used to predict the unknown concentration of cardiac biomarkers based on Raman spectral data. In contrast, the second option cross-validates and get the lowest predictive error, thus it is more suitable and reliable compared to the first option with a larger increase of variance. Despite the fact that the PLS model was built with the lowest predictive error will help to preserve a better accuracy for unknown cardiac biomarkers concentration prediction.

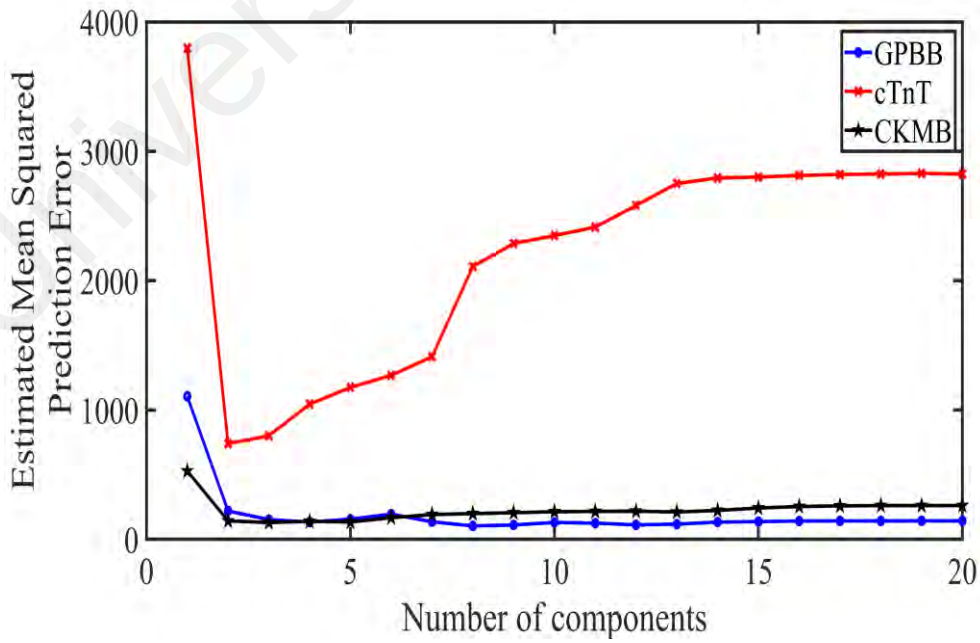

Figure 4.30: Estimated root mean square prediction of three cardiac biomarkers across the first 20 PLS components (Option 2: the optimal PLS components was chosen based on the lowest root mean square prediction value).

Next, the predictive ability of the developed models was assessed by comparing the predicted concentration with actual concentration and then the coefficient of determination was identified (also known as R-squared, goodness-of-fit), as shown in **Figure 4.31**. R^2 indicated how well the data points fit a regression line. The best fit model was GPBB assay, with $R^2 = 0.94$. On the other hand, performance of CK−MB assay prediction was recorded with $R^2 = 0.80$. For cTnT assay, R^2 was reported at 0.86. Herein, the findings revealed a satisfactory performance of the developed PLS model in the prediction of the unknown concentration of respective cardiac biomarkers. Due to the reason of the R^2 three cardiac biomarkers obtained at ≥ 0.80, this indicated that it is a good fit to the data, owing to low discrepancy between the observed values and values expected under the model.

University of Malaya

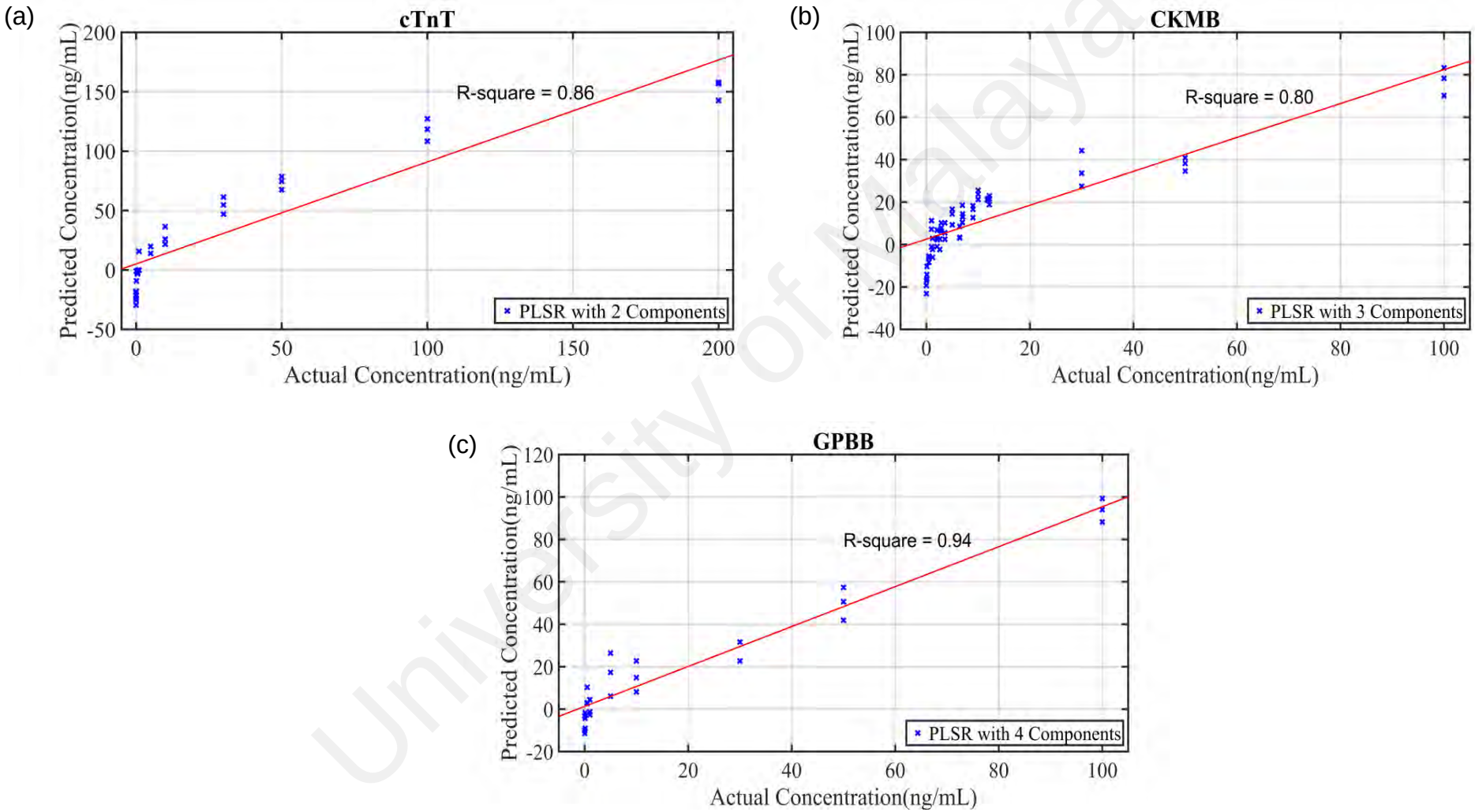

Figure 4.31: Goodness-of-fit of three cardiac biomarkers ─ (a) GPBB, (b) CK−MB and (c) cTnT.

University of Malaya

Furthermore, the parsimonious model of three cardiac biomarkers with their respective PLS components (based on the second selection option in **Figure 4.30**) were evaluated and plotted, as shown in **Figure 4.32**. For GPBB assay (**Figure 4.32a**), the loading of 4 components which contained 4-nitroanilline (Raman reporter molecules), as evidenced by these peaks at 848 cm^{-1} (NO); 1286 cm^{-1} (NO_2 bonds); 1329 cm^{-1}, 1372 cm^{-1}, and 1387 cm^{-1} (C−NO_2 and NO_2 stretching); 1438 cm^{-1} (C−C aromatic ring vibration); 1552 (C−C aromatic ring vibration); and 1610 cm^{-1} (C−C aromatic ring vibration). For CK−MB assay (**Figure 4.32b)**, the loading of 3 components which contained tert-Butylhydroquinone (Raman reporter molecules), as evidenced by those peaks identified at 858 cm^{-1} attributed to (NO); 1283 cm^{-1} (NO_2 bonds); 1368 cm^{-1} (C−NO_2 vibration); 1450cm^{-1} (C−C aromatic ring vibration); and 1650 cm^{-1} (C−C aromatic ring vibration). For cTnT assay (**Figure 4.32c**), the loading of 2 components which contained the following specific Raman peaks from Raman reporter molecules, Methyl red at 855 cm^{-1} (NO); 1291 cm^{-1} (NO_2 bonds); 1372 cm^{-1} (aromatic C−N bond vibration); 1400 cm^{-1} (N=N aromatic stretching); and 1423 cm^{-1} (CH_2 and CH_3 stretching). In short, Renishaw InVia Raman Microscope is found to be associated with PLS modelling using 4 components, 3 components and 2 components to provide highly specific Raman signatures for GPBB, CK−MB and cTnT assay, respectively.

University of Malaya

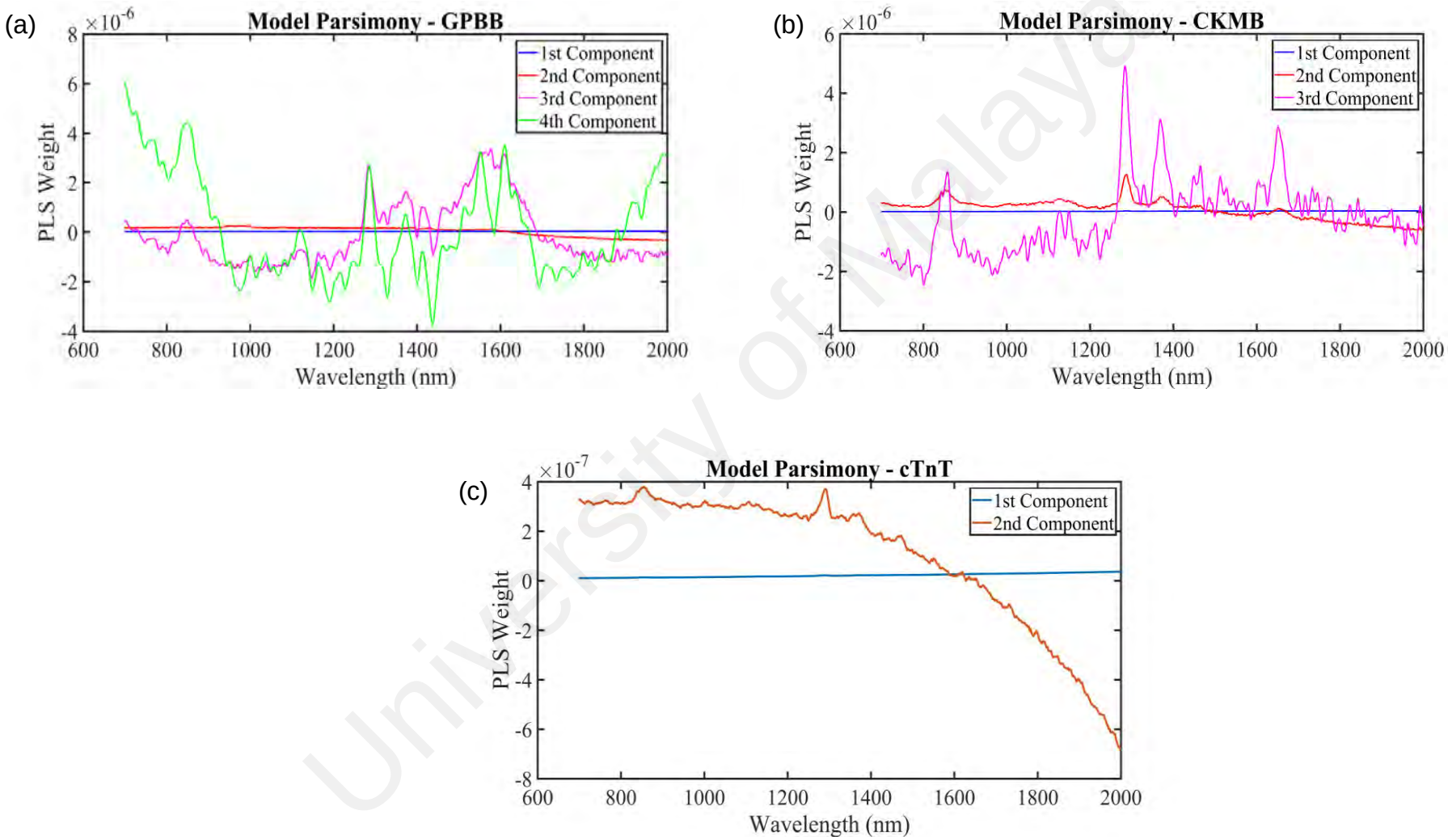

Figure 4.32: Model parsimony of three cardiac biomarkers ─ (a) GPBB, (b) CK−MB and (c) cTnT.

University of Malaya

Overall, the PCA and PLS were performed for two purposes in the regression analysis. First, both techniques are used to convert a set of highly correlated variables to a set of independent variables by using linear transformations. Second, both of the techniques are used for variable reductions. When a dependent variable for a regression is specified, the PLS technique is more efficient than the PCA technique for dimension reduction due to the supervised nature of its algorithm. Last but not least, the developed algorithms have provided three cardiac biomarkers identification and allow for the detection of their unknown using SERS spectra, which is potentially useful in clinical applications. With this approach, the conventional calibration curve for unknown sample analysis can be excluded in the future. The quantification of cardiac biomarkers levels can be determined by the PLS model sensitively and rapidly with their obtained Raman spectral. In the near future, this developed algorithm can also be programmed into the smartphone technology and then used as a custom digital reader application in hospital, to provide fast analysis for rule-in at risk patients with AMI and rule-out chest pain patients with non-AMI.

University of Malaya

CHAPTER 5: CONCLUSIONS AND FUTURE PERSPECTIVES

5.1 Conclusions

In this project, μPAD was developed for simultaneous multiplex detection of cardiac biomarkers, measured and analysed with two detection techniques which were colourimetric and SERS. This μPAD is inexpensive, user-friendly and disposable to suit the demand for effective AMI care to rule in and rule out the suspected ACS patient. A combination testing of the early cardiac marker (GPBB) with prognosis biomarkers (CK−MB and cTnT) on μPAD offers the best approach for early diagnosis and prognosis of AMI, to prompt diagnosis and save the individual from possible heart attack.

For colourimetric detection, the colour signal generated on μPAD can be determined qualitatively using the naked eye. In order to exclude the requirement of using costly instruments for quantitative assay, especially in remote area; a smartphone-based camera and desktop scanner suffice to be an alternative detector for colourimetric assay on the fabricated μPAD. My study shows that the analytical performance of colourimetric-based μPAD obtained from a smartphone-based camera and desktop scanner was reproducible and correlates well to the laboratory standard method (Siemens Centaur XPT Immunoassay System). Indeed, the colourimetric-based μPAD has the potential to be used as a POCT as it had covered the clinical ranges of cardiac biomarkers in the human body.

To further improve the μPAD with higher resource setting (adequate resources in medication, equipment and medical personnel), SERS-based μPAD can be an alternative option for the quantification of cardiac biomarkers. The SERS signal can be determined via the respective Raman reporter in SERS probe (nanotags) using Renishaw InVia Raman Microscope by trained personnel. In comparison to the

University of Malaya

colourimetric method, this SERS method have a more higher quantitative ability and sensitivity, because Raman signal still could be measured when there are no colour seen at lower biomarkers concentration. This study shows that SERS technique could achieve a lower *LOD* and wider dynamic range, but a higher cost instrument is required if compared to colourimetric analysis.

Moreover, three predictive PLS models were designed with MATLAB software for the quantification of cardiac biomarkers based on the obtained Raman spectra. These PLS models are able to provide effective analysis results from the obtained spectrum and aid the medical personnel in providing prompt therapy to at-risk patients.

The present findings indicate the potential of my fabricated μPAD as a POCT device meant for early diagnosis and prognosis of AMI, by using colourimetric and/or SERS method. Overall, the fabricated μPAD offered advantages such as low sample volume requirement (10 μL), fast analysis time (10 minutes), portability, and easy to use. Thus, it is promising to provide better healthcare, and reducing waiting time for result dissemination. By using my fabricated uPAD, the device is able to provide faster and accurate detection, thus patients with MI can receive their treatment early thus giving them higher survival rate. In addition, both detection techniques can be chosen dependent on the available resource for healthcare setting (e.g., medical supplies, equipment and medical personnel).

5.2 Future Perspectives

It can be produced as a μPAD test kit and a portable reader for the final product of colorimetric μPAD, where a smartphone color intensity measurement app can be downloaded. Whereas the μPAD focused on SERS, the built-in predictive PLS models can be integrated in future diagnostic settings in a portable reader or phone camera app

University of Malaya

and can be used to diagnose AMI quickly. Then the unknown biomarker concentration can be automatically estimated without the need for a quantitative calibration measurement curve.

There is also a new sensing approach which can be proposed for AMI detection. A conducting polymer-nanoparticles composite modified electrochemical sensor can be developed for simultaneous multiplex detection of cardiac biomarkers. The conducting polymer-gold nanoparticle nanocomposites can be prepared by in-situ polymerization, wherein the nanoparticles and polymer are produced simultaneously. For the surface modification, the electrode (e.g., glassy carbon) is coated with the synthesized composites. This approach can improve the sensitivity of electrochemical sensors owing to their high stability and electrical conductivity. For that reason, the composites served as an excellent conductive skeleton with high electro-catalytic surface area to lower the activation energy barrier and the over-potential of the reactions. Consequently, promoting the reaction rate and efficiency of electrode activity towards the desired oxidation reaction. In this case, the sensor will exhibit high response to cardiac biomarkers in a wide concentration range with a low detection limit. Furthermore, their complex shape of composite also offers advantages for the incorporation and functionalisation of the antibody without any loss of activity.

In addition, the quantitative detection of cardiac biomarkers can be obtained based on the oxidation peaks of redox labels metal such as lead (Pb), copper (Cu), Zinc (Zn) by using differential pulse voltammetry (DPV). The redox nanomaterial modified antibodies (i.e., copper nanoparticles@anti-GPBB detecting antibody; lead nanoparticles@anti-CK-MB detecting antibody; and zinc nanoparticles@anti-cTnT detecting antibody will be used as the labels for sandwiching the target antigen on electrode. Thus, the DPV was applied for the simultaneous quantitative detection of

three cardiac biomarkers by determining their specific oxidation potential of redox label nanomaterial such as Pb, Cu, and Zn.

5.3 Recommendations

There are some recommendations to improve the detection of AMI in colourimetry, especially when using smartphone-based camera and Image J software. This is despite the fact that linearity is an important parameter for image sensors (e.g., phone camera) in many applications. Nowadays, most of the phone camera have always used CMOS technology for image-processing, which accounts for the non-linear response of the pixel intensity values obtained from the sensor. Generally, when light from an image falls on a camera sensor, it is collected by a matrix of small potential wells called pixels. Therefore the lighting condition during imaging needs to maintain in consistent as it may influence the pixel signal. To solve this limitation, the phone camera need to be calibrated to observe its linearity by turning off the camera's automatic gain contract control (AGC) setting and then use it to measure well calibrated light sources at different intensity levels. Besides that, elimination of a gamma correction or apply gamma transformation to the RGB values can be performed to smartphone camera before using for colour analysis (Priye et al., 2018). This is because the gamma correction function of the CMOS detector distorts the linear response (Shen et al., 2011; Soda & Bakker, 2019). Indeed, the colour generated on the image without gamma correction reflects the actual light intensity. Therefore, the direct linear model that converts the gamma-corrected RGB values can be used to find out the sample concentration accurately. In addition, the curve fitting method in Image J software can be used to select the suitable calibration function for the quantitative measurement of the image. Before use, the captured image can be calibrated by measuring the mean intensity of each standard concentration, and then enter the known standard value in the

University of Malaya

“calibration dialogue box” in Image J for comparison. At last, Image J will display the ideal calibration function (linear or non-linear) for measurement.

For assay, the adsorption method has been used in many applications such as ELISA, and immuno-sensors (e.g. LFA and μPAD) due to its simple procedure with no modification of antibody is required and high antibody-binding capacity. Nevertheless, the antibodies are immobilised in a randomly oriented manner. Hence, there are some covalent immobilisations and modification methods such as covalent coupling and antibody binding protein which could be recommended for oriented antibody/protein on NC membrane to ensure robust immobilisation and to improve orientation outcomes at the substrate (Holstein et al., 2016; Jung et al., 2008). The NC membrane or antibody can be custom modified for covalent coupling antibody. For instance, (i) the membrane can be chemically activated with aldehyde group for covalent cross-linking of antibodies. The amino groups on the antibody surface can be readily coupled with aldehyde-modified membrane for protein (antibody). (ii) Covalent modification of antibodies with affinity tags such as biotin as amino groups of antibodies are also used for biotinylation. Then, the biotinylated antibodies can be strongly immobilised on streptavidin- or avidin-coated surfaces. On the other hand, antibody-binding proteins such as protein G (contains 2 binding sites) and protein A (contains 4 binding size) specifically target the Fc region of an antibody which could be used to maximum range of specificity and binding capacity and fulfil the requirement of ideal antibody orientation. For proper orientation to obtain optimal antigen binding, the antibody can be immobilised on a surface that is pre-coated with an antibody binding protein. However, it has also been reported that the antibody-binding proteins are not suitable for certain assays using multiplex sandwich sensing systems as it has the potential to cross-react with detection or secondary antibody, where the primary antibody does not block all IgG binding sites. Moreover, the drawback related to the above immobilisation

University of Malaya

methods require the additional immobilisation steps or modification process on the membrane or antibody before capturing antibody immobilisation.

University of Malaya

REFERENCES

Abdullah, W. M. S. W., Yusoff, Y. S., Basir, Nurlida, & Yusuf, M. M. (2017). *Mortality rates due to coronary heart disease by specific sex and age groups among malaysians.* Paper presented at the Proceeding of the World Congress on Engineering and Computer Science, San Francisco, United States.

Abe, K., Suzuki, K., & Citterio, D. (2008). Inkjet-printed microfluidic multianalyte chemical sensing paper. *Analytical Chemistry, 80*(18), 6928-6934.

Ahirwar, Rajesh, Bariar, Shilpi, Balakrishnan, Abitha, & Nahar, Pradip. (2015). BSA blocking in enzyme-linked immunosorbent assays is a non-mandatory step: a perspective study on mechanism of BSA blocking in common ELISA protocols. *RSC Advances, 5*(121), 100077-100083.

Ahmad, MI, & Sharma, N. (2012). Biomarkers in acute myocardial infarction. *Journal of Clinical & Experimental Cardiology, 3*(11), 1-8.

Al-Hadi, H. A., & Fox, K. A. (2009). Cardiac markers in the early diagnosis and management of patients with acute coronary syndrome. *Sultan Qaboos University Medical Journal, 9*(3), 231-246.

Alpert, JS, Thygesen, K, Antman, E, & Bassand, JP. (2000). for the Joint European Society of Cardiology/American College of Cardiology Committee. Myocardial infarction redefined—a consensus document of the Joint European Society of Cardiology/American College of Cardiology Committee for the Redefinition of Myocardial Infarction. *Journal of the American College of Cardiology, 36*(3), 959-969.

Altman, Douglas G, & Bland, J Martin. (1983). Measurement in medicine: the analysis of method comparison studies. *Journal of the Royal Statistical Society: Series D (The Statistician), 32*(3), 307-317.

Amsterdam, Ezra A, Wenger, Nanette K, Brindis, Ralph G, Casey, Donald E, Ganiats, Theodore G, Holmes, David R, . . . Kontos, Michael C. (2014). 2014 AHA/ACC guideline for the management of patients with non-ST-elevation acute coronary syndromes. *Circulation, 64*(24), e139-e228.

Amundson, Beret E, & Apple, Fred S. (2015). Cardiac troponin assays: a review of quantitative point-of-care devices and their efficacy in the diagnosis of myocardial infarction. *Clinical Chemistry and Laboratory Medicine (CCLM), 53*(5), 665-676.

Apple, F. S., Parvin, C. A., Buechler, K. F., Christenson, R. H., Wu, A. H., & Jaffe, A. S. (2005a). Validation of the 99th percentile cutoff independent of assay imprecision (CV) for cardiac troponin monitoring for ruling out myocardial infarction. *Clinical Chemistry, 51*(11), 2198-2200.

Apple, F. S., Wu, A. H., Mair, J., Ravkilde, J., Panteghini, M., Tate, J., . . . Committee on Standardization of Markers of Cardiac Damage of the, Ifcc. (2005b). Future

University of Malaya

biomarkers for detection of ischemia and risk stratification in acute coronary syndrome. *Clinical Chemistry, 51*(5), 810-824.

Arunkumar, Shantala, Arunkumar, JS, Krishna, NB, & Shakunthala, GK. (2014). Developments in diagnostic applications of saliva in oral and systemic diseases-A comprehensive review. *Journal of Scientific and Innovative Research, 3*(3), 372-387.

Batteiger, Byron, & Jones, Robert B. (1982). The use of Tween 20 as a blocking agent in the immunological detection of proteins transferred to nitrocellulose membranes. *Journal of Immunological Methods, 55*(3), 297-307.

Bernard, R. (1979). Nomenclature and criteria for diagnosis of ischemic heart disease: Report of the Joint International Society and Federation of Cardiology/World Health Organization task force on standardization of clinical nomenclature. *Circulation, 59*, 607-609.

Bertrand, ME, Simoons, ML, Fox, KAA, Wallentin, LC, Hamm, CW, McFadden, Eugene, . . . Ruzyllo, Witold. (2000). Management of acute coronary syndromes: acute coronary syndromes without persistent ST segment elevation. Recommendations of the Task Force of the European Society of CardiologyRecommendations of the Task Force of the European Society of Cardiology. *European Heart Journal, 21*(17), 1406-1432.

Bhakta, Samir A, Borba, Rubiane, Taba Jr, Mario, Garcia, Carlos D, & Carrilho, Emanuel. (2014). Determination of nitrite in saliva using microfluidic paper-based analytical devices. *Analytica Chimica Acta, 809*, 117-122.

Bhattacharjee, Sourav. (2016). DLS and zeta potential–What they are and what they are not? *Journal of Controlled Release, 235*, 337-351.

Bhayana, V, & Henderson, A Ralph. (1995). Biochemical markers of myocardial damage. *Clinical Biochemistry, 28*(1), 1-29.

Bhimji, A., Zaragoza, A. A., Live, L. S., & Kelley, S. O. (2013). Electrochemical enzyme-linked immunosorbent assay featuring proximal reagent generation: detection of human immunodeficiency virus antibodies in clinical samples. *Analytical Chemistry, 85*(14), 6813-6819.

Bird, Christopher R, Gearing, Andrew JH, & Thorpe, Robin. (1988). The use of Tween 20 alone as a blocking agent for immunoblotting can cause artefactual results. *Journal of Immunological Methods, 106*(2), 175-179.

Blicharz, Timothy M, Rissin, David M, Bowden, Michaela, Hayman, Ryan B, DiCesare, Christopher, Bhatia, Jasvinder S, . . . Loscalzo, Joseph. (2008). Use of colorimetric test strips for monitoring the effect of hemodialysis on salivary nitrite and uric acid in patients with end-stage renal disease: a proof of principle. *Clinical Chemistry, 54*(9), 1473-1480.

Bozbas, H., Yildirir, A., & Muderrisoglu, H. (2006). Cardiac enzymes, renal failure and renal transplantation. *Clinical Medicine & Research, 4*(1), 79-84.

University of Malaya

Bozkurt, S., Kaya, E. B., Okutucu, S., Aytemir, K., Coskun, F., & Oto, A. (2011). The diagnostic and prognostic value of first hour glycogen phosphorylase isoenzyme BB level in acute coronary syndrome. *Cardiology Journal, 18*(5), 496-502.

Brar, Satinder K, & Verma, M. (2011). Measurement of nanoparticles by light-scattering techniques. *Trends in Analytical Chemistry, 30*(1), 4-17.

Braunwald, Eugene, Antman, Elliott M, Beasley, John W, Califf, Robert M, Cheitlin, Melvin D, Hochman, Judith S, . . . Levin, Thomas N. (2000). ACC/AHA guidelines for the management of patients with unstable angina and non–ST-segment elevation myocardial infarction: executive summary and recommendations: a report of the American College of Cardiology/American Heart Association Task Force on Practice Guidelines (Committee on the Management of Patients With Unstable Angina). *Circulation, 102*(10), 1193-1209.

Bruzewicz, Derek A, Reches, Meital, & Whitesides, George M. (2008). Low-cost printing of poly (dimethylsiloxane) barriers to define microchannels in paper. *Analytical Chemistry, 80*(9), 3387-3392.

Carrilho, E., Martinez, A. W., & Whitesides, G. M. (2009a). Understanding wax printing: a simple micropatterning process for paper-based microfluidics. *Analytical Chemistry, 81*(16), 7091-7095.

Carrilho, Emanuel, Phillips, Scott T, Vella, Sarah J, Martinez, Andres W, & Whitesides, George M. (2009b). Paper microzone plates. *Analytical Chemistry, 81*(15), 5990-5998.

Cassano, Christopher L, & Fan, Z Hugh. (2013). Laminated paper-based analytical devices (LPAD): fabrication, characterization, and assays. *Microfluidics and Nanofluidics, 15*(2), 173-181.

Castro, Kepa, de Vallejuelo, Silvia Fdez-Ortiz, & Manuel Madariaga, Juan. (2012). Fireworks: Composition and chemistry through Raman spectroscopy and SEM-EDS imaging. *Spectroscopy Europe, 24*, Retrieved on January 2, 2018 from https://www.spectroscopyeurope.com/article/fireworks-composition-and-chemistry-through-raman-spectroscopy-and-sem-eds-imaging.

Cazes, Jack. (2004). *Analytical instrumentation handbook*. Boca Raton: CRC Press.

Chacko, Sanoj, Haseeb, Sohaib, Glover, Benedict M, Wallbridge, David, & Harper, Alan. (2017). The role of biomarkers in the diagnosis and risk stratification of acute coronary syndrome. *Future Science OA, 4*(1), Article#FSO251.

Chaita, T. M., Graham, S. M., Maxwell, S. M., Sirivasin, W., Sabchareon, A., & Beeching, N. J. (1995). Salivary sampling for hepatitis B surface antigen carriage: a sensitive technique suitable for epidemiological studies. *Annals of Tropical Paediatrics, 15*(2), 135-139.

Chen, Yu, Wang, Jie, Liu, Zhongming, Wang, Xingang, Li, Xin, & Shan, Guiqiu. (2018). A simple and versatile paper-based electrochemiluminescence

University of Malaya

biosensing platform for hepatitis B virus surface antigen detection. *Biochemical Engineering Journal, 129*, 1-6.

Chial, HJ, & Splittgerber, AG. (1993). A comparison of the binding of Coomassie brilliant blue to proteins at low and neutral pH. *Analytical Biochemistry, 213*(2), 362-369.

Choi, Dong Hwan, Lee, Seok Ki, Oh, Young Kyoung, Bae, Byeong Woo, Lee, Sung Dong, Kim, Sanghyo, . . . Kim, Min-Gon. (2010). A dual gold nanoparticle conjugate-based lateral flow assay (LFA) method for the analysis of troponin I. *Biosensors and Bioelectronics, 25*(8), 1999-2002.

Clayton, Katherine N, Salameh, Janelle W, Wereley, Steven T, & Kinzer-Ursem, Tamara L. (2016). Physical characterization of nanoparticle size and surface modification using particle scattering diffusometry. *Biomicrofluidics, 10*(5), Article#054107.

Cone, E. J. (1993). Saliva testing for drugs of abuse. *Annals of the New York Academy of Sciences, 694*, 91-127.

Cowart, Steven L, & Stachura, Max E. (1990). Glucosuria (Chapter 139). In H. Walker, W. Hall & J. Hurst (Eds.), *Clinical Methods: The History, Physical, and Laboratory Examinations* (3rd ed.) (pp. 653-657). Boston: Butterworths.

Crowley, Timothy A, & Pizziconi, Vincent. (2005). Isolation of plasma from whole blood using planar microfilters for lab-on-a-chip applications. *Lab on a Chip, 5*(9), 922-929.

Cubranic, Z., Madzar, Z., Matijevic, S., Dvornik, S., Fisic, E., Tomulic, V., . . . Zaputovic, L. (2012). Diagnostic accuracy of heart fatty acid binding protein (H-FABP) and glycogen phosphorylase isoenzyme BB (GPBB) in diagnosis of acute myocardial infarction in patients with acute coronary syndrome. *Biochemia Medica, 22*(2), 225-236.

Cutler, Christopher W, Stanford, Thomas W, Abraham, Celeste, Cederberg, Robert A, Boardman, Thomas J, & Ross, Candy. (2000). Clinical benefits of oral irrigation for periodontitis are related to reduction of pro - inflammatory cytokine levels and plaque. *Journal of Clinical Periodontology, 27*(2), 134-143.

Daniel, Marie-Christine, & Astruc, Didier. (2004). Gold nanoparticles: assembly, supramolecular chemistry, quantum-size-related properties, and applications toward biology, catalysis, and nanotechnology. *Chemical Reviews, 104*(1), 293-346.

Daubert, M. A., & Jeremias, A. (2010). The utility of troponin measurement to detect myocardial infarction: review of the current findings. *Vascular Health and Risk Management, 6*, 691-699.

de Lemos, J. A. (2013). Increasingly sensitive assays for cardiac troponins: a review. *JAMA, 309*(21), 2262-2269.

University of Malaya

de Tarso Garcia, Paulo, Cardoso, Thiago Miguel Garcia, Garcia, Carlos Diego, Carrilho, Emanuel, & Coltro, Wendell Karlos Tomazelli. (2014). A handheld stamping process to fabricate microfluidic paper-based analytical devices with chemically modified surface for clinical assays. *RSC Advances, 4*(71), 37637-37644.

De Winter, Robbert J, Koster, Rudolph W, Sturk, Augueste, & Sanders, Gerard T. (1995). Value of myoglobin, troponin T, and CK-MB mass in ruling out an acute myocardial infarction in the emergency room. *Circulation, 92*(12), 3401-3407.

Delaney, Jacqui L, Hogan, Conor F, Tian, Junfei, & Shen, Wei. (2011). Electrogenerated chemiluminescence detection in paper-based microfluidic sensors. *Analytical Chemistry, 83*(4), 1300-1306.

Dereli, Ö, Erdogdu, Y, Gulluoglu, MT, Türkkan, E, Özmen, A, & Sundaraganesan, N. (2012). Vibrational spectral and quantum chemical investigations of tert-butyl-hydroquinone. *Journal of Molecular Structure, 1012*, 168-176.

Deshpande, Alok, & Birnbaum, Yochai. (2014). ST-segment elevation: Distinguishing ST elevation myocardial infarction from ST elevation secondary to nonischemic etiologies. *World Journal of Cardiology, 6*(10), 1067-1079.

Dickstein, K. (2008). ESC Committee for Practice Guidelines (CPG): ESC Guidelines for the diagnosis and treatment of acute and chronic heart failure 2008: The Task Force for the Diagnosis and Treatment of Acute and Chronic Heart Failure 2008 of the European Society of Cardiology: Developed in collaboration with the Heart Failure Association of the ESC (HFA) and endorsed by the European Society of Intensive Care Medicine (ESICM). *European Heart Journal, 29*(10), 2388-2442.

Diris, J. H., Hackeng, C. M., Kooman, J. P., Pinto, Y. M., Hermens, W. T., & van Dieijen-Visser, M. P. (2004). Impaired renal clearance explains elevated troponin T fragments in hemodialysis patients. *Circulation, 109*(1), 23-25.

Do Kim, Ki, & Kim, Hee Taik. (2002). Formation of silica nanoparticles by hydrolysis of TEOS using a mixed semi-batch/batch method. *Journal of Sol-Gel Science and Technology, 25*(3), 183-189.

Dungchai, W., Chailapakul, O., & Henry, C. S. (2009). Electrochemical detection for paper-based microfluidics. *Analytical Chemistry, 81*(14), 5821-5826.

Dungchai, Wijitar, Chailapakul, Orawon, & Henry, Charles S. (2011). A low-cost,simple, and rapid fabrication method for paper-based microfluidics using wax screen-printing. *Analyst, 136*(1), 77-82.

Emmons, W. (1997). Accuracy of oral specimen testing for human immunodeficiency virus. *American Journal of Medicine, 102*(4A), 15-20.

Fenton, Erin M, Mascarenas, Monica R, López, Gabriel P, & Sibbett, Scott S. (2008). Multiplex lateral-flow test strips fabricated by two-dimensional shaping. *ACS Applied Materials & Interfaces, 1*(1), 124-129.

University of Malaya

Fiorini, Gina S, & Chiu, Daniel T. (2005). Disposable microfluidic devices: fabrication, function, and application. *BioTechniques, 38*(3), 429-450.

Foo, J. Y., Wan, Y., Kostner, K., Arivalagan, A., Atherton, J., Cooper-White, J., . . . Punyadeera, C. (2012). NT-ProBNP levels in saliva and its clinical relevance to heart failure. *PLOS One, 7*(10), Article# e48452.

Freda, Benjamin J, Tang, WH Wilson, Van Lente, Frederick, Peacock, W Franklin, & Francis, Gary S. (2002). Cardiac troponins in renal insufficiency: review and clinical implications. *Journal of the American College of Cardiology, 40*(12), 2065-2071.

Free, Alfred H, Adams, Ernest C, Kercher, Mary Lou, Free, Helen M, & Cook, Marion H. (1957). Simple specific test for urine glucose. *Clinical Chemistry, 3*(3), 163-168.

Gao, X., Zheng, P., Kasani, S., Wu, S., Yang, F., Lewis, S., . . . Wu, N. (2017). Paper-Based Surface-Enhanced Raman Scattering Lateral Flow Strip for Detection of Neuron-Specific Enolase in Blood Plasma. *Analytical Chemistry, 89*(18), 10104-10110.

Ghosh, Sujit Kumar, & Pal, Tarasankar. (2007). Interparticle coupling effect on the surface plasmon resonance of gold nanoparticles: from theory to applications. *Chemical Reviews, 107*(11), 4797-4862.

Giannitsis, E., Becker, M., Kurz, K., Hess, G., Zdunek, D., & Katus, H. A. (2010). High-sensitivity cardiac troponin T for early prediction of evolving non-ST-segment elevation myocardial infarction in patients with suspected acute coronary syndrome and negative troponin results on admission. *Clinical Chemistry, 56*(4), 642-650.

Giavarina, D. (2015). Understanding Bland Altman analysis. *Biochemia Medica, 25*(2), 141-151.

Gibbs, Judy, & Kennebunk, ME. (2001). Effective blocking procedures, *ELISA Technical Bull,* pp. 1-6. Retrieved on July 20, 2017 from http://www.gongyingshi.com/item/doc/20141221/elisa20141223.pdf.

Grieshaber, Dorothee, MacKenzie, Robert, Vörös, Janos, & Reimhult, Erik. (2008). Electrochemical biosensors-sensor principles and architectures. *Sensors, 8*(3), 1400-1458.

Gross, Erin M, Durant, Hannah E, Hipp, Kenneth N, & Lai, Rebecca Y. (2017). Electrochemiluminescence detection in paper ‐ based and other inexpensive microfluidic devices. *ChemElectroChem, 4*(7), 1594-1603.

Gupta, Sanjiv, Singh, KN, Bapat, V, Mishra, V, Agarwal, DK, & Gupta, P. (2008). Diagnosis of acute myocardial infarction: CK-MB versus cTn-T in Indian patients. *Indian Journal of Clinical Biochemistry, 23*(1), 89-91.

University of Malaya

Hamblin, Michael R, Avci, Pinar, & Gupta, Gaurav K. (2016). *Imaging in dermatology*. Boston, Massachusetts, United State: Academic Press.

Hamm, Christian W, Bassand, Jean-Pierre, Agewall, Stefan, Bax, J, Boersma, Eric, Bueno, Hector, . . . Huber, Kurt. (2011). ESC Committee for Practice Guidelines. ESC Guidelines for the management of acute coronary syndromes in patients presenting without persistent ST-segment elevation: The Task Force for the management of acute coronary syndromes (ACS) in patients presenting without persistent ST-segment elevation of the European Society of Cardiology (ESC). *European Heart Journal, 32*(23), 2999-3054.

He, Qiaohong, Ma, Cuicui, Hu, Xianqiao, & Chen, Hengwu. (2013). Method for fabrication of paper-based microfluidic devices by alkylsilane self-assembling and UV/O3-patterning. *Analytical Chemistry, 85*(3), 1327-1331.

He, Yong, Wu, Yan, Xiao, Xiao, Fu, JianZhong, & Xue, GuangHuai. (2014). A low-cost and rapid microfluidic paper-based analytical device fabrication method: flash foam stamp lithography. *RSC Advances, 4*(109), 63860-63865.

Holstein, Carly A, Chevalier, Aaron, Bennett, Steven, Anderson, Caitlin E, Keniston, Karen, Olsen, Cathryn, . . . Fu, Elain. (2016). Immobilizing affinity proteins to nitrocellulose: a toolbox for paper-based assay developers. *Analytical and Bioanalytical Chemistry, 408*(5), 1335-1346.

Hu, Lianzhe, & Xu, Guobao. (2010). Applications and trends in electrochemiluminescence. *Chemical Society Reviews, 39*(8), 3275-3304.

Huang, Y. X., Wu, Z. J., Huang, B. T., & Luo, M. (2013). Pathway and mechanism of pH dependent human hemoglobin tetramer-dimer-monomer dissociations. *PLOS One, 8*(11), Article#e81708.

Inoue, T., & Tanaka, Y. (2016). Hepatitis B virus and its sexually transmitted infection - an update. *Microbial Cell, 3*(9), 420-437.

Jaffe, Allan S, Apple, Fred S, Morrow, David A, Lindahl, Bertil, & Katus, Hugo A. (2010). Being rational about (im) precision: A statement from the Biochemistry Subcommittee of the Joint European Society of Cardiology/American College of Cardiology Foundation/American Heart Association/World Heart Federation Task force for the definition of myocardial infarction. *Clinical Chemistry, 56*(6), 941-943.

Jaffe, Allan S, Babuin, Luciano, & Apple, Fred S. (2006). Biomarkers in acute cardiac disease. *Journal of the American College of Cardiology, 48*(1), 1-11.

Jalal, Uddin M, Kim, Sang C, & Shim, Joon S. (2017). Histogram analysis for smartphone-based rapid hematocrit determination. *Biomedical Optics Express, 8*(7), 3317-3328.

Jayawardane, B Manori, Wei, Shen, McKelvie, Ian D, & Kolev, Spas D. (2014). Microfluidic paper-based analytical device for the determination of nitrite and nitrate. *Analytical Chemistry, 86*(15), 7274-7279.

University of Malaya

Jazayeri, Mir Hadi, Amani, Hamed, Pourfatollah, Ali Akbar, Pazoki-Toroudi, Hamidreza, & Sedighimoghaddam, Bijan. (2016). Various methods of gold nanoparticles (GNPs) conjugation to antibodies. *Sensing and Bio-sensing Research, 9*, 17-22.

Jung, Yongwon, Jeong, Jin Young, & Chung, Bong Hyun. (2008). Recent advances in immobilization methods of antibodies on solid supports. *Analyst, 133*(6), 697-701.

Kaneta, Takashi, Alahmad, Waleed, & Varanusupakul, Pakorn. (2019). Microfluidic paper-based analytical devices with instrument-free detection and miniaturized portable detectors. *Applied Spectroscopy Reviews, 54*(2), 1-25.

Karamizadeh, Sasan, Abdullah, Shahidan M, Manaf, Azizah A, Zamani, Mazdak, & Hooman, Alireza. (2013). An overview of principal component analysis. *Journal of Signal and Information Processing, 4*(3), 173-175.

Kaski, Juan Carlos, & Holt, David W. (2013). Myocardial Damage: Early detection by novel biochemical markers *Myocardial Damage*. London, UK: Springer

Kaufman, Eliaz, & Lamster, Ira B. (2002). The diagnostic applications of saliva—a review. *Critical Reviews in Oral Biology & Medicine, 13*(2), 197-212.

Kawasaki, Ernest S. (1990). Sample preparation from blood, cells and other fluids. In M. A. Innis, D. H. Gelfand, J. J. Sninsky & T. J. White (Eds.), *PCR protocols: A guide to methods and applications* (pp. 461-482). San Diego: Academic Press.

Ke, YC, & Stroeve, Pieter. (2005). Polymer-layered silicate and silica nanocomposites. Amsterdam, Boston: Elsevier.

Kemp, M, Donovan, J, Higham, H, & Hooper, J. (2004). Biochemical markers of myocardial injury. *British Journal of Anaesthesia, 93*(1), 63-73.

Khlebtsov, B. N., Bratashov, D. N., Byzova, N. A., Dzantiev, B. B., & Khlebtsov, N. G. (2019). SERS-based lateral flow immunoassay of troponin I by using gap-enhanced Raman tags. *Nano Research, 12*(2), 413-420.

Kidwell, David A, Holland, Janel C, & Athanaselis, Sotiris. (1998). Testing for drugs of abuse in saliva and sweat. *Journal of Chromatography B: Biomedical Sciences and Applications, 713*(1), 111-135.

Kilickap, S, Barista, I, Akgul, E, Aytemir, K, Aksoyek, S, Aksoy, S, . . . Tekuzman, G. (2005). cTnT can be a useful marker for early detection of anthracycline cardiotoxicity. *Annals of Oncology, 16*(5), 798-804.

Klasner, S. A., Price, A. K., Hoeman, K. W., Wilson, R. S., Bell, K. J., & Culbertson, C. T. (2010). Paper-based microfluidic devices for analysis of clinically relevant analytes present in urine and saliva. *Analytical and Bioanalytical Chemistry, 397*(5), 1821-1829.

Kobayashi, Yoshio, Katakami, Hironori, Mine, Eiichi, Nagao, Daisuke, Konno, Mikio, & Liz-Marzán, Luis M. (2005). Silica coating of silver nanoparticles using a

University of Malaya

modified Stöber method. *Journal of Colloid and Interface Science, 283*(2), 392-396.

Kong, Jilie, & Yu, Shaoning. (2007). Fourier transform infrared spectroscopic analysis of protein secondary structures. *Acta Biochimica et Biophysica Sinica, 39*(8), 549-559.

Kontos, M. C., Diercks, D. B., & Kirk, J. D. (2010). Emergency department and office-based evaluation of patients with chest pain. *Mayo Clinic Proceedings, 85*(3), 284-299.

Kumar, A., & Cannon, C. P. (2009a). Acute coronary syndromes: diagnosis and management, part I. *Mayo Clinic Proceedings, 84*(10), 917-938.

Kumar, A., & Cannon, C. P. (2009b). Acute coronary syndromes: Diagnosis and management, part II. *Mayo Clinic Proceedings, 84*(11), 1021-1036.

Lang, K, Börner, A, & Figulla, HR. (2000). Comparison of biochemical markers for the detection of minimal myocardial injury: superior sensitivity of cardiac troponin–T ELISA. *Journal of Internal Medicine, 247*(1), 119-123.

Lang, N. P., Joss, A., Orsanic, T., Gusberti, F. A., & Siegrist, B. E. (1986). Bleeding on probing. A predictor for the progression of periodontal disease? *Journal of Clinical Periodontology, 13*(6), 590-596.

Lee, Linda G, Nordman, Eric S, Johnson, Martin D, & Oldham, Mark F. (2013). A low-cost, high-performance system for fluorescence lateral flow assays. *Biosensors, 3*(4), 360-373.

Lee, William M. (1997). Hepatitis B virus infection. *New England Journal of Medicine, 337*(24), 1733-1745.

Lee, Y. H., & Wong, D. T. (2009). Saliva: an emerging biofluid for early detection of diseases. *American Journal of Dentistry, 22*(4), 241-248.

Li, X., Scida, K., & Crooks, R. M. (2015). Detection of hepatitis B virus DNA with a paper electrochemical sensor. *Analytical Chemistry, 87*(17), 9009-9015.

Li, X., Tian, J., Nguyen, T., & Shen, W. (2008). Paper-based microfluidic devices by plasma treatment. *Analytical Chemistry, 80*(23), 9131-9134.

Li, Xu, Tian, Junfei, Garnier, Gil, & Shen, Wei. (2010a). Fabrication of paper-based microfluidic sensors by printing. *Colloids and Surfaces, B: Biointerfaces, 76*(2), 564-570.

Li, Xu, Tian, Junfei, & Shen, Wei. (2010b). Quantitative biomarker assay with microfluidic paper-based analytical devices. *Analytical and Bioanalytical Chemistry, 396*(1), 495-501.

Lim, W. Y., Thevarajah, T. M., Goh, B. T., & Khor, S. M. (2017). Microfluidic paper-based analytical devices for potential use in quantitative and direct detection of

University of Malaya

disease biomarkers in clinical analysis. *Journal of Chromatography B, 1060*, 424-442.

Liu, Hong, & Crooks, Richard M. (2011). Three-dimensional paper microfluidic devices assembled using the principles of origami. *Journal of the American Chemical Society, 133*(44), 17564-17566.

Liu, Hongxing, Zhou, Xiaoming, Liu, Weipeng, Yang, Xiaoke, & Xing, Da. (2016). based bipolar electrode electrochemiluminescence switch for label-free and sensitive genetic detection of pathogenic bacteria. *Analytical Chemistry, 88*(20), 10191-10197.

Liu, Rui, Zhang, Chunsun, & Liu, Min. (2015). Open bipolar electrode-electrochemiluminescence imaging sensing using paper-based microfluidics. *Sensors and Actuators, B: Chemical, 216*, 255-262.

Liu, X. Y., Cheng, C. M., Martinez, A. W., Mirica, K. A., Li, X. J., Phillips, S. T., . . . Whitesides, G. M. (2011). *A portable microfluidic paper-based device for ELISA.* Paper presented at the Proceedings of the IEEE International Conference on Micro Electro Mechanical Systems (MEMS), Cancun, Mexico.

Ljungblad, Jonas. (2009). *Antibody-conjugated gold nanoparticles integrated in a fluorescence based biochip.* (Master's thesis, Linköping University, Sweden). Retrieved on June 20, 2015 from http://liu.diva-portal.org/smash/get/diva2:271859/FULLTEXT01.pdf.

Lopez-Ruiz, Nuria, Curto, Vincenzo F, Erenas, Miguel M, Benito-Lopez, Fernando, Diamond, Dermot, Palma, Alberto J, & Capitan-Vallvey, Luis F. (2014). Smartphone-based simultaneous pH and nitrite colorimetric determination for paper microfluidic devices. *Analytical Chemistry, 86*(19), 9554-9562.

Lu, Y., Shi, W., Jiang, L., Qin, J., & Lin, B. (2009a). Rapid prototyping of paper-based microfluidics with wax for low-cost, portable bioassay. *Electrophoresis, 30*(9), 1497-1500.

Lu, Y., Shi, W., Qin, J., & Lin, B. (2009b). Fabrication and characterization of paper-based microfluidics prepared in nitrocellulose membrane by wax printing. *Analytical Chemistry, 82*(1), 329-335.

MacRae, Andrew R, Kavsak, Peter A, Lustig, Viliam, Bhargava, Rakesh, Vandersluis, Rudy, Palomaki, Glenn E, . . . Jaffe, Allan S. (2006). Assessing the requirement for the 6-hour interval between specimens in the American Heart Association Classification of Myocardial Infarction in Epidemiology and Clinical Research Studies. *Clinical Chemistry, 52*(5), 812-818.

Mair, P, Mair, J, Krause, E-G, Balogh, D, Puschendorf, B, & Rabitzsch, G. (1994). Glycogen phosphorylase isoenzyme BB mass release after coronary artery bypass grafting. *Clinical Chemistry and Laboratory Medicine, 32*(7), 543-548.

Malamud, Daniel. (1997). Oral diagnostic testing for detecting human immunodeficiency virus-1 antibodies: a technology whose time has come. *The American Journal of Medicine, 102*(4), 9-14.

University of Malaya

Marquette, Christophe A, & Blum, Loïc J. (2006). Applications of the luminol chemiluminescent reaction in analytical chemistry. *Analytical and Bioanalytical Chemistry, 385*(3), 546-554.

Martinez, A. W., Phillips, S. T., Butte, M. J., & Whitesides, G. M. (2007). Patterned paper as a platform for inexpensive, low-volume, portable bioassays. *Angewandte Chemie International Edition, 46*(8), 1318-1320.

Martinez, A. W., Phillips, S. T., Carrilho, E., Thomas, S. W., 3rd, Sindi, H., & Whitesides, G. M. (2008a). Simple telemedicine for developing regions: camera phones and paper-based microfluidic devices for real-time, off-site diagnosis. *Analytical Chemistry, 80*(10), 3699-3707.

Martinez, A. W., Phillips, S. T., Nie, Zhihong, Cheng, Chao-Min, Carrilho, Emanuel, Wiley, Benjamin J, & Whitesides, George M. (2010a). Programmable diagnostic devices made from paper and tape. *Lab on a Chip, 10*(19), 2499-2504.

Martinez, A. W., Phillips, S. T., & Whitesides, G. M. (2008b). Three-dimensional microfluidic devices fabricated in layered paper and tape. *Proceedings of the National Academy of Sciences of the United States of America, 105*(50), 19606-19611.

Martinez, A. W., Phillips, S. T., Wiley, B. J., Gupta, M., & Whitesides, G. M. (2008c). FLASH: a rapid method for prototyping paper-based microfluidic devices. *Lab on a Chip, 8*(12), 2146-2150.

Martinez, Andres W, Phillips, Scott T, Whitesides, George M, & Carrilho, Emanuel (2010b). Diagnostics for the developing world: microfluidic paper-based analytical devices. *Analytical Chemistry, 82*(1), 3-10.

Mirzaii-Dizgah, I., & Jafari-Sabet, M. (2011). Unstimulated whole saliva creatine phosphokinase in acute myocardial infarction. *Oral Diseases, 17*(6), 597-600.

Mirzaii-Dizgah, I., & Riahi, E. (2013). Salivary high-sensitivity cardiac troponin T levels in patients with acute myocardial infarction. *Oral Diseases, 19*(2), 180-184.

Mittal, Amit Kumar, & Banerjee, Uttam Chand. (2016). Current status and future prospects of nanobiomaterials in drug delivery. In A. M. Grumezescu (Ed.), *Nanobiomaterials in Drug Delivery* (pp. 147-170). Massachusetts, United Stated: Elsevier.

Mogensen, C. E. (1984). Microalbuminuria predicts clinical proteinuria and early mortality in maturity-onset diabetes. *New England Journal of Medicine, 310*(6), 356-360.

Mohammed, Mazher-Iqbal, & Desmulliez, Marc PY. (2011). Lab-on-a-chip based immunosensor principles and technologies for the detection of cardiac biomarkers: a review. *Lab on a Chip, 11*(4), 569-595.

Moore, D. S., & McGrane, S. D. (2003). Comparative infrared and Raman spectroscopy of energetic polymers. *Journal of Molecular Structure, 661*, 561-566.

University of Malaya

Moradpour, D., Wakita, T., Tokushige, K., Carlson, R. I., Krawczynski, K., & Wands, J. R. (1996). Characterization of three novel monoclonal antibodies against hepatitis C virus core protein. *Journal of Medical Virology, 48*(3), 234-241.

Nagesh, CM, & Roy, Ambuj. (2010). Role of biomarkers in risk stratification of acute coronary syndrome. *The Indian Journal of Medical Research, 132*(5), 627-633.

Nagler, Rafael M. (2008). Saliva analysis for monitoring dialysis and renal function. *Clinical Chemistry 54*(9), 1415-1417.

Nie, Jinfang, Liang, Yuanzhi, Zhang, Yun, Le, Shangwang, Li, Dunnan, & Zhang, Songbai. (2013). One-step Patterning of hollow microstructures in paper by laser cutting to create microfluidic analytical devices. *Analyst, 138*(2), 671-676.

Nie, Z., Deiss, F., Liu, X., Akbulut, O., & Whitesides, G. M. (2010a). Integration of paper-based microfluidic devices with commercial electrochemical readers. *Lab on a Chip, 10*(22), 3163-3169.

Nie, Zhihong, Nijhuis, Christian A, Gong, Jinlong, Chen, Xin, Kumachev, Alexander, Martinez, Andres W, . . . Whitesides, George M. (2010b). Electrochemical sensing in paper-based microfluidic devices. *Lab on a Chip, 10*(4), 477-483.

Nilsen, Dennis WT, Mjelva, Øistein Rønneberg, Leon de la Fuente, Ricardo A, Naesgaard, Patrycja, Pönitz, Volker, Brügger-Andersen, Trygve, . . . Nilsen, Stein Tore. (2015). Borderline Values of Troponin-T and High Sensitivity C-Reactive Protein Did Not Predict 2-Year Mortality in TnT Positive Chest-Pain Patients, Whereas Brain Natriuretic Peptide Did. *Frontiers in Cardiovascular Medicine, 2*(16), 1-10.

Noginov, MA, Zhu, G, Bahoura, M, Adegoke, J, Small, C, Ritzo, BA, . . . Shalaev, VM. (2007). The effect of gain and absorption on surface plasmons in metal nanoparticles. *Applied Physics B, 86*(3), 455-460.

Noiphung, J., Nguyen, M. P., Punyadeera, C., Wan, Y., Laiwattanapaisal, W., & Henry, C. S. (2018). Development of Paper-Based Analytical Devices for Minimizing the Viscosity Effect in Human Saliva. *Theranostics, 8*(14), 3797-3807.

O'Gara, Patrick T, Kushner, Frederick G, Ascheim, Deborah D, Casey, Donald E, Chung, Mina K, De Lemos, James A, . . . Franklin, Barry A. (2013). 2013 ACCF/AHA guideline for the management of ST-elevation myocardial infarction: a report of the American College of Cardiology Foundation/American Heart Association Task Force on Practice Guidelines. *Journal of the American College of Cardiology, 61*(4), e78-e140.

Ochnio, Jan J, Scheifele, David W, Ho, Margaret, & Mitchell, Leslie A. (1997). New, ultrasensitive enzyme immunoassay for detecting vaccine-and disease-induced hepatitis A virus-specific immunoglobulin G in saliva. *Journal of Clinical Microbiology, 35*(1), 98-101.

Odum, Ehimen Phyllis, & Wakwe, Victor Chukwuma. (2017). Clinical Significance of Creatine Kinase-MB Elevation in Patients with Chronic Kidney Disease before

University of Malaya

Initiation of Hemodialysis. *Cardiology and Angiology: An International Journal, 6*(4), 1-7.

Oh, Jung-Min, & Chow, Kwok-Fan. (2015). Recent developments in electrochemical paper-based analytical devices. *Analytical Methods, 7*(19), 7951-7960.

Ohman, E Magnus, Armstrong, Paul W, Christenson, Robert H, Granger, Christopher B, Katus, Hugo A, Hamm, Christian W, . . . Harrell Jr, Frank E. (1996). Cardiac troponin T levels for risk stratification in acute myocardial ischemia. *New England Journal of Medicine, 335*(18), 1333-1342.

Olkkonen, J., Lehtinen, K., & Erho, T. (2010). Flexographically printed fluidic structures in paper. *Analytical Chemistry, 82*(24), 10246-10250.

Out, D., Hall, R. J., Granger, D. A., Page, G. G., & Woods, S. J. (2012). Assessing salivary C-reactive protein: longitudinal associations with systemic inflammation and cardiovascular disease risk in women exposed to intimate partner violence. *Brain, Behavior, and Immunity, 26*(4), 543-551.

Overbaugh, Kristen J. (2009). Acute coronary syndrome. *American Journal of Nursing, 109*(5), 42-52.

Panteghini, Mauro, Pagani, Franca, Yeo, Kiang-Teck J, Apple, Fred S, Christenson, Robert H, Dati, Francesco, . . . Wu, Alan HB. (2004). Evaluation of imprecision for cardiac troponin assays at low-range concentrations. *Clinical Chemistry, 50*(2), 327-332.

Papautsky, Ian, Shen, Li, Hagen, Joshua, & Stone, Morley. (2016). *United State Patent No. US9506855B2.* Retrieved on May 18, 2017 from https://patents.google.com/patent/US9506855B2/en.

Peacock IV, W Frank, De Marco, Teresa, Fonarow, Gregg C, Diercks, Deborah, Wynne, Janet, Apple, Fred S, & Wu, Alan HB. (2008). Cardiac troponin and outcome in acute heart failure. *New England Journal of Medicine, 358*(20), 2117-2126.

Priye, Aashish, Ball, Cameron S, & Meagher, Robert J. (2018). Colorimetric-luminance readout for quantitative analysis of fluorescence signals with a smartphone CMOS sensor. *Analytical Chemistry, 90*(21), 12385-12389.

Prochazka, Marek. (2016). Basics of surface-enhanced raman scattering (SERS) *Surface-Enhanced Raman Spectroscopy*. Switzerland: Springer.

Qureshi, Anjum, Gurbuz, Yasar, & Niazi, Javed H. (2012). Biosensors for cardiac biomarkers detection: A review. *Sensors and Actuators, B: Chemical, 171*, 62-76.

Rabitzsch, G., Mair, J., Lechleitner, P., Noll, F., Hofmann, U., Krause, E. G., . . . Puschendorf, B. (1995). Immunoenzymometric assay of human glycogen phosphorylase isoenzyme BB in diagnosis of ischemic myocardial injury. *Clinical Chemistry, 41*(7), 966-978.

University of Malaya

Ramya, Atmakuri Shanmukha, Uppala, Divya, Majumdar, Sumit, Surekha, Ch, & Deepak, KGK. (2015). Are salivary amylase and pH–Prognostic indicators of cancers? *Journal of Oral Biology and Craniofacial Research, 5*(2), 81-85.

Rao, Lokinendi V, Petersen, John R, Mohammad, Amin A, Bissell, Michael G, & Okorodudu, Anthony O. (1999). Chemistry: Cost-Effective Utilization of CK-MB Mass and Activity Assays. *Laboratory Medicine, 30*(4), 271-275.

Roth, G. A., Johnson, C., Abajobir, A., Abd-Allah, F., Abera, S. F., Abyu, G., . . . Murray, C. (2017). Global, Regional, and National Burden of Cardiovascular Diseases for 10 Causes, 1990 to 2015. *Journal of the American College of Cardiology, 70*(1), 1-25.

Rubio, F, Rubio, J, & Oteo, JL. (1998). A FT-IR study of the hydrolysis of tetraethylorthosilicate (TEOS). *Spectroscopy Letters, 31*(1), 199-219.

Schmid, Günter (Eds.). (2011). *Nanoparticles: from theory to application*. New York: John Wiley & Sons.

Schneider, Astrid, Hommel, Gerhard, & Blettner, Maria. (2010). Linear regression analysis: part 14 of a series on evaluation of scientific publications. *Deutsches Ärzteblatt International, 107*(44), 776-782.

Scida, Karen, Li, Bingling, Ellington, Andrew D, & Crooks, Richard M. (2013). DNA detection using origami paper analytical devices. *Analytical Chemistry, 85*(20), 9713-9720.

Sechi, D., Greer, B., Johnson, J., & Hashemi, N. (2013). Three-dimensional paper-based microfluidic device for assays of protein and glucose in urine. *Analytical Chemistry, 85*(22), 10733-10737.

Shah, Kwok Wei. (2018). Nanosynthesis Techniques of Silica-Coated Nanostructures. In G. Z. Kyzas & A. C. Mitropoulos (Eds.), *Novel Nanomaterials-Synthesis and Applications* (pp. 91-109). London, UK: IntechOpen.

Shah, Vinod P, Midha, Kamal K, Dighe, Shrikant, McGilveray, Iain J, Skelly, Jerome P, Yacobi, Avraham, . . . McDowall, RD. (1992). Analytical methods validation: bioavailability, bioequivalence, and pharmacokinetic studies. *Journal of Pharmaceutical Sciences, 81*(3), 309-312.

Shen, Li, Ratterman, Michael, Klotzkin, David, & Papautsky, Ian. (2011). A CMOS optical detection system for point-of-use luminescent oxygen sensing. *ensors and Actuators, B: Chemical, 155*(1), 430-435.

Soda, Yoshiki, & Bakker, Eric. (2019). Quantification of Colorimetric Data for Paper-Based Analytical Devices. *ACS Sensors*. doi: 10.1021/acssensors.9b01802

Soman, Matthew, Stefanov, Konstantin, Weatherill, Daniel, Holland, Andrew, Gow, Jason, & Leese, Mark. (2015). Non-linear responsivity characterisation of a CMOS Active Pixel Sensor for high resolution imaging of the Jovian system. *Journal of Instrumentation, 10*(02), Article#C02012.

University of Malaya

Songjaroen, T., Dungchai, W., Chailapakul, O., Henry, C. S., & Laiwattanapaisal, W. (2012). Blood separation on microfluidic paper-based analytical devices. *Lab on a Chip, 12*(18), 3392-3398.

Songjaroen, Temsiri, Dungchai, Wijitar, Chailapakul, Orawon, & Laiwattanapaisal, Wanida. (2011). Novel, simple and low-cost alternative method for fabrication of paper-based microfluidics by wax dipping. *Talanta, 85*(5), 2587-2593.

Steinitz, M. (2000). Quantitation of the blocking effect of tween 20 and bovine serum albumin in ELISA microwells. *Analytical Biochemistry, 282*(2), 232-238.

Stejskal, David, Lacnak, Borek, Jedelsky, Libor, Stepanova, Leona, Proskova, Jitka, Solichova, Pavlina, . . . Karpisek, Michal. (2007). Use of glycogen phosphorylase BB measurement with POCT in the diagnosis of acute coronary syndromes. A comparison with the ELISA method. *Biomedical Papers of the Medical Faculty of Palacky University in Olomouc, 151*(2), 247-249.

Subramanian, N, Sundaraganesan, N, Dereli, Ö, & Türkkan, E. (2011). FT-IR, FT-Raman spectra, density functional computations of the vibrational spectra and molecular conformational analysis of 2, 5-di-tert-butyl-hydroquinone. *Spectrochimica Acta Part A: Molecular and Biomolecular Spectroscopy, 83*(1), 165-174.

Sun, Jie, Zhang, Xueji, Broderick, Mark, & Fein, Harry. (2003). Measurement of nitric oxide production in biological systems by using Griess reaction assay. *Sensors, 3*(8), 276-284.

Tam, Justina O, de Puig, Helena, Yen, Chun-wan, Bosch, Irene, Gómez-Márquez, Jose, Clavet, Charles, . . . Gehrke, Lee. (2017). A comparison of nanoparticle-antibody conjugation strategies in sandwich immunoassays. *Journal of Immunoassay and Immunochemistry, 38*(4), 355-377.

Teasdale, Peter R, Hayward, Sean, & Davison, William. (1999). In situ, high-resolution measurement of dissolved sulfide using diffusive gradients in thin films with computer-imaging densitometry. *Analytical Chemistry, 71*(11), 2186-2191.

Thobhani, Smita, Attree, Simon, Boyd, Robert, Kumarswami, Neelam, Noble, James, Szymanski, Mateusz, & Porter, Robert A. (2010). Bioconjugation and characterisation of gold colloid-labelled proteins. *Journal of Immunological Methods, 356*(1), 60-69.

Thygesen, K. A., & Alpert, J. S. (2001). The definitions of acute coronary syndrome, myocardial infarction, and unstable angina. *Current Cardiology Reports, 3*(4), 268-272.

Utsumi, T., & Lusida, M. I. (2015). Viral hepatitis and human immunodeficiency virus co-infections in Asia. *World Journal of Virology, 4*(2), 96-104.

Vella, S. J., Beattie, P., Cademartiri, R., Laromaine, A., Martinez, A. W., Phillips, S. T., . . . Whitesides, G. M. (2012). Measuring markers of liverfunction using a micropatterned paper device designed for blood from a fingerstick. *Analytical Chemistry, 84*(6), 2883-2891.

University of Malaya

Wang, Fei, & Theuwissen, Albert. (2017). Linearity analysis of a CMOS image sensor. *Electronic Imaging, 2017*(11), 84-90.

Wang, Wei, Wu, Wen-Ya, & Zhu, Jun-Jie. (2010). Tree-shaped paper strip for semiquantitative colorimetric detection of protein with self-calibration. *Journal of Chromatography A, 1217*(24), 3896-3899.

Wei, F., & Wong, D. T. (2012). Point-of-care platforms for salivary diagnostics. *Chinese Journal of Dental Research, 15*(1), 7-15.

Whalley, Simon A, Murray, John M, Brown, Dave, Webster, George JM, Emery, Vincent C, Dusheiko, Geoffrey M, & Perelson, Alan S. (2001). Kinetics of acute hepatitis B virus infection in humans. *Journal of Experimental Medicine, 193*(7), 847-854.

Wölcken, Piet Christof, & Papadopoulos, Michael. (2015). *Smart intelligent aircraft structures (SARISTU): proceedings of the final project conference*. Switzerland: Springer.

Wu, AH, & Feng, YJ. (1998). Biochemical differences between cTnT and cTnI and their significance for diagnosis of acute coronary syndromes. *European Heart Journal, 19*, N25-N29.

Xia, Yanyan, Si, Jin, & Li, Zhiyang. (2016). Fabrication techniques for microfluidic paper-based analytical devices and their applications for biological testing: A review. *Biosensors and Bioelectronics, 77*, 774-789.

Xiao, Yuhong, & Isaacs, Stuart N. (2012). Enzyme-linked immunosorbent assay (ELISA) and blocking with bovine serum albumin (BSA)—not all BSAs are alike. *Journal of Immunological Methods, 384*(1), 148-151.

Yang, Xiaoxi, Forouzan, Omid, Brown, Theodore P, & Shevkoplyas, Sergey S. (2012). Integrated separation of blood plasma from whole blood for microfluidic paper-based analytical devices. *Lab on a Chip, 12*(2), 274-280.

Yetisen, Ali Kemal, Akram, Muhammad Safwan, & Lowe, Christopher R. (2013). based microfluidic point-of-care diagnostic devices. *Lab on a Chip, 13*(12), 2210-2251.

Yu, J., Ge, L., Huang, J., Wang, S., & Ge, S. (2011). Microfluidic paper-based chemiluminescence biosensor for simultaneous determination of glucose and uric acid. *Lab on a Chip, 11*(7), 1286-1291.

Yuen, V. G., & McNeill, J. H. (2000). Comparison of the glucose oxidase method for glucose determination by manual assay and automated analyzer. *Journal of Pharmacological and Toxicological Methods, 44*(3), 543-546.

Zaret, Barry L, Battler, Alexander, Berger, Harvey J, Bodenheimer, Monty M, Borer, Jeffrey S, Brochier, Mireille, . . . Pfisterer, Matthias E. (1984). Report of the joint international society and federation of cardiology/world health organization task force on nuclear cardiology. *European Heart Journal, 5*(10), 850-863.

University of Malaya

Zhang, D., Huang, L., Liu, B., Ni, H. B., Sun, L. D., Su, E. B., . . . Zhao, X. W. (2018a). Quantitative and ultrasensitive detection of multiplex cardiac biomarkers in lateral flow assay with core-shell SERS nanotags. *Biosensors and Bioelectronics, 106*, 204-211.

Zhang, D., Huang, L., Liu, B., Su, E. B., Chen, H. Y., Gu, Z. Z., & Zhao, X. W. (2018b). Quantitative detection of multiplex cardiac biomarkers with encoded SERS nanotags on a single T line in lateral flow assay. *Sensors and Actuators, B: Chemical, 277*, 502-509.

Zhang, Xiaowei, Li, Jing, Chen, Chaogui, Lou, Baohua, Zhang, Lingling, & Wang, Erkang. (2013). A self-powered microfluidic origami electrochemiluminescence biosensing platform. *Chemical Communications, 49*(37), 3866-3868.

Zhang, Yin, Hong, Hao, & Cai, Weibo. (2010). Imaging with Raman spectroscopy. *Current Pharmaceutical Biotechnology, 11*(6), 654-661.

Zhao, C., & Liu, X. (2016). A portable paper-based microfluidic platform for multiplexed electrochemical detection of human immunodeficiency virus and hepatitis C virus antibodies in serum. *Biomicrofluidics, 10*(2), Article#024119.

Zhao, Pengxiang, Li, Na, & Astruc, Didier. (2013). State of the art in gold nanoparticle synthesis. *Coordination Chemistry Reviews, 257*(3-4), 638-665.

University of Malaya

LIST OF PUBLICATIONS

PUBLICATIONS

Lim, W. Y., Thevarajah, T. M., Goh, B. T., & Khor, S. M. (2017). Microfluidic paper-based analytical devices for potential use in quantitative and direct detection of disease biomarkers in clinical analysis. *Journal of Chromatography B*, *1060*, 424-442.

Lim, W. Y., Thevarajah, T. M., Goh, B. T., & Khor, S. M. (2019). Paper microfluidic device for early diagnosis and prognosis of acute myocardial infarction via quantitative multiplex cardiac biomarker detection. *Biosensors and Bioelectronics*, *128*, 176-185.

Lim, W. Y., Goh, C. H., Thevarajah, T. M., Goh, B. T., & Khor, S. M. (2020). Using SERS-based microfluidic paper-based device (μPAD) for calibration-free quantitative measurement of AMI cardiac biomarkers. *Biosensors and Bioelectronics*, *147*, Article#111792.

University of Malaya